## Signal Propagation on a Network

A thesis submitted to the School of Engineering, Mathematics and Physics at the University of East Anglia in partial fulfilment of the requirements for the degree of Doctor of Philosophy

Asmaa Alqarni

31/January/2025

© This copy of the thesis has been supplied on condition that anyone who consults it is understood to recognise that its copyright rests with the author and that use of any information derived there from must be in accordance with current UK Copyright Law. In addition, any quotation or extract must include full attribution.

## **Abstract**

This thesis investigates the behaviour of signals in networked systems by applying diffusion and reaction-diffusion equations on a variety of network topologies, which include path graphs, tree graphs, Y-shaped graphs, and square grid graphs.

We employ mathematical models, including the diffusion equation, the Fisher equation, and the FitzHugh-Nagumo equations, to describe concentration and excitation across networks. Using methods such as eigenvalue analysis, finite-difference methods, and the Method of Lines (MOL), numerical simulations were performed to solve these equations and analyse the impact of network topology on signal propagation.

Key findings include the adaptation of continuous diffusion models to discrete network structures, the successful application of the Crank-Nicholson method for solving diffusion equations on networks, and the analysis of pulse dynamics and stability in reaction-diffusion models. The FitzHugh-Nagumo model was particularly useful for exploring excitable systems and the propagation of pulses across networks, showing how topology influences wave formation and stability.

#### **Access Condition and Agreement**

Each deposit in UEA Digital Repository is protected by copyright and other intellectual property rights, and duplication or sale of all or part of any of the Data Collections is not permitted, except that material may be duplicated by you for your research use or for educational purposes in electronic or print form. You must obtain permission from the copyright holder, usually the author, for any other use. Exceptions only apply where a deposit may be explicitly provided under a stated licence, such as a Creative Commons licence or Open Government licence.

Electronic or print copies may not be offered, whether for sale or otherwise to anyone, unless explicitly stated under a Creative Commons or Open Government license. Unauthorised reproduction, editing or reformatting for resale purposes is explicitly prohibited (except where approved by the copyright holder themselves) and UEA reserves the right to take immediate 'take down' action on behalf of the copyright and/or rights holder if this Access condition of the UEA Digital Repository is breached. Any material in this database has been supplied on the understanding that it is copyright material and that no quotation from the material may be published without proper acknowledgement.

A	bstra	ct			11
Li	st of	Figur	es		х
Li	st of	Table	${f s}$	3	ζV
A	cknov	wledge	ements	x	vi
1	Intr	oduct	ion		1
	1.1	Motiv	ation for the study		1
		1.1.1	Calcium wave propagation in plant leaves		1
		1.1.2	Broader applications of network diffusion models		1
	1.2	Backg	round of diffusion on a network		2
	1.3	Introd	luction to graph theory		3
		1.3.1	Definition and terminology		3
		1.3.2	Relevance to network modelling		5
		1.3.3	Edge directions and vertex degrees		5

	1.4	Diffus	ion on a graph literature review and novel contribution	7
		1.4.1	Discretising approach	7
		1.4.2	Random walks on a graph	10
		1.4.3	Metric graph	12
		1.4.4	Quantum graphs	12
		1.4.5	Novel contributions of this work	14
	1.5	Aim a	and outline	15
2	Diff	usion	in networks: analysis and asymptotic behaviour	18
	2.1	Found	lations of diffusion	18
		2.1.1	Basic concepts	19
		2.1.2	Fick's Law of diffusion	19
		2.1.3	Derivation of the one-dimensional diffusion equation	19
	2.2	Diffus	ion on a network	20
		2.2.1	General case	20
		2.2.2	Mathematical formulation	21
		2.2.3	Boundary and continuity conditions	22
		2.2.4	Governing equation	23
		2.2.5	Separation of variables for network diffusion	24
		2.2.6	Special case	25
		2.2.7	Flux conditions	26

2.3	Eigenv	value analysis and matrix formulation	26
	2.3.1	Matrix formulation and eigenvalue problem	27
	2.3.2	Generalized eigenvalue problem for nu	28
	2.3.3	Eigenvalue analysis using Gershgorin's theorem	29
2.4	_	arity of the modified Laplacian matrix $\mathbf{L}^*$ and eigenvalue is	33
	2.4.1	Regular graph	33
2.5	Nume	rical results for eigenvalue analysis of the modified Laplacian	
	matrix	c	34
	2.5.1	Graphs with four vertices	34
	2.5.2	Graphs with four vertices decay rate analysis	37
	2.5.3	Graphs with six vertices	37
	2.5.4	Normalized Laplacian	37
2.6	Square	e grid graph	41
	2.6.1	Klopotek's results for a square grid graph	41
	2.6.2	Eigenvalues of a square grid graph	55
	2.6.3	Key Observations on a Square Grid Graph	57
2.7	Asymj	ptotic theory for a square grid graph	61
	2.7.1	Case 1: $(z1, z2) = (0, 1)$ or $(z1, z2) = (1, 0) \dots \dots$	63
	2.7.2	Case 2: $(z1, z2) = (1, 1) \dots \dots \dots \dots$	65
	2.7.3	Case 3: $(z1, z2) = (0, 0) \dots \dots \dots \dots \dots$	65

*Contents* vi

		2.7.4	Results of asymptotic analysis	66
3	Diff	usion o	on a network: finite-difference approach	71
	3.1	Brief i	ntroduction to the finite difference method	72
	3.2	Crank	-Nicholson method to solve the diffusion equation on a network	73
		3.2.1	Crank-Nicholson method to solve the diffusion equation for path graph P2	73
		3.2.2	Numerical results for a path graph $P_2$	78
		3.2.3	Crank–Nicholson method to solve diffusion equation for path graph $P_3$	82
		3.2.4	Numerical results for a path graph $P_3$	88
		3.2.5	The general formula of the fictitious point for the continuity of flux condition for any network	91
		3.2.6	Initial condition	94
		3.2.7	Numerical results for the Y-shaped graph	96
		3.2.8	Numerical results for square grid graph $3 \times 3$	99
		3.2.9	Numerical results for square grid graph $6 \times 6$	104
4	Rea	ction- $c$	diffusion equation on network	L <b>08</b>
	4.1	Reacti	on diffusion equation	109
	4.2	Steady	v-state and stability analysis for the reaction-diffusion equation	110
		4.2.1	Steady states for the reaction-diffusion equation	110

Contents vii

		4.2.2	Stability analysis for the reaction-diffusion equation on a network
		4.2.3	Stability analysis for $P_2$
	4.3	Metho	od of Lines
		4.3.1	Method of lines for path graph $P_2$
		4.3.2	Numerical results and analysis for path graph $P_2$ 123
		4.3.3	Method of Lines for path graph $P_3$
		4.3.4	Numerical results and analysis for path graph $P_3$ 128
		4.3.5	Method of lines on general network
		4.3.6	Numerical results and analysis for general network 133
5	The	e FitzH	Iugh–Nagumo model: simulation of pulse dynamics in
5		e FitzH work	Iugh-Nagumo model: simulation of pulse dynamics in  141
5		work	
5	netv	work The F	141
5	<b>netv</b> 5.1	work The F	141 itzHugh—Nagumo model
5	<b>netv</b> 5.1	work The F	141 itzHugh–Nagumo model
5	<b>netv</b> 5.1	work The F Nume 5.2.1 5.2.2	itzHugh–Nagumo model
5	5.1 5.2	work The F Nume 5.2.1 5.2.2	141         itzHugh-Nagumo model
5	5.1 5.2	The F Nume 5.2.1 5.2.2 Spatia	141         itzHugh-Nagumo model
5	5.1 5.2	work The F Nume 5.2.1 5.2.2 Spatia 5.3.1	141         itzHugh-Nagumo model

Contents viii

		5.3.5	Small amplitude stationary solution on a network: wave	
			number compatibility	. 162
		5.3.6	Small amplitude stationary solution on a network: example	es 167
		5.3.7	Small amplitude stationary solution on a network: initial	
			guess for the numerical method	. 169
	5.4	Unifor	rm solution on a network	. 172
	5.5	Statio	nary solutions on a network: stability	. 174
		5.5.1	Stability of the uniform state	. 178
	5.6	Nume	rical results	. 184
		5.6.1	The path graph $P_2$	. 185
		5.6.2	The path graph $P_3$	. 187
		5.6.3	The Y-shaped graph	. 190
		5.6.4	Square grid graph $3 \times 3$	. 193
6	Con	clusio	n	198
	6.1	Summ	nary and conclusions	. 198
	6.2	Future	e work	. 200
$\mathbf{A}_{\mathbf{j}}$	ppen	dices		202
$\mathbf{A}$	Fine	$_{ m d}$ the $_{ m e}$	eigenvalue of square grid graph by applying Klopotek	c's
	equ	ation		202
	A.1	Case	of $3 \times 3$ square grid graph	. 202

	A.1.1	Observation on the table for odd number of vertices along
		one side n=3
A.2	Case o	of $4 \times 4$ square grid graph
	A.2.1	Observation on the table for even number of vertices along
		one side n=4
A.3	Case o	of $5 \times 5$ square grid graph
	A.3.1	Case of $6 \times 6$ square grid graph
	A.3.2	Observation

## List of Figures

1.3.1 A simple undirected graph
1.3.2 A bipartite graph
1.3.3 A directed graph
1.3.4 A high-degree vertex and low-degree vertex
1.4.1 Path graph $P_2$
2.1.1 The diffusion process
2.2.1 A typical edge $e_{ij}$ in the network
2.2.2 A typical network
2.5.1 Path graph $P_4$ and its eigenvalues
2.5.2 A square graph with 4 vertices and its eigenvalues
2.5.3 A Y-shaped graph and its eigenvalues
2.5.4 Triangular graph with 4 vertices and its eigenvalue
2.5.5 Triangular graph with one edge added and its eigenvalues $36$
2.5.6 Two connected triangles and its eigenvalues

List of Figures xi

2.5.7 Tree graph with 6 vertices and its eigenvalue	39
$2.5.8$ Triangular grid graph with 6 vertices with its eigenvalues $\dots$	39
2.6.1 Initial guesses for $\delta_1$ and $\delta_2$	46
2.6.2 multiplicity of zero eigenvalue for a square grid graph	52
2.6.3 A $4 \times 4$ square grid graph with 16 vertices	56
2.6.4 Eigenvalues of square grid graphs of various sizes vs. $\lambda \in [-1,1]$	57
2.7.1 Value of $\tau$ closest to the eigenvalue 2 for different values of $n$ on a square grid graph	62
2.7.2 Asymptotic approximation of a square grid graph $(z_1, z_2) = (1, 0)$ .	67
2.7.3 Asymptotic approximation of a square grid graph $(z_1,z_2)=(1,1)$ .	68
2.7.4 Asymptotic approximation of a square grid graph $(z_1, z_2) = (0, 0)$ .	69
3.2.1 A path graph $P_2$ with two vertices	73
3.2.2 A path graph $P_2$ with two vertices	79
3.2.3 Results of solving diffusion equation by (FDM) for a path graph $P_2$ .	80
3.2.4 Applying Crank–Nicholson discretization on path graph $P_3$	81
3.2.5 Applying Crank–Nicholson discretization on path graph $P_3$	85
3.2.6 Directed path graph $P_3$ with three vertices connected by two edges.	88
3.2.7 Results of solving diffusion equation by (FDM) for a path graph $P_3$ .	89
3.2.8 Results of solving diffusion equation by (FDM) for a path graph $P_3$ with varying spatial step size h	90

List of Figures xii

3.2.9 Results of solving diffusion equation by (FDM) for a path graph
$P_3$ with varying time steps $\Delta t$
3.2.10Y-shape graph with four vertices and three edges 96
3.2.1 Results of solving diffusion equation by (FDM) for a Y-shaped graph. 97
3.2.12Square grid graph $3 \times 3$
3.2.1 $\Re$ esults of solving diffusion equation by (FDM) for a 3 × 3 square grid graph
3.2.14Results of solving diffusion equation by (FDM) for a $6 \times 6$ square grid graph
4.2.1 plot the reaction term of Fisher equation to show regions is positive and negative
4.2.2 Sketch of one conceivable steady state configuration $U(x)$ 112
4.2.3 Numerical simulation of the Fisher equation
4.2.4 Numerical simulation of the Fisher equation
4.3.1 A path graph $P_2$ with two vertices
4.3.2 Evaluation of concentration $u(x,t)$ over time for a Fisher equation. 123
4.3.3 Numerical result of a $P_2$ graph for reaction-diffusion equation 124
4.3.4 path graph $P_3$ with three vertices connected by two edges 125
4.3.5 The concentration distribution of $P_3$ for the Fisher equation 128
4.3.6 Numerical result of a $P_3$ graph for reaction-diffusion equation 129
$4.3.7 \mathrm{On}P_3$ , the flux dynamics at the edge boundary over time $130$
4.3.8 Cycle graph with 3 vertices arranged as a triangle 135

List of Figures xiii

4.3.9 Propagation of concentration on a triangular graph for a reaction-
diffusion equation
4.3.10 Numerical converge study in triangle graph
4.3.1 Numerical result of a triangle graph for reaction-diffusion equation 136
4.3.12Fluxes entering edges
4.3.13Tree graph with 6 vertices
4.3.14Concentration spread in a tree graph composed of 6 vertices 139
4.3.15Numerical result of reaction diffusion equation by using (MOL) $140$
4.3.16 Fluxes entering edge
5.2.1 A path graph $P_2$ with two vertices
5.2.2 Pulse of voltage in the axon on $P_2$
5.2.3 Pulse of recovery dynamics on $P_2$
5.2.4 Final profile pulse of the voltage in the axon on $P_2$
5.2.5 Final profile of recovery dynamics of $v(x,t)$ on a $P_2$ 146
5.2.6 Temporal evolution of maximum amplitudes
5.2.7 Y-shape graph with four vertices and three edges
5.2.8 Voltage axon pulse propagation in Y-shaped graph
5.2.9 Recovery dynamics pulse propagation in Y-shaped graph 149
5.2.10Time evolution of the voltage in the axon on Y-shaped graph $150$
5.2.1 Time evolution of the recovery dynamic of Y-shaped graph 150
5.3.1 The spatial dynamics evolution of (FHN) on $P_2$

List of Figures xiv

5.3.2 The zeros of function $F$ , defined in (5.3.58)
5.3.3 Demonstrating the set of possible $k$ values
5.4.1 Uniform solutions
5.5.1 Uniform state: left branch stability
5.5.2 Uniform state: right branch stability
5.6.1 A path graph $P_2$ with two vertices
5.6.2 Bifurcation diagram of (FHN) of $P_2$
5.6.3 path graph $P_3$ with three vertices connected by two edges 189
5.6.4 Bifurcation diagram of (FHN) of $P_3$
5.6.5 Y-shape graph with four vertices and three edges 192
5.6.6 Bifurcation diagram of (FHN) of Y-shaped graph 192
5.6.7 Square grid graph $3 \times 3$
5.6.8 Bifurcation diagram of (FHN) of $3 \times 3$ square grid graph 195

## List of Tables

2.1	Minimum decay rate for graphs with four vertices
2.2	Eigenvalues of modified Laplacian for 16-Vertex Square Grid Graph 58
2.3	Chosen values of $z_1, z_2, \delta_1, \delta_2$ , and corresponding eigenvalues $\tau$ for a 16-vertex grid graph
3.1	The eigenvalue $\lambda$ of the modified Laplacian $\mathbf{L}^*$ and their corresponding $\nu$ for square grid graph Y-shaped graph 98
3.2	The eigenvalue $\lambda$ of the modified Laplacian $\boldsymbol{L}^*$ and their corresponding $\nu$ for square grid graph $3 \times 3 \dots $
3.3	The eigenvalue $\lambda$ of the modified Laplacian $\boldsymbol{L}^*$ and their corresponding $\nu$ for square grid graph $6\times 6.$
4.1	The smallest decay rate $\nu_{\min}$ for a range of different networks 116

## Acknowledgements

First and foremost, I would like to express my heartfelt thanks to my supervisor, Prof. Mark Blyth, for his exceptional mentorship, unwavering support, and invaluable guidance throughout this journey. His expertise, insightful feedback, and encouragement were crucial in shaping this work, and I am deeply grateful for the time and effort he dedicated to my growth as a researcher. It has been a privilege to benefit from both his remarkable knowledge and his outstanding character.

To my beloved parents, whose sacrifices, unconditional love, and steadfast belief in education laid the foundation for every achievement in my life—thank you. Your resilience and support, even in the most challenging times, have been my anchor and inspiration.

To my precious kids, Raseel and Abdullah, who brighten my world with their laughter and curiosity: thank you for your patience during the countless hours I spent immersed in this work. You reminded me daily of what truly matters, and your love gave me the strength to persevere.

Finally, to my siblings, whose unwavering support and cheerleading carried me through moments of doubt—thank you for always being my loudest advocates and for keeping me grounded with your humour and love.

### Introduction

#### 1.1 Motivation for the study

#### 1.1.1 Calcium wave propagation in plant leaves

The motivation for this work originates from the experiments conducted by Annalisa Bellandi, who investigated the propagation of diffusion waves in plant leaves triggered by localised stimuli [4]. In her study, a needle was used to induce a pressure disturbance at a specific point on a leaf, generating a calcium wave that diffused across the entire leaf. The mechanism was attributed to the diffusion and bulk flow of amino acid messengers, which activated calcium-permeable channels as they travelled through the plant vasculature. In this thesis, the focus shifts away from biological specifics to develop generalised mathematical models of diffusion and reaction-diffusion processes on graphs. This abstraction allows for the study of wave dynamics in a variety of contexts, making the findings relevant beyond plant systems.

#### 1.1.2 Broader applications of network diffusion models

Beyond the biological systems that motivated this study, diffusion processes on networks find extensive applications across diverse fields where substances, information, or influences propagate through interconnected structures. In epidemiology, the spread of infectious diseases can be modelled as diffusion processes on social contact networks, where individuals represent vertices and their interactions form edges, allowing researchers to predict outbreak patterns and evaluate intervention strategies [29]. Social networks exhibit similar diffusion phenomena in the propagation of information, opinions, or behaviours, where ideas spread from person to person following network connectivity In neuroscience, the brain's neural networks demonstrate patterns [17]. diffusion-like processes in the transmission of electrical signals and chemical messengers between neurons, making network diffusion models valuable for understanding cognitive processes and neurological disorders [10]. Urban transportation systems represent another domain where diffusion models apply, as traffic flow, congestion patterns, and public transport dynamics can be analysed using network-based diffusion equations [3]. These diverse applications highlight the fundamental importance of understanding diffusion dynamics on networks, as the mathematical frameworks developed in this thesis—including eigenvalue analysis, boundary conditions, and reaction-diffusion.

#### 1.2 Background of diffusion on a network

Understanding the principle of diffusion processes is essential, which will serve as a foundation for developing more generalised models of diffusion in networks. Diffusion is the process by which particles move from areas of high concentration to areas of low concentration due to molecular interactions between the particles themselves [35]. These molecular interactions are what drive the transfer of substances from one molecule to another, causing the diffusion process to unfold. Although the essential mechanism is inherently discrete and involves individual molecular collisions, diffusion is often modelled as a continuous process for practical reasons.

One classical approach to modelling diffusion is Fick's law, which treats diffusion as a smooth, continuous process [25]. Although this continuous model is effective in many scenarios, a more refined approach is needed when diffusion occurs in

systems structured as networks, such as in Turing's model of biological pattern formation. In these cases, diffusion occurs between cells or nodes in a network, with the medium represented as a set of discrete vertices and edges. This brings us to the work of Alan Turing, who, in the early twentieth century, applied diffusion processes between cells arranged in a network-like structure to explain the formation of patterns in biological systems [43].

Our approach focusses on solving the diffusion equation for each individual edge within the network. This differs from the finite-difference technique commonly used in network diffusion studies, where the diffusion operator is discretised across the entire network. Later in this chapter, we will provide a more detailed analysis of this methodology and its differences from the approach we employ, but first, it is essential to introduce some foundational concepts from graph theory that will help us understand networks in this context.

#### 1.3 Introduction to graph theory

In this section, we provide a basic overview of graph theory, which serves as the mathematical framework for analysing networks in this thesis. We begin by defining essential concepts, such as vertices, edges, and degrees, which form the basis of the network structure. These definitions are crucial for understanding how diffusion processes operate in networks, as the structure and properties of a graph directly influence the dynamics of diffusion. In addition, we will explore key graph types, including bipartite and directed graphs.

#### 1.3.1 Definition and terminology

Graph theory provides a mathematical framework for studying networks, which are made up of a set of vertices (or nodes) V and a set of edges E. Each edge connects two vertices and represents a relationship or interaction between them. In a  $directed\ graph$  (or digraph), each edge has a direction, indicating a one-way

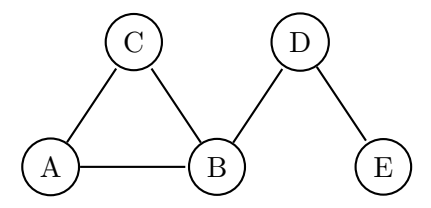


Figure 1.3.1: A simple undirected graph. Each edge represents a bidirectional relationship.

relationship from one vertex to another. Conversely, in an *undirected graph*, edges do not have a direction, implying a bidirectional relationship between connected vertices [45].

The degree of a vertex is the number of edges connected to it. In directed graphs, we distinguish between the *in-degree*, which is the number of incoming edges, and the *out-degree*, which is the number of outgoing edges [36]. These basic concepts form the foundation for the analysis of more complex structures and behaviours in networks.

A *loop-less graph* which will be the focus of this thesis, is defined as a graph that contains no loops. A loop is characterised as an edge that connects a vertex to itself, or equivalently as an edge whose endpoints are identical [7].

A bipartite graph G = (V, E) is a graph whose vertex set V can be partitioned into two non-empty subsets A and B (i.e.,  $A \cup B = V$  and  $A \cap B = \emptyset$ ) such that each edge of G has one endpoint in A and one endpoint in B. A bipartite graph does not contain self-loops [40].

A path graph  $P_n$  is a graph with n vertices and n-1 edges that lie on a single straight line [28], where vertex i is connected to vertex i+1 for  $i=1,2,\ldots,n-1$ . A grid graph or a lattice is a regular tiling of the Euclidean space  $\mathbb{R}^n$  that forms a repetitive structure. These graphs are characterised by a group of bijective transformations that map the graph onto itself. Examples of grid graphs include the square grid graph and the triangular grid graph, each with distinct geometric properties [37].

A regular graph is a graph that has the same number of vertex neighbours; in other words, every vertex has the same degree [20].

A connected graph, any two vertices in the graph are connected by a path [46].

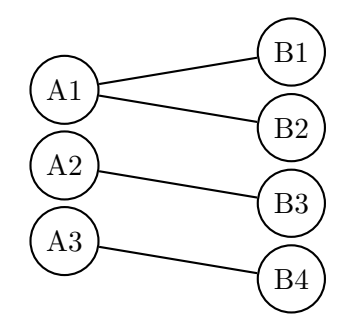


Figure 1.3.2: A bipartite graph.

In a *tree*, there is exactly one edge connecting every distinct pair of vertices i and j on the graph, where  $i \neq j$  [5].

#### 1.3.2 Relevance to network modelling

In the previous section, we introduced concepts such as vertices, edges, and degrees, which play an essential role in modelling how substances or information propagate through a network. The vertices represent the locations or entities where diffusion occurs, and the edges represent the pathways for diffusion. The structure of the graph, whether it is directed or undirected, and the degree distribution of its vertices can significantly influence the dynamics of diffusion [2]. Therefore, understanding these concepts of graph theory is essential for effectively modelling and analysing diffusion in networks.

#### 1.3.3 Edge directions and vertex degrees

The direction of the edges in a network determines the pathways through which diffusion can occur. In a directed graph, diffusion can occur only along the direction of the edges, which may lead to asymmetric diffusion patterns. For instance, if the vertex A has an outgoing edge to the vertex B but not vice versa, diffusion from A to B is possible, but the reverse is not [36].

The degree of a vertex plays a significant role in the diffusion process. Vertices with a high degree, which means that they are connected to many other vertices,

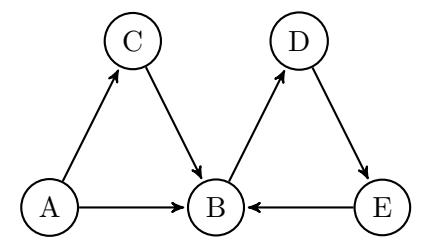


Figure 1.3.3: A directed graph. Note that vertex B has both incoming edges (in-degree) and outgoing edges (out-degree).

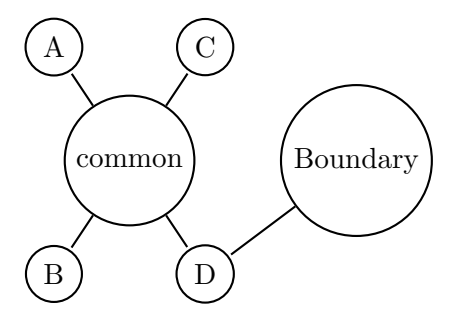


Figure 1.3.4: A high-degree vertex (common vertex) connected to multiple vertices and a low-degree vertex (Boundary vertex) with limited connections.

are often referred to as *common vertices*. These common vertices serve as hubs, facilitating rapid diffusion across the network by connecting different parts of the graph. In contrast, low-degree vertices, known as *boundary vertices*, have fewer connections and may act to slow down the diffusion process.

The distinction between *in-degree* and *out-degree* in directed graphs becomes important. The in-degree refers to the number of incoming edges to a vertex, while the out-degree refers to the number of outgoing edges. These properties influence how substances or information accumulate or disperse from specific vertices, shaping the overall dynamics of diffusion in the network [45].

Graph theory provides a framework for representing networks, but to understand how processes such as chemical substances occur within these networks, we must delve into the physical principles governing such phenomena. Specifically, diffusion plays a central role in many network processes. Before applying diffusion models to networks, we will review the core principles of diffusion in a continuous medium.

# 1.4 Diffusion on a graph literature review and novel contribution

The mathematical modelling of diffusion processes on networks has evolved through several distinct approaches, each offering unique insights into how substances spread through discrete structures. Understanding these existing methodologies is crucial for positioning our novel contributions within the broader landscape of network diffusion theory. The following sections review the primary approaches found in the literature, beginning with traditional discretization methods before introducing the innovative edge-by-edge analytical framework developed in this work.

#### 1.4.1 Discretising approach

In most approaches, the network is represented as a graph, with each vertex corresponding to a location (such as a cell) and each edge representing a connection (such as a pathway between cells) [26]. A common method to discretise the diffusion process in these graphs involves solving a diffusion equation as follows:

$$u_t = u_{xx},$$

where u represents the concentration of substance,  $u_t$  represents the temporal change in concentration, and  $u_{xx}$  represents the spatial diffusion. On a simple path graph denoted by  $P_2$  where subscript 2 represents the number of vertices of the graph (see Figure 1.4.1), the diffusion of a substance along the edges of the graph from vertex i to vertex j can be discretised by assigning concentration values  $u_i$  to each vertex, where i = 1, ..., N. The second derivative is approximated using finite differences:

$$\frac{u_{i+1} - 2u_i + u_{i-1}}{h^2},$$



Figure 1.4.1: Path graph  $P_2$ 

where h is the distance between adjacent vertices, essentially discretising the network in terms of spatial steps.

More generally, for a graph structure, diffusion is modelled from each vertex to its neighbours. Let D be the diffusion rate across the edge, then the amount of substance that moves from vertex i to vertex j over a time period dt is  $D(u_i - u_j)$  and from vertex j to vertex i is  $D(u_j - u_i)$ . then

$$\frac{du_i}{dt} = D(u_i - u_j), \quad \frac{du_j}{dt} = D(u_j - u_i)$$

When considering diffusion to and from the vertex i, we must take into consideration all the vertices of the graph. The connectivity of the graph is represented by the adjacency matrix. Now for a simple graph we assume D = 1, then the rate at which  $u_i$  is changing is given by:

$$\frac{du_i}{dt} = \sum_{j=1}^{N} A_{ij}(u_j - u_i),$$
 (1.4.1)

where the sum is over all N vertices in the graph, and  $A_{ij}$  is the adjacency matrix and  $u_i$  is the concentration at vertex i. The following form can be used to express Equation (1.4.1):

$$\frac{du_i}{dt} = \sum_{j=1}^{N} A_{ij} u_j - u_i \sum_{j=1}^{N} A_{ij}.$$
 (1.4.2)

The degree of vertex i, denoted  $d_i$ , can be written in terms of the adjacency matrix as  $d_i = \sum_{j=1}^{N} A_{ij}$  [35], the equation (1.4.2) can be expressed as:

$$\frac{du_i}{dt} = \sum_{j=1}^{N} A_{ij} u_j - u_i d_i,$$
(1.4.3)

We define the Kronecker delta,  $\delta_{ij}$  [35], as follows

$$\delta_{ij} = \begin{cases} 1 & \text{if } i = j \\ 0 & \text{if } i \neq j. \end{cases}$$

Using the Kronecker delta definition in equation (1.4.3), which leads to:

$$\frac{du_i}{dt} = \sum_{j=1}^{N} A_{ij} u_j - \sum_{j=1}^{N} \delta_{ij} u_j d_i.$$

(Note that there is no implied summation over a repeated index here). Since  $\delta_{ij}d_j = D_{ij}$ , this simplifies to:

$$\frac{du_i}{dt} = \sum_{j=1}^{N} (A_{ij} - D_{ij})u_j.$$

In vector form, this can be written as:

$$\frac{d\mathbf{u}}{dt} = (\mathbf{A} - \mathbf{D})\mathbf{u},$$

where  $\mathbf{u}$  is the vector of concentration values at the graph vertices and  $\mathbf{D}$  is the degree matrix. Thus, the equation becomes:

$$\frac{d\mathbf{u}}{dt} = \mathbf{L}\mathbf{u},$$

where  $\mathbf{L} = \mathbf{A} - \mathbf{D}$  is the Laplacian matrix for the graph. We seek a solution in the form

$$\mathbf{u} = e^{\lambda t} \mathbf{a}$$

where **a** is a constant vector, and  $\lambda$  is a constant. Substituting this into the differential equation yields:

$$\lambda \mathbf{a} = \mathbf{L} \mathbf{a}$$

which implies that  $\lambda$  is an eigenvalue of the Laplacian matrix **L**. Thus, in this model, the decay rates over the network correspond to the eigenvalues of the

Laplacian. This formulation of the equation is commonly referred to as the diffusion equation on a graph or the graph Laplacian [35].

#### 1.4.2 Random walks on a graph

A random walk on a graph is a stochastic process in which a walker moves from one vertex to an adjacent vertex based on transition probabilities. This discrete process can be viewed as an analogy to diffusion, where the spread of a substance follows a continuous medium. Let G = (V, E) represent a graph, and let P denote the transition matrix of the random walk, where:

$$\mathbf{P}_{ij} = \begin{cases} \frac{1}{d_i} & \text{if } (i,j) \in E, \\ 0 & \text{otherwise,} \end{cases}$$

where  $(i, j) \in E$  indicates that there is an edge connecting vertices i and j in the graph [32].

For a graph G = (V, E), the normalised Laplacian  $\mathbf{L}_{norm}$  is defined as:

$$\mathbf{L}_{norm} = \mathbf{D}^{-1/2} \mathbf{L} \mathbf{D}^{-1/2},$$

where  $\mathbf{L} = \mathbf{D} - \mathbf{A}$  is the combinatorial Laplacian,  $\mathbf{A}$  is the adjacency matrix and  $\mathbf{D}$  is the degree matrix [19]. Substituting  $\mathbf{L} = \mathbf{D} - \mathbf{A}$  into the expression for  $\mathbf{L}_{\text{norm}}$ , we have:

$$\mathbf{L}_{\text{norm}} = \mathbf{D}^{-1/2}(\mathbf{D} - \mathbf{A})\mathbf{D}^{-1/2}.$$

Expanding this expression:

$$L_{norm} = D^{-1/2}DD^{-1/2} - D^{-1/2}AD^{-1/2}$$

Since  $\mathbf{D}^{-1/2}\mathbf{D}\mathbf{D}^{-1/2} = \mathbf{I}$  (the identity matrix), this simplifies to:

$$\mathbf{L}_{\text{norm}} = \mathbf{I} - \mathbf{D}^{-1/2} \mathbf{A} \mathbf{D}^{-1/2}.$$

The random walk transition matrix P defined above can be written as:

$$\mathbf{P} = \mathbf{D}^{-1} \mathbf{A}.$$

which describes the probabilities of transition between vertices in a random walk [33]. To express  $\mathbf{P}$  in terms of normalized matrices, we observe that:

$$P = D^{-1/2}(D^{-1/2}AD^{-1/2})D^{1/2}.$$

Let  $\mathbf{A}^* = \mathbf{D}^{-1/2} \mathbf{A} \mathbf{D}^{-1/2}$ , which is often referred to as the normalized adjacency matrix. Substituting  $\mathbf{A}^*$  into  $\mathbf{P}$ , we have:

$$\mathbf{P} = \mathbf{D}^{-1/2} \mathbf{A}^* \mathbf{D}^{1/2}.$$

When we replace  $\mathbf{A}^* = \mathbf{D}^{-1/2} \mathbf{A} \mathbf{D}^{-1/2}$  in the Laplacian matrix, we obtain:

$$\mathbf{L}_{norm} = \mathbf{I} - \mathbf{A}^*.$$

Since  $\mathbf{A}^* = \mathbf{D}^{-1/2} \mathbf{A} \mathbf{D}^{-1/2}$ , and from the relation  $\mathbf{P} = \mathbf{D}^{-1} \mathbf{A}$ , we observe that:

$$A^* = I - L_{norm}$$
.

Thus, substituting this into  $L_{norm}$ , we finally obtain:

$$\mathbf{L}_{\text{norm}} = \mathbf{I} - \mathbf{P}.$$

This relationship highlights the intrinsic connection between random walks and spectral graph theory [9], since the normalised Laplacian governs diffusion-like processes on graphs as will be discussed in chapter 2.

#### 1.4.3 Metric graph

In this section, we introduce an approach to how we can structure a graph that is similar to the approach we use in the thesis, which is a metric graph. A metric graph is a mathematical structure in which each edge is treated as a continuous interval, giving it a 1D geometric character rather than a purely combinatorial one. Formally, a metric graph  $\Gamma$  consists of a set V of vertices and a set E of edges, where each edge  $e \in E$  is assigned a positive length  $l_e \in (0, \infty]$ . The edge e is identified with an interval  $[0, l_e]$  of the real line, and a coordinate  $x_e$  is defined along the edge, with  $x_e = 0$  and  $x_e = l_e$  corresponding to the two vertices connected by the edge. This representation introduces a natural topology and a metric on the graph [31].

The finite metric graphs are graphs that have a finite number of vertices and edges. The distances between two points are always finite, and the graph structure can often be represented compactly. A path in a metric graph is a sequence of connected edges  $\{e_j\}_{j=1}^M$ . The total length of the path is given by the sum of the edge lengths  $\sum_{j=1}^M l_{e_j}$  [31].

#### 1.4.4 Quantum graphs

Expanding on the concept of metric graphs, we present quantum graphs, which are a natural extension of metric graphs used to study problems involving differential operators on graphs. A quantum graph is a metric graph equipped with a differential operator, such as the Laplacian, acting on functions defined on the edges of the graph. These functions describe physical quantities like wave functions or diffusion densities, making quantum graphs a framework for solving various physical and mathematical problems which is similar to the method that is used in this thesis.

A function f defined on a quantum graph can be expressed as a tuple  $(f_e)_{e \in E}$ , where each  $f_e(x_e)$  is a function defined on the interval  $[0, l_e]$  corresponding to the

edge e. The Hilbert space of the quantum graph is given by

$$\bigoplus_{e \in E} L^2([0, l_e]),$$

where  $L^2([0, l_e])$  is the space of square-integrable functions on the edge e. The inner product of two functions f and g on this space is defined as

$$\langle f, g \rangle = \sum_{e \in E} \int_0^{l_e} f_e^*(x_e) g_e(x_e) dx_e.$$

The simplest operator considered on a quantum graph is the Laplace operator, which acts on each edge as

$$-\frac{d^2}{dx_a^2}$$
,

where  $x_e$  is the coordinate along edge e. To solve problems on a quantum graph, suitable boundary conditions must be imposed at the vertices to ensure the operator is self-adjoint. Common boundary conditions include:

- Dirichlet conditions: The function  $f_e(x_e)$  vanishes at the endpoints of the edge, i.e.,  $f_e(0) = f_e(l_e) = 0$ .
- Neumann (natural) conditions: The function is continuous at vertices, and the sum of the outgoing derivatives at each vertex is zero:

$$\sum_{e \sim v} \frac{df_e}{dx_e}(v) = 0.$$

By solving the eigenvalue problem

$$-\frac{d^2 f_e}{dx_e^2} = \lambda f_e,$$

subject to the chosen boundary conditions, one can determine the eigenvalues  $\lambda$  and eigenfunctions  $f_e(x_e)$ , which describe the natural modes of the system [31].

While the approaches discussed above—discretization methods, random walks,

and quantum/metric graphs—have provided valuable frameworks for understanding diffusion on networks, they each possess inherent limitations. Traditional discretization approaches sacrifice analytical precision for computational tractability, random walk methods primarily capture stochastic behaviour rather than deterministic concentration dynamics, and quantum graph approaches, while mathematically elegant, often lack direct connections to practical network applications. Recognizing these gaps in the existing literature, this thesis develops a fundamentally different approach that addresses these limitations through exact analytical solutions coupled with systematic eigenvalue analysis.

#### 1.4.5 Novel contributions of this work

This thesis introduces several new methodological approaches:

- Exact edge-by-edge solutions: Unlike previous finite-difference approaches
  that discretize across the entire network, we solve the diffusion equation
  analytically on each individual edge, then couple solutions through vertex
  conditions.
- 2. Modified Laplacian eigenvalue analysis: We develop a comprehensive eigenvalue analysis using the modified Laplacian matrix  $\boldsymbol{L}^*(\nu) = \boldsymbol{A} \cos(\nu)\boldsymbol{D}$ , providing exact decay rates for arbitrary network topologies—a systematic analysis not previously available in the literature.
- 3. Asymptotic theory for large networks: We derive asymptotic eigenvalue behaviour for square grid graphs as network size approaches infinity, extending Klopotek's results [30] to diffusion problems.
- 4. Unified numerical framework: We integrate exact analytical solutions with the method of lines for reaction-diffusion systems, enabling treatment of both linear diffusion and non-linear Fisher and FitzHugh-Nagumo dynamics on the same network framework.

These contributions provide new theoretical insights into how network topology fundamentally affects diffusion dynamics, bridging the gap between discrete graph theory and continuous PDE approaches.

#### 1.5 Aim and outline

In this thesis, we explore the phenomenon of diffusion and reaction-diffusion in networks, focusing on the structural properties of graphs. We use graph theory to explain the network structure, employing concepts such as the adjacency matrix and degree matrix.

Chapter 2 introduces the physical principles of diffusion and their application to networks. It begins by defining key terms such as concentration, flux, and diffusion coefficient, followed by the derivation of the one-dimensional diffusion equation using Fick's Law. The chapter then extends these principles to network structures, where diffusion occurs across discrete vertices and edges, unlike the continuous media in physical space. The mathematical formulation of diffusion on networks is developed, including the general case of diffusion across edges with varying lengths and diffusivity constants. The chapter further explores boundary and continuity conditions for solving diffusion equations and employs methods such as separation of variables and eigenvalue analysis to understand the longterm behaviour of diffusion processes in networks. Special attention is given to the eigenvalue analysis of a modified form of the Laplacian matrix to reveal insights into the structure of the network and the diffusion characteristics. The chapter concludes with numerical examples and the asymptotic behaviour of diffusion in square grid graphs, highlighting the significance of eigenvalues in determining the decay rate of substances across networks.

In chapter 3, we employ a finite-difference method to numerically solve the diffusion equation on networks. Instead of solving the diffusion equation exactly on each edge and using eigenvalue analysis for decay rates, we discretise the

problem using a set of equally spaced collocation points along each edge. This approach provides a simplified framework that enables the subsequent inclusion of non-linear terms in Chapters 4 and 5, facilitating the solution of the diffusion equation with more complex dynamics in later stages of the study. We enforce continuity conditions at the vertices and apply the Crank-Nicholson method to evolve the system over time. The chapter begins with a brief introduction to the finite-difference method, followed by the application of the Crank-Nicholson method to simple network structures, such as a path graph with two vertices,  $P_2$ . The methodology is extended to more complex networks, such as a path graph with three vertices  $P_3$  and a Y-shaped graph, ensuring the continuity of concentration and flux at the common vertices. Numerical results are presented for various network topologies, including square grid graphs, where the concentration profiles and decay rates are compared with theoretical The chapter concludes by generalising the approach to handle predictions. networks with arbitrary numbers of vertices and edges, introducing fictitious points to maintain continuity at common vertices, and extending the analysis to large networks.

In chapter 4, we focus on solving reaction-diffusion equations on networks using the Method of Lines (MOL). The chapter begins by discretising the spatial domain into a grid, transforming the partial differential equations (PDEs) into a system of ordinary differential equations (ODEs) that can be efficiently solved using standard numerical integration techniques. We emphasise enforcing the continuity of flux and concentration at the vertices and applying zero-flux boundary conditions at the boundary vertices. Various network topologies are considered, starting from simple path graphs and extending to more complex structures. The chapter also explores the stability of steady-state solutions for the reaction-diffusion equation, comparing numerical decay rates with theoretical predictions introduced in Chapter 2. Additionally, the chapter includes numerical simulations conducted using MATLAB to analyse the dynamic behaviour of concentration, demonstrating the propagation and

stabilisation of concentration profiles over time. The results provide an understanding of both dynamic and steady-state behaviours of reaction-diffusion systems on networks, offering insight into the stability conditions and decay rates for different network structures.

In Chapter 5, we investigate the application of the Fitzhugh-Nagumo (FHN) model to simulate pulse dynamics in network structures. This chapter is motivated by experimental observations made by Annalisa, who identified distinct pulse-like phenomena in calcium wave dynamics [4]. The Fitzhugh-Nagumo model, consisting of two coupled reaction diffusion equations that describe the membrane potential and recovery variables of neurones, is used to explore the underlying mechanisms of pulse propagation within these networks. We explore pulse propagation in simple network topologies, starting with a path graph  $P_2$  and extending to more complex structures, such as a Y-shaped network. External forces are applied at the head node to initiate pulse propagation, and the effects of this stimulation are observed in both one-dimensional edge networks and more complex multi-edge networks. particular, the study examines how pulses split and propagate when they reach a junction point, illustrating how the network topology influences the pulse The chapter also explores boundary conditions and introduces dynamics. numerical methods for solving the (FHN) equations, including the application of finite-difference methods and time-stepping techniques. Finally, bifurcation points and the stability analysis of pulse solutions are studied, with results showing how the pulse propagation behaviour depends on the network structure and parameter values. The thesis is then summarised with some conclusions.

# Diffusion in networks: analysis and asymptotic behaviour

In this chapter, we delve into the mathematical foundation for understanding diffusion in networks, beginning with the concepts of concentration, flux, and the diffusion coefficient. We will start by exploring the basic principles of diffusion, including Fick's Law, which leads to the derivation of the diffusion equation. We use the concepts of graph theory to represent the network topologies by vertices and edges. We then apply zero flux conditions at the boundary vertices and continuity of flux and concentration at the common vertices. From there, we solve the diffusion equation exactly on each edge of the network and then formulate an eigenvalue problem for the decay rate.

#### 2.1 Foundations of diffusion

In this section, we introduce the physical principles of diffusion, which govern the spread of substances or information through a medium. These concepts are critical for understanding how diffusion occurs in networks, where the medium is represented by the connections between vertices. We will begin by defining key terms such as concentration, flux, and diffusion coefficient. Then, we will derive the one-dimensional diffusion equation based on Fick's Law, which will serve as the mathematical foundation for extending diffusion to more complex network structures in the following sections.

#### 2.1.1 Basic concepts

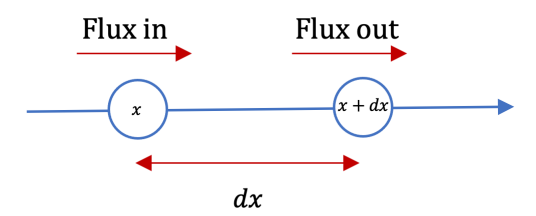


Figure 2.1.1: The diffusion process showing concentration gradients and flux.

To understand diffusion processes, we begin by defining several key terms. The concentration u(x,t) represents the quantity of a substance per unit length at position x and time t. The flux q(x,t) denotes the rate at which the substance flows through a point per unit time at a given position x and time t. The diffusion coefficient D is a proportionality constant that characterizes the rate of diffusion in a particular medium, with units of  $m^2/s$  [24].

#### 2.1.2 Fick's Law of diffusion

Fick's First Law states that the flux q(x,t) is proportional to the negative gradient of the concentration:

$$q(x,t) = -D\frac{\partial u(x,t)}{\partial x},$$
(2.1.1)

where D is the diffusion coefficient. This relationship implies that the substance flows from regions of high concentration to regions of low concentration, with the rate of flow being higher where the concentration gradient is steeper [24].

#### 2.1.3 Derivation of the one-dimensional diffusion equation

To derive the one-dimensional diffusion equation, consider the conservation of mass within a differential element of length dx. The rate of change of the concentration within this element is given by the difference between the flux

entering and leaving the element:

$$\frac{\partial u(x,t)}{\partial t} = -\frac{\partial q(x,t)}{\partial x}. (2.1.2)$$

Substituting Fick's First Law into this equation yields:

$$\frac{\partial u(x,t)}{\partial t} = D \frac{\partial^2 u(x,t)}{\partial x^2}.$$
 (2.1.3)

This is the one-dimensional diffusion equation, which describes how the concentration of a substance evolves over time in a given medium [24], forming the basis for our subsequent analysis of diffusion on networks.

# 2.2 Diffusion on a network

In this section, we extend the principles of diffusion to networks built on both the graph theory and diffusion foundations. While diffusion in physical space occurs in continuous media, network diffusion involves discrete structures where vertices and edges represent locations and connections, respectively. We will develop the mathematical formulation of diffusion on networks and introduce boundary and continuity conditions specific to network structures. The governing diffusion equation for networks will then be derived, followed by an exploration of methods to solve it, including separation of variables and eigenvalue analysis.

#### 2.2.1 General case

In this section, we explore the diffusion of a chemical substance across a network, which consists of vertices V connected by edges E. The diffusivity constant D is assumed to be uniform across all edges, while the length of each edge connecting vertex i to vertex j is denoted by  $L_{ij}$ . The edges in the network can have different lengths, allowing for a more generalized model of diffusion. We define  $e_{ij}$  as the edge connecting vertex i to vertex j, where j > i. In this structure, vertex i

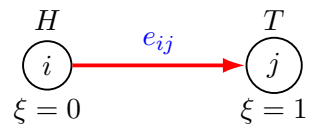


Figure 2.2.1: A typical edge  $e_{ij}$  in the network of length  $L_{ij}$  with head H at vertex i and tail T at vertex j. The red arrow designates the positive direction of flow.

is designated as the head (H), and vertex j as the tail (T), with the positive direction of flow along the edge  $e_{ij}$  being from head to tail, as depicted in Figure (2.2.1).

#### 2.2.2 Mathematical formulation

The concentration of the substance on edge  $e_{ij}$  is denoted by  $u_{ij}$ . The diffusion equation governing the concentration over time is given by:

$$\frac{\partial u(t,x)}{\partial t} = D \frac{\partial^2 u(t,x)}{\partial x^2},\tag{2.2.1}$$

We will transform each edge of the network into an interval of canonical length one. To achieve this, we introduce a new variable  $\xi$ , defined such that  $x = L_{ij}\xi$  with  $\xi \in [0,1]$  representing a scaled version of the position x along the edge, and  $x \in [0, L_{ij}]$  corresponds to the actual position along the edge of length. Substituting into equation (2.2.1), we obtain:

$$\frac{\partial u_{ij}(t,\xi)}{\partial t} = \beta_{ij} \frac{\partial^2 \xi u_{ij}(t,\xi)}{\partial \xi^2},$$
(2.2.2)

where  $\beta_{ij} = \frac{D_{ij}}{L_{ij}^2}$  and  $D_{ij}$  are the diffusivity constant specific to edge  $e_{ij}$ . To analyse the mass of the chemical on edge  $e_{ij}$ , we define:

$$m_{ij} = \int_0^1 u_{ij}(t,\xi) d\xi,$$
 (2.2.3)

where  $m_{ij}$  represents the total mass of the substance along the edge, and  $u_{ij}(\xi)$  is the concentration at position  $\xi$  [27]. Taking the positive direction of flow from

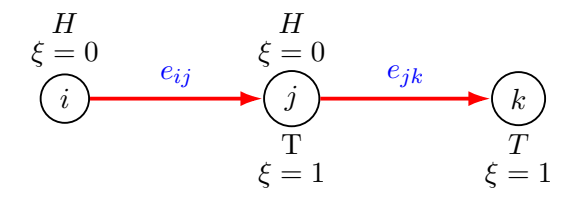


Figure 2.2.2: A typical network where vertices i and k are boundary vertices, and vertex j is a common vertex.

head to tail as indicated by the red arrow in Figure 2.2.1, we define the fluxes at the head and tail of edge  $e_{ij}$  as follows:

$$q_{ij}^{H} = -\alpha_{ij} \frac{\partial u_{ij}(t,\xi)}{\partial \xi}$$
 at  $\xi = 0$ , (2.2.4)

$$q_{ij}^{T} = -\alpha_{ij} \frac{\partial u_{ij}(t,\xi)}{\partial \xi}$$
 at  $\xi = 1$ , (2.2.5)

where

$$\alpha_{ij} = \frac{D_{ij}}{L_{ij}}. (2.2.6)$$

In this context,  $D_{ij}$  remains the diffusivity constant, and  $L_{ij}$  is the length of the edge from vertex i to vertex j.

#### 2.2.3 Boundary and continuity conditions

To uniquely determine the solution to the network diffusion problem, appropriate boundary and initial conditions must be imposed. Consider the network structure depicted in Figure 2.2.2, where vertices i and k are boundary vertices connected to a common vertex j via edges  $e_{ij}$  and  $e_{jk}$ , respectively. In a network, vertices can be classified as either boundary or common vertices. Boundary vertices are those connected by only one edge, implying that the flux cannot extend beyond these vertices ( $\xi = 0$  if the boundary node is the head, and  $\xi = 1$  if the boundary node is the tail). Common vertices, on the other hand, are connected by two or more edges, allowing flux to be continuous across them ( $\xi = 1$  when the vertex is a tail or  $\xi = 0$  when the vertex is a head). Specifically:

• Boundary vertex at head ( $\xi = 0$ ): For a boundary vertex connected as the head of edge  $e_{ij}$ , the zero-flux condition is:

$$-\alpha_{ij} \left. \frac{\partial u_{ij}}{\partial \xi} \right|_{\xi=0} = 0. \tag{2.2.7}$$

• Boundary vertex at tail ( $\xi = 1$ ): For a boundary vertex connected as the tail of edge  $e_{jk}$ , the zero-flux condition is:

$$-\alpha_{jk} \left. \frac{\partial u_{jk}}{\partial \xi} \right|_{\xi=1} = 0. \tag{2.2.8}$$

Common vertices, such as vertex j in Figure 2.2.2, are connected by two or more edges, allowing flux continuity across them. The conditions at a common vertex are:

• Continuity of flux: The net flux into the common vertex must equal the net flux out. For vertex j, this condition is:

$$-\alpha_{ij} \left. \frac{\partial u_{ij}}{\partial \xi} \right|_{\xi=1} = -\alpha_{jk} \left. \frac{\partial u_{jk}}{\partial \xi} \right|_{\xi=0}. \tag{2.2.9}$$

• Continuity of concentration: The concentration must be continuous across the common vertex. Thus, for vertex j:

$$u_{ij}(t,\xi)\Big|_{\xi=0} = u_{jk}(t,\xi)\Big|_{\xi=1}.$$
 (2.2.10)

These conditions ensure the proper diffusion dynamics across a network, accounting for both boundary and common vertices.

# 2.2.4 Governing equation

Consider a network consisting of N vertices, where the diffusion process is governed by a differential equation defined on each edge  $e_{ij}$  connecting vertices i and j. Assuming a uniform network with diffusivity D and edge length L, the

diffusion equation on edge  $e_{ij}$  is given by:

$$\beta^2 \frac{\partial u_{ij}}{\partial t} = \frac{\partial^2 u_{ij}}{\partial \xi^2}, \quad \beta^2 = \frac{L^2}{D}$$
 (2.2.11)

where  $u_{ij}(\xi, t)$  represents the concentration of a substance at a scaled position  $\xi \in [0, 1]$  along the edge and at time t.

## 2.2.5 Separation of variables for network diffusion

To solve the diffusion equation on a network, we employ the method of separation of variables. This approach assumes that the temporal behaviour of the solution is uniform across the network, allowing us to express the concentration function  $u_{ij}(\xi,t)$  on any edge  $e_{ij}$  as a product of a spatial function  $X_{ij}(\xi)$  and a temporal function T(t):

$$u_{ij}(\xi, t) = X_{ij}(\xi)T(t).$$
 (2.2.12)

Substituting this assumed form into the governing diffusion equation, we obtain two ordinary differential equations (ODEs) by separating the variables:

$$\frac{d^2 X_{ij}}{d\xi^2} + \nu^2 X_{ij} = 0, (2.2.13)$$

$$\frac{dT}{dt} + \mu^2 T = 0, (2.2.14)$$

where  $\nu$  and  $\mu$  are separation constants with  $\nu = \beta \mu$ . The ODE for the temporal component, Equation (2.2.14), has a solution of the form:

$$T_{ij}(t) = e^{-\mu^2 t}. (2.2.15)$$

The ODE for the spatial component, Equation (2.2.13), represents a second-order linear homogeneous differential equation. The general solution is given by:

$$X_{ij}(\xi) = \frac{1}{\sin \nu} \left( U_j \sin(\nu \xi) + U_i \sin(\nu (1 - \xi)) \right), \qquad (2.2.16)$$

where  $U_i$  and  $U_j$  denote the concentrations at vertices i and j, respectively. This formula (2.2.16) holds unless  $\sin(\nu) = 0$ , which will be considered in the next section (2.2.6). This form of  $X_{ij}(\xi)$  is chosen to ensure continuity of concentration across the network. By satisfying the boundary conditions at the endpoints of each edge,

$$X_{ij}(0) = U_i, \quad X_{ij}(1) = U_j$$

the solution maintains a smooth transition of concentration between connected edges, which is a necessary condition for physically realistic diffusion across the network. Thus, the general solution for the concentration function on edge  $e_{ij}$  is:

$$u_{ij}(\xi, t) = e^{-\mu^2 t} \left( \frac{U_j \sin(\nu \xi) + U_i \sin(\nu (1 - \xi))}{\sin \nu} \right).$$
 (2.2.17)

This expression demonstrates how the diffusion evolves both spatially along each edge and temporally over time, governed by the network's structure and the diffusion coefficients.

#### 2.2.6 Special case

In certain cases, the general solution to the diffusion equation may require modification due to special conditions, such as when  $\sin(\nu) = 0$ . When this occurs, the form of the solution needs to be adjusted to maintain consistency with the boundary and continuity conditions.

$$X_{ij}(\xi) = \frac{1}{\sin \nu} \left( [U_j - U_i \cos \nu] \sin(\nu \xi) + [U_i \sin \nu] \cos(\nu \xi) \right). \tag{2.2.18}$$

Taking the limit as  $\nu \to k\pi$  for integer k, the expression simplifies to:

$$X_{ij}(\xi) = U_i \cos(\nu \xi), \tag{2.2.19}$$

where we must choose  $U_i = (-1)^k U_j$  to maintain consistency.

#### 2.2.7 Flux conditions

In addition to solving the diffusion equation, it is important to ensure that the flux is well defined. The flux conditions describe how the substance moves between the vertices of the network, ensuring that the flow is continuous . The flux along an edge  $e_{ij}$ , connecting vertices i and j, is defined by:

$$q_{ij}^{H} = -\alpha_{ij} \left. \frac{\partial u_{ij}}{\partial \xi} \right|_{\xi=0}, \tag{2.2.20}$$

$$q_{ij}^{T} = -\alpha_{ij} \left. \frac{\partial u_{ij}}{\partial \xi} \right|_{\xi=1}. \tag{2.2.21}$$

where  $\alpha_{ij}$  is the diffusion coefficient along the edge, and  $q_{ij}^H$  and  $q_{ij}^T$  are the fluxes at the head and tail of the edge, respectively. For a common vertex j, connected by multiple edges, the flux into the vertex must equal the flux out:

$$blue \sum_{k \in S(i)^{-}} q_{ik}^{H} - \sum_{k \in S(i)^{+}} q_{ki}^{T} = 0,$$
(2.2.22)

where  $S(i)^-$  and  $S(i)^+$  denote the sets of vertices connected to i with indices less than or greater than i, respectively. The elements  $a_{ij}$  of the adjacency matrix A represent the connectivity of the network.

- $S(i)^- = \{ j \in V : j < i \text{ and } a_{ij} = 1 \},$
- $S(i)^+ = \{ j \in V : j > i \text{ and } a_{ij} = 1 \}.$

# 2.3 Eigenvalue analysis and matrix formulation

In this section, we will explore the mathematical formulation of the diffusion process on networks, specifically through matrix representation and eigenvalue analysis. We will first introduce the matrix formulation of the diffusion equation, representing the network's structure using the adjacency and degree matrices. This leads to an eigenvalue problem. We will apply Gershgorin's Theorem, which

offers a method for determining how network topology affects the eigenvalue spectrum.

#### 2.3.1 Matrix formulation and eigenvalue problem

The matrix formulation of the diffusion process on a network leads naturally to an eigenvalue problem. By analysing the eigenvalues of this matrix, we gain insight into the long-term behaviour of the diffusion process. We define a function

$$c(\nu) = \nu \cos \nu$$

and express the flux terms as:

$$q_{ik}^H = \nu U_k - cU_i, \tag{2.3.1}$$

$$q_{ki}^T = cU_i - \nu U_k. \tag{2.3.2}$$

Thus, the continuity condition becomes:

$$\nu \left( \sum_{k \in S(i)^{-}} U_k + \sum_{k \in S(i)^{+}} U_k \right) - c \left( \sum_{k \in S(i)^{-}} U_i + \sum_{k \in S(i)^{+}} U_i \right) = 0.$$
 (2.3.3)

Simplifying, we have:

$$\nu \left( \sum_{k \in S(i)^{-}} U_k + \sum_{k \in S(i)^{+}} U_k \right) - cd_i U_i = 0, \tag{2.3.4}$$

where  $d_i$  is the degree of vertex i. We can express this as the matrix equation

$$\begin{bmatrix} -cd_1 & \nu & \dots & \nu \\ \nu & -cd_2 & \nu & \dots & \nu \\ \vdots & \ddots & \ddots & \ddots & \vdots \\ \nu & \ddots & \ddots & -cd_{N-1} & \nu \\ \nu & \ddots & \ddots & \nu & -cd_N \end{bmatrix} \begin{bmatrix} U_1 \\ U_2 \\ \vdots \\ U_{N-1} \\ U_N \end{bmatrix} = \mathbf{0},$$

where the  $\nu$ 's occupy positions depending on the connectivity of the network. This is made more clear by expressing the equation in the more succinct form

$$L^*(\nu)x = \mathbf{0},\tag{2.3.5}$$

where  $\boldsymbol{x} = (U_1, U_2, \dots, U_N)^T$ , and

$$\boldsymbol{L}^*(\nu) = \boldsymbol{A} - \frac{c}{\nu} \boldsymbol{D} = \boldsymbol{A} - \cos(\nu) \boldsymbol{D}.$$
 (2.3.6)

$$L^*(\nu) = A - \cos(\nu)D \tag{2.3.7}$$

This formulation (2.3.7) is referred to as the modified Laplacian matrix, where  $\boldsymbol{A}$  denotes the adjacency matrix, and  $\boldsymbol{D}$  represents the degree matrix of the network. Before proceeding to these examples, we want to determine the values of  $\nu$ .

### 2.3.2 Generalized eigenvalue problem for $\nu$

To determine the values of  $\nu$ , we must solve the generalized eigenvalue problem that arises from the matrix formulation discussed earlier (2.3.5). Specifically, we solve the equation:

$$\mathbf{A}x = \lambda \mathbf{D}x,\tag{2.3.8}$$

To establish the relationship between the parameter  $\nu$  and the eigenvalue  $\lambda$ , we observe that, by comparing Equation (2.3.7) to the corresponding eigenvalue expression,  $\lambda$  is related to  $\nu$  through the equation

$$\lambda = \cos(\nu). \tag{2.3.9}$$

meaning that for each eigenvalue  $\lambda$ , there corresponds a countably infinite set of values for  $\nu$ . This formulation provides insight into the spectral properties of the network. To further analyse this relationship, we need to establish bounds on the eigenvalues  $\lambda$ , which can be done effectively using Gershgorin's Theorem. By

applying this theorem, we can determine where the eigenvalues are located.

#### 2.3.3 Eigenvalue analysis using Gershgorin's theorem

As the matrix formulation of the diffusion process has been established, the next step is to estimate the bounds of eigenvalues based on the entries of the matrix. In this section, we will use Gershgorin's Theorem to establish these bounds and guide our understanding of the eigenvalue spectrum of  $\mathbf{L}^*$ .

Consider a loop-less graph G with n vertices. Let A denote its adjacency matrix, which is an  $n \times n$  square matrix defined as:

$$\mathbf{A} = \begin{bmatrix} 0 & a_{12} & \dots & & & & & \\ a_{21} & 0 & a_{23} & \dots & & a_{2n} \\ a_{31} & a_{32} & \ddots & \ddots & & \vdots \\ \vdots & \vdots & \ddots & \ddots & & a_{(n-1)n} \\ a_{n1} & a_{n2} & \dots & a_{n(n-1)} & 0 \end{bmatrix}$$

where each entry  $a_{ij}$  represents the edge weights between vertices i and j, and  $a_{ii} = 0$  since the graph is loop-less. Let  $\mathbf{D}$  represent the degree matrix of the graph, which is also an  $n \times n$  diagonal matrix:

$$\mathbf{D} = \begin{bmatrix} d_{11} & 0 & \dots & 0 \\ 0 & d_{22} & 0 & \dots & 0 \\ 0 & 0 & \ddots & \ddots & \vdots \\ \vdots & \vdots & \ddots & \ddots & 0 \\ 0 & 0 & \dots & 0 & d_{nn} \end{bmatrix}$$

where  $d_{ii}$  is the degree of vertex i (i.e., the sum of the weights of the edges connected to vertex i).

#### Eigenvalue equation

We seek to find the eigenvalues  $\lambda \in \mathbb{R}$  that satisfy the following eigenvalue equation for the adjacency matrix  $\boldsymbol{A}$  and the degree matrix  $\boldsymbol{D}$ :

$$\mathbf{A}\mathbf{x} = \lambda \mathbf{D}\mathbf{x}.\tag{2.3.10}$$

Since the degree matrix D is diagonal and non-singular for connected graphs, we can multiply both sides of this equation by  $D^{-1}$  to simplify the problem. This yields the modified eigenvalue equation:

$$D^{-1}Ax = \lambda x.$$

Let us define a new matrix  $\boldsymbol{B}$  as:

$$\boldsymbol{B} = \boldsymbol{D}^{-1} \boldsymbol{A}.$$

This allows us to rewrite the modified eigenvalue equation as:

$$\boldsymbol{B}\boldsymbol{x} = \lambda \boldsymbol{x},$$

indicating that  $\lambda$  is an eigenvalue of  $\boldsymbol{B}$ . The matrix  $\boldsymbol{B}$ , which represents the normalized adjacency matrix, can be written explicitly as:

$$\boldsymbol{B} = \begin{bmatrix} 0 & \frac{a_{12}}{d_{11}} & \dots & & \frac{a_{1n}}{d_{11}} \\ \frac{a_{21}}{d_{22}} & 0 & \frac{a_{23}}{d_{22}} & \dots & \frac{a_{2n}}{d_{22}} \\ \frac{a_{31}}{d_{33}} & \frac{a_{32}}{d_{33}} & \ddots & \ddots & \vdots \\ \vdots & \vdots & \ddots & \ddots & \frac{a_{(n-1)n}}{d_{(n-1)(n-1)}} \\ \frac{a_{n1}}{d_{nn}} & \frac{a_{n2}}{d_{nn}} & \dots & \frac{a_{n(n-1)}}{d_{nn}} & 0 \end{bmatrix}.$$

Here, each off-diagonal entry  $\frac{a_{ij}}{d_{ii}}$  represents the ratio of the edge weight between vertices i and j to the degree of vertex i.

## Applying Gershgorin's theorem

We apply Gershgorin's circle theorem to analyse the eigenvalues of  $\boldsymbol{B}$ . Gershgorin's theorem states that every eigenvalue of a matrix lies within at least one of the Gershgorin discs, centred at each diagonal element of the matrix, with radius equal to the sum of the absolute values of the off-diagonal elements in the corresponding row [13]. For each row i of the matrix  $\boldsymbol{B}$ , the diagonal element is 0 (since the graph is loop-less), and the radius  $R_i$  of the Gershgorin disc is:

$$R_i = \sum_{\substack{j=1 \ j \neq i}}^n \left| \frac{a_{ij}}{d_{ii}} \right| = \frac{1}{d_{ii}} \sum_{j \neq i} a_{ij} = \frac{1}{d_{ii}} \cdot d_{ii} = 1.$$

Thus, each Gershgorin disc is centred at 0 with a radius of 1

#### Proof that the Eigenvalue $\lambda$ is Real

The generalized eigenvalue problem is given as follows:

$$\mathbf{A}\mathbf{x} = \lambda \mathbf{D}\mathbf{x},\tag{2.3.11}$$

 $\boldsymbol{A}$  and  $\boldsymbol{D}$  are both real and symmetric matrices. First, we take the complex conjugate of the eigenvalue equation (2.3.11):

$$ar{A}ar{x} = ar{\lambda}ar{D}ar{x}.$$

Since  $\boldsymbol{A}$  and  $\boldsymbol{D}$  are real matrices, their complex conjugates are equal to themselves:

$$A\bar{x} = \bar{\lambda}D\bar{x}.$$

Next, we transpose the equation to get:

$$\bar{\boldsymbol{x}}^T \boldsymbol{A}^T = \bar{\lambda} \bar{\boldsymbol{x}}^T \boldsymbol{D}^T.$$

Because  $\boldsymbol{A}$  and  $\boldsymbol{D}$  are symmetric ( $\boldsymbol{A} = \boldsymbol{A}^T$  and  $\boldsymbol{D} = \boldsymbol{D}^T$ ), we simplify this expression to:

$$\bar{\boldsymbol{x}}^T \boldsymbol{A} = \bar{\lambda} \bar{\boldsymbol{x}}^T \boldsymbol{D}.$$

Multiply both sides of the equation by x on the right:

$$\bar{\boldsymbol{x}}^T \boldsymbol{A} \boldsymbol{x} = \bar{\lambda} \bar{\boldsymbol{x}}^T \boldsymbol{D} \boldsymbol{x}.$$

We can rearrange this to express  $\bar{\lambda}$  as:

$$ar{\lambda} = rac{ar{m{x}}^T m{A} m{x}}{ar{m{x}}^T m{D} m{x}}.$$

From equation (2.3.11), we multiply both sides by  $\bar{x}^T$ :

$$\bar{\boldsymbol{x}}^T \boldsymbol{A} \boldsymbol{x} = \lambda \bar{\boldsymbol{x}}^T \boldsymbol{D} \boldsymbol{x}.$$

Thus, we express  $\lambda$  as:

$$\lambda = \frac{\bar{\boldsymbol{x}}^T \boldsymbol{A} \boldsymbol{x}}{\bar{\boldsymbol{x}}^T \boldsymbol{D} \boldsymbol{x}}.$$

Since  $\lambda$  and  $\bar{\lambda}$  are both expressed as the same ratio, we conclude:

$$\lambda = \bar{\lambda},$$

meaning that the eigenvalue  $\lambda$  is real:  $\lambda \in \mathbb{R}$ . According to Gershgorin's Circle Theorem, all eigenvalues of any loop-less graph are contained within a disc of radius 1 centred at 0. Since we have proven that the eigenvalue  $\lambda$  is real, it must lie within the interval [-1,1]. Hence  $\lambda \in [-1,1]$ .

# 2.4 Singularity of the modified Laplacian matrix $L^*$ and eigenvalue analysis

In the analysis of diffusion processes in networks, it is essential to determine the values of  $\nu$  for which the matrix  $\mathbf{L}^*$  becomes singular. A matrix is singular if it has at least one zero eigenvalue, which occurs when its determinant is zero. The modified Laplacian matrix  $\mathbf{L}^*$  is defined as:

$$\mathbf{L}^*(\nu) = \mathbf{A} - \cos(\nu)\mathbf{D},\tag{2.4.1}$$

where **A** is the adjacency matrix of the network, and **D** is the degree matrix.

#### 2.4.1 Regular graph

Consider the case of a graph in which all vertices have the same degree. In such a graph, the degree matrix D can be expressed as a scalar multiple of the identity matrix:

$$\mathbf{D} = (N-1)\mathbf{I} \tag{2.4.2}$$

where N is the total number of vertices in the graph. This structure occurs in regular graphs, such as the complete graph or the cyclic graph, where each vertex has a degree N-1. Substituting the form of D (2.4.2) into equation (2.3.7) then equation (2.3.5) yields:

$$\mathbf{A}\mathbf{x} = \gamma\mathbf{x}$$

where  $\gamma = (N-1)\cos(\nu)$ . This simplified equation reveals that  $\gamma$  is an eigenvalue of the adjacency matrix **A**. Consequently, the possible values of  $\nu$  are determined by the spectrum of **A**, that is, the eigenvalues of the adjacency matrix.

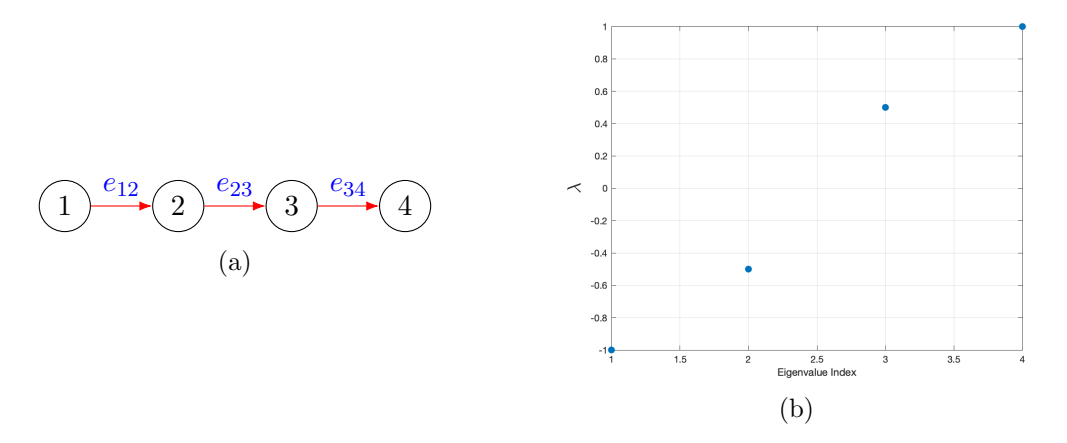


Figure 2.5.1: (a) Path graph with 4 vertices  $P_4$ . (b) The eigenvalues  $\lambda$  of the modified Laplacian matrix  $L^*$  of  $P_4$ .

# 2.5 Numerical results for eigenvalue analysis of the modified Laplacian matrix

In this section, we analyse the spectral properties of various graph topologies using the modified Laplacian matrix  $L^*$  as defined in Equation (2.4.1). The adjacency matrix A is used to describe the connectivity of the graphs in MATLAB, and the degree matrix D is calculated to obtain the eigenvalues for the graphs. The numerical results and visualisations for various graph structures are presented, including all possible graphs with 4 vertices and selected examples with 5 and 6 vertices. These results illustrate how eigenvalue spectra vary between graph topologies.

#### 2.5.1 Graphs with four vertices

- The path graph P<sub>4</sub> is one of the simplest graph structures, where vertices
  are connected sequentially in a straight line. The topology of the path graph
  is shown in Figure 2.5.1(a). The eigenvalues λ of the modified Laplacian
  matrix L\* for this graph are presented in Figure 2.5.1(b).
- The square graph, depicted in Figure 2.5.2(a), is a cycle graph with 4 vertices. The eigenvalues  $\lambda$  of the modified Laplacian matrix  $L^*$  for this

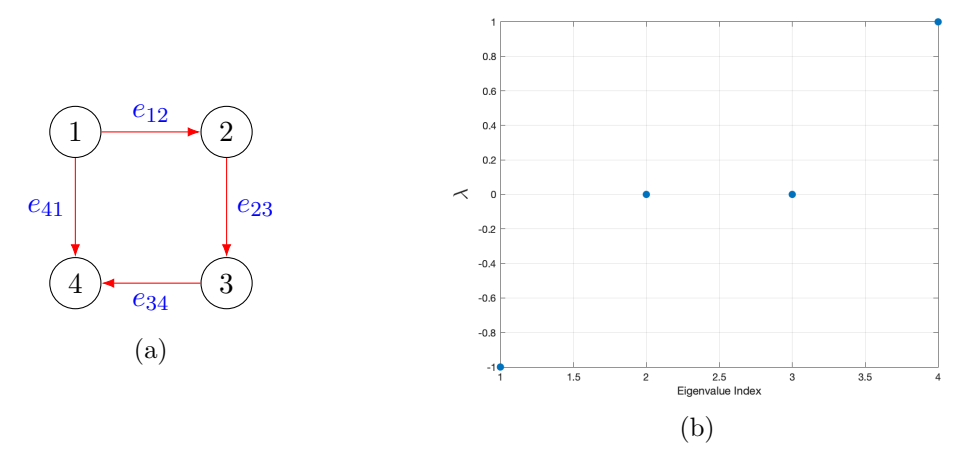


Figure 2.5.2: (a) Square graph with 4 vertices. (b) The eigenvalues  $\lambda$  of the modified Laplacian matrix  $L^*$  of the square graph.

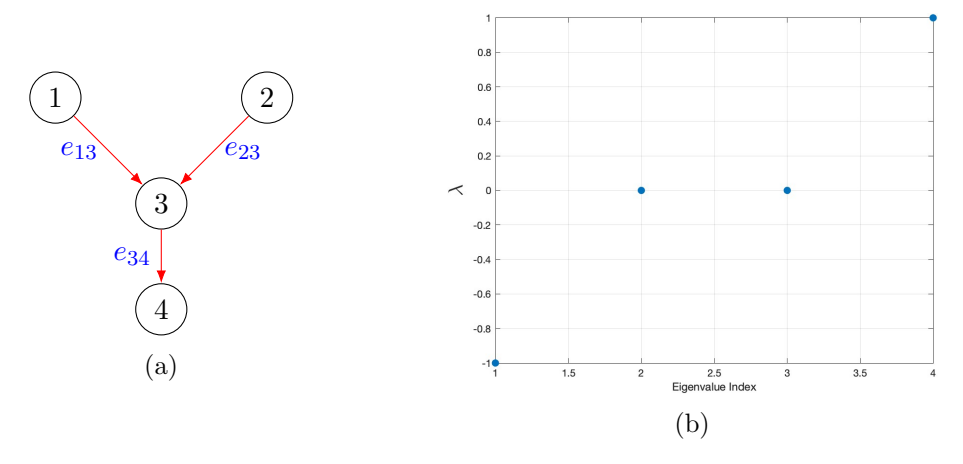


Figure 2.5.3: (a) Y-shaped tree graph with 4 vertices. (b) The eigenvalues  $\lambda$  of the modified Laplacian matrix  $L^*$  of the Y-shaped tree graph.

graph are presented in Figure 2.5.2(b).

- The Y-shaped graph is a type of tree graph where three paths converge at a single vertex. The topology of this graph is shown in Figure 2.5.3(a). The eigenvalues  $\lambda$  of the modified Laplacian matrix  $\boldsymbol{L}^*$  for this graph are presented in Figure 2.5.3(b).
- The complete graph of 4 vertices has a shape of triangular with a middle vertex is a graph where three vertices form a triangle, and the fourth vertex is connected to all three. The topology of this graph is shown in Figure 2.5.4(a). The eigenvalues λ of the modified Laplacian matrix L\* for this graph are presented in Figure 2.5.4(b).

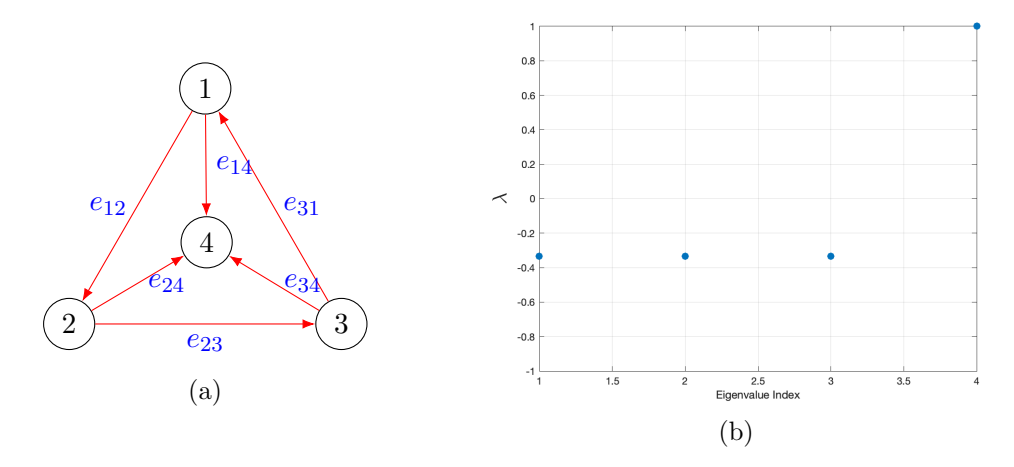


Figure 2.5.4: (a) Triangular graph with 4 vertices and a middle vertex. (b) The eigenvalues  $\lambda$  of the modified Laplacian matrix  $L^*$  of the graph.

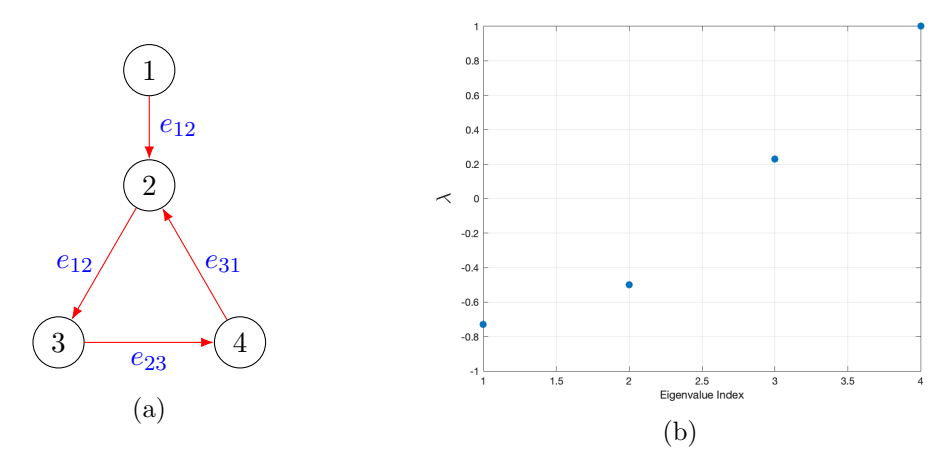


Figure 2.5.5: (a) Triangular graph with one edge added. (b) The eigenvalues  $\lambda$  of the modified Laplacian matrix  $L^*$  of the graph.

- The graph consists of a triangle with an additional edge connecting one of the triangle's vertices to an external vertex. The topology of the graph is shown in Figure 2.5.5(a). The eigenvalues  $\lambda$  of the modified Laplacian matrix  $L^*$  are shown in Figure 2.5.5(b).
- Two connected triangles is a graph consisting of two triangles connected by a shared edge. The topology of the graph is shown in Figure 2.5.6(a). The eigenvalues  $\lambda$  of the modified Laplacian matrix  $L^*$  are shown in Figure 2.5.6(b).

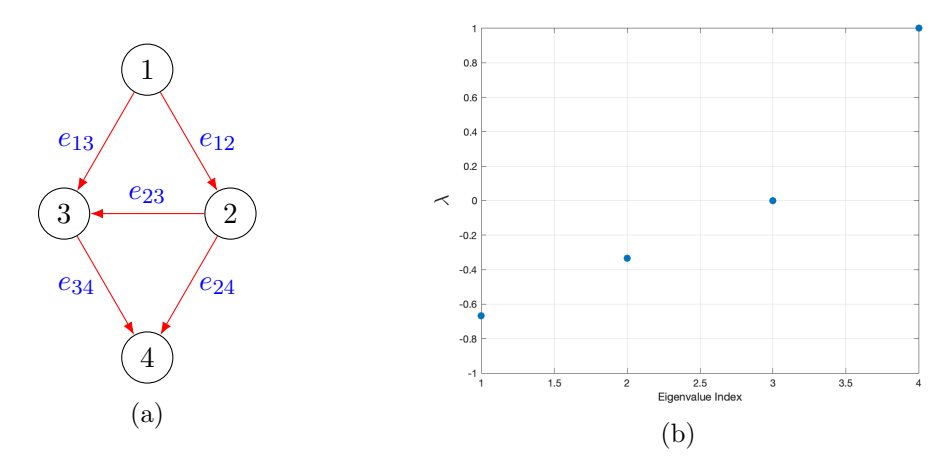


Figure 2.5.6: (a) Two connected triangles. (b) The eigenvalue  $\lambda$  of the modified Laplacian matrix  $L^*$  of the graph.

#### 2.5.2 Graphs with four vertices decay rate analysis

The smallest decay rate  $\nu_{\min}$  for various graphs containing four vertices is presented in Table 2.1. The table illustrates how the shape of the graph influences the rate of decay of the substance. The graphs are ordered by increasing decay rate.

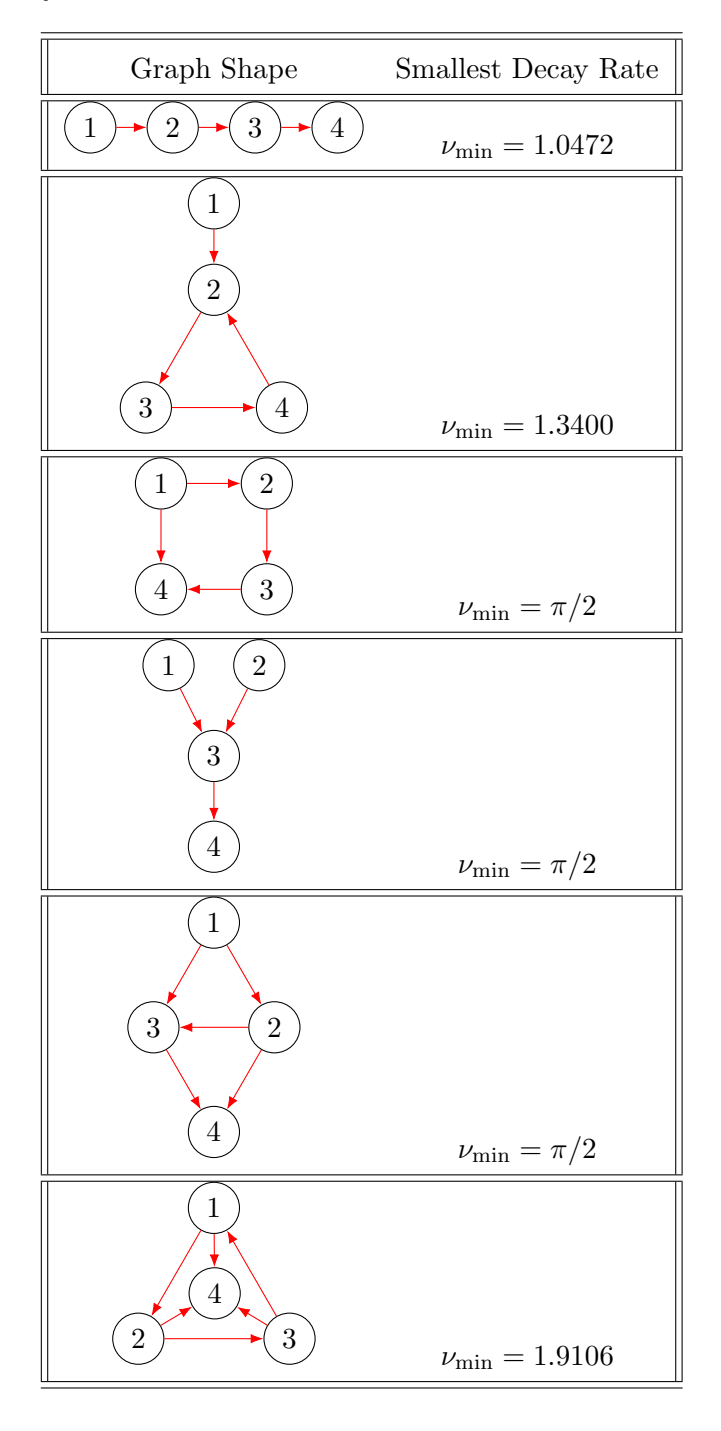
#### 2.5.3 Graphs with six vertices

- The tree graph (see Figure 2.5.7(a)) where every two vertices are connected by exactly one path. The eigenvalues of the modified Laplacian matrix for that graph are presented in Figure (2.5.7) (b).
- The triangular grid graph consists of vertices arranged in a triangular lattice. Its topology is shown in Figure 2.5.8(a). The eigenvalues  $\lambda$  of the modified Laplacian matrix  $L^*$  are presented in Figure 2.5.8(b).

#### 2.5.4 Normalized Laplacian

There exists a relationship between the modified Laplacian matrix  $L^*$  and the normalized Laplacian matrix denoted as  $\mathcal{L}$ , which we aim to establish. The

Table 2.1: Minimum decay rate  $\nu_{\min}$  for graphs with four vertices, ordered by increasing decay rate



normalized Laplacian matrix  $\mathcal{L}$  is defined as follows:

$$\mathcal{L} = D^{-\frac{1}{2}} L D^{-\frac{1}{2}} = I - D^{-\frac{1}{2}} A D^{-\frac{1}{2}}, \tag{2.5.1}$$

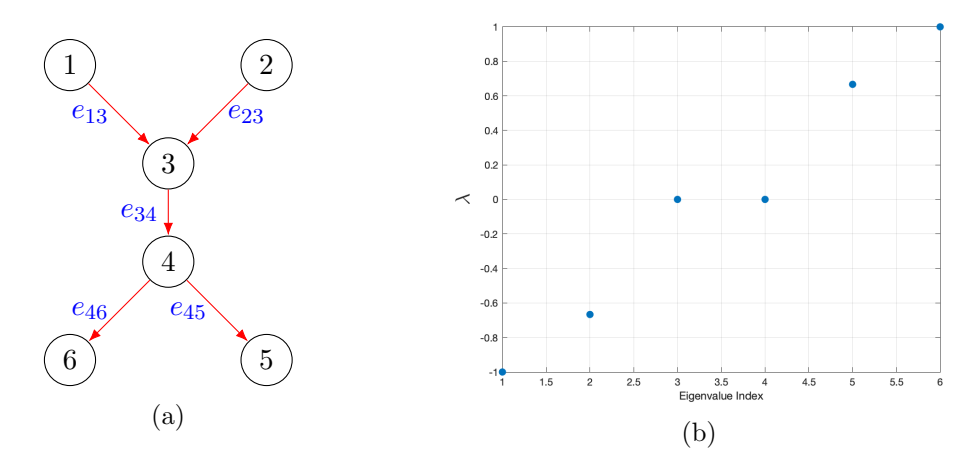


Figure 2.5.7: (a) Tree graph with 6 vertices and 5 edges. (b) The eigenvalue  $\lambda$  of the modified Laplacian matrix  $L^*$  of that tree graph.

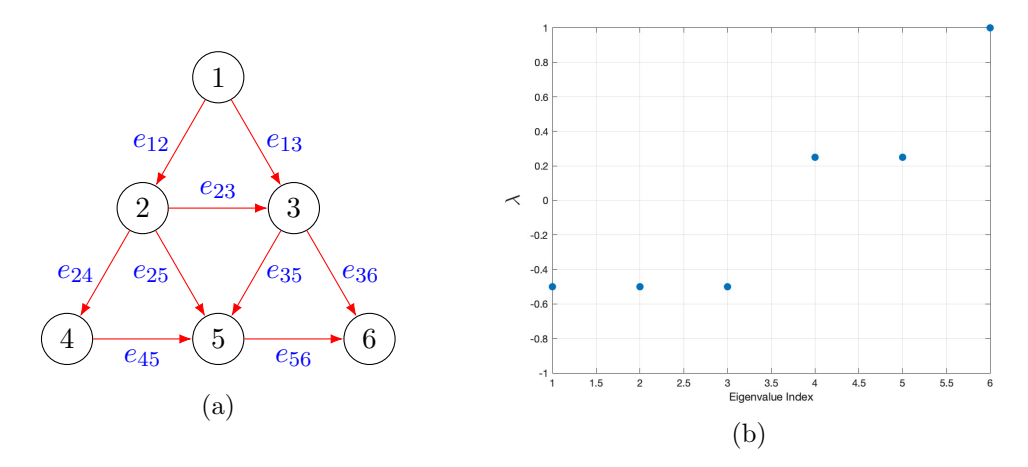


Figure 2.5.8: (a) Triangular grid graph with 6 vertices. (b) The eigenvalues  $\lambda$  of the modified Laplacian matrix  $L^*$  of the triangular grid graph.

where L = D - A is the combinatorial Laplacian [22], D is the degree matrix, A is the adjacency matrix of the graph and  $D^{-\frac{1}{2}}$  is a diagonal square matrix defined as:

$$D^{-\frac{1}{2}} = \begin{bmatrix} \frac{1}{\sqrt{d_1}} & 0 & 0 & 0 & \dots & 0\\ 0 & \frac{1}{\sqrt{d_2}} & 0 & 0 & \dots & 0\\ 0 & 0 & \frac{1}{\sqrt{d_3}} & 0 & \dots & 0\\ 0 & 0 & 0 & \frac{1}{\sqrt{d_4}} & \dots & 0\\ \vdots & \vdots & \vdots & \vdots & \ddots & \vdots\\ 0 & 0 & 0 & 0 & \dots & \frac{1}{\sqrt{d_n}} \end{bmatrix}$$

We refer to the generalized eigenvalue for the normalized Laplacian as  $\tau$ . It satisfies

$$\mathcal{L}\boldsymbol{x} = \tau \boldsymbol{D}\boldsymbol{x}.\tag{2.5.2}$$

Consider the generalized eigenvalue problem given as:

$$Ay = \lambda Dy, \tag{2.5.3}$$

where  $\lambda$  is the eigenvalue corresponding to the eigenvector  $\mathbf{y}$ . To transform this equation into a form involving the normalized Laplacian, we multiply both sides of equation (2.5.3) by  $\mathbf{D}^{-\frac{1}{2}}$ :

$$\boldsymbol{D}^{-\frac{1}{2}}\boldsymbol{A}\boldsymbol{y} = \lambda \boldsymbol{D}^{\frac{1}{2}}\boldsymbol{y}. \tag{2.5.4}$$

Now, assume that  $y = D^{-\frac{1}{2}}x$ , where x is an eigenvector of the normalized Laplacian. Substituting this into the above equation, we obtain:

$$D^{-\frac{1}{2}}AD^{-\frac{1}{2}}x = \lambda x. \tag{2.5.5}$$

From the eigenvalue equation of the normalized Laplacian  $\mathcal{L}x = \tau x$ , and substituting the definition of  $\mathcal{L}$  we get:

$$(I - D^{-\frac{1}{2}}AD^{-\frac{1}{2}})x = \tau x.$$
 (2.5.6)

Expanding the left-hand side to get

$$Ix - D^{-\frac{1}{2}}AD^{-\frac{1}{2}}x = \tau x.$$
 (2.5.7)

Simplifying, and using (2.5.5),

$$x - \lambda x = \tau x. \tag{2.5.8}$$

We see that the eigenvalues  $\lambda$  of the adjacency matrix and the eigenvalues  $\tau$  of the normalized Laplacian are related by:

$$\lambda = 1 - \tau. \tag{2.5.9}$$

This relationship shows that the spectrum of the normalized Laplacian can be used to infer the eigenvalues of our problem, that is the set of values  $\lambda$  which makes the modified Laplacian  $L^*$  singular. In the next section we will exploit this relationship to determine the relevant eigenvalues  $\lambda$  for diffusion on a grid graph.

# 2.6 Square grid graph

In this section we discuss diffusion over a grid network. In principle to do this we must seek  $\lambda$  such that  $L^*$  is singular and in general this is a numerical task. However, at the end of the previous section we established a connection between  $\lambda$  and the eigenvalues of the normalized Laplacian. We shall now use this to calculate  $\lambda$  for a grid graph. In particular we may appeal to recent work by Klopotek [30] which provides an analytical treatment of the problem of calculating the eigenvalues of the normalized Laplacian on a grid graph. Leveraging Klopotek's work, we aim to investigate diffusion processes on grid graphs to construct a model that can reflect laboratory observations of diffusion processes occurring in biological systems, such as a plant leaf exposed to a localized stimulus, like a needle prick [4].

#### 2.6.1 Klopotek's results for a square grid graph

In this section, we apply results from Klopotek [30] to our diffusion problem on grid graphs. Klopotek's work provides analytical formulas for computing eigenvalues and eigenvectors of normalised Laplacian on multidimensional grid graphs. While Klopotek focused on the general spectral properties of grid graphs

for clustering applications, our work extends his results specifically to analyse diffusion processes and compute the dominant decay rates for biological modelling applications. We leverage his eigenvalue formulas but develop new approaches for solving the resulting larger systems and analysing asymptotic behaviour.

we will discuss the eigenvalues for a square grid graph with  $n \times n = n^2$  vertices. An example of a  $4 \times 4$  grid graph with n = 4 vertices is shown in Figure 2.6.3. Klopotek's [30] work provides essential formulas for determining the eigenvalues of grid graphs. In particular, the normalized Laplacian eigenvalue  $\tau$  is given by

$$\tau = 1 + \frac{1}{2}(\cos \xi_1 + \cos \xi_2), \tag{2.6.1}$$

$$\tau = 1 + \cos \xi_1 + \tan(\delta_1) \sin \xi_1, \tag{2.6.2}$$

and

$$\tau = 1 + \cos \xi_2 + \tan(\delta_2) \sin \xi_2. \tag{2.6.3}$$

where

$$\xi_j = \frac{2}{n-1} \left( \frac{z_j \pi}{2} - \delta_j \right), \tag{2.6.4}$$

for j = 1, 2. Here the  $z_j$  (j = 1, 2) are numbers to be chosen from the set  $\{0, 1, 2, ...., n - 1\}$ , whereas, as mentioned above, n is the number of vertices. While Klopotek provided these fundamental equations, he did not develop systematic methods for solving them numerically or analyse their asymptotic behaviour for large networks. Our contribution lies in:

- Developing robust numerical solution strategies using phase plots and Newton's method.
- Systematically analysing all possible  $(z_1, z_2)$  combinations.
- Extending the analysis to understand diffusion dynamics.

The  $\delta_j$  are shift terms to be found along with the  $\xi_j$ . Having selected a pair  $(z_1, z_2)$ , we substitute (2.6.4) into (2.6.1)-(2.6.3) to eliminate the  $\xi_j$ . We are then

left with three non-linear algebraic equations to be solved for the three unknowns  $\tau$ ,  $\delta_1$ , and  $\delta_2$ .

Prior to doing this, however, it is convenient to first eliminate  $\tau$ . To this end we multiply (2.6.1) by 2 to obtain

$$2\tau = 2 + \cos \xi_1 + \cos \xi_2. \tag{2.6.5}$$

Adding (2.6.2) to (2.6.3) gives:

$$2\tau = 2 + \cos \xi_1 + \tan(\delta_1)\sin \xi_1 + \cos \xi_2 + \tan(\delta_2)\sin \xi_2. \tag{2.6.6}$$

By subtracting (2.6.5) from (2.6.6), we obtain:

$$\tan \delta_1 \sin \xi_1 + \tan \delta_2 \sin \xi_2 = 0,$$

which can be expressed as

$$-\tan \delta_1 \sin \xi_1 = \tan \delta_2 \sin \xi_2 \tag{2.6.7}$$

Next we rewrite (2.6.2) and (2.6.3), by using equation (2.6.7), resulting in:

$$\tau - 1 = \cos \xi_1 + \tan(\delta_1) \sin \xi_1, \tag{2.6.8}$$

and

$$\tau - 1 = \cos \xi_2 - \tan(\delta_1) \sin \xi_1. \tag{2.6.9}$$

By subtracting these two equations and utilizing the result from (2.6.7), we find that

$$\cos \xi_2 = \cos \xi_1 + 2 \tan \delta_1 \sin \xi_1. \tag{2.6.10}$$

Finally we eliminate the  $\xi_j$  using (2.6.4), in which case (2.6.7) and (2.6.10) become

$$\tan \delta_1 \sin \left( \frac{2}{n-1} \left[ \frac{z_1 \pi}{2} - \delta_1 \right] \right) + \tan \delta_2 \sin \left( \frac{2}{n-1} \left[ \frac{z_2 \pi}{2} - \delta_2 \right] \right) = 0, \quad (2.6.11)$$

$$\cos \left( \frac{2}{n-1} \left[ \frac{z_2 \pi}{2} - \delta_2 \right] \right) = \cos \left( \frac{2}{n-1} \left[ \frac{z_1 \pi}{2} - \delta_1 \right] \right)$$

$$+ 2 \tan \delta_1 \sin \left( \frac{2}{n-1} \left[ \frac{z_1 \pi}{2} - \delta_1 \right] \right).$$

The goal now for a given grid size  $n \times n$  is to solve (2.6.11) and (2.6.12) numerically, for a chosen pair  $(z_1, z_2)$ , in order to determine  $\delta_1$  and  $\delta_2$  and thus  $\xi_1, \xi_2$ . Then we use (2.6.1) to compute the eigenvalue  $\tau$ . The following analysis of the solution space and numerical methods represents our extension of Klopotek's theoretical framework to practical computation of eigenvalues for diffusion modelling.

#### General case for $z_1$ and $z_2$

It is important to note that the equations (2.6.11) and (2.6.12) are invariant under the transformations:

$$(z_1, z_2) \mapsto (z_2, z_1), \qquad (\delta_1, \delta_2) \mapsto (\delta_2, \delta_1).$$

This symmetry implies that we may restrict our calculations to the case  $z_1 \geq z_2$  without loss of generality. However, allowing all possible values of  $z_1$  and  $z_2$  makes it easier to observe the multiplicities of eigenvalues.

If  $z_1 = z_2$ , the permutation  $(\delta_1, \delta_2) \mapsto (\delta_2, \delta_1)$  is valid. Hence, we expect that if  $z_1 = z_2$ , both  $(\delta_1, \delta_2)$  and  $(\delta_2, \delta_1)$  will yield solutions.

Note that (2.6.11) and (2.6.12) are also invariant under the transformations

$$z_i \mapsto z_i + 2m, \quad \delta_i \mapsto \delta_i + m\pi,$$
 (2.6.13)

where  $m \in \mathbb{Z}$ . This suggests that we can restrict the values of  $z_i$  to  $z_i \in \{0,1\}$ .

Thus, the pairs  $(z_1, z_2)$  can be chosen from the set:

$$S = \{(0,0), (1,0), (1,1)\}. \tag{2.6.14}$$

The equations (2.6.11) and (2.6.12) are also invariant under the transformation:

$$\delta_i \mapsto \delta_i + \frac{2\pi}{2/(n-1)}$$
 i.e.  $\delta_i \mapsto \delta_i + (1-n)\pi$ 

We can limit our search for the values of  $\delta_1$  and  $\delta_2$  to the interval:

$$D = [0, (n-1)\pi) \tag{2.6.15}$$

We will solve (2.6.11) and (2.6.12) numerically using Newton iterations and a suitable initial guess. The initial guess can be selected by analysing the phase behaviour of the complex function:

$$w(z) = (\tan \delta_1 \sin \xi_1 + \tan \delta_2 \sin \xi_2) + i(-\cos \xi_2 + \cos \xi_1 + 2\tan \delta_1 \sin \xi_1), (2.6.16)$$

where  $z = \delta_1 + i\delta_2$ , and the relationship (2.6.4) is used to eliminate the  $\xi_j$  in favour of the  $\delta_j$  as before. The function w(z) vanishes when both (2.6.11) and (2.6.12) are satisfied. To visualize where w(z) = 0, it is useful to plot its phase  $\phi$ , defined as:

$$\phi = \arg(w)/\pi$$

where  $\phi \in [-1, 1]$ . This plot helps identify the correct starting values  $\delta_1, \delta_2$  for solving the system. An example is shown in figure (2.6.1). The red dot indicates the point where we expect to find w = 0 and therefore gives a guide as to an appropriate initial guess for  $\delta_1, \delta_2$ .

In summary the task of solving (2.6.11) and (2.6.12) is fulfilled by selecting pairs  $(z_1, z_2)$  from the set S defined in (2.6.14) and then solving for  $\delta_1$ ,  $\delta_2$  numerically using Newton's method. Having done this we reconstruct the possible eigenvalues

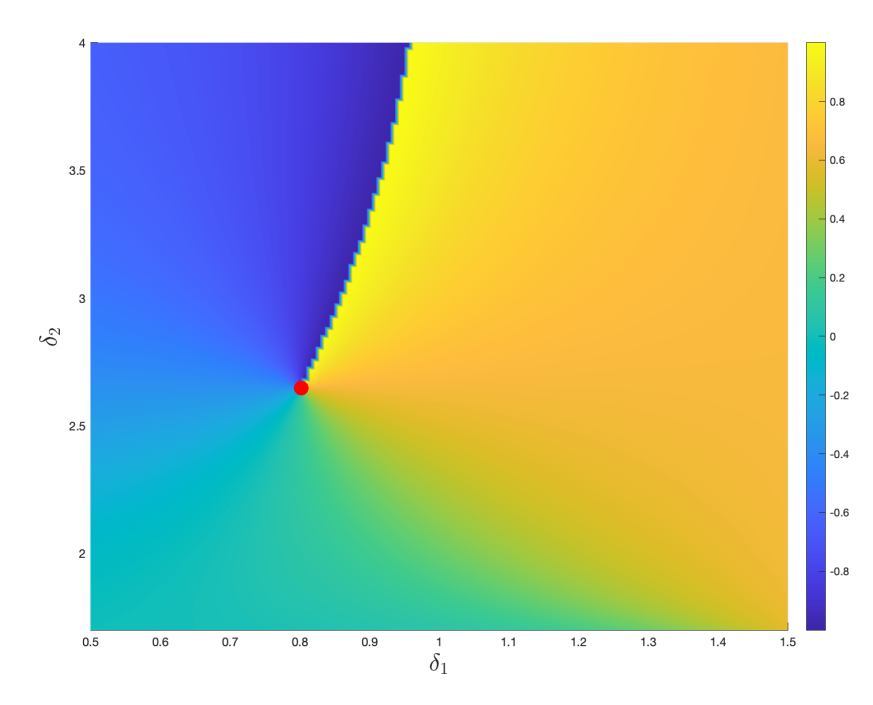


Figure 2.6.1: The initial guesses for the parameters  $\delta_1$  and  $\delta_2$ , with a red dot indicating the point where the solution w = 0 is expected

 $\tau$  using the formula (2.6.1), namely

$$\tau = 1 + \frac{1}{2}\cos\left(\frac{2}{n-1}\left[\frac{z_1\pi}{2} - \delta_1\right]\right) + \frac{1}{2}\cos\left(\frac{2}{n-1}\left[\frac{z_2\pi}{2} - \delta_2\right]\right). \tag{2.6.17}$$

**case I:**  $z_1 = z_2$ 

In the case when  $z_1 = z_2 = z$ , say, equations (2.6.11) and (2.6.12) reduce to

$$\tan \delta_1 \sin \left( \frac{2}{n-1} \left[ \frac{z\pi}{2} - \delta_1 \right] \right) + \tan \delta_2 \sin \left( \frac{2}{n-1} \left[ \frac{z\pi}{2} - \delta_2 \right] \right) = 0, \quad (2.6.18)$$

$$\cos \left( \frac{2}{n-1} \left[ \frac{z\pi}{2} - \delta_2 \right] \right) = \cos \left( \frac{2}{n-1} \left[ \frac{z\pi}{2} - \delta_1 \right] \right)$$

$$+ 2 \tan \delta_1 \sin \left( \frac{2}{n-1} \left[ \frac{z\pi}{2} - \delta_1 \right] \right). \quad (2.6.19)$$

If we assume that  $\delta_1 = \delta_2 = \delta$ , say, these reduce to the single condition that

$$\tan \delta \sin \left( \frac{2}{n-1} \left[ \frac{z\pi}{2} - \delta \right] \right) = 0. \tag{2.6.20}$$

One option is to set  $\tan \delta = 0$  in which case  $\delta = k\pi$ , for integer k. Then (2.6.1) yields with z = 0 or z = 1,

$$\tau(z=0) = 1 + \cos\left(\frac{2k\pi}{n-1}\right), \qquad \tau(z=1) = 1 + \cos\left(\frac{(2k-1)\pi}{n-1}\right).$$

So either way we get the eigenvalue set

$$\tau = 1 + \cos\left(\frac{q\pi}{n-1}\right), \qquad q = 0, 1, 2, \dots, n-1.$$
 (2.6.21)

This furnishes n of the normalised Laplacian's  $n^2$  eigenvalues. So there remains a further n(n-1) eigenvalues to be identified. Alternatively we could take  $z\pi/2 - \delta = m\pi$  so that the sine term in (2.6.20) vanishes. This merely produces a subset of the values already accounted for in (2.6.21). By way of example, consider the square grid with n = 2. Then (2.6.21) yields

$$au = 2 \quad (q = 0); \qquad \frac{3}{2} \quad (q = 1); \qquad \frac{1}{2} \quad (q = 2); \qquad 0 \quad (q = 3).$$

Let us now consider the case when  $\delta_1 \neq \delta_2$ . Setting z = 0 in (2.6.18), (2.6.19) yields

$$\tan \delta_1 \sin \left(\frac{2\delta_1}{n-1}\right) + \tan \delta_2 \sin \left(\frac{2\delta_2}{n-1}\right) = 0,$$

$$\cos \left(\frac{2\delta_2}{n-1}\right) = \cos \left(\frac{2\delta_1}{n-1}\right) - 2\tan \delta_1 \sin \left(\frac{2\delta_1}{n-1}\right).$$

These must be solved numerically for  $\delta_1$ ,  $\delta_2$ . Instead setting z = 1 in (2.6.18), (2.6.19) yields

$$\tan \delta_1 \sin \left( \frac{2}{n-1} \left[ \frac{\pi}{2} - \delta_1 \right] \right) + \tan \delta_2 \sin \left( \frac{2}{n-1} \left[ \frac{\pi}{2} - \delta_2 \right] \right) = 0, \qquad (2.6.22)$$

$$\cos \left( \frac{2}{n-1} \left[ \frac{\pi}{2} - \delta_2 \right] \right) = \cos \left( \frac{2}{n-1} \left[ \frac{\pi}{2} - \delta_1 \right] \right)$$

$$+ 2 \tan \delta_1 \sin \left( \frac{2}{n-1} \left[ \frac{\pi}{2} - \delta_1 \right] \right). \qquad (2.6.23)$$

These must be solved numerically for  $\delta_1$ ,  $\delta_2$ .

## Case II: $z_1 \neq z_2$

As mentioned above, the values of  $z_1$  and  $z_2$  must be chosen from the set S defined in (2.6.14), namely,

$$S = \{(0,0), (1,0), (1,1)\}$$

Therefore, by definition, we have  $\delta_1 \neq \delta_2$ . For the case  $(z_1, z_2) = (1, 0)$  equations (2.6.11) and (2.6.12) become

$$\tan \delta_1 \sin \left( \frac{2}{n-1} \left[ \frac{\pi}{2} - \delta_1 \right] \right) - \tan \delta_2 \sin \left( \frac{2\delta_2}{n-1} \right) = 0, \tag{2.6.24}$$

$$\cos\left(\frac{2\delta_2}{n-1}\right) = \cos\left(\frac{2}{n-1}\left[\frac{\pi}{2} - \delta_1\right]\right) + 2\tan\delta_1\sin\left(\frac{2}{n-1}\left[\frac{\pi}{2} - \delta_1\right]\right).$$

$$(2.6.25)$$

In general, these equations must be solved numerically to find  $\delta_1$  and  $\delta_2$ .

We might try to seek a solution assuming that  $\delta_1 = \delta_2 = \delta$ , say. In this case (2.6.24) and (2.6.25) require that  $\sin \xi_1 = \sin \xi_2$ . Hence we have two possibilities:

$$(i): \quad \xi_2 = \pi - \xi_1, \qquad (ii): \quad \xi_2 = \xi_1$$

both to within an addition of an integer multiple of  $2\pi$ . Taking the second option first, namely (ii), this requires  $\cos \xi_2 = \cos \xi_1$  and (2.6.24) and (2.6.25) reduce to

$$\tan \delta \sin \xi_1 = 0 \tag{2.6.26}$$

In this case (2.6.26) requires that  $\delta = m\pi$  or  $\xi_1 = m\pi$  for integer m. The latter implies  $\delta = (1 - 4m)\pi/2$  so that  $\tan \delta = \infty$ , so we disregard this possibility. The former cannot be satisfied as it implies  $\xi_1 \neq \xi_2$ .

Inserting the definitions of  $\xi_1$  and  $\xi_2$  into option (i), we require that

$$\frac{2\delta}{n-1} = \pi - \frac{2}{n-1} \left[ \frac{\pi}{2} - \delta \right],$$

which rearranges to

$$\pi\left(1 - \frac{1}{n-1}\right) = 0,$$

which is only possible if n=2. So this case only works for a  $2 \times 2$  grid graph. Assuming n=2 then, we have  $\cos \xi_2 = -\cos \xi_1$  and (2.6.24) and (2.6.25) reduce to

$$1 = \tan \delta \tan 2\delta$$
.

Using the double angle formula for tan this simplifies to

$$\tan \delta = \frac{1}{\sqrt{3}}.\tag{2.6.27}$$

Hence  $\delta = \tan^{-1}(1/\sqrt{3}) \approx 0.524$ . Then by (2.6.17) we have since  $\cos \xi_2 = -\cos \xi_1$ 

$$\tau = 1$$
.

To analyse the eigenvalue of  $\tau = 1$ , we consider the case  $(z_1, z_2) = (1, 0)$ , where the parameters  $\xi_1$  and  $\xi_2$  are defined as follows:

$$\xi_1 = \frac{2}{n-1} \left( \frac{\pi}{2} - \delta_1 \right), \quad \xi_2 = \frac{2}{n-1} (-\delta_2).$$

By choosing  $\xi_2$  in terms of  $\xi_1$  such that  $\xi_1 + \xi_2 = -\pi$ , we obtain the relation:

$$\pi + \xi_1 = -\xi_2$$
.

Given this choice, the eigenvalue  $\tau$  of the normalized Laplacian, represented by equation (2.6.1), can be expressed by substituting the value of  $\xi_2$  as:

$$\tau = 1 + \frac{1}{2}(\cos \xi_1 + \cos(\pi + \xi_1)).$$

Since  $\cos(\pi + \xi_1) = -\cos \xi_1$ , the expression simplifies to:

$$\tau = 1 + \frac{1}{2}(\cos \xi_1 - \cos \xi_1) = 1. \tag{2.6.28}$$

Thus, the eigenvalue  $\tau = 1$  is inherently satisfied when  $\xi_1 + \xi_2 = -\pi$ .

The Normalized Laplacian  $\tau$  which is equation (2.6.2) is:

$$\tau = 1 + [\cos \xi_1 + \tan(\delta_1) \sin \xi_1]. \tag{2.6.29}$$

Using the relation  $\cos \xi_2 = -\cos \xi_1$ , into equation (2.6.3), we have:

$$\tau = 1 + [-\cos \xi_1 + \tan(\delta_2)\sin \xi_2]. \tag{2.6.30}$$

Thus, under the condition  $\pi + \xi_1 = -\xi_2$ , we find

$$\sin \xi_2 = \sin(\pi + \xi_1) = -\sin \xi_1, \tag{2.6.31}$$

which leads to

$$\tau = 1 - [\cos \xi_1 - \tan(\delta_2) \sin \xi_1]. \tag{2.6.32}$$

By equating (2.6.29) and (2.6.32), the following relation holds:

$$\tan \delta_1 = -\tan \delta_2. \tag{2.6.33}$$

Substituting the condition  $\pi + \xi_1 = -\xi_2$  into the definition of  $\xi_1$  and  $\xi_2$ , we obtain:

$$\pi + \frac{2}{n-1} \left( \frac{\pi}{2} - \delta_1 \right) = \frac{2\delta_2}{n-1}.$$

Rearranging, this leads to:

$$\frac{2}{n-1}(\delta_1 + \delta_2) = \pi + \frac{\pi}{n-1} = \frac{\pi}{n-1}(n-1+1) = \frac{n\pi}{n-1},$$

simplifying further gives:

$$\delta_1 + \delta_2 = \frac{n\pi}{2} \quad \Rightarrow \quad \delta_1 = \frac{n\pi}{2} - \delta_2.$$

From equation (2.6.33), we can rewrite (2.6.11) as:

$$\tan \delta_1 \sin \xi_1 - \tan \delta_1 \sin \xi_2 = 0.$$

And from equation (2.6.12), we have:

$$\cos \xi_2 = \cos \xi_1 + 2 \tan \delta_1 \sin \xi_1.$$

Using relation where  $\pi + \xi_1 = -\xi_2$ , we have:

$$\cos(\pi + \xi_1) = \cos \xi_1 + 2 \tan \delta_1 \sin \xi_1.$$

Leads to

$$-\cos\xi_1 = \cos\xi_1 + 2\tan\delta_1\sin\xi_1.$$

Rearranging, we have

$$0 = 2\cos\xi_1 + 2\tan\delta_1\sin\xi_1.$$

This leads to:

$$\tan \delta_1 = -\cot \xi_1,$$

where

$$\tan \delta_1 = -\cot \left(\frac{2}{n-1} \left(\frac{\pi}{2} - \delta_1\right)\right).$$

Defining  $A = \frac{\pi}{n-1}$  and  $B = \frac{2}{n-1}\delta_1$ , and using the trigonometric identity:

$$\tan(A+B) = \frac{\tan A + \tan B}{1 - \tan A \tan B}.$$

In summary, to satisfy  $\tau = 1$ , the conditions  $\xi_1 + \xi_2 = -\pi$  and  $\delta_1 + \delta_2 = \frac{n\pi}{2}$  must

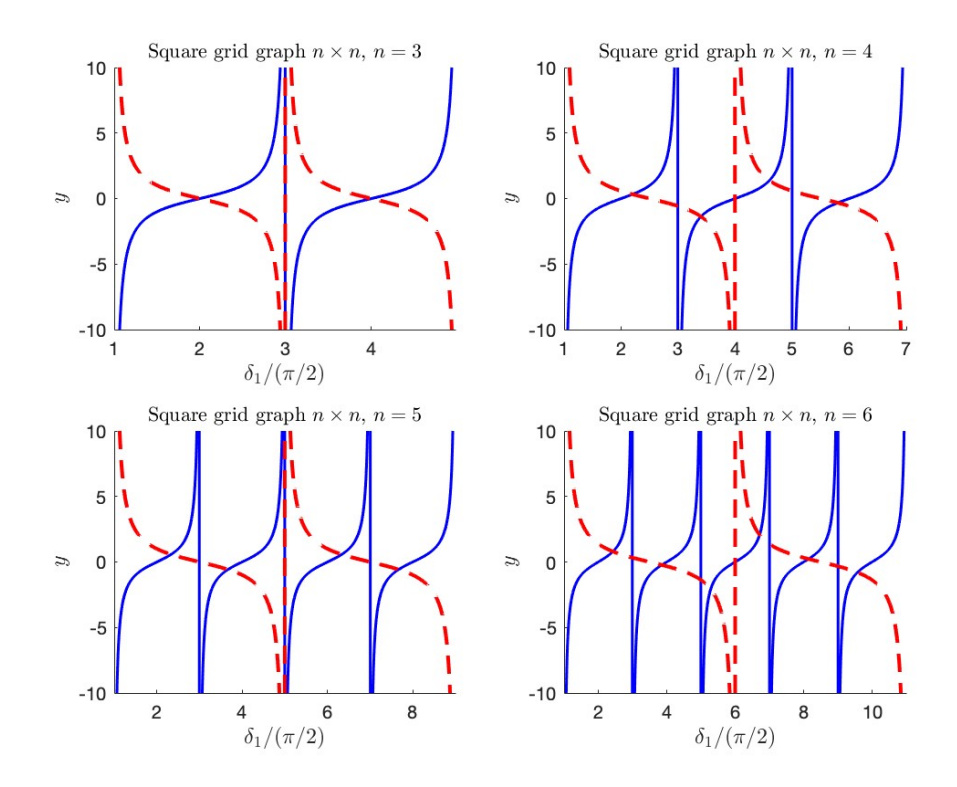


Figure 2.6.2: Graphical solution for  $\tau = 1$  in a square grid graph  $4 \times 4$  to  $6 \times 6$ . The intersections of  $\tan(\delta_1)$  (blue solid line) and  $-\cot\left(\frac{\pi}{n-1} - \frac{2\delta_1}{n-1}\right)$  (red dashed line) represent the roots of the system. which is shows the multiplicity of the eigenvalue of  $\tau = 1$  on each graph

hold. This implies:

$$\tan \delta_1 = -\tan \delta_2,\tag{2.6.34}$$

and

$$\tan \delta_1 = -\cot \xi_1 = -\cot \left(\frac{\pi}{n-1} - \frac{2\delta_1}{n-1}\right).$$
(2.6.35)

Here,  $\tan \delta_1$  is periodic with  $\pi$ , while  $-\cot\left(\frac{\pi}{n-1} - \frac{2\delta_1}{n-1}\right)$  has a period of  $\frac{(n-1)\pi}{2}$ .

The graphical solution for  $\tau = 1$  is illustrated in Figure (2.6.2), which depicts the intersections of the functions  $\tan(\delta_1)$  and  $-\cot\left(\frac{\pi}{n-1} - \frac{2\delta_1}{n-1}\right)$  for square grid graphs with dimensions ranging from  $4 \times 4$  to  $6 \times 6$ . The intersections represent the roots of the system, corresponding to the multiplicity of the eigenvalue  $\tau = 1$  in each graph.

The x-axis represents the normalized parameter  $\delta_1/(\pi/2)$ , while the y-axis

shows the values of the functions  $\tan(\delta_1)$  (solid blue line) and  $-\cot\left(\frac{\pi}{n-1} - \frac{2\delta_1}{n-1}\right)$  (dashed red line). The intersections indicate the values of  $\delta_1$  that satisfy both equations simultaneously.

For square grid graphs with an even number of vertices per side, the number of intersections aligns with the number of vertices per side. In contrast, for grids with an odd number of vertices, the intersections are fewer by one, with the final point of intersection occurring asymptotically where the asymptotes of both functions coincide.

Klopotek's formulas for determining the eigenvalues of grid graphs. In particular, the normalized Laplacian eigenvalue  $\tau$  is given by

$$\tau = 1 + \frac{1}{2}(\cos \xi_1 + \cos \xi_2) \tag{2.6.36}$$

To make  $\tau = 1$  choose either

Case A: 
$$\xi_1 + \xi_2 = -\pi$$
, (2.6.37)

or

Case B: 
$$\xi_1 - \xi_2 = \pi$$
. (2.6.38)

For the case where  $(z_1, z_2) = (1, 0)$ , where the parameters  $\xi_1$  and  $\xi_2$  are defined as follows:

$$\xi_1 = \frac{2}{n-1} \left( \frac{\pi}{2} - \delta_1 \right), \quad \xi_2 = \frac{2}{n-1} (-\delta_2).$$

Then, for case A we can write  $\delta_1$  to be

$$\delta_1 = \frac{n\pi}{2} - \delta_2$$

and for case B we can write  $\delta_2 - \delta_1$  to be

$$\delta_2 - \delta_1 = \frac{n\pi}{2} - \pi$$

Note that from case A we have:

$$\tan \delta_2 = \tan \left(\frac{n\pi}{2} - \delta_1\right) = -\tan \left(\delta_1 - \frac{n\pi}{2}\right).$$

From case B we have:

$$\tan \delta_2 = \tan \left(\frac{n\pi}{2} - \pi + \delta_1\right) = \tan \left(\delta_1 + \frac{n\pi}{2}\right).$$

Now we want to study the case where the number of vertices along one side of the square grid graph are even.

Case I: n is even; n = 2k,  $k \in \mathbb{Z}$ 

For case A we have

$$\tan \delta_2 = -\tan(\delta_1 - k\pi) = -\tan \delta_1$$

For Klopotek's equation we must solve

$$\tan \delta_1 = -\tan \delta_2$$
  $\tan \delta_1 = -\cot \xi_1 = -\cot \left(\frac{\pi}{n-1} - \frac{2\delta_1}{n-1}\right)$ 

NB: Since  $\delta_1, \delta_2$  periodic with period  $(n-1)\pi$  is the fact that  $\delta_1 + \delta_2 = \frac{n\pi}{2} + m(n-1)\pi$ , some integer m. For case B we have

$$\tan \delta_2 = \tan \left(\frac{n\pi}{2} + \delta_1\right) = \tan \delta_1$$

since n is even From equation (2.6.11)

$$\tan \delta_1 \sin \xi_1 + \tan \delta_2 \sin \xi_2 = 0,$$

and from (2.6.12)

$$\cos \xi_2 = \cos \xi_1 + 2 \tan \delta_1 \sin \xi_1$$

Then from case B we know  $\sin(\xi_1) = \sin(-\pi - \xi_2)$ , then we can say

$$\sin \xi_1 = -\sin \xi_2$$

we know from B that

$$\cos(\xi_1 - \pi) = \cos \xi_1 + 2 \tan \delta_1 \sin \xi_1.$$

Leads to

$$-\cos\xi_1 = \cos\xi_1 + 2\tan\delta_1\sin\xi_1.$$

Rearranging, we have

$$0 = 2\cos\xi_1 + 2\tan\delta_1\sin\xi_1.$$

This leads to:

$$\tan \delta_1 = -\cot \xi_1$$

i.e. is the same as A.

IN summary, for n even, solve  $\tan \delta_1 = -\cot \xi_1$  for  $\delta_1$  and then constrict  $\delta_2$  either from

$$\delta_1 + \delta_2 = \frac{n\pi}{2} + m(n-1)\pi$$

or

$$\delta_2 - \delta_1 = \frac{n\pi}{2} + m(n-1)\pi$$

e.g. for n=4:

$$\delta_1 + \delta_2 = 2\pi + m(n-1)\pi$$

$$\delta_2 - \delta_1 = \pi + m(n-1)\pi$$

### 2.6.2 Eigenvalues of a square grid graph

In this section, we use MATLAB to compute the eigenvalues, denoted as  $\lambda$ , of the modified Laplacian for square grid graphs with sizes of 9, 16, 25, and 36 vertices.

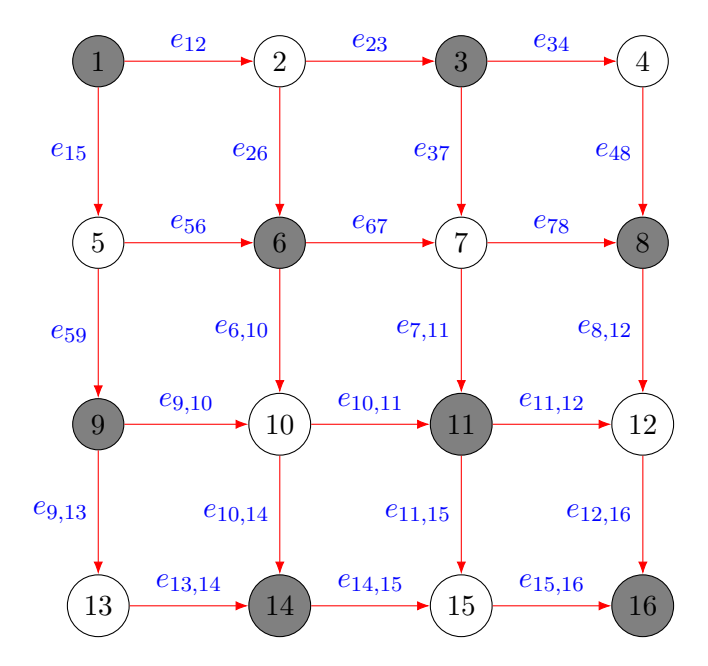


Figure 2.6.3: A  $4 \times 4$  square grid graph with 16 vertices.

For the 16-vertex grid, we further calculate the eigenvalues of the normalized Laplacian, denoted as  $\tau$ , using results from Section(2.5.4). Additionally, we apply Klopotek's main equation from Section(2.6.1) by selecting values for  $z_1$  and  $z_2$  and solving for  $\delta_1$  and  $\delta_2$  to validate these eigenvalues.

The square grid graph with 16 vertices is shown in Figure (2.6.3). To understand its eigenvalues, we first establish that it is bipartite. According to bipartite graph theory, the vertex set V can be divided into two disjoint sets such that no edges connect vertices within the same set; such graphs are also known as 2-colourable [34].

In this square grid graph G, we assign colours based on the parity of the sum of the vertex coordinates (x, y). A vertex (x, y) is coloured gray if (x + y) is even and white if (x + y) is odd. This ensures adjacent vertices always have different colours, confirming that G is bipartite [39].

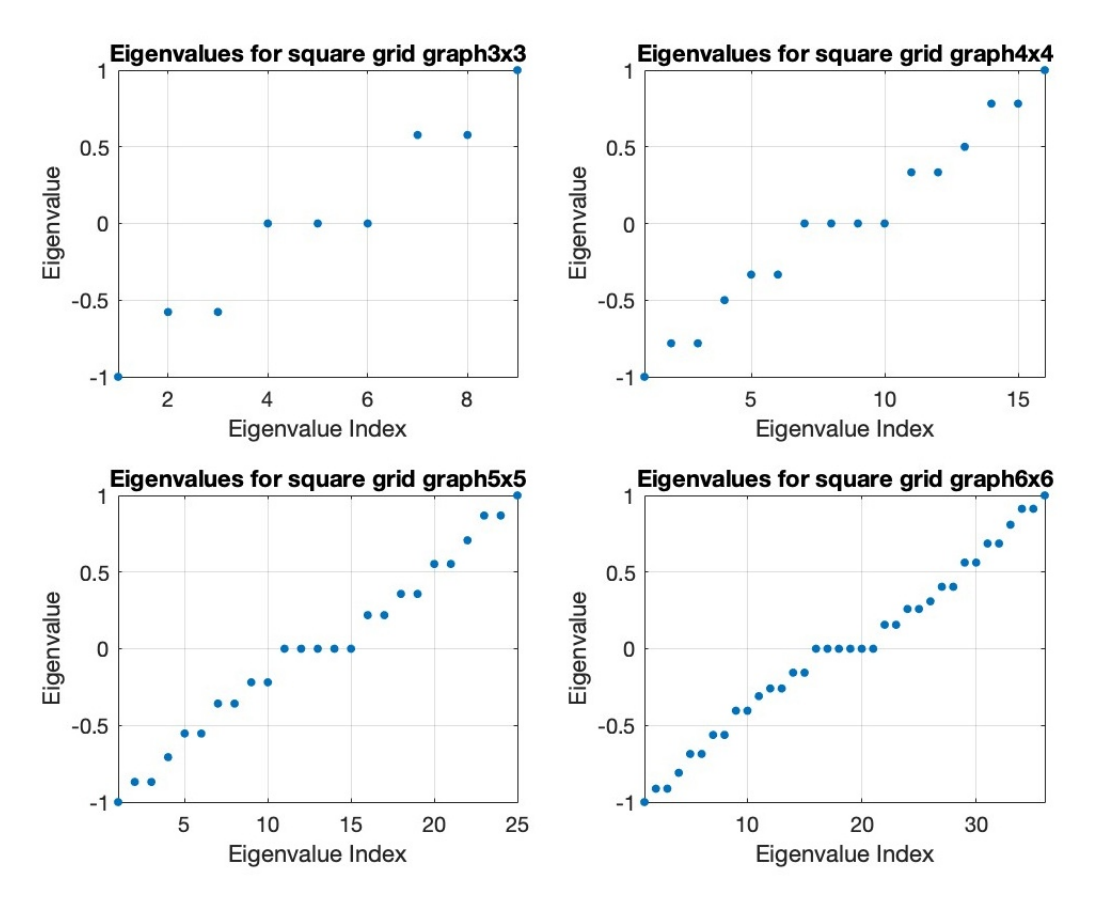


Figure 2.6.4: Eigenvalues of square grid graphs of various sizes vs.  $\lambda \in [-1, 1]$ .

### 2.6.3 Key Observations on a Square Grid Graph

We analysed square grid graphs and performed experiments with both odd and even numbers of vertices along one side of the grid, varying the grid size up to  $100 \times 100$ , resulting in 1000 vertices. Figure (2.6.4) shows some examples. Based on these experiments, we made the following key observations:

- Zero Eigenvalue Multiplicity: The multiplicity of the zero eigenvalue corresponds directly to the grid's side length. For instance, in a 3 × 3 grid, the zero eigenvalue has a multiplicity of 3, while in a 4 × 4 grid, the multiplicity is 4. This pattern is consistent with the results presented in Section 2.6.1.
- Antisymmetry About Zero: The eigenvalues of our eigenvalue problem matrix  $\lambda$  exhibit antisymmetry around zero. This indicates a balanced

spectrum, with an equal distribution of positive and negative eigenvalues.

• **Eigenvalue Range:** The eigenvalues of the graph are bounded within the interval [-1,1], which aligns with the theoretical bounds established in Section 2.3.3. These bounds were anticipated based on our analysis.

Additionally, since a square grid graph is bipartite, we observed that the eigenvalue properties of our eigenvalue problem are similar to those of the graph's adjacency matrix, as noted in [12]. Specifically, bipartite graphs have the property that if  $\lambda$  is an eigenvalue, then  $-\lambda$  is also an eigenvalue with the same multiplicity [12]. This antisymmetry is also evident in the eigenvalue problem (2.3.10), where  $\mathbf{A}\mathbf{x} = \lambda \mathbf{D}\mathbf{x}$ . This behaviour is confirmed by the Matlab computations shown in some results in Figure 2.6.4.

λ	au	multiplicity
-1.0000	2.0000	1
-0.7817	1.7817	2
-0.5000	1.5000	1
-0.3333	1.3333	2
0.0000	1.0000	4
0.3333	0.6667	2
0.5000	0.5000	1
0.7817	0.2183	2
1.0000	0.0000	1

Table 2.2: Eigenvalues of modified Laplacian  $\lambda$  and Corresponding Normalized Laplacian Eigenvalues  $\tau$  for a 16-Vertex Square Grid Graph

As established in Section (2.5.4), we derived a relationship between the eigenvalues of the normalized Laplacian matrix, denoted by  $\tau$ , and the modified Laplacian eigenvalues,  $\lambda$ . This relationship is expressed by the following equation:

$$\lambda = 1 - \tau \tag{2.6.39}$$

Table (2.2) presents the eigenvalues that were calculated using MATLAB for a

square grid graph with 16 vertices. The first column, labelled  $\lambda$ , contains the eigenvalues directly computed from the graph's modified Laplacian matrix. The second column shows the corresponding normalized Laplacian eigenvalues obtained by applying equation (2.6.39). According to this relationship, the normalized Laplacian eigenvalues should fall within the interval [0, 2].

By using MATLAB to solve the non-linear equations derived by Klopotek (2.6.7)-(2.6.10) discussed in Section (2.6.1) on a square grid graph, we explored all possible values of  $z_1$  and  $z_2$ . In order to ensure the convergence of the solution, we determined the initial values of  $\delta_1$  and  $\delta_2$  by plotting the phases, which allowed us to locate the regions where w(z) = 0. These initial values of  $\delta_1$  and  $\delta_2$  were then used in MATLAB to solve the system numerically.

Table (2.3) presents the chosen values of  $z_1$ ,  $z_2$ ,  $\delta_1$ , and  $\delta_2$ , and their corresponding normalized Laplacian eigenvalues  $\tau$ .

$\boxed{\{z_1, z_2\}}$	$(\delta_1,\delta_2)$	au
(0,0)	(0,0)	2
(0,0)	(0.80217 , 6.7762)	1.3333
(0,0)	(0.8021734, 2.648612)	1.3333
(0,0)	(2.6486, 8.6226)	1.3333
(0,0)	(2.6486, 0.8022)	1.3333
(0,0)	(6.7762, 8.62260)	1.3333
(0,0)	(6.7762, 0.8022)	1.3333
(0,0)	(8.6226 , 6.7762)	1.3333
(0,0)	(8.6226 , 2.6486)	1.3333
(0,0)	(3.1416 , 6.2832)	0.5
(0,0)	(3.1416 , 3.1416)	0.5
(0,0)	(6.2832, 6.2832)	0.5
(0,0)	(6.2832, 3.1416)	0.5
(1,1)	$(2\pi \ ,  2\pi)$	0

	$(\delta_1,\delta_2)$	au
(1,1)	(3.6346 , 7.0854)	0.6667
(1,1)	(3.6346 , 5.4810 )	0.6667
(1,1)	(5.4810, 8.9318)	0.6667
(1,1)	(5.4810 , 3.6346)	0.6667
(1,1)	(7.0854, 8.9318)	0.6667
(1,1)	(7.0854, 3.6346)	0.6667
(1,1)	(8.9318, 7.0854)	0.6667
(1,1)	(8.9318, 5.4810)	0.6667
(1,1)	( 3.1416 , 3.1416)	1.5
(1,1)	$(0,\pi)$	1.5
(1,0)	(0.2083, 8.9408)	1.781736
(1,0)	(0.2083, 0.48396)	1.781736
(1,0)	(2.9333, 8.9408)	1.781736
(1,0)	(2.9333, 0.48394)	1.781736
(1,0)	(5.79923, 6.07487)	0.21826
(1,0)	(5.7992, 3.3499)	0.21826
(1,0)	(6.7671, 3.3499)	0.21826
(1,0)	(6.76714, 6.0749)	0.21826
(1,0)	(3.45575, 6.59734)	1
(1,0)	(3.4557, 2.8274)	1
(1,0)	(5.3407, 8.4823)	1
(1,0)	(5.3407, 0.9425)	1
(1,0)	(7.2257, 8.4823)	1
(1,0)	(7.2257, 0.9425)	1
(1,0)	(9.1106, 6.5973)	1
(1,0)	(9.1106, 2.8274)	1

Table 2.3: Chosen values of  $z_1, z_2, \delta_1, \delta_2,$  and corresponding eigenvalues  $\tau$  for a 16-vertex grid graph.

From these results, we observe that the eigenvalues computed using Klopotek's method, as shown in Table (2.3), are consistent with those obtained from the first table (2.2), which were calculated using MATLAB's internal eigenvalue solver, specifically the eig command, to directly solve the eigenvalue problem for the grid graph. However, the multiplicity of the eigenvalues was not accurately determined using Klopotek's method.

While it is possible to compute the eigenvalues of smaller networks directly, understanding the behaviour of eigenvalues in large networks requires an asymptotic approach. We will explore the asymptotic behaviour of eigenvalues in square grid graphs as the network grows in size in the following section.

### 2.7 Asymptotic theory for a square grid graph

In this section, we analyse the asymptotic behaviour of the eigenvalues, denoted by  $\tau$ , for the normalized Laplacian of a square grid graph  $n_1 \times n_2$ , where  $n_1 = n_2 = M$ , representing the number of vertices along one dimension, and M is taken to be large. The asymptotic behaviour of the eigenvalues is derived using the formulae of Klopotek [30] that we used in the previous section. Our primary interest is in computing the dominant decay rate, that is the first non-zero value of  $\nu$ . We recall that  $\lambda = \cos \nu$ , and that, as was established in section (2.3.3),  $\lambda \in [-1,1]$ . Hence we seek the eigenvalue  $\lambda$  which is closest to unity. Furthermore, since  $\lambda = 1 - \tau$ , and  $\tau \in [0,2]$  for a normalized Laplacian,and considering that the eigenvalues of a grid graph are symmetric about  $\tau = 1$ , due to the bipartite nature of the graph as we discussed in section (2.6.2), we aim to find the eigenvalue closest to  $\tau = 2$  as M become large.

In figure (2.7.1) we show the value of  $\tau$  closest to 2 for different values of n on a square grid graph, together with the corresponding values of  $\delta_1$  and  $\delta_2$ . For each n the value of  $\tau$  was found by solving Klopotek's equations (2.6.24) and (2.6.25) for  $(z_1, z_2) = (1, 0)$  using Newton's method. It can be seen that as n increases,  $\tau$ 

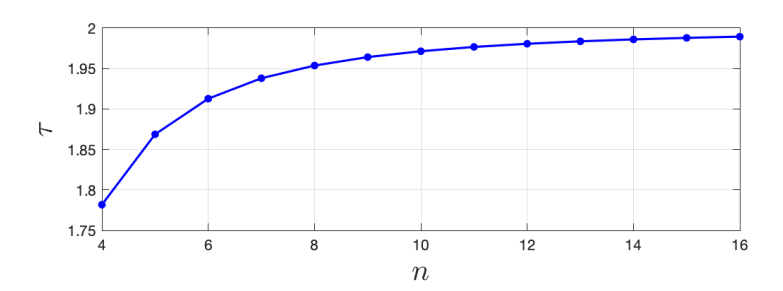


Figure 2.7.1: Value of  $\tau$  closest to the eigenvalue 2 for different values of n on a square grid graph.

approaches 2 from below while  $\delta_1$  and  $\delta_2$  both approach zero. We may conclude that when  $n \gg 1$ , we calculate the slowest decay rate by choosing  $(z_1, z_2) = (1, 0)$  and taking small values as the initial guesses for the  $\delta_j$ .

The normalized Laplacian eigenvalue  $\tau$  is given by the following expressions:

$$\tau = 1 + \frac{1}{2}(\cos \xi_1 + \cos \xi_2),\tag{2.7.1}$$

$$\tau = 1 + \cos \xi_j + \tan \delta_j \sin \xi_j \quad (j = 1, 2),$$
 (2.7.2)

where

$$\xi_j = \frac{z_j \pi - 2\delta_j}{n - 1}.$$

Based on the discussion above, we know that when  $n \gg 1$ ,  $\delta_1$  and  $\delta_2$  are both small, and hence  $|\xi_j|$  is small. To approximate the eigenvalue nearest to  $\tau = 2$ , then, we apply a Taylor expansion to both equations (2.7.1) and (2.7.2), yielding:

$$\tau \approx 1 + \frac{1}{2} \left[ \left( 1 - \frac{\xi_1^2}{2} \right) + \left( 1 - \frac{\xi_1^2}{2} \right) \right] = 2 - \frac{1}{4} (\xi_1^2 + \xi_2^2), \tag{2.7.3}$$

$$\tau \approx 1 + \left(1 - \frac{\xi_j^2}{2}\right) + \tan \delta_j \left(\xi_j - \frac{\xi_j^3}{6}\right)$$

$$= 2 + (\tan \delta_j)\xi_j - \frac{\xi_j^2}{2} + \dots \quad (j = 1, 2).$$
(2.7.4)

### **2.7.1** Case I: $(z_1, z_2) = (0, 1)$ , or $(z_1, z_2) = (1, 0)$

We first consider the case where  $z_1 = 0$  and  $z_2 = 1$ , or equivalently  $z_1 = 1$  and  $z_2 = 0$  due to symmetry, as discussed in Section (2.6.1). We aim to find the second-largest eigenvalue, to get the growth rate  $\nu$  which is corresponding to the eigenvalue nearest to 2. The eigenvalues of the normalized Laplacian lie within the range [0, 2].

Let M = n - 1 and assume that M is large  $(M \gg 1)$ . In this case,  $\xi_1$  and  $\xi_2$  are approximated as:

$$\xi_1 = \frac{-2\delta_1}{M}, \quad \xi_2 = \frac{\pi - 2\delta_2}{M}.$$

We express  $\delta_1$  and  $\delta_2$  in terms of M:

$$\delta_1 = \frac{1}{2}\beta_1 M^{-a}, \quad \delta_2 = \frac{1}{2}\beta_2 M^{-b}, \quad a, b > -1,$$

where  $\beta_1$  and  $\beta_2$  are constants of order O(1). Substituting into  $\xi_1$  and  $\xi_2$ , we have:

$$\xi_1 = \frac{-\beta_1}{M^{1+a}}, \quad \xi_2 = \frac{\pi}{M} - \frac{\beta_2}{M^{1+b}}.$$

Substituting these values of  $\xi_1, \xi_2$  into equation (2.7.3) gives:

$$\tau = 2 - \frac{1}{4} \left( \frac{\beta_1^2}{M^{2+2a}} + \dots + \frac{\pi^2}{M^2} + \dots \right). \tag{2.7.5}$$

Similarly, applying  $\xi_1$  and  $\xi_2$  in (2.7.4) for j=1 leads to the following expressions for  $\tau$ :

$$\tau = 1 + \left(1 - \frac{\xi_1^2}{2} + \dots\right) + \left[\frac{1}{2}\beta_1 M^{-a} + \dots\right] (\xi_1 + \dots)$$

$$\tau = 2 + \frac{\frac{1}{2}\beta_1(-\beta_1)}{M^{1+2a}} + \dots$$
(2.7.6)

For j=2 equation (2.7.4) leads to the following expressions for  $\tau$ :

$$\tau = 1 + \left(1 - \frac{\xi_2^2}{2} + \dots\right) + \left[\frac{1}{2}\beta_2 M^{-b} + \dots\right] (\xi_2 + \dots)$$

$$= 2 + \frac{1}{2}\beta_2 M^{-b} \left(\frac{\pi}{M} + \dots\right) - \frac{1}{2} \left[\frac{\pi}{M} + \dots\right]^2$$

$$\tau = 2 + \frac{\left(\frac{1}{2}\pi\beta_2\right)}{M^{1+b}} + \dots - \frac{1}{2}\pi^2 M^{-2} + \dots$$
(2.7.7)

To ensure consistency between these equations, we compare the powers of M from (2.7.7) and (2.7.6). This gives the conditions:

$$1 + 2a = 1 + b = 2$$
  $\Rightarrow$   $a = \frac{1}{2}, b = 1.$ 

Thus,  $\delta_1$  and  $\delta_2$  are given by:

$$\delta_1 = \frac{1}{2}\beta_1 M^{-\frac{1}{2}}, \quad \delta_2 = \frac{1}{2}\beta_2 M^{-1}$$

Substituting the value of a and b into equation (2.7.5), we obtain:

$$\tau = 2 - \frac{\pi^2}{4} M^{-2} + \dots \tag{2.7.8}$$

Similarly, equation (2.7.6) becomes:

$$\tau = 2 + \left(\frac{1}{2}\pi\beta_2 - \frac{1}{2}\pi^2\right)M^{-2} + \cdots$$
 (2.7.9)

And for equation (2.7.7), we have:

$$\tau = 2 - \frac{1}{2}\beta_1^2 M^{-2} + \dots {(2.7.10)}$$

By comparing the coefficients of  $M^{-2}$  from equations (2.7.8) through (2.7.10), we obtain the following relation:

$$\frac{1}{2}\beta_1^2 = \frac{\pi^2}{4} = -\frac{1}{2}\pi(\beta_2 - \pi),$$

As a result, we conclude

$$\beta_1 = \frac{\pi}{\sqrt{2}}, \quad \beta_2 = \frac{\pi}{2}.$$

Thus, in fact,

$$\delta_1 \sim \frac{\pi}{2\sqrt{2}} M^{-\frac{1}{2}}, \quad \delta_2 \sim \frac{\pi}{4} M^{-1},$$

and the asymptotic behaviour of  $\tau$  for large M for case  $(z_1, z_2) = (0, 1)$  is given by:

$$\tau \sim 2 - \frac{\pi^2}{4M^2}$$

### **2.7.2** Case II: $(z_1, z_2) = (1, 1)$

We now consider the case where  $z_1 = z_2 = 1$ . The goal is to find the second-largest eigenvalue, with  $\tau$  symmetric around 1. For large M,  $\xi_1$  and  $\xi_2$  are given by:

$$\xi_1 = \frac{\pi - 2\delta_1}{M}, \quad \xi_2 = \frac{\pi - 2\delta_2}{M}.$$

To ensure consistency between equations (2.7.3) and (2.7.4), we observe that these only agree if  $\delta_j = 0$ . This leads to the simplified expressions:

$$\xi_j = \frac{\pi}{M}, \quad j = 1, 2.$$

Substituting this value of  $\xi_j$  into the expressions for  $\tau$  in equations (2.7.3) and (2.7.4), we find that  $\tau$  can be expressed as:

$$\tau = 2 - \frac{\pi^2}{2M^2} + \dots.$$

Therefore, the asymptotic behaviour of  $\tau$  for large M for case  $(z_1, z_2) = (1, 1)$  is given by:

$$\tau \sim 2 - \frac{\pi^2}{2M^2}$$

### **2.7.3** Case III: $(z_1, z_2) = (0, 0)$

We now consider the case where  $z_1 = z_2 = 0$ . The goal is to find the secondlargest eigenvalue, with  $\tau$  symmetric around 1. For large M,  $\xi_1$  and  $\xi_2$  are given by:

$$\xi_1 = \frac{-2\delta_1}{M}, \quad \xi_2 = \frac{-2\delta_2}{M}.$$

To ensure consistency between equations (2.7.3) and (2.7.4), we observe that these only agree if  $\delta_j = \pi$ . This leads to the simplified expressions:

$$\xi_j = \frac{4\pi^2}{M^2}, \quad j = 1, 2.$$

Substituting this value of  $\xi_j$  into the expressions for  $\tau$  in equations (2.7.3) and (2.7.4), we find that  $\tau$  can be expressed as:

$$\tau = 2 - \frac{2\pi^2}{M^2} + \dots$$

Therefore, the asymptotic behaviour of  $\tau$  for large M for case  $(z_1, z_2) = (0, 0)$  is given by:

$$\tau \sim 2 - \frac{2\pi^2}{M^2}$$

### 2.7.4 Results of asymptotic analysis

In this section, we present the results of the asymptotic analysis of the eigenvalues of the normalized Laplacian  $\tau$  for a square grid graph. The analysis builds upon the theoretical derivations discussed in Section (2.7), where the eigenvalues of the normalized Laplacian were approximated asymptotically for large grid sizes. Here, we will compare these asymptotic results with the actual eigenvalues computed numerically for a square grid graph with sizes  $3 \times 3$  to  $20 \times 20$ , which corresponds to a grid graph with 9 vertices to 400 vertices. Specifically, we aim to validate the accuracy of the asymptotic expression, particularly for the second-largest eigenvalue to study the growth rate  $\nu$ , as the number of grid vertices, denoted by M, increases, with our chosen values for  $z_1$  and  $z_2$ .

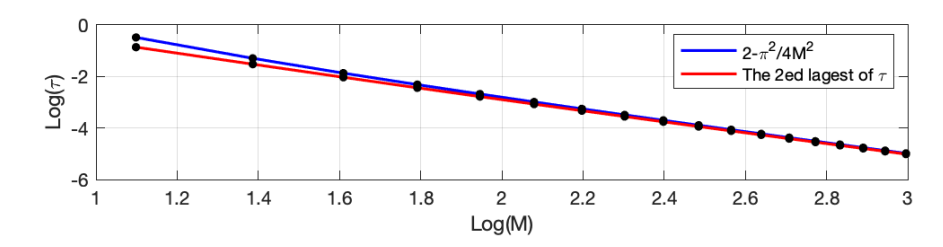


Figure 2.7.2: The red line represents the second-largest eigenvalue of the normalized Laplacian  $\tau$  for grid sizes ranging from M=3 to M=20. The blue line shows the asymptotic approximation for the chosen values  $(z_1, z_2) = (1, 0)$  over the same range of M.

Case I: 
$$(z_1, z_2) = (0, 1) = (1, 0)$$

We derived the asymptotic expression for the eigenvalue closest to  $\tau=2$  when  $(z_1,z_2)=(0,1)=(1,0)$  in Section (2.7) The result was:

$$\tau \sim 2 - \frac{\pi^2}{4M^2},$$

where M is the number of vertices along one dimension in the grid. This approximation is valid for large M.

Figure 2.7.2 obtained by using MATLAB, we computed the actual second-largest eigenvalue of the normalized Laplacian for grid sizes ranging from M=3 to M=20, and the asymptotic approximation and then plots them for comparison. The plot displays:

- Red line: The second-largest eigenvalue of the normalized Laplacian for each M from 3 to 20.
- Blue line: The asymptotic approximation  $\tau \sim 2 \frac{\pi^2}{4M^2}$ .

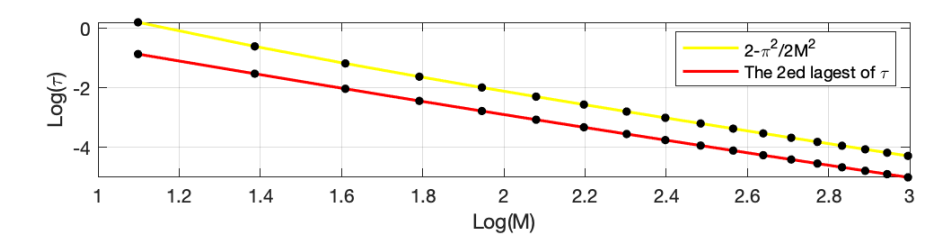


Figure 2.7.3: The red line represents the second-largest eigenvalue of the normalized Laplacian  $\tau$  for grid sizes ranging from M=3 to M=20. The yellow line shows the asymptotic approximation for the chosen values  $(z_1,z_2)=(1,1)$  over the same range of M.

Case II: 
$$(z_1, z_2) = (1, 1)$$

We derived the asymptotic expression for the eigenvalue closest to  $\tau = 2$  when  $(z_1, z_2) = (1, 1)$  in Section (2.7) The result was:

$$\tau \sim 2 - \frac{\pi^2}{2M^2},$$

where M is the number of vertices along one dimension in the grid. This approximation is valid for large M.

Figure 2.7.3 obtained by using MATLAB, we computed the actual second-largest eigenvalue of the normalized Laplacian for grid sizes ranging from M=3 to M=20, and the asymptotic approximation and then plots them for comparison. The plot displays:

- ullet Red line: The second-largest eigenvalue of the normalized Laplacian for each M from 3 to 20.
- Yellow line: The asymptotic approximation  $\tau \sim 2 \frac{\pi^2}{2M^2}$ .

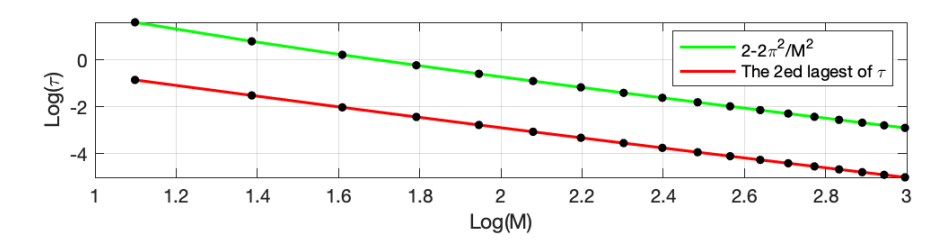


Figure 2.7.4: The red line represents the second-largest eigenvalue of the normalized Laplacian  $\tau$  for grid sizes ranging from M=3 to M=20. The green line shows the asymptotic approximation for the chosen values  $(z_1, z_2) = (0, 0)$  over the same range of M.

Case III:  $(z_1, z_2) = (0, 0)$ 

We derived the asymptotic expression for the eigenvalue closest to  $\tau = 2$  when  $(z_1, z_2) = (0, 0)$  in Section (2.7) The result was:

$$\tau \sim 2 - \frac{2\pi^2}{M^2},$$

where M is the number of vertices along one dimension in the grid. This approximation is valid for large M.

Figure 2.7.4 obtained by using MATLAB, we computed the the actual second-largest eigenvalue of the normalized Laplacian for grid sizes ranging from M=3 to M=20, and the asymptotic approximation and then plots them for comparison. The plot displays:

- ullet Red line: The second-largest eigenvalue of the normalized Laplacian for each M from 3 to 20.
- Green line: The asymptotic approximation  $\tau \sim 2 \frac{2\pi^2}{M^2}$ .

### Conclusion

The plot (2.7.2) demonstrates a high degree of agreement between the computed eigenvalues and the asymptotic approximation when  $(z_1, z_2) = (0, 1) = (1, 0)$ , particularly as M increases. For larger grid sizes, the

two curves essentially overlap, indicating that the asymptotic formula accurately approximates the second-largest eigenvalue for large grids.

# Diffusion on a network: finite-difference approach

In this chapter we take a different approach to calculating diffusion on a network. Rather than solving the diffusion equation exactly on each edge of the network and then formulating an eigenvalue problem for the decay rate (as done in chapter 2), we instead develop a novel finite-difference discretization approach to solve the full partial differential diffusion equation directly on the network structure.

Previous work on PDEs on metric networks has primarily focused on other types of equations. For example, Böttcher and Porter [8] recently developed spectral methods for solving Schrödinger, Poisson, heat, and wave equations on metric networks, while Brio et al. [11] compared spectral, finite-difference, and discontinuous Galerkin methods for Helmholtz and telegrapher's equations. However, to our knowledge, no previous work has specifically developed finite-difference methods for the diffusion equation on networks with the particular boundary conditions and vertex coupling conditions we consider here.

Our original contribution in this chapter is the development and implementation of a Crank-Nicholson finite-difference scheme specifically tailored for the diffusion equation on network structures. We discretize the domain using equally spaced collocation points along each edge and develop novel methods for enforcing continuity of flux and concentration conditions at common vertices, as well as zero flux conditions at boundary vertices. This

approach is fundamentally different from existing work because:

- 1. We focus specifically on the diffusion equation rather than other PDE types.
- We develop custom finite-difference stencils for network vertex conditions.
- We use fictitious points to maintain second-order accuracy at vertices.
- We validate our numerical decay rates against the eigenvalue analysis from Chapter 2.

The evolution in time is computed using the Crank-Nicholson method, and we demonstrate that our numerical results accurately capture the decay rates predicted by the theoretical eigenvalue analysis.

### 3.1 Brief introduction to the finite difference method

The finite difference method (FDM) is an approximate solution to differential equations. The fundamental idea behind finite difference methods, when applied to boundary-value problems, is to replace the governing differential equations and corresponding boundary conditions with suitable finite difference equations. This is achieved by approximating the derivatives in the differential equations using finite difference quotients, which are combinations of the dependent (unknown) function values at specific values of the independent variables. By formulating the difference equations at these specific values, we are led to systems of simultaneous algebraic equations [21], which can be solved using MATLAB, as will be demonstrated in this chapter. Therefore, a finite difference method is understood as a numerical procedure that approximates exact differential equations and boundary conditions [21], such as those in a diffusion equation problem, which will be illustrated in this chapter for solving a network graph. The resulting approximate equations can then be solved exactly

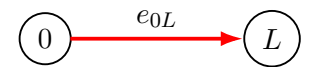


Figure 3.2.1: A path graph  $P_2$  with two vertices.

or approximately to find the growth rate of our network. The Crank-Nicholson method is a second-order method in numerical analysis used to solve diffusion equations and similar partial differential equations [15]. In the next section, we will apply that method to simple graphs to introduce the concept of solving more complex graphs.

# 3.2 Crank-Nicholson method to solve the diffusion equation on a network

In this section, we introduce the application of the Crank-Nicholson method for solving the linear diffusion equation on various network structures. We begin with the simplest case, a path graph  $P_2$ , to establish a foundational understanding of solving the diffusion equation on a network with Neumann boundary conditions applied at the boundary vertices. Next, we extend the analysis to a slightly more complex path graph,  $P_3$ , where we apply the principles of continuity of concentration and flux at a common (interior) vertex. This ensures that the flux transitions smoothly across the network. Finally, the concepts are generalized and applied to larger, more complex networks.

## 3.2.1 Crank-Nicholson method to solve the diffusion equation for path graph $P_2$

In this section, we discuss the Crank-Nicholson method for solving the linear diffusion equation on a simple path graph  $P_2$  as shown in figure (3.2.1). The diffusion equation, governing the spread of a substance over the graph, is expressed as:

$$u_t = Du_{xx} (3.2.1)$$

where u(x,t) denotes the concentration of the substance at position x and time t, and D is the diffusion coefficient. The domain considered is  $0 \le x \le L$ , with initial conditions prescribed as:

$$u(x,0) = f(x), (3.2.2)$$

where f(x) is some selected function.

We apply the Crank-Nicholson method to discretize the diffusion equation (3.2.1). The discretization begins by defining a uniform grid of points over the path graph  $P_2$ . These points are distributed over the interval  $0 \le \xi \le 1$  such that

$$\xi_i = (i-1)h, \qquad i = 1, \dots, N,$$
 (3.2.3)

where h = 1/N is the step length. We then denote by  $u_i^n$  the approximated value of u at grid point  $\xi_i$  at time level  $t = t_n$ , where  $t_n = n\Delta t$  for some chosen time step  $\Delta t$ . The finite difference discretisation for the diffusion equation is:

$$\frac{u_i^{n+1} - u_i^n}{\Delta t} = \frac{D}{2} \left( \frac{u_{i+1}^{n+1} - 2u_i^{n+1} + u_{i-1}^{n+1}}{h^2} \right) + \frac{D}{2} \left( \frac{u_{i+1}^n - 2u_i^n + u_{i-1}^n}{h^2} \right)$$
(3.2.4)

Multiplying both sides of equation (3.2.4) by  $\Delta t$ , we have:

$$u_i^{n+1} - u_i^n = \frac{D\Delta t}{2h^2} (u_{i+1}^{n+1} - 2u_i^{n+1} + u_{i-1}^{n+1}) + \frac{D\Delta t}{2h^2} (u_{i+1}^n - 2u_i^n + u_{i-1}^n)$$
 (3.2.5)

Defining  $\hat{\alpha} = \frac{D\Delta t}{2h^2}$ , equation (3.2.5) becomes:

$$u_i^{n+1} - u_i^n = \hat{\alpha}(u_{i+1}^{n+1} - 2u_i^{n+1} + u_{i-1}^{n+1}) + \hat{\alpha}(u_{i+1}^n - 2u_i^n + u_{i-1}^n)$$
(3.2.6)

Thus, the discrete diffusion equation for the path graph  $P_2$  is given by:

$$-\hat{\alpha}u_{i-1}^{n+1} + (1+2\hat{\alpha})u_i^{n+1} - \hat{\alpha}u_{i+1}^{n+1} = \hat{\alpha}u_{i-1}^n + (1-2\hat{\alpha})u_i^n + \hat{\alpha}u_{i+1}^n$$
 (3.2.7)

where  $u_i^n$  represents the numerical solution at the *i*-th grid point and *n*-th time

level. Equation (3.2.7) leads to a system of equations, which will be detailed further by taking into consideration the boundary conditions at the boundary vertices. The following section will focus on the application of Neumann boundary conditions.

### Neumann boundary conditions on path graph $P_2$

Neumann boundary conditions specify the derivative of the solution at the boundaries of the domain [41]. For the path graph  $P_2$  on the interval  $0 \le x \le 1$ , the Neumann boundary conditions are expressed as:

$$u_x(0,t) = Q_1, \quad u_x(1,t) = Q_2,$$

where  $Q_1$  and  $Q_2$  are specified fluxes. To approximate the derivative at the boundaries, we use finite difference approximations. At the left boundary,in the simplest implementation we use a forward difference:

$$\frac{u_2 - u_1}{h} = Q_1 \quad \Rightarrow \quad u_1 - u_2 = -hQ_1.$$

This method, however, is only first-order accurate with respect to h. In the following section, we will explore the use of fictitious points at the boundaries to achieve second-order accuracy,  $h^2$ . Similarly, at the right boundary, we use a backward difference:

$$\frac{u_N - u_{N-1}}{h} = Q_2 \quad \Rightarrow \quad u_{N-1} - u_N = -hQ_2$$

In equation (3.2.7) the Crank-Nicholson discretization can be represented in matrix form as follows:

$$\begin{bmatrix} 1 & -1 & 0 & \dots & 0 \\ -\hat{\alpha} & 1 + 2\hat{\alpha} & -\hat{\alpha} & \ddots & \vdots \\ 0 & \ddots & \ddots & \ddots & 0 \\ \vdots & \ddots & -\hat{\alpha} & 1 + 2\hat{\alpha} & -\hat{\alpha} \\ 0 & \dots & 0 & 1 & -1 \end{bmatrix} \begin{bmatrix} u_1^{n+1} \\ u_2^{n+1} \\ \vdots \\ u_{N-1}^{n+1} \\ u_N^{n+1} \end{bmatrix}$$

$$= \begin{bmatrix} -hQ_1 & 0 & 0 & \dots & 0 \\ \hat{\alpha} & 1 - 2\hat{\alpha} & \hat{\alpha} & \ddots & \vdots \\ 0 & \ddots & \ddots & \ddots & 0 \\ \vdots & \ddots & \hat{\alpha} & 1 - 2\hat{\alpha} & \hat{\alpha} \\ 0 & 0 & 0 & 0 & hO \end{bmatrix} \begin{bmatrix} u_1^n \\ u_2^n \\ \vdots \\ u_{N-1}^n \\ u_N^n \end{bmatrix}$$

Here,  $\hat{\alpha} = \frac{Ddt}{2h^2}$ , and n and n+1 denote the current and next time levels, respectively. For the matrix representation, the first and last rows correspond to the Neumann boundary conditions, while the interior rows correspond to the diffusion equation discretization (3.2.7). To maintain the accuracy of the finite difference method near the boundaries, we use fictitious points to allow us consistent treatment of the boundary conditions while preserving the structure of the numerical grid [23]. Further details will be discussed in the next section.

### Fictitious points in finite differences for path graph $P_2$

To impose boundary conditions at x = 0 and x = L on the path graph  $P_2$ , we use fictitious points  $u_0^{n+1}$  and  $u_{N+1}^{n+1}$ , which lie outside the interval of interest. At x = 0, the derivative is approximated by:

$$u_x|_{x=0} \simeq \frac{u_2^{n+1} - u_0^{n+1}}{2h} = Q_1.$$

Solving for  $u_0^{n+1}$  gives:

$$u_0^{n+1} = u_2^{n+1} - 2hQ_1. (3.2.8)$$

The finite difference of the diffusion equation (3.2.7) at x = 0 is given by:

$$-\hat{\alpha}u_0^{n+1} + (1+2\hat{\alpha})u_1^{n+1} - \hat{\alpha}u_2^{n+1} = \hat{\alpha}u_0^n + (1-2\hat{\alpha})u_1^n + \hat{\alpha}u_2^n.$$
 (3.2.9)

Substituting the value of  $u_0^{n+1}$  from (3.2.8) into the finite difference equation (3.2.9), we obtain:

$$-\hat{\alpha}(u_2^{n+1} - 2hQ_1) + (1 + 2\hat{\alpha})u_1^{n+1} - \hat{\alpha}u_2^{n+1} = \hat{\alpha}(u_2^n - 2hQ_1) + (1 - 2\hat{\alpha})u_1^n + \hat{\alpha}u_2^n.$$
(3.2.10)

Simplifying and rearranging (3.2.10), we get

$$(1+2\hat{\alpha})u_1^{n+1} - 2\hat{\alpha}u_2^{n+1} = -4\hat{\alpha}hQ_1 + (1-2\hat{\alpha})u_1^n + 2\hat{\alpha}u_2^n.$$
(3.2.11)

At x = L, we similarly approximate the derivative and obtain a fictitious point  $u_{N+1}^{n+1}$ :

$$u_x|_{x=L} \simeq \frac{u_{N+1}^{n+1} - u_{N-1}^{n+1}}{2h} = Q_2,$$

where  $Q_2$  is an approximation for the derivative. Solving for  $u_{N+1}^{n+1}$  gives:

$$u_{N+1}^{n+1} = u_{N-1}^{n+1} - 2hQ_2. (3.2.12)$$

The finite difference of the diffusion equation (3.2.7) at x=L is given by:

$$-\hat{\alpha}u_{N-1}^{n+1} + (1+2\hat{\alpha})u_N^{n+1} - \hat{\alpha}u_{N+1}^{n+1} = \hat{\alpha}u_{N-1}^n + (1-2\hat{\alpha})u_N^n + \hat{\alpha}u_{N+1}^n$$
 (3.2.13)

Substituting the value of  $u_{N+1}^{n+1}$  from (3.2.12) into the finite difference equation (3.2.13), we obtain:

$$-\hat{\alpha}u_{N-1}^{n+1} + (1+2\hat{\alpha})u_N^{n+1} - \hat{\alpha}(2hQ_2 + u_{N-1}^{n+1})$$

$$= \hat{\alpha}u_{N-1}^n + (1-2\hat{\alpha})u_N^n + \hat{\alpha}(2hQ_2 + u_{N-1}^n) \quad (3.2.14)$$

Simplifying and rearranging (3.2.14), we get

$$-2\hat{\alpha}u_{N-1}^{n+1} + (1+2\hat{\alpha})u_N^{n+1} = 4\hat{\alpha}hQ_2 + 2\hat{\alpha}u_{N-1}^n + (1-2\hat{\alpha})u_N^n$$
 (3.2.15)

Thus, using fictitious points, we arrive at the following system of equations in matrix form:

$$\begin{bmatrix} (1+2\hat{\alpha}) & -2\hat{\alpha} & 0 & \dots & 0 \\ -\hat{\alpha} & 1+2\hat{\alpha} & -\hat{\alpha} & \dots & 0 \\ 0 & \ddots & \ddots & \ddots & \vdots \\ \vdots & 0 & -\hat{\alpha} & 1+2\hat{\alpha} & -\hat{\alpha} \\ 0 & 0 & \dots & -2\hat{\alpha} & (1+2\hat{\alpha}) \end{bmatrix} \begin{bmatrix} u_1^{n+1} \\ u_2^{n+1} \\ \vdots \\ u_{N-1}^{n+1} \\ u_N^{n+1} \end{bmatrix}$$

$$= \begin{bmatrix} -4\hat{\alpha}hQ_1 & 2\hat{\alpha} & 1-2\hat{\alpha} & \dots & 0 \\ \hat{\alpha} & 1-2\hat{\alpha} & \hat{\alpha} & \dots & 0 \\ 0 & \ddots & \ddots & \ddots & \vdots \\ \vdots & 0 & \hat{\alpha} & 1-2\hat{\alpha} & \hat{\alpha} \\ 0 & 0 & 4\hat{\alpha}hQ_1 & 2\hat{\alpha} & 1-2\hat{\alpha} \end{bmatrix} \begin{bmatrix} u_1^n \\ u_2^n \\ \vdots \\ u_{N-1}^n \\ u_N^n \end{bmatrix}$$

Here,  $\hat{\alpha} = \frac{D\Delta t}{2h^2}$ , and n and n+1 denote the current and next time levels, respectively. The first and last rows of the matrix impose the Neumann boundary conditions, while the remaining rows correspond to the discretized diffusion equation on the path graph  $P_2$ . The result of this analysis is explained in the following section.

### 3.2.2 Numerical results for a path graph $P_2$

This section presents the results obtained by MATLAB simulations of the diffusion equation

$$u_t = Du_{rr}$$

on the path graph  $P_2$  that represents the path graph  $P_2$ , which consists of two vertices connected by a single edge (see figure 3.2.2). We use a finite difference



Figure 3.2.2: A path graph  $P_2$  with two vertices.

method; the simulation considers the interval [0,1] with Neumann boundary conditions applied.

The adjacency and degree matrices characterise the network's topology, enabling analysis of diffusion dynamics. The growth or decay rate of the diffusion process is theoretically determined by the eigenvalues of the *modified Laplacian* matrix,  $\mathbf{L}^*$ , as discussed in detail in section (2.3.1) defined as:

$$\mathbf{L}^* = \mathbf{A} - \cos(\nu)\mathbf{D}.$$

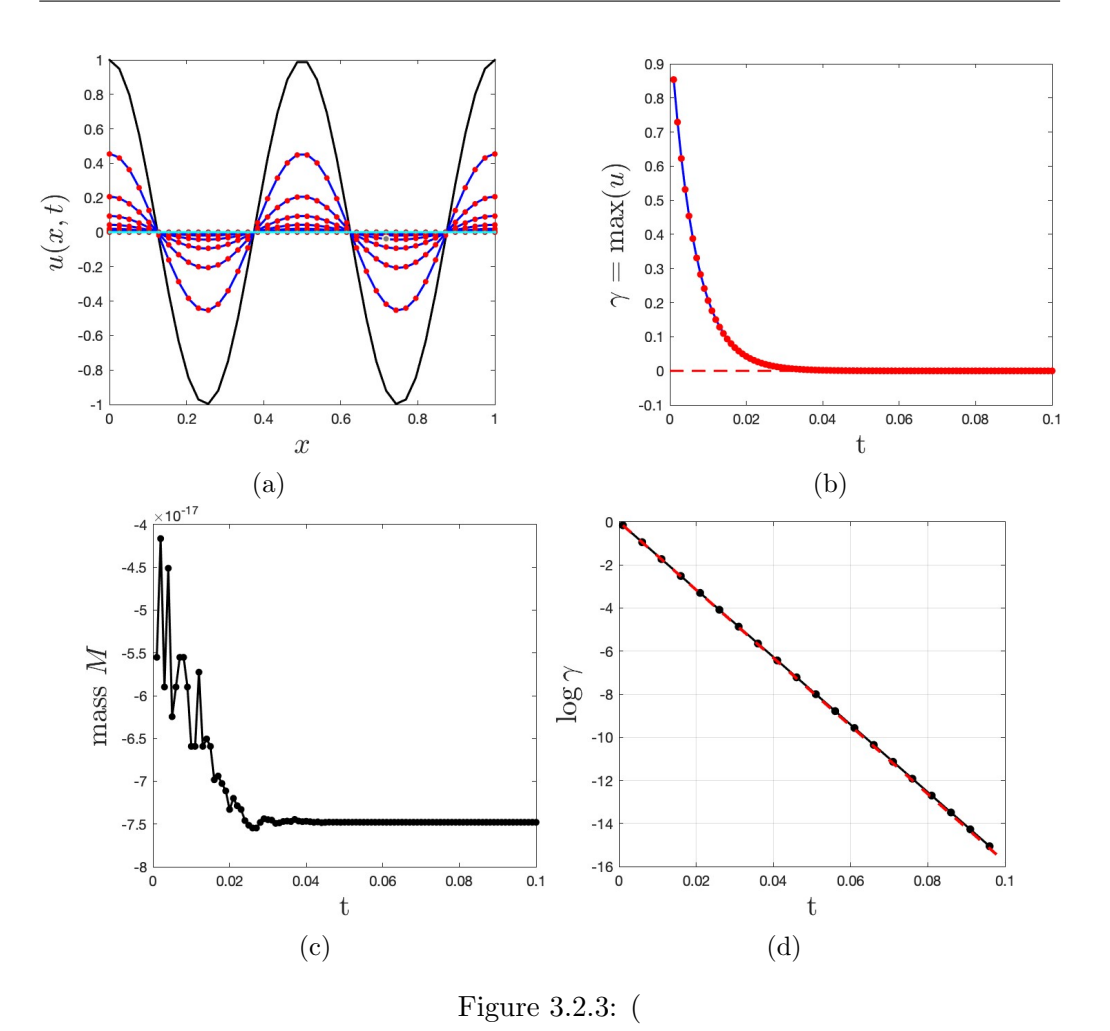
Here,  $\cos(\nu)$  represents an eigenvalue  $\lambda$ , such that from section (2.3.2) we know  $\cos(\nu) = \lambda$ . By reformulating, the matrix can be expressed as:

$$\mathbf{L}^* = \mathbf{A} - \lambda \mathbf{D}.$$

For any given network, the eigenvalues of  $\mathbf{L}^*$  can be computed numerically. The decay rate  $\nu$  is then determined using the relation  $\cos^{-1}(\lambda) = \nu$ , as established in section (2.3.2). The smallest positive decay rate corresponds to the slowest diffusion mode and is compared with theoretical predictions obtained through eigenvalue analysis.

The results obtained from MATLAB for the path graph  $P_2$  are illustrated in Figure (3.2.3), with choosing values  $\hat{\alpha} = 0.76$ , dt = 0.0001 and h = 0.03 which captures key aspects of diffusion dynamics:

• Figure (3.2.3)(a): shows the evaluation of the concentration profiles u(x,t) of  $P_2$  in different time steps t. The initial condition  $u(x,0) = \cos(4\pi x)$  (black curve) evolves over time. with intermediate steps in (blue curve), the (red dots) indicate the exact solution. The numerical solution (blue curve) is compared with the exact analytical solution (red dots) during the



a): shows the concentration profile u(x,t) of  $P_2$  along the network at different time steps t, the black curve shows the initial condition, the blue curves different time steps with cyan dotes that represent exact solution which indicate the agreement of the numerical and theoretical solutions. , and the red line the final step. (b): Maximum value  $\gamma$  as a function of time, comparing numerical (blue) and analytical solutions(red dots). (c): shows total mass conserved of the system as a function of time. (d): logarithmic plot of maximum concentration  $\gamma$  over time t (black line with dots), and analytical calculation of the smallest

positive eigenvalue of decay rate of the modified Laplacian  $\nu$  (red dash).

simulation, and both solutions show excellent agreement, the final state in (cyan line). Mathematically, this behaviour aligns with the diffusion equation's tendency to minimise concentration differences across the domain.

• Figure (3.2.3)(b): illustrates the temporal evolution of the maximum value of u,  $\gamma = \max(u(x,t))$ . Two curves are presented numerically computed maximum values (blue line) and (red dots) exact analytical

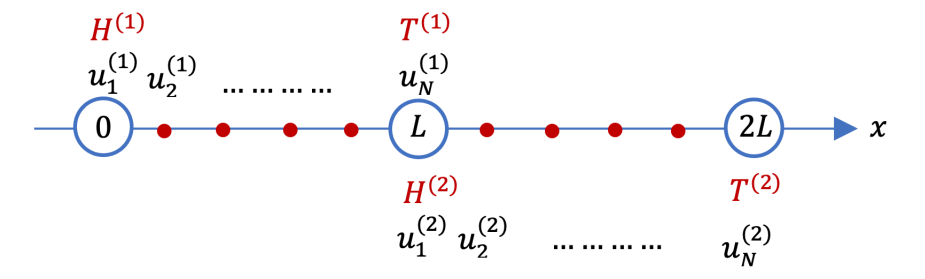


Figure 3.2.4: Applying Crank–Nicholson discretization on path graph  $P_3$ 

solution maximum values. As expected, the maximum value decreases exponentially with time, which is characteristic of diffuse processes.

- Figure (3.2.3)(c): shows the total mass of the system over time. The nearly constant mass confirms the numerical ability to preserve the total quantity of the diffusing substance, a crucial property of correct numerical implementations of diffusion equations.
- Figure (3.2.3)(d): shows  $\gamma = \max(u)$  on a logarithmic scale with time. This logarithmic scale represents the decay of  $\gamma$ , providing a clear visualisation of the decay rate. The slope of the line in this graph corresponds to the rate of exponential decay, which aligns with the theoretical prediction based on the smallest positive decay of the modified Laplacian  $\nu$ . This plot serves as a powerful confirmation of the agreement between numerical and analytical approaches, showing that the decay behaviour of the system is accurately captured by the Crank-Nicholson method.

To extend this analysis to more general cases, we begin by solving the diffusion equation on a path graph with three vertices, denoted as  $P_3$ . This will serve as a foundational example, allowing us to later generalise the approach for solving the diffusion equation on any loop-less graph structure.

### 3.2.3 Crank–Nicholson method to solve diffusion equation for path graph $P_3$

In this section, we consider the domain  $0 \le x \le 2L$  and apply the Crank-Nicholson method for the numerical approximation of the diffusion equation on a path graph  $P_3$ . This path graph consists of three vertices and two edges, representing a simple yet foundational graph structure for solving the diffusion equation that contains a common vertex. To begin, we discretise the domain into mesh points along the two edges of the path graph  $P_3$  as depicted in figure (3.2.4).

### Neumann boundary condition for path graph $P_3$

The boundary conditions for the vertices are imposed as follows. We begin with the zero-flux boundary condition at the point x = 0, which is expressed as:

$$u_x^{(1)}|_{x=0} = 0.$$

This condition signifies that there is no flux across the boundary at x = 0, meaning the derivative of u with respect to x is zero. Using a forward finite difference approximation, we have:

$$\frac{u_2^{(1)} - u_1^{(1)}}{h} = 0 \quad \Rightarrow \quad u_1^{(1)} = u_2^{(1)} \tag{3.2.16}$$

Next, we impose the zero-flux boundary condition at x=2L, which is expressed as:

$$u_x^{(2)}|_{x=2L} = 0.$$

Using a backward finite difference approximation, we get:

$$\frac{u_N^{(2)} - u_{N-1}^{(2)}}{h} = 0 \quad \Rightarrow \quad u_{N-1}^{(2)} = u_N^{(2)}. \tag{3.2.17}$$

### Continuity conditions on common vertex for path graph $P_3$

The continuity of flux at the midpoint x = L, which is the common vertex, implies that:

$$-\alpha u_x^{(1)}|_{x=L} = q_1$$
 on  $T^{(1)}$ ,  $-\alpha u_x^{(2)}|_{x=L} = q_2$  on  $H^{(2)}$ ,

with the condition  $q_2 - q_1 = 0$  ensuring continuity of flux between the two edges. Assuming  $\alpha = 1$ , the forward finite difference approximation for flux is given as:

$$q_1 = \frac{u_N^{(1)} - u_{N-1}^{(1)}}{h}, \quad q_2 = \frac{u_2^{(2)} - u_1^{(2)}}{h}.$$

The condition  $q_2 - q_1 = 0$  gives:

$$\frac{u_N^{(1)} - u_{N-1}^{(1)}}{h} - \frac{u_2^{(2)} - u_1^{(2)}}{h} = 0.$$

Simplifying, we obtain:

$$u_N^{(1)} - u_{N-1}^{(1)} - u_2^{(2)} + u_1^{(2)} = 0. (3.2.18)$$

Finally, we impose the continuity of concentration at the common vertex L:

$$u_N^{(1)} = u_1^{(2)}. (3.2.19)$$

This continuity condition, combined with the previous flux condition, ensures smooth behaviour of the diffusion process across the edges of the path graph  $P_3$ .

The matrix form for solving the diffusion equation on the path graph  $P_3$ , incorporating the conditions from equations (3.2.16), (3.2.17), (3.2.18), and

(3.2.19), is given by:

$$\begin{bmatrix} 1 & -1 & 0 & \dots & \dots & \dots & 0 \\ -\hat{\alpha} & 1 + 2\hat{\alpha} & -\hat{\alpha} & \ddots & \dots & \dots & \dots & 0 \\ 0 & \ddots & \ddots & \ddots & 0 & \dots & \dots & \vdots \\ 0 & 0 & -1 & 1 & 1 & -1 & 0 & \dots & 0 \\ 0 & \dots & 1 & -1 & 0 & \dots & \dots & \vdots \\ \vdots & 0 & \dots & -\hat{\alpha} & 1 + 2\hat{\alpha} & -\hat{\alpha} & 0 & \dots & \vdots \\ 0 & \dots & \dots & \ddots & \ddots & \ddots & \ddots & \vdots \\ 0 & \dots & \dots & \ddots & \ddots & \ddots & \ddots & \ddots \\ 0 & 0 & \dots & \dots & \dots & \dots & \dots & 0 & 1 & -1 \end{bmatrix} \begin{bmatrix} u_1^{(1)n+1} \\ \vdots \\ u_{N-1}^{(1)n+1} \\ u_N^{(1)n+1} \\ u_1^{(2)n+1} \\ \vdots \\ \vdots \\ u_N^{(2)n+1} \end{bmatrix}$$

$$= \begin{bmatrix} -hQ_1 & 0 & 0 & \cdots & \cdots & \cdots & 0 \\ \hat{\alpha} & 1 - 2\hat{\alpha} & \hat{\alpha} & \ddots & \cdots & \cdots & \cdots & 0 \\ 0 & \ddots & \ddots & \ddots & 0 & \cdots & \cdots & \vdots \\ 0 & 0 & 0 & 1 & -1 & 0 & 0 & \cdots & 0 \\ \vdots & 0 & \cdots & \hat{\alpha} & 1 - 2\hat{\alpha} & \hat{\alpha} & 0 & \cdots & \vdots \\ 0 & \cdots & \ddots & \ddots & \ddots & \ddots & \vdots \\ 0 & \cdots & \cdots & \ddots & \ddots & \ddots & \ddots & \vdots \\ 0 & 0 & \cdots & \cdots & \cdots & \ddots & \ddots & \ddots & 0 \\ 0 & 0 & \cdots & \cdots & \cdots & \cdots & 0 & 0 & -hQ_2 \end{bmatrix} \begin{bmatrix} u_1^{(1)n} \\ \vdots \\ u_{N-1}^{(1)n} \\ u_1^{(1)n} \\ u_1^{(2)n} \\ \vdots \\ \vdots \\ u_N^{(2)n} \end{bmatrix}$$

Here,  $\hat{\alpha} = \frac{D\Delta t}{2h^2}$ , with n and n+1 denoting the current and next time levels, respectively. Superscripts (1) and (2) refer to the first and second edges on the path graph, respectively. The first and last rows of the matrix correspond to the Neumann boundary conditions at x=0 and x=2L. The remaining rows represent the discretized diffusion equation for the path graph  $P_3$ .

### Fictitious points on the continuity of flux for path graph $P_3$

We now introduce the concept of fictitious points to handle the continuity of flux conditions at the common points of the path graph  $P_3$ . According to Figure

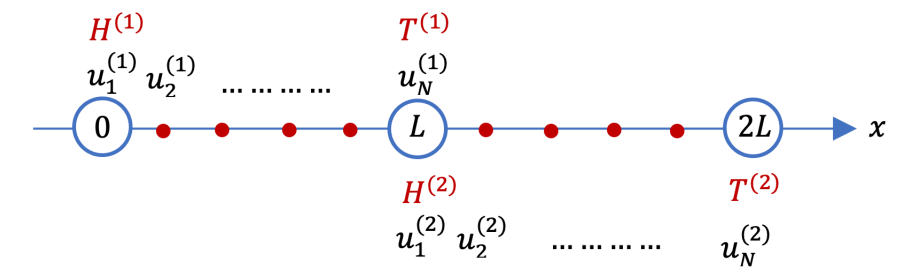


Figure 3.2.5: Applying Crank–Nicholson discretization on path graph  $P_3$ 

(3.2.5), there is a common vertex, denoted by L, shared between two edges in the graph. To enforce the continuity of flux condition at this common vertex, fictitious points are applied. As illustrated in Figure (3.2.5), the common vertex L is designated as the tail of the first edge, denoted by  $T^{(1)}$ , and as the head of the second edge, denoted by  $H^{(2)}$ . Here, the superscripts (1) and (2) correspond to edges one and two, respectively.

The finite difference scheme of the diffusion equation at the fictitious point for the first edges is given by:

$$-\hat{\alpha}u_{N-1}^{n+1} + (1+2\hat{\alpha})u_N^{n+1} - \hat{\alpha}u_{N+1}^{n+1} - \hat{\alpha}u_{N-1}^{n} - (1-2\hat{\alpha})u_N^{n} - \hat{\alpha}u_{N+1}^{n} = 0. \quad (3.2.20)$$

Similarly, the finite difference at the fictitious point for the second edge is:

$$-\hat{\alpha}u_0^{n+1} + (1+2\hat{\alpha})u_1^{n+1} - \hat{\alpha}u_2^{n+1} - \hat{\alpha}u_0^n - (1-2\hat{\alpha})u_1^n - \hat{\alpha}u_2^n = 0.$$
 (3.2.21)

At the tail of the first edge, the flux condition at x = L implies  $-\alpha u_x^{(1)}|_{x=L}$ . Assuming  $\alpha = 1$ , we can use the central difference method to obtain an expression for this condition using a fictitious point. We can write:

$$q_1^{n+1} = \frac{u_{N+1}^{n+1} - u_{N-1}^{n+1}}{2h}. (3.2.22)$$

At the head of the second edge, the flux condition at x = L implies  $-\alpha u_x^{(2)}|_{x=L}$ . Assuming  $\alpha = 1$ , we can use the central difference method to obtain an expression for this condition using a fictitious point. We can write:

$$q_2^{n+1} = \frac{u_2^{n+1} - u_0^{n+1}}{2h} \tag{3.2.23}$$

To define the continuity of flux at the common vertex, we need to consider whether it corresponds to a tail or a head on the segment. If it corresponds to a tail, we take minus the flux, and if it corresponds to a head, we take plus the flux. This means that for the node at x = L, we have:

$$q_2^{n+1} - q_1^{n+1} = 0. (3.2.24)$$

We substitute the value of (3.2.22) and (3.2.23) into (3.2.24) to obtain the expression for the continuity of flux condition:

$$(u_{N+1}^{n+1} - u_{N-1}^{n+1}) - (u_2^{n+1} - u_0^{n+1}) = 0. (3.2.25)$$

Next, we proceed by segregating the terms that involve the fictitious points to the left-hand side of the equation, while retaining the remaining terms on the right-hand side:

$$u_{N+1}^{n+1} + u_0^{n+1} = u_{N-1}^{n+1} + u_2^{n+1}. (3.2.26)$$

In addition, the expression for the previous time steps for equation (3.2.26) can be expressed as follows:

$$u_{N+1}^n + u_0^n = u_{N-1}^n + u_2^n. (3.2.27)$$

By adding equations (3.2.20) and (3.2.21), we obtain the following expression:

$$-\hat{\alpha}(u_{N+1}^{n+1} + u_0^{n+1}) - \hat{\alpha}(u_{N+1}^n + u_0^n) = -(1 + 2\hat{\alpha})u_N^{n+1} + \hat{\alpha}u_{N-1}^{n+1}$$

$$+ (1 - 2\hat{\alpha})u_N^n + \hat{\alpha}u_{N-1}^n + \hat{\alpha}u_2^{n+1} - (1 + 2\hat{\alpha})u_1^{n+1} + \hat{\alpha}u_2^n + (1 - 2\hat{\alpha})u_1^n. \quad (3.2.28)$$

We define the non-fictitious part of the equation as R, which can be expressed as

follows:

$$R = -(1+2\hat{\alpha})u_N^{n+1} + \hat{\alpha}u_{N-1}^{n+1} + (1-2\hat{\alpha})u_N^n + \hat{\alpha}u_{N-1}^n$$
$$+ \hat{\alpha}u_2^{n+1} - (1+2\hat{\alpha})u_1^{n+1} + \hat{\alpha}u_2^n + (1-2\hat{\alpha})u_1^n. \quad (3.2.29)$$

By utilizing the information provided by equations (3.2.26) and (3.2.27), we can substitute the term involving fictitious points in equation (3.2.28) with the corresponding expression from equations (3.2.26) and (3.2.27). This allows us to obtain an expression that solely involves non-fictitious points, which can be expressed as follows:

$$-\hat{\alpha}(u_{N-1}^{n+1} + u_2^{n+1}) - \hat{\alpha}(u_{N-1}^n + u_2^n) = -(1 + 2\hat{\alpha})u_N^{n+1} + \hat{\alpha}u_{N-1}^{n+1}$$

$$+ (1 - 2\hat{\alpha})u_N^n + \hat{\alpha}u_{N-1}^n + \hat{\alpha}u_2^{n+1} - (1 + 2\hat{\alpha})u_1^{n+1} + \hat{\alpha}u_2^n + (1 - 2\hat{\alpha})u_1^n.$$
 (3.2.30)

We can then rearrange equation (3.2.30) to obtain the continuity of flux condition at the common vertex on two edges as follows:

$$-2\hat{\alpha}u_{N-1}^{n+1} - 2\hat{\alpha}u_{2}^{n+1} + (1+2\hat{\alpha})u_{N}^{n+1} + (1+2\hat{\alpha})u_{1}^{n+1}$$

$$= 2\hat{\alpha}u_{N-1}^{n} + 2\hat{\alpha}u_{2}^{n} + (1-2\hat{\alpha})u_{N}^{n} + (1-2\hat{\alpha})u_{1}^{n}. \quad (3.2.31)$$

The continuity of concentration at the common vertex (equation (3.2.19):  $u_N^{(1)} = u_1^{(2)}$ ) is enforced implicitly throughout our numerical scheme. When implementing the finite difference method at the junction between edges, the fictitious points (such as  $u_{N+1}^{(1)}$  and  $u_0^{(2)}$ ) are introduced and then eliminated using the flux continuity conditions. During this process, the concentration values at the common vertex are treated as a single value across all connected edges, which naturally enforces the concentration continuity.



Figure 3.2.6: Directed path graph  $P_3$  with three vertices connected by two edges.

### 3.2.4 Numerical results for a path graph $P_3$

This section presents the numerical solution of the diffusion equation

$$u_t = Du_{xx}$$

on the path graph  $P_3$  (see Figure (3.2.6), using the Crank-Nicholson method with Neumann boundary conditions and continuity of flux and concentration at a common vertex. The method and mathematical framework are consistent with those applied in Section (3.2.2). The results are summarized in Figure (3.2.7), choosing values  $\hat{\alpha} = 1.8$ ,  $\Delta t = 0.01$  and h = 0.0526 which highlights the diffusion dynamics through the following key plots:

- Figure (3.2.7)(a): This plot illustrates the evolution of the concentration profiles u(x,t) at different time steps t. The initial condition, represented as a cosine wave black curve  $\cos(\frac{\pi x}{2})$ , evolves over time toward equilibrium, with intermediate states in blue and the final state in red. This behaviour reflects the intrinsic property of the diffusion equation of minimising concentration gradients across the domain.
- Figure (3.2.7)(b): This graph shows the maximum concentration value  $\gamma = \max(u)$  over time t, with the blue line representing the numerical solution and the red dots indicating the exact solution. The red dashed line marks the initial mass, which remains constant as expected as a result of mass conservation.
- Figure (3.2.7)(c): The total mass M in the system is plotted over time, which confirms mass conservation throughout the simulation. The black line with dots demonstrates that the Neumann boundary conditions maintain the system's integrity since no mass is gained or lost.

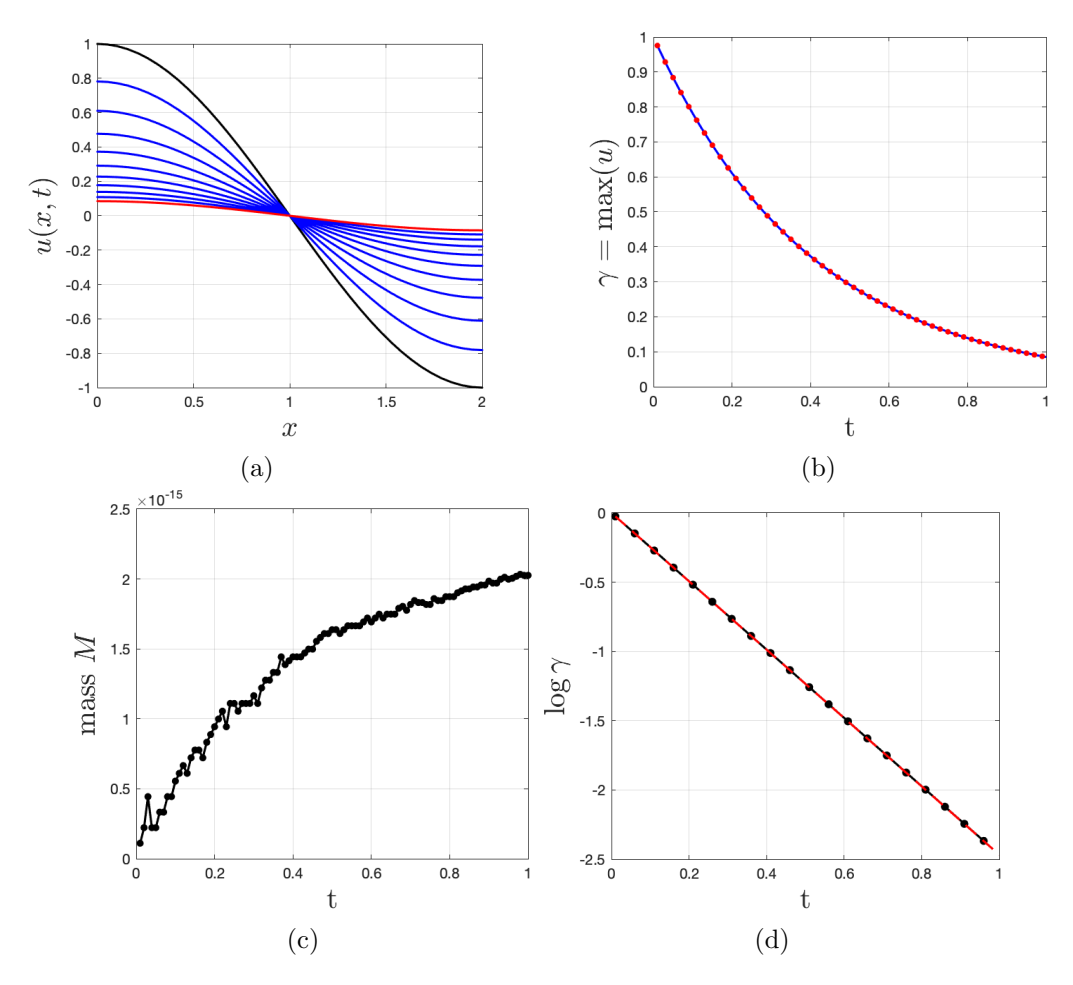


Figure 3.2.7: On the path graph  $P_3$ , figure (a): shows the concentration profile u(x,t) along the network at different time steps t, the black cure shows the initial condition, the blue cures different times, and the red curve the final step. (b): displays the maximum concentration  $\gamma$  over time t The blue curve represents the numerical solution, while red dots show the exact solution. (d): logarithmic plot of maximum concentration  $\gamma$  represent decay rate of  $\gamma$  over time t (black line with dots), and theoretical calculation of the smallest positive eigenvalue of decay rate of the modified Laplacian  $\nu$ .

• Figure (3.2.7)(d): This plot shows  $\gamma = \max(u)$  on a logarithmic scale with time t. The logarithmic scale representation provides a clear view of the decay rate, with the slope corresponding to the exponential decay rate. This rate is closely aligned with theoretical predictions based on the smallest positive decay rate of the modified Laplacian  $\nu$ , validating the numerical approach and its consistency with the analytical framework.

The numerical convergence of our results is established in Figure 3.2.8 which shows that convergence is achieved on reducing the size of the mesh spacing h,

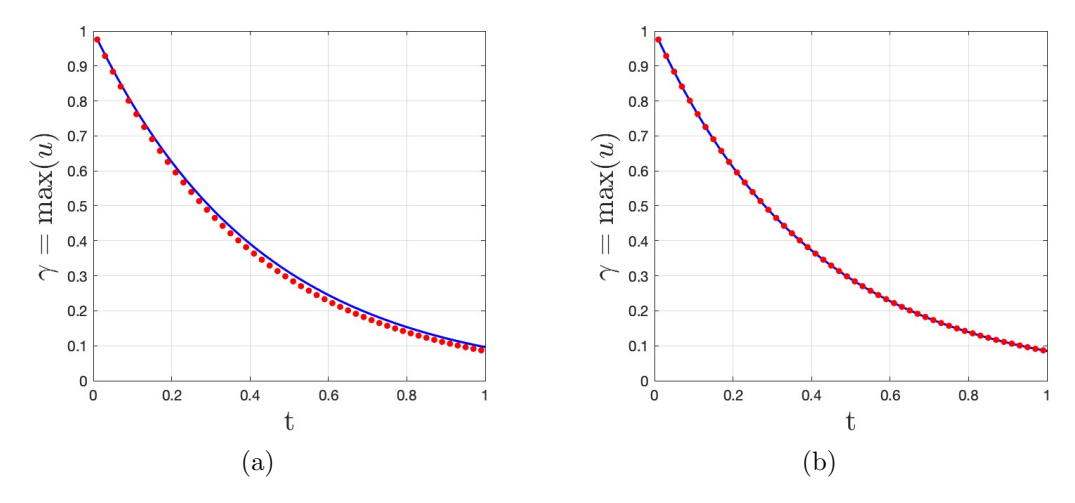


Figure 3.2.8: Numerical convergence study in h for the path graph  $P_3$ . Showing the maximum concentration  $\gamma$  over time t. The blue curve represents the numerical solution, while red dots show the exact solution. Comparison shown for: (a) h = 0.5,  $\hat{\alpha} = 0.02$ ,  $\Delta t = 0.01$ , and (b) h = 0.005,  $\hat{\alpha} = 178.6$ ,  $\Delta t = 0.01$ 

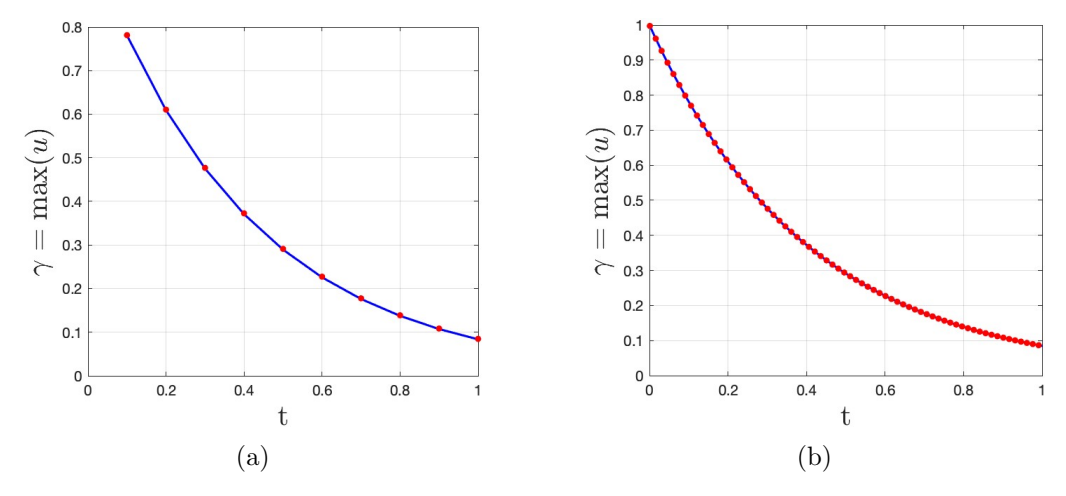


Figure 3.2.9: Numerical convergence study in  $\Delta t$  for the path graph  $P_3$ . Showing the maximum concentration  $\gamma$  over time t. The blue curve represents the numerical solution, while red dots show the exact solution. Comparison shown for: (a) h = 0.005,  $\hat{\alpha} = 178.6$ ,  $\Delta t = 0.1$ , and (b) h = 0.005,  $\hat{\alpha} = 178.6$ ,  $\Delta t = 0.001$ 

and in figure 3.2.9 which shows that convergence is achieved for fixed h and lowering  $\Delta t$ .

### 3.2.5 The general formula of the fictitious point for the continuity of flux condition for any network

Consider a network with a common vertex i having more than two connected edges. To ensure continuity of flux, we introduce the following condition:

$$\sum_{m \in S_{+}^{(i)}} q_{im}^{H} - \sum_{m \in S_{-}^{(i)}} q_{mi}^{T} = 0$$
(3.2.32)

where the sets

$$S_{-}^{(i)} = \{ j \in V : j < i \text{ and } a_{ij} = 1 \}$$

and

$$S_{+}^{(i)} = \{ j \in V : j > i \text{ and } a_{ij} = 1 \}$$

where  $S_{-}^{(i)}$  and  $S_{+}^{(i)}$  represent the sets of vertices with indices less than and greater than i, respectively, that are connected to vertex i via edges in the network. Here,  $a_{ij}$  is the ijth element of the adjacency matrix A for the network, and V is the set of all vertices in the network.

To discretise this condition, we introduce the notation  $u_i^{j,n}$ , which represents the concentration on edge j at time level  $t_n$  at discretisation point i. Each edge is discretised into N points so that point i = 1 is in the head and i = N is at the tail. We can then write (3.2.32) in discrete form and introduce fictitious points as follows:

$$\sum_{j \in C_k^H} \frac{u_2^{j,n} - u_0^{j,n}}{2h} - \sum_{i \in C_k^T} \frac{u_{N+1}^{i,n} - u_{N-1}^{i,n}}{2h} = 0, \tag{3.2.33}$$

where h is the grid spacing and

- $C_k^H$  denotes the set of elements with a vertex common to vertex k such that this common vertex lies at the head of the edge.
- $C_k^T$  denotes the set of elements with a vertex common to vertex k such that this common vertex lies at the tail of the edge.

Next we apply the diffusion equation at grid point i = N (the tail) on edge j to obtain, using Crank- Nicholson:

$$\frac{u_N^{n+1} - u_N^n}{dt} = \frac{D}{2} \left( \frac{u_{N+1}^{n+1} - 2u_N^{n+1} + u_{N-1}^{n+1}}{h^2} \right) + \frac{D}{2} \left( \frac{u_{N+1}^n - 2u_N^n + u_{N-1}^n}{h^2} \right)$$

Reorganising the terms to bring all of the fictitious points to the left hand side, we have

$$-\hat{\alpha}u_{N+1}^{j,n+1} - \hat{\alpha}u_{N+1}^{j,n} = -(1+2\hat{\alpha})u_N^{j,n+1} + \hat{\alpha}u_{N-1}^{j,n+1} + \hat{\alpha}u_{N-1}^{j,n} + (1-2\hat{\alpha})u_N^{j,n} \quad (3.2.34)$$

where

$$\hat{\alpha} = \frac{dtD}{2h^2}$$

Then, let  $R_T^j$  denote the set of terms in the discretized diffusion equation that do not involve fictitious points. Then, we can express Equation (3.2.34) as:

$$-\hat{\alpha}u_{N+1}^{j,n+1} - \hat{\alpha}u_{N+1}^{j,n} = R_T^j \tag{3.2.35}$$

where we have moved all terms involving fictitious points to the left hand side. Summing over all edges in  $C_k^T$  we obtain

$$\sum_{j \in C_k^T} \left( -\hat{\alpha} u_{N+1}^{j,n+1} - \hat{\alpha} u_{N+1}^{j,n} \right) = R_T^j$$
(3.2.36)

Similarly we apply the diffusion equation at grid point i = 1 (The head) on edge j to obtain, using Crank- Nicholson:

$$\frac{u_1^{n+1} - u_1^n}{dt} = \frac{D}{2} \left( \frac{u_2^{n+1} - 2u_1^{n+1} + u_0^{n+1}}{h^2} \right) + \frac{D}{2} \left( \frac{u_2^n - 2u_1^n + u_0^n}{h^2} \right)$$

Reorganising the terms to bring all of the fictitious points to the left hand side, we have

$$-\hat{\alpha}u_0^{j,n+1} - \hat{\alpha}u_0^{j,n} = -(1+2\hat{\alpha})u_1^{j,n+1} + \hat{\alpha}u_2^{j,n+1} + \hat{\alpha}u_2^{j,n} + (1-2\hat{\alpha})u_1^{j,n} \quad (3.2.37)$$

Let  $R_H^j$  denote the set of terms in the discretized diffusion equation that do not involve fictitious points. Then, we can express Equation (3.2.37) as:

$$-\hat{\alpha}u_0^{j,n+1} - \hat{\alpha}u_0^{j,n} = R_H^j \tag{3.2.38}$$

where, again, we have moved all terms involving fictitious points to the left hand side. Summing over all edges in  $C_k^H$  we obtain

$$\sum_{j \in C_k^H} \left( -\hat{\alpha} u_0^{j,n+1} - \hat{\alpha} u_0^{j,n} \right) = R_H^j \tag{3.2.39}$$

Now, multiplying (3.2.33) by  $2h\hat{\alpha}$  and rearranging yields

$$-\sum_{j \in C_k^H} \hat{\alpha} u_0^{j,n} - \sum_{j \in C_k^T} \hat{\alpha} u_{N+1}^{j,n} = -\hat{\alpha} \left[ \sum_{j \in C_k^H} u_2^{j,n} + \sum_{j \in C_k^T} u_{N-1}^{j,n} \right], \quad (3.2.40)$$

We define

$$P_k^n = -\hat{\alpha} \left[ \sum_{j \in C_k^H} u_2^{j,n} + \sum_{j \in C_k^T} u_{N-1}^{j,n} \right]$$
 (3.2.41)

Similarly, the next time level n + 1 can be expressed as:

$$P_k^{n+1} = -\hat{\alpha} \left[ \sum_{j \in C_k^H} u_2^{j,n+1} + \sum_{j \in C_k^T} u_{N-1}^{j,n+1} \right]$$
 (3.2.42)

Next we add (3.2.39) to (3.2.36) to obtain

$$\sum_{j \in C_k^T} \left( -\hat{\alpha} u_{N+1}^{j,n+1} - \hat{\alpha} u_{N+1}^{j,n} \right) + \sum_{j \in C_k^H} \left( -\hat{\alpha} u_0^{j,n+1} - \hat{\alpha} u_0^{j,n} \right) = R_T^j + R_H^j. \quad (3.2.43)$$

Rearranging slightly, we have

$$\left(-\sum_{j \in C_k^T} \hat{\alpha} u_{N+1}^{j,n+1} - \sum_{j \in C_k^H} \hat{\alpha} u_0^{j,n+1}\right) + \left(-\sum_{j \in C_k^T} \hat{\alpha} u_{N+1}^{j,n} - \sum_{j \in C_k^H} \hat{\alpha} u_0^{j,n}\right) = R_T^j + R_H^j.$$
(3.2.44)

Using (3.2.41), (3.2.42) and (3.2.40) into (3.2.44), the continuity of flux condition

for any common vertex in network with fictitious points becomes:

$$P_k^{n+1} + P_k^n = R_T^j + R_H^j (3.2.45)$$

We consider the continuity of concentration as we discussed in section 3.2.3. This condition is not explicitly imposed as a separate constraint at common vertices, but rather is implicitly enforced when we formulate the flux continuity conditions. When fictitious points  $(u_{N+1}^{(j)} \text{ or } u_0^{(j)})$  are introduced and then eliminated using equations (3.2.32)-(3.2.45), the resulting numerical scheme naturally preserves the concentration continuity at all common vertices.

### 3.2.6 Initial condition

In the next few sections we will present some numerical computations over different networks including a Y-shaped graph, a  $3 \times 3$  square grid graph, and a  $6 \times 6$  square grid graph. In each case we choose an initial condition that corresponds either to an eigenfunction of the eigenvalue problem discussed in Chapter 2 or to a more general initial condition to be discussed below.

In the former case, selecting an initial condition at t=0 that corresponds to an eigenfunction means that the time evolution in the numerical calculation will follow that eigenfunction (to within numerical error) for all t>0. This is true because the diffusion problem is linear. We can therefore use this as a check on our numerical method to confirm that the decay rate computed numerically by integrating forwards in time agrees with that computed by solving the normalised Laplacian eigenvalue problem.

More generally, if we do not want to follow an eigenfunction throughout the calculation, we may start from a general initial condition that does not correspond to an eigenfunction. In setting this initial condition we must be careful to respect the continuity conditions at the network vertices (including both common and boundary vertices), that is our initial condition must satisfy continuity of flux and

continuity of concentration; otherwise the numerical implementation discussed earlier will simply propagate the discontinuity throughout the calculation. With this in mind on each edge of the network we demand that the concentration on the j edge of the network is equal to  $U_0(\xi)$ ,  $0 \le \xi \le 1$ , where

$$U_0(\xi) = \cos(2\pi i \xi) \tag{3.2.46}$$

Note that initial condition (3.2.46) guarantees continuity at every vertex, irrespective of the network structure, by setting the initial concentration at each vertex to unity and the initial concentration gradient at each vertex equal to zero. The index j is included in (3.2.46) to prevent it from coincidentally conforming to an eigenfunction. For example for a Y-shaped graph as depicted in Figure 3.2.10 one of the eigenvalues is  $\nu = 2\pi$  corresponding to the eigenfunction (2.2.19), namely  $\cos(2\pi\xi)$ .

One practical issue with the initial condition (3.2.46) is that for a graph with many edges j becomes potentially large and this creates an initial profile across the network that is difficult to resolve without a large number of collocation points. Therefore, for a graph with more than a certain number of edges we prefer to impose the condition

$$U_0(\xi) = \cos(2\pi j^* \xi), \tag{3.2.47}$$

where

$$j^* = \begin{cases} 1 & \text{if } j = 2\\ 0 & \text{if } j \neq 2. \end{cases}$$

This also precludes the possibility of the initial condition coinciding with an eigenfunction whilst simultaneously restricting the size of the frequency of the assumed cosine profile.

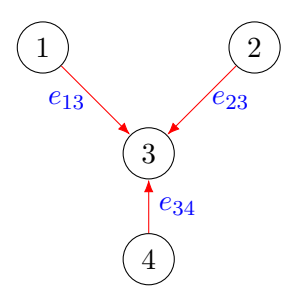


Figure 3.2.10: Y-shape graph with four vertices and three edges

### 3.2.7 Numerical results for the Y-shaped graph

In this section, we extend our analysis to a Y-shaped graph (see figure 3.2.10). The graph consists of a central common vertex connected to three boundary vertices by three edges.

The method and mathematical framework are consistent with those applied in Section (3.2.2). The methodology is adapted to the topology of the Y-shaped graph by recalculating the modified Laplacian matrix  $L^*$ . The eigenfunctions and eigenvalues are computed for this topology, and the dynamics of the diffusion process are analysed using both specific eigenfunctions and a general initial condition. We also verify that the total mass, represented by the integral of u(x,t) across the entire network, remains constant over time, confirming the mass-preserving nature of the Crank-Nicholson method under Neumann boundary conditions. The results of the analyses are discussed in the following way:

- The eigenvalues of the modified Laplacian matrix, denoted as  $\lambda$ , and their corresponding decay rate are (see table 3.1):
- For the eigenvalue  $\lambda = -1$ , we have the corresponding decay rate  $(\nu = \pi)$ , the eigenfunction corresponding to this eigenvalue was chosen as the initial condition. The results in Figure (3.2.11) (a) show the concentration profile of the diffusion equation on the Y-shaped graph. The black curve represents the initial condition, the blue curves show intermediate time steps, and the red curve represents the final time step. Figure 3.2.11 (b) shows the

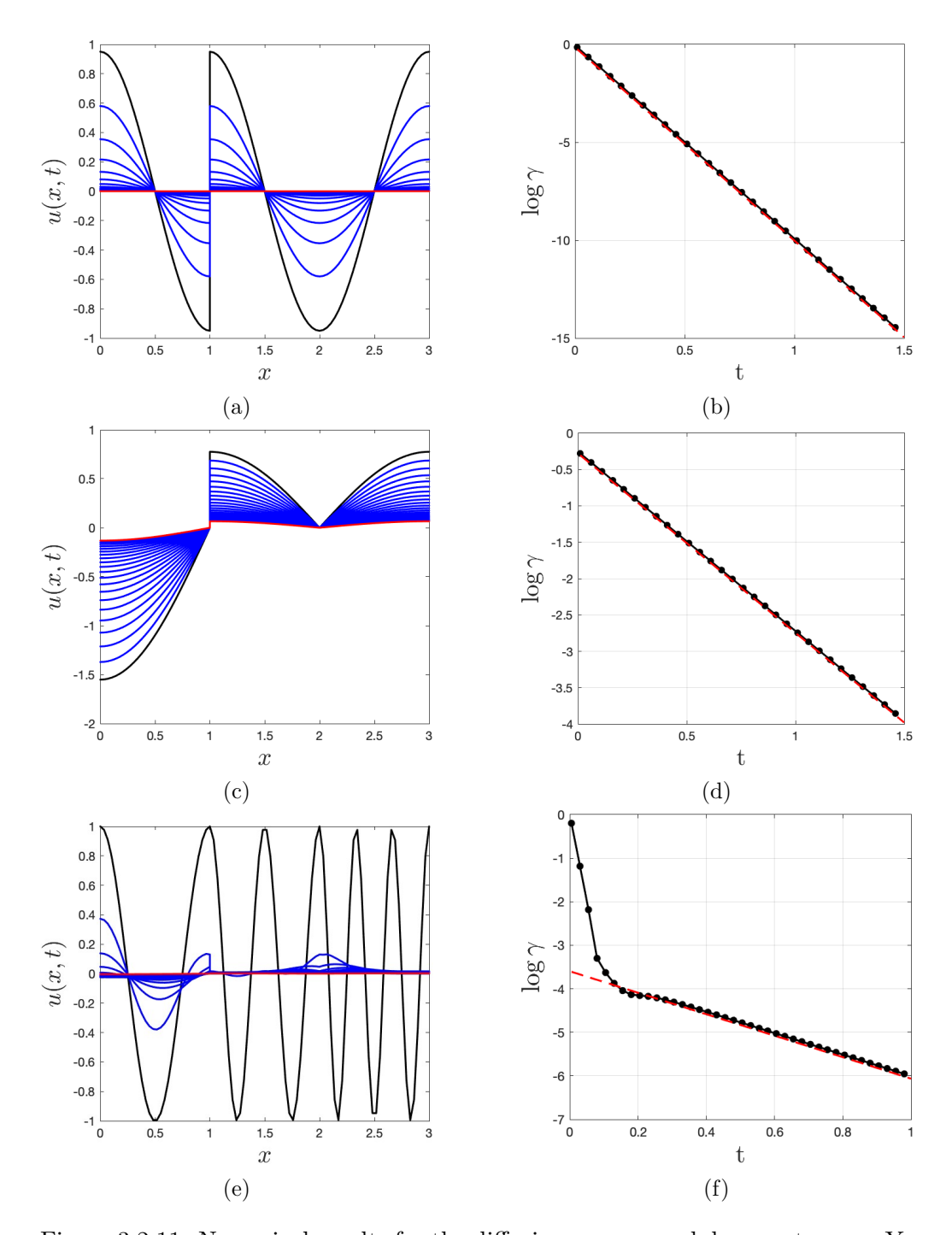


Figure 3.2.11: Numerical results for the diffusion process and decay rates on a Y-shaped graph. (a, c, e): Concentration profiles u(x,t) for different eigenfunctions and initial conditions. The black curve shows the initial condition, blue curves represent intermediate time steps, and the red curve represents the final time step. (b, d, f): Decay rates of the maximum concentration  $\gamma$  over time t. The black line with dots represents the numerical decay rate, while the red dashed line represents the theoretical decay rate. (b),  $\lambda = -1, \nu = \pi$ , the red dashed line has slope  $-\pi^2$ . (d)  $\lambda = 0, \nu = \pi/2$ : the red dashed line has slope  $-\pi^2/4$ . (f) Taking initial condition (3.2.46): the red dashed line has slope  $-\nu_1^2 = -\pi^2/4$ .

λ	multiplicity	ν
-1	1	$\pi$
0	2	$\pi/2$
1	1	0

Table 3.1: The eigenvalue  $\lambda$  of the modified Laplacian  $\mathbf{L}^*$  and their corresponding  $\nu$  for square grid graph Y-shaped graph.

decay rate of the chosen eigenfunction, demonstrating excellent agreement between the numerical decay rate (black line) and the theoretical prediction (red line).

- For the eigenvalue  $\lambda=0$ , we have the corresponding decay rate ( $\nu=\pi/2$ ), the eigenfunction corresponding to this eigenvalue was used as the initial condition. The results, shown in Figure (3.2.11) (c), the concentration profile of this case . Figure 3.2.11 (d) confirms the perfect match between the numerical (black line with dots) and theoretical decay rates (red line).
- Figure 3.2.11 (e, f) shows the result for the initial condition (3.2.46) that does not correspond to an eigenfunction. The concentration is shown in Figure 3.2.11(e), while Figure 3.2.11(f) shows the decay of maximum concentration γ with time. Two points are striking in the latter panel. First, the solid black curve eventually aligns with with red dashed curve. The latter has slope equal to the smallest decay rate. Hence, the solution ultimately settles to decay at the minimum decay rate. Second, the initial slope of the black line is much steeper than that of the red dashed line, suggesting that the initial decay is much more rapid than the ultimate decay at the smallest value of ν. This can be explained by noting that γ, the maximum concentration, can be expressed as a linear combination of all of the eigenfunctions for the network, namely,

$$\gamma = \sum_{n=1}^{\infty} c_n e^{-\nu_n^2 t}$$

for some coefficients  $c_n$ . Thus

$$\left. \frac{d\gamma}{dt} \right|_{t=0} = -\sum_{n=1}^{\infty} c_n \nu_n^2$$

(assuming the series converges). Then

$$\left. \frac{d\log \gamma}{dt} \right|_{t=0} = \left. \frac{d\gamma/dt}{\gamma} \right|_{t=0} = -\frac{\sum_{n=1}^{\infty} c_n \nu_n^2}{\sum_{n=1}^{\infty} c_n}$$

This corresponds to the slope of the black line in Figure 3.2.11(f) at t = 0. Evidently

$$\frac{\sum_{n=1}^{\infty} c_n \nu_n^2}{\sum_{n=1}^{\infty} c_n} > \nu_1^2.$$

This holds because

$$\sum_{n=1}^{\infty} c_n \nu_n^2 > \nu_1^2 \sum_{n=1}^{\infty} c_n,$$

since  $\nu_1 > \nu_2 > \nu_3 \cdots$ .

In conclusion, the decay rate of the chosen eigenfunctions agrees with the theoretical decay rates, as the eigenfunctions correspond to specific eigenvalues of the system's Laplacian matrix, determining their respective decay rates in the diffusion process. Furthermore, for a general initial condition, the function is expressed as a linear combination of eigenfunctions, each decaying independently at a rate determined by its eigenvalue. This results in an overall decay dominated by the slowest-decaying mode in the long term. The agreement between the numerical results (black lines) and the theoretical predictions (red lines) confirms the accuracy of the Crank-Nicholson method and the theoretical framework.

### 3.2.8 Numerical results for square grid graph $3 \times 3$

In this section, we solve the diffusion equation

$$u_t = Du_{xx}$$

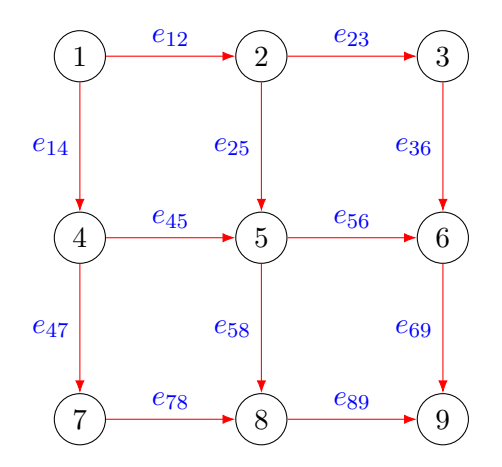


Figure 3.2.12: Square grid graph  $3 \times 3$ .

numerically on a square grid graph  $3 \times 3$  (see Figure 3.2.12), using the Crank-Nicholson method with Neumann boundary conditions and continuity of flux and concentration at common vertices. The method and mathematical framework are consistent with those applied on the Y-shaped graph.

To analyse the behaviour, we start by selecting specific eigenfunctions as initial conditions. The eigenfunctions correspond to the eigenvalues of the modified Laplacian matrix of the system  $L^* = A - \lambda D$ , where  $\cos(\nu) = \lambda$ . The results are summarised as follows:

• The eigenvalues of the modified Laplacian matrix, denoted as  $\lambda$ , and their corresponding decay rate are (see table 3.2):

λ	multiplicity	ν
-1	1	$\pi$
-0.5774	2	2.1863
0	3	$\pi/2$
0.5774	2	0.9553
1	1	0

Table 3.2: The eigenvalue  $\lambda$  of the modified Laplacian  $L^*$  and their corresponding  $\nu$  for square grid graph  $3 \times 3$ .

• For the eigenvalue  $\lambda = -1$  (corresponding to  $\nu = \pi$ ), the eigenfunction

that corresponds to that eigenvalue was chosen as the initial condition for the calculation. The result in Figure (3.2.13)(a) shows the concentration profiles u(x,t) at various time steps t. The initial condition, represented as the black curve, evolves over time with intermediate states (blue) and the final state (red). This behaviour reflects the tendency of the diffusion equation to reduce concentration gradients. Figure (3.2.13)(b) shows logarithmic plot of the maximum concentration  $\gamma = \max(u)$  over time, revealing the decay rate. The slope corresponds to the exponential decay rate, aligning with the theoretical prediction for the chosen eigenfunction. This validates the ability of the Crank-Nicholson method to capture the decay dynamics of the system accurately.

- For λ = -0.5774 (corresponding to ν = 2.1863), the other eigenfunction has been chosen as an initial condition for the calculation. Figure (3.2.13)(c): This plot shows the concentration profiles u(x,t) in various time steps t. The initial condition, represented as a black curve, evolves over time, with intermediate states in blue and the final state in red. Figure (3.2.13)(d): The logarithmic plot of the maximum concentration γ = max(u) over time reveals the decay rate. The slope corresponds to the exponential decay rate, aligning with the theoretical prediction for the chosen eigenfunction.
- Figure (3.2.13)(e,f) we use the same methodology as the Y-shaped graph for the initial condition that does not correspond to the eigenfunction. we set the initial condition to satisfy the continuity of flux and concentration condition as we discussed in detailed on section (3.2.7). The concentration is shown in Figure 3.2.13(e), while Figure 3.2.13(f) shows the decay of maximum concentration γ with time. Two points are striking in the latter panel. First, the solid black curve eventually aligns with with red dashed curve. The latter has slope equal to the smallest decay rate. Hence, the solution ultimately settles to decay at the minimum decay rate. Second, the initial slope of the black line is much steeper than that of the red dashed line, suggesting that the initial decay is much more rapid than the ultimate

decay at the smallest value of  $\nu$  that is explained in section (3.2.7).

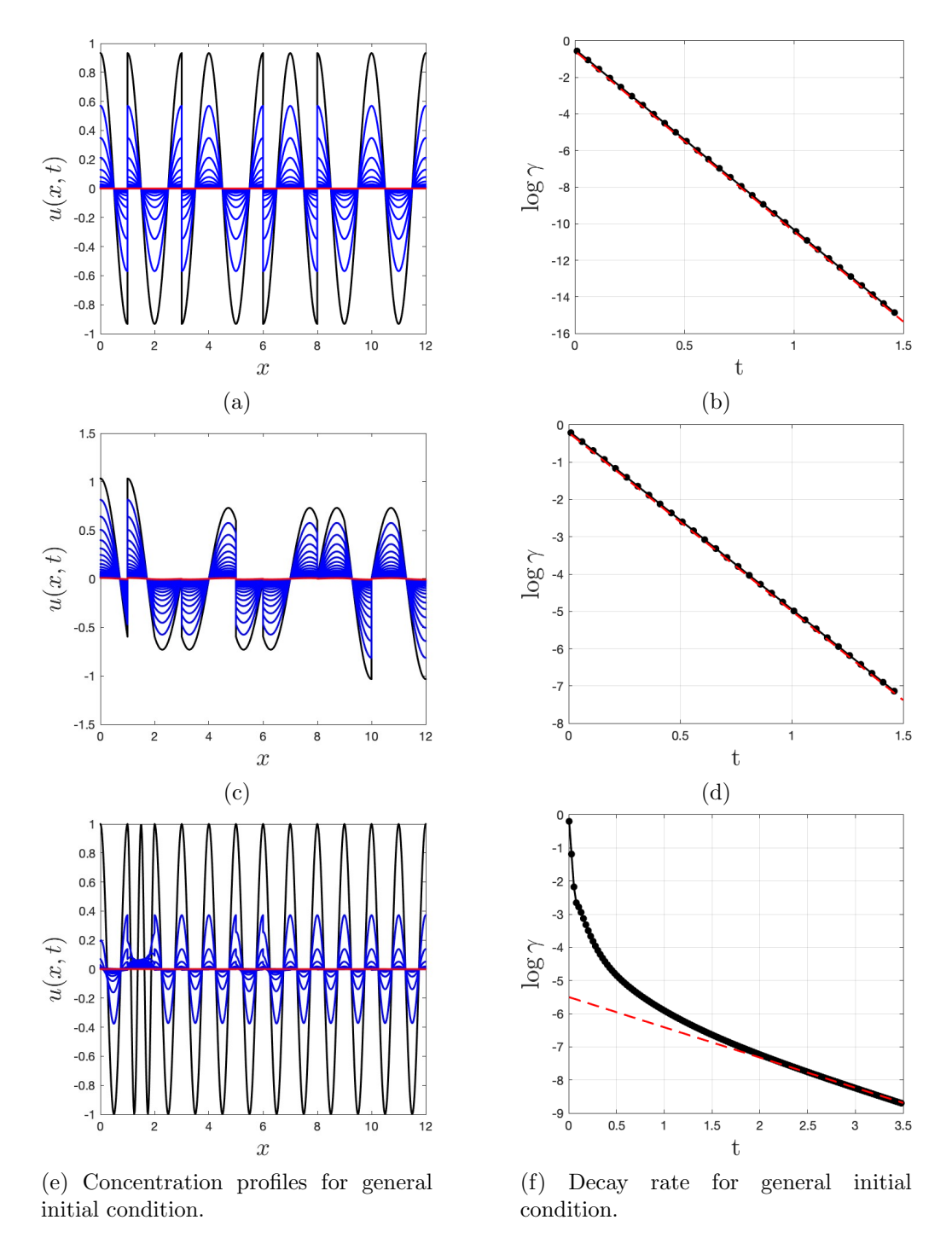


Figure 3.2.13: Numerical results for the diffusion process and decay rates on a  $3\times 3$  square grid graph. (a, c, e) are the concentration profile u(x,t) along the network at different time steps t for different eigenfunction and initial condition. The black cure shows the initial condition, blue curves represent intermediate time steps, and the red curve represents the final time step. (b, d, f) are the decay rates of maximum concentration  $\gamma$  over time t. (black line with dots) represents the numerical decay rate , and theoretical decay rates represented by red dashed. (b)  $\lambda = -1$ , and  $\nu = \pi$ , the red dashed line has slop  $-\pi^2$ . (d)  $\lambda = -0.5774$ , and  $\nu = 2,1863$ , the red dashed line has slop  $-\pi^2$ . (f) the initial condition (3.2.47) the red dashed line has a slope  $-(0.9553)^2$ .

### 3.2.9 Numerical results for square grid graph $6 \times 6$

In this section, we extend our analysis to a larger square grid graph  $6 \times 6$ . This graph consists of 36 vertices and 60 edges. The diffusion equation

$$u_t = Du_{xx}$$

is solved numerically using the Crank-Nicholson method, imposing Neumann boundary conditions and ensuring the continuity of flux and concentration at all common vertices.

We maintain the same methodology as for the  $3 \times 3$  grid graph, but adapt the system to account for the increased number of vertices and edges in the  $6 \times 6$  graph. The modified Laplacian matrix  $L^*$  is recalculated to reflect the new topology, with the eigenfunctions and eigenvalues adjusted accordingly. We analyse the dynamics using both eigenfunctions as initial conditions and general initial conditions. Furthermore, we verify that the total mass, represented by the integral of u(x,t) throughout the network, remains constant over time, confirming that the Crank-Nicholson method preserves mass as expected for a diffusion process governed by Neumann boundary conditions.

- The eigenvalues of the modified Laplacian matrix, denoted as  $\lambda$ , and their corresponding decay rate  $\nu$  are (see table 3.3):
- For the eigenvalue  $\lambda=0.8090$  (corresponding to  $\nu=0.6283$ ), the eigenfunction that corresponds to that eigenvalue was chosen as the initial condition for the calculation. The result in Figure (3.2.14)(a) shows logarithmic plot of the maximum concentration  $\gamma=\max(u)$  over time, revealing the decay rate. The slope corresponds to the exponential decay rate (black line with dots), aligning with the theoretical prediction for the chosen eigenfunction (red dash). the red dashed line has a slop  $-(0.6283)^2$ .

λ	multiplicity	ν
-1	1	$\pi$
-0.9128	2	2.7209
-0.8090	1	2.5132
-0.6863	2	2.3272
-0.5621	2	2.1677
-0.4043	2	1.9870
-0.3090	1	1.8849
-0.2591	2	1.8329
-0.1562	2	1.7276
0	6	$\pi/2$
0.1562	2	1.4140
0.2591	2	1.3087
0.3090	1	1.2567
0.4043	2	1.1546
0.5621	2	0.9739
0.6863	2	0.8144
0.8090	1	0.6283
0.9128	2	0.4207
1	1	0

Table 3.3: The eigenvalue  $\lambda$  of the modified Laplacian  $L^*$  and their corresponding  $\nu$  for square grid graph  $6 \times 6$ .

- For λ = 0.9128 (corresponding to ν = 0.4208), the other eigenfunction has been chosen as an initial condition for the calculation. Figure (3.2.14)(b)
   The logarithmic plot of the maximum concentration γ = max(u) over time reveals the decay rate. The slope corresponds to the exponential decay rate (black line with dots), aligning with the theoretical (red dash) prediction for the chosen eigenfunction. the red dashed line has a slop -(0.4208)².
- Figure (3.2.13)(c) we use the same methodology as the Y-shaped graph for the initial condition that does not correspond to the eigenfunction. we

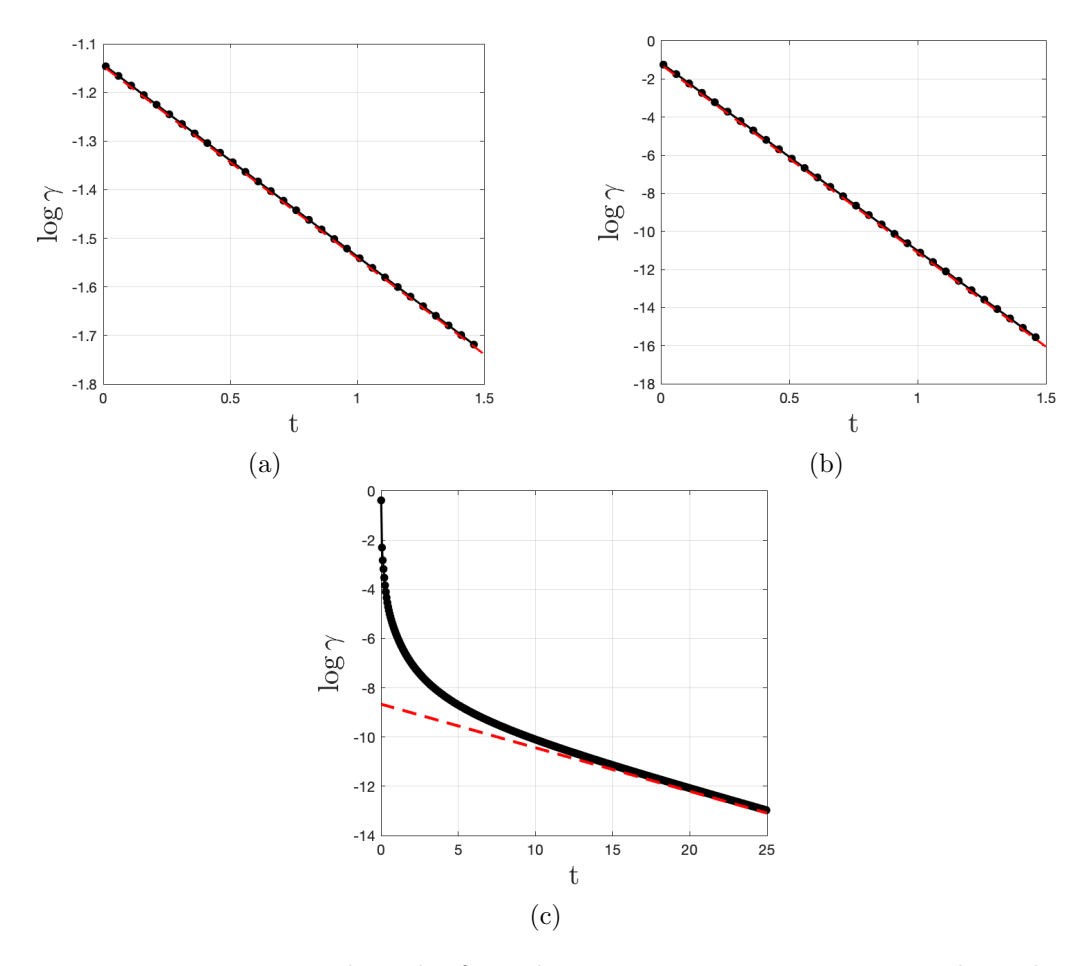


Figure 3.2.14: Numerical results for a decay rates on a  $6 \times 6$  square grid graph. (a, b, c) are the decay rates of maximum concentration  $\gamma$  over time t. (black line with dots) represents the numerical decay rate , and theoretical decay rates represented by red line dashed. (a)  $\lambda = 0.8090$ , and  $\nu = 0.6283$ , the red dashed line has slope  $-(0.6283)^2$ . (b)  $\lambda = -1$ , and  $\nu = \pi$ , the red dashed line has slope  $-(0.4208)^2$ .

set the initial condition to satisfy the continuity of flux and concentration condition as we discussed in detail in section (3.2.7). The figure shows the decay of maximum concentration  $\gamma$  with time. Two points are striking in the latter panel. First, the solid black curve eventually aligns with the red dashed curve. The latter has a slope equal to the smallest decay rate. Hence, the solution eventually settles and decays at the minimum decay rate. Second, the initial slope of the black line is much steeper than that of the red dashed line, suggesting that the initial decay is much more rapid than the ultimate decay at the smallest value of  $\nu$  which is explained in Section (3.2.7).

In conclusion, the decay rate of the chosen eigenfunction agrees with the theoretical decay rate because the eigenfunction corresponds to a specific eigenvalue of the system's Laplacian matrix, which determines the rate at which that mode decays in the diffusion process. Furthermore, if the initial condition is a general function, it can be expressed as a linear combination of the eigenfunctions of the Laplacian matrix. Each eigenfunction will decay independently at a rate determined by its corresponding eigenvalue. Consequently, the overall decay behaviour of the system will be governed by a combination of these rates, with the slowest decay mode (associated with the smallest non-zero eigenvalue) dominating the long-term dynamics of the diffusion process. This explains the observed agreement between the black line, representing the decay rate of the chosen function, and the red line, representing the theoretical calculation.

# Reaction-diffusion equation on network

In this chapter, we solve the reaction-diffusion equations in a network. We use the method of lines to discretise the spatial domain into a grid and transform the reaction-diffusion equation into a system of ordinary differential equations. This allows us to efficiently solve the system using standard numerical integration techniques. We focus on enforcing continuity of flux and concentration at common vertices, as well as zero-flux boundary conditions at boundary vertices. The approach is applied to various networks, starting from simple path graphs and extending to more complex structures.

The numerical results for the dynamic behaviour of concentration are obtained using MATLAB and analysed in detail. In particular, we explore the stability of steady-state solutions for the reaction-diffusion equation. Numerical decay rates obtained using the method of lines are compared with the theoretical predictions derived from the eigenvalues of the modified Laplacian matrix, as discussed in Chapter (2). This provides a comprehensive understanding of both the dynamic and steady-state behaviours of reaction-diffusion systems on networks.

### 4.1 Reaction diffusion equation

Reaction—diffusion equations have been used primarily in chemical physics to model the evolution of concentration and temperature distributions in reactive and diffusive systems. The theoretical foundations of reaction—diffusion waves were established in the 1930s by works by Fisher and Kolmogorov, Petrovskii, Piskunov on the propagation of the dominant gene, and Zeldovich, Frank-Kamenetskii in combustion theory. They have introduced the scalar reaction—diffusion equation:

$$u_t(x,t) = u_{xx}(x,t) + f(u),$$
 (4.1.1)

where f(u) represents the reaction term [44]. This equation serves as the foundation for understanding a wide variety of phenomena, including wave propagation in biological, chemical, and physical systems.

The Fisher equation shows the interplay between non-linear reaction mechanisms and spatial diffusion, which leads to phenomena such as wave propagation and spatial patterning.

$$u_t(x,t) = u(1-u) + Du_{xx}(x,t), (4.1.2)$$

where u(x,t) represents the concentration of chemical, u(1-u) is a given function representing a reaction term which describes the growth dynamics, and D is the diffusion [18]. We aim to solve this equation using the Method of Lines under Neumann boundary conditions, continuity constraints, and continuity of flux at common vertices, enabling the analysis of the dynamic behaviour throughout the entire network.

Before presenting a discussion of the Method of Lines and its implementation for a network, it is instructive to first discuss the possible equilibria and stability thereof associated with the reaction-diffusion equation, and the particular form of the Fisher equation. This we do in the next section.

## 4.2 Steady-state and stability analysis for the reaction-diffusion equation

In this section we discuss the possible steady states, for which u = u(t), that can occur for the reaction-diffusion equation. The next subsection is devoted to this point. The following two subsections discuss stability.

### 4.2.1 Steady states for the reaction-diffusion equation

We consider the partial differential equation

$$u_t = f(u) + Du_{xx},$$
 (4.2.1)

For definiteness we examine the possibility of steady states, u(t), for the graph  $P_2$ , that is over the domain  $0 \le x \le 1$ . The boundary conditions  $u_x(0,t) = u_x(1,t) = 0$  are imposed. In particular we investigate the behaviour of the solution as t tends to infinity on a one-edge graph, namely  $P_2$ . In particular we wish to decide whether or not the solution u(x,t) can approach a steady state.

Evidently a uniform steady state  $u = U^*$ , a constant, is possible provided that

$$f(U^*) = 0, (4.2.2)$$

and this depends on the existence of zeros for the function f. In any case our particular interest here is in non-uniform, that is, spatially-varying, steady states of the form u = U(x), for some U(x).

If such a steady state exists then it is the infinite time limit of the solution to equation (4.2.1), i.e.

$$\lim_{t \to \infty} u(x, t) = U(x).$$

From (4.2.1) we have that

$$0 = f(U) + DU'', (4.2.3)$$

where a prime denotes a derivative with respect to x.

We define the spatially-averaged value, m(t), of u(x,t) over the domain  $0 \le x \le 1$  to be

$$m = \int_0^1 u(x,t) \, dx. \tag{4.2.4}$$

Integrating equation (4.2.1) over the spatial domain, and making use of the boundary conditions, we obtain an expression relating the time derivative of m to the integral of f(u) over the domain

$$\frac{dm}{dt} = \int_0^1 f(u) \, dx. \tag{4.2.5}$$

At steady state, we have

$$\frac{dm}{dt} = 0,$$

yielding from (4.2.5) the following equation

$$\int_0^1 f(U) \, dx = 0. \tag{4.2.6}$$

It is clear from this result that f(U) must change sign in  $0 \le x \le 1$ .

At this point we specialise to the particular case

$$f(U) = U(1 - U), (4.2.7)$$

that is the form of the reaction term in the Fisher equation (4.1.2). In this case we shall now show that no spatially non-uniform steady states can exist. Equation (4.2.6) becomes

$$\int_0^1 U(1-U) \, dx = 0. \tag{4.2.8}$$

In Figure 4.2.1 we sketch the integrand against U. Evidently for (4.2.8) to hold we will need 0 < U < 1 over some portion of the domain  $0 \le x \le 1$ , and U > 1 over some other portion, in order to ensure that f changes sign (note that we do not allow U < 0, which we consider to be unphysical). In Figure 4.2.2 we sketch

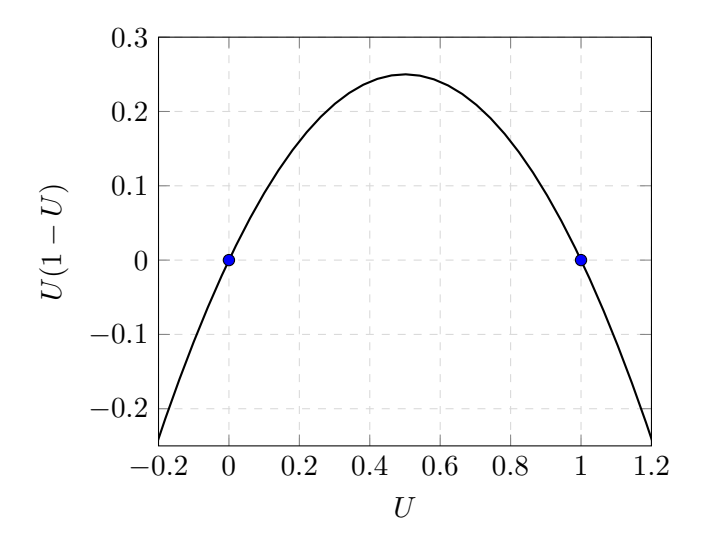


Figure 4.2.1: Sketch of the Fisher equation reaction term f(U) = U(1-U) against U showing regions where f(U) is positive (0 < U < 1) and negative (U < 0) and U > 1.

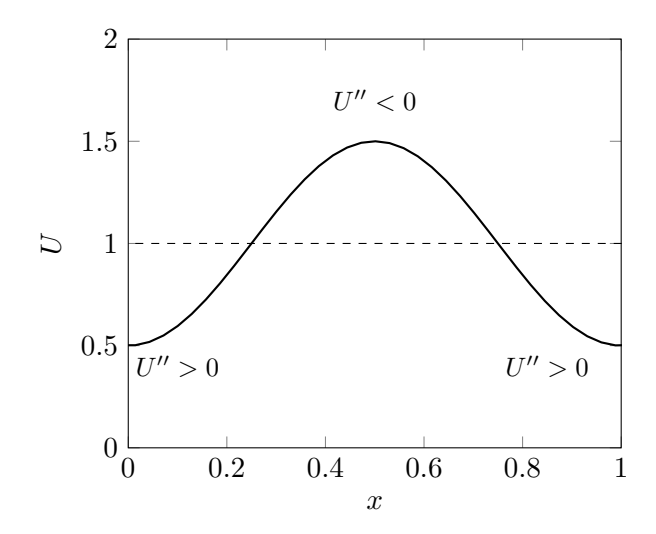


Figure 4.2.2: Sketch of one conceivable steady state configuration U(x).

the type of scenario envisaged. Also included in the sketch is the sign of U''. Now from (4.2.3) it must be the case that the sign of U'' must be opposite to the sign of f(U) (since D > 0). This means that in the region in Figure 4.2.2 where U'' < 0 we must have f(U) > 0. But, U > 1 in this region and, according to the sketch in Figure 4.2.1, when U > 1 we have f(U) < 0 yielding a contradiction. The same contradiction will be reached for any smooth U(x) and we conclude therefore that no steady state is possible.

In the case of the Fisher reaction term f(U) = U(1 - U), then, the steady-state

solution must be constant across the domain. There are two possible steady states, and these are

$$U = 0$$
 and  $U = 1$ . (4.2.9)

An important question now arises. Which of these two states is stable? This question will be addressed in the next section.

### 4.2.2 Stability analysis for the reaction-diffusion equation on a network

In (4.2.9) we noted that for the Fisher equation there are two possible steady states, namely u = 0 and u = 1. While that section was devoted to the graph  $P_2$ , it is clear that either of the steady states in (4.2.9) can be attained in principle on any network. Therefore, in this section, we analyse the stability of the steady states but broaden the discussion to encompass any network.

We maintain our focus on the Fisher equation, namely

$$u_t = u(1 - u) + Du_{xx}. (4.2.10)$$

Numerical calculations discussed later in this chapter suggest that in some cases as  $t \to \infty$ , the concentration u tends to 1. This suggests that the steady state u = 1 is stable, while u = 0 is possibly unstable. Herein we analyse carefully the stability of both steady states. Our results will be compared with the results of numerical calculations later in the chapter.

To analyse the stability near to u = 0, we assume u is small so that  $|u| \ll 1$ . Linearising (4.2.10) on this basis we obtain

$$u_t = u + Du_{xx}.$$
 (4.2.11)

To solve, we consider a solution of the form  $u = e^t q(t, x)$ , which leads upon

substitution into (4.2.11) to:

$$e^t q + e^t q_t = e^t q + De^t q_{xx}.$$

Simplifying, we obtain the diffusion equation:

$$q_t = Dq_{xx}. (4.2.12)$$

The decay rates of the diffusion equation on a network were discussed at length in chapter (2). As discussed there, these are computed by first determining the eigenvalues of the associated modified Laplacian matrix,  $L^*$  – see section (2.3.1). We know from section (2.2.5) that  $\nu = \mu \beta$ , and  $\beta = \frac{L^2}{D}$ . Assuming D = L = 1, then  $\beta = 1$  and the decay rate is given by  $\nu^2$ , that is q will behave like  $e^{-\nu^2 t}$ . Consequently, u behaves as:

$$e^{(1-\nu^2)t}. (4.2.13)$$

If  $1 - \nu^2 > 0$  for any network eigenvalue  $\nu$ , the steady state u = 0 is unstable; otherwise if  $1 - \nu^2 < 0$  for all network eigenvalues then the steady state u = 0 is stable. However, it is not possible that  $1 - \nu^2 < 0$  for all eigenvalues across a network. For we know that the diffusion problem on any network must have an eigenvalue corresponding to the zero decay rate  $\mu = 0$ . In this case  $1 - \nu^2 = 1$  which is positive.

To analyse the stability near to u=1, we write v=1-u and aim to determine v. In particular we will assume that v is small so that  $|v| \ll 1$ . Linearising (4.2.10) on this basis we obtain

$$v_t = -v + Dv_{xx}. (4.2.14)$$

To solve, we consider a solution of the form  $v=e^{-t}q(t,x)$ , which leads upon substitution into (4.2.14) to:

$$-e^{-t}q + e^{-t}q_t = -e^{-t}q + De^{-t}q_{xx}.$$

Simplifying, we obtain the diffusion equation:

$$q_t = Dq_{xx}. (4.2.15)$$

As mentioned above, the decay rates of the diffusion equation on a network were discussed at length in chapter (2). However, it makes no difference to the outcome here since as q behaves like  $e^{-\nu^2 t}$  it follows that v behaves as

$$e^{-(1+\nu^2)t},$$
 (4.2.16)

and hence, since  $1 + \nu^2 > 0$  irrespective of the network eigenvalue  $\nu$ , the steady state u = 1 is stable.

We can generalise this argument for any reaction-diffusion equation of the form

$$u_t = f(u) + Du_{xx}, (4.2.17)$$

where f is a non-linear function of u. Suppose for illustration that f(u) = 0 is satisfied by  $u = u^*$ , a constant, i.e.  $u = u^*$  is steady state of the system. In this case the linearisation procedure carried out above will lead to the linearised form

$$v_t = f'(u^*)v + Dv_{xx}. (4.2.18)$$

Making the same change of variable as before from v to q we again obtain the diffusion equation, and this time the conclusion that for large t, u behaves as

$$e^{(m-\nu^2)t}$$
,

where  $m = f'(u^*)$ . The stability then depends on the sign of  $m - \nu^2$ . In particular, if  $m - \nu^2$  is positive for any eigenvalue  $\nu$  then the steady state  $u = u^*$  is unstable.

Network Shape	$ u_{ m min}$	Network topology
1 2	$\pi$	Path graph $P_2$

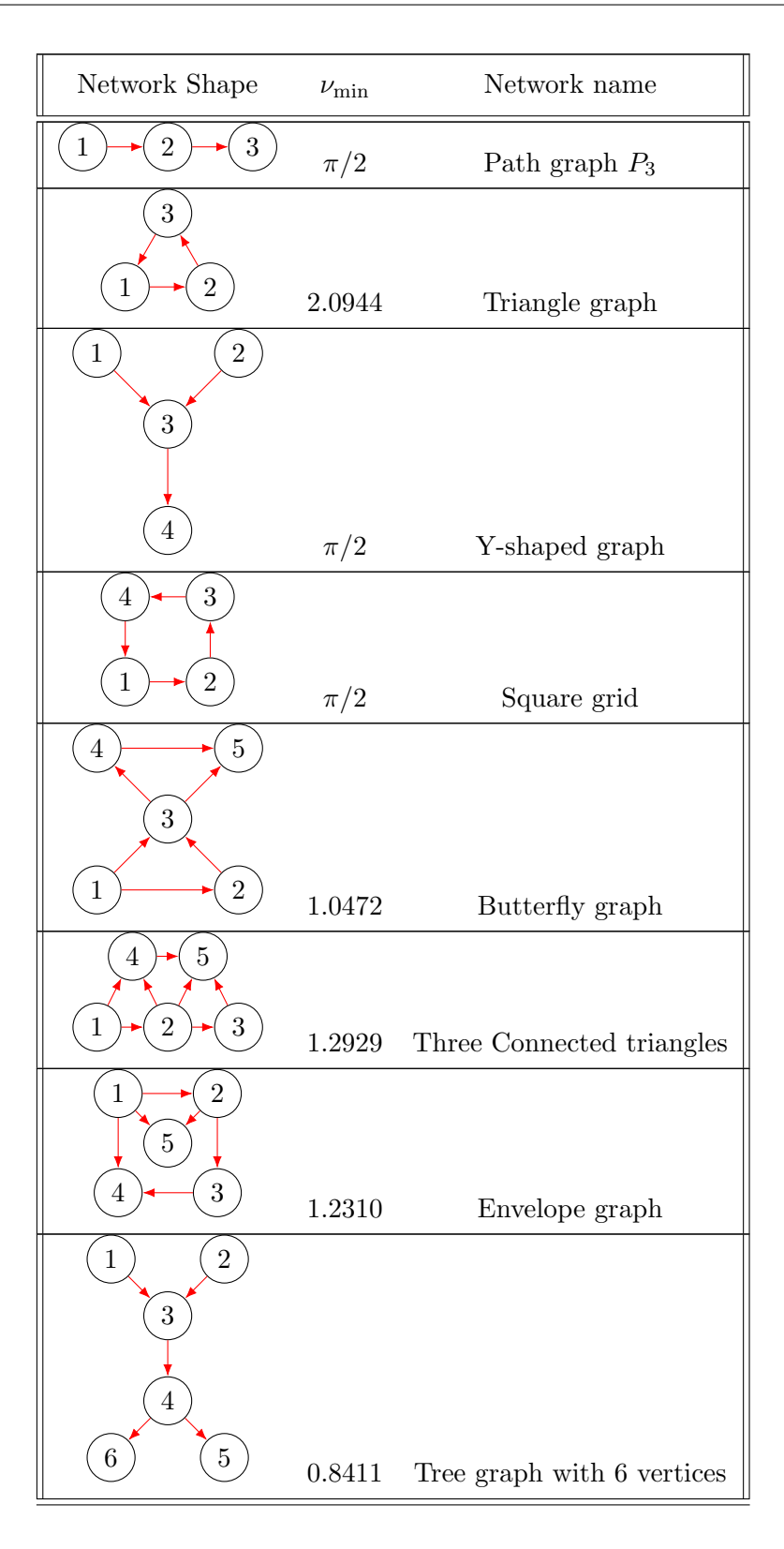


Table 4.1: The smallest decay rate  $\nu_{\min}$  for a range of different networks.

For a given network we can compute the smallest decay rate for the associated

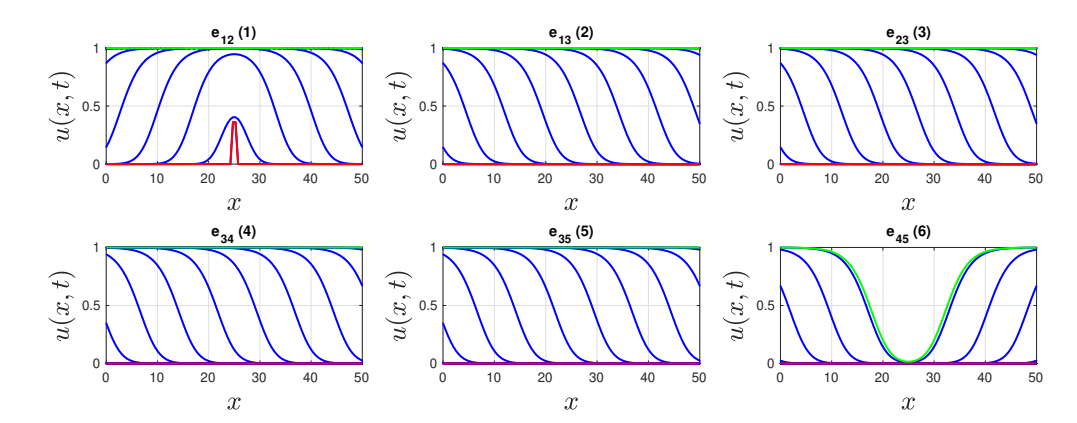


Figure 4.2.3: Numerical simulation of the Fisher equation (4.2.10) on a butterfly network (see Table (4.1)). The coloured lines are explained in the text. Each panel shows the concentration on a particular edge (for subset of all edges).

diffusion problem. Clearly if m < 0 then  $u^*$  is stable since then  $m - \nu^2 < 0$ . But if m > 0 then  $u^*$  is unstable for the reason given above that  $\nu = 0$  is always an eigenvalue for any network. The latter alludes to the fact that any spatially-independent concentration u = u(t) will grow over time away from a steady state at which m > 0. If u = u(t) the network structure is irrelevant. However, we can attempt to quantify the rate of growth or decay for spatially-varying perturbations away from a steady state. Of interest in this case is the smallest  $\nu$  in absolute value. We call this  $\nu_{min}$ .

Returning to the form of f for the Fisher equation, viz. f(u) = u(1 - u), we have m = f'(0) = 1 as noted above. In Table (4.1) we show values of  $\nu_{\min}$  for an assortment of networks. In figure 4.2.3 and 4.2.4 we show numerical simulations for the Fisher equation over the butterfly and envelope networks, whose  $\nu_{\min}$  value is given in Table (4.1). In each of these figures the initial condition is shown as the red line, representing a perturbation away from the unstable steady state u = 0. The blue lines indicate the concentration u on the edges of the network at later times. The red line shows the final state at the end of the simulation at t = 75.0.

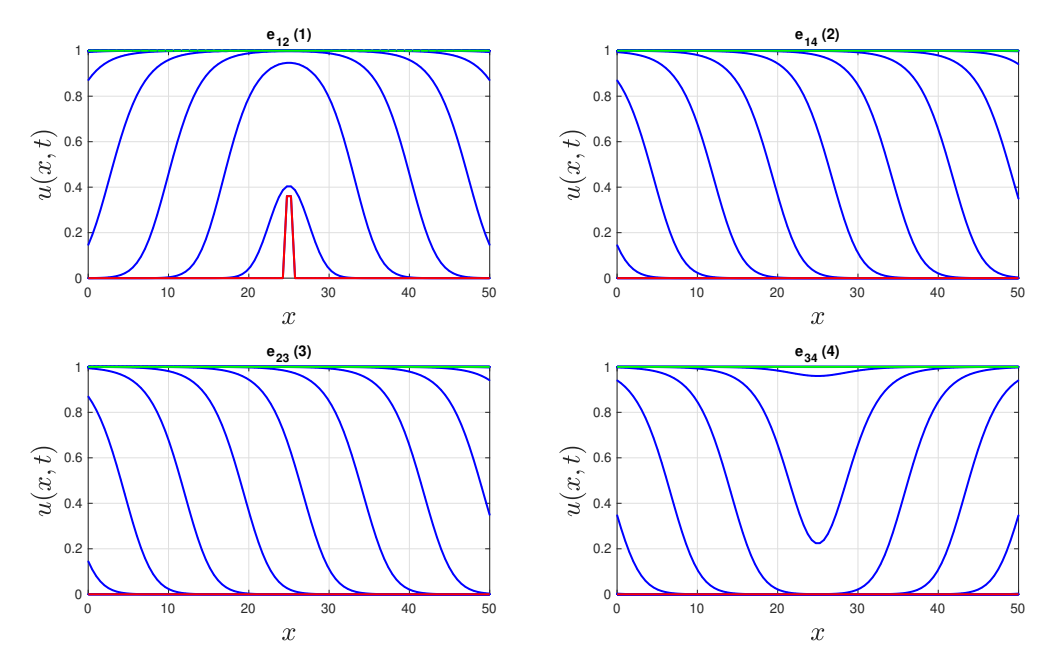


Figure 4.2.4: Numerical simulation of the Fisher equation (4.2.10) on a envelope network (see Table (4.1)). The coloured lines are explained in the text. Each panel shows the concentration on a particular edge (for subset of all edges).

### 4.2.3 Stability analysis for $P_2$ .

In this section we present a particular case of the stability analysis for the graph  $P_2$ . The reaction-diffusion equation is given by:

$$u_t = f(u) + u_{xx}. (4.2.19)$$

We assume steady states exist at u = 0 and u = 1.

To explore their stability properties we introduce a small perturbation around the steady-state solution.

For u=0 we write  $u=0+\eta(x,t)$ , where  $|\eta|\ll 1$ . This leads to the linearised equation:

$$\eta_t = f'(0)\eta + \eta_{xx},\tag{4.2.20}$$

where f'(0) is the derivative of the function f(u) evaluated at u = 0, denoted by  $\lambda$ . In the case of the Fisher equation, we have  $f(u) = u - u^2$ , and  $f'(0) = 1 = \lambda$ .

By assuming  $\eta$  takes the form  $\eta(x,t)=e^{\lambda t}q(x,t)$ , we find that q(x,t) satisfies the

diffusion equation:

$$q_t = q_{xx}.$$
 (4.2.21)

We work on the domain [0, L] and assume Neumann boundary conditions at the ends. We posit the solution in the form

$$q(x,t) = e^{-s^2 t} v(x),$$
 (4.2.22)

where s is to be determined, and v(x) satisfies the ordinary differential equation:

$$v'' + s^2 v = 0. (4.2.23)$$

The solution which satisfies the boundary conditions is

$$v(x) = \cos(sx),\tag{4.2.24}$$

provided that

$$s = \frac{n\pi}{L}.$$

We now have that

$$q(x,t) = e^{-s^2t}\cos(sx).$$
 (4.2.25)

and hence

$$\eta(x,t) = e^{\mu t} \cos(sx),$$

where

$$\mu = \lambda - s^2 = \lambda - \left(\frac{n\pi}{L}\right)^2 = \mu_n,$$

say. In the case of the Fisher equation,  $\lambda = 1$ , so that

$$\mu = 1 - \left(\frac{n\pi}{L}\right)^2.$$

To investigate stability, we analyse the sign of  $\mu$ . If  $\mu > 0$ , the perturbations grow exponentially over time, indicating instability. If  $\mu < 0$ , the perturbations decay exponentially, implying stability. When  $\mu = 0$ , there is neither growth nor

decay, and the system is said to be neutrally stable.

When n=1 we obtain  $\mu_1=1-\frac{\pi^2}{L^2}<1$ . Therefore, if  $L>\pi$ ,  $\mu_1$  is positive, indicating instability. If  $L<\pi$ ,  $\mu_1$  is negative, indicating stability. The critical value of  $L=\pi$  corresponds to a neutrally stable mode. When n=0: In this case,  $\mu_0=1>0$ , indicating that the perturbations definitely grow, making the system unstable, irrespective of the value of L. General case  $(n\neq 0 \text{ and } n\neq 1)$ : The stability of the system depends on the values of  $\mu_n$  as determined by the domain size L. In conclusion, this analysis indicates that the stability of the system is influenced by the mode number n and the domain size L, and provides valuable insight into the behaviour of perturbations around the steady-state solution.

In summary, as the domain size L increases, the decay rate of the perturbations tends to converge to a slower rate, approaching a decay rate of 1. This behaviour is a consequence of the stability analysis and the value of  $\mu_n$ . Recall that  $\mu_n = \lambda - s^2$ , where  $\lambda = 1$  for the specific function  $f(u) = u - u^2$  and  $s = \frac{n\pi}{L}$  (where n is the mode number). So,  $\mu_n = 1 - \frac{n^2\pi^2}{L^2}$ . When L is large (compared to the mode number n),  $\frac{n^2\pi^2}{L^2}$  becomes small, and consequently  $\mu_n$  becomes close to 1. As  $\mu_n$  approaches 1, the decay rate of the perturbations becomes slower, and the system takes more time to stabilise. In contrast, when L is small (compared to the mode number n),  $\frac{n^2\pi^2}{L^2}$  becomes large, and  $\mu_n$  moves further away from 1. In this case, the decay rate is faster and the system stabilizes more quickly. This behaviour is a fundamental characteristic of the stability analysis and is consistent with the behaviour of perturbations around the steady-state solution in the context of the Fisher equation.

Note that the above analysis can be repeated for the steady state at u = 1, with the result that the corresponding value of  $\mu$  is given by

$$\mu = 1 - \left(\frac{n\pi}{L}\right)^2. \tag{4.2.26}$$

### 4.3 Method of Lines

The Method of Lines (MOL) is a numerical technique that simplifies the solution of partial differential equations (PDEs) by discretizing the spatial domain into discrete grid points while keeping the time variable continuous. This approach transforms the original PDE into a system of ordinary differential equations (ODEs), which can then be solved using established time-integration methods [38].

For the Fisher equation:

$$u_t = u(1 - u) + Du_{xx}, (4.3.1)$$

consider a spatial domain [0,1] that is divided into N grid points:

$$x_i = (i-1)h, \quad h = \frac{1}{N-1}, \quad i = 1, 2, \dots, N.$$
 (4.3.2)

The equation is then approximated at each grid point using finite differences. The second derivative  $u_{xx}$  is discretized as:

$$u_{xx} \approx \frac{u_{i+1} - 2u_i + u_{i-1}}{h^2} \tag{4.3.3}$$

where  $u_i(t)$  denotes the value of u at the i-th grid point at time t. Substituting this approximation into the Fisher equation (4.3.1) results in a system of ODEs for the interior grid points:

$$\frac{du_i}{dt} = f(u_i) + D\frac{u_{i+1} - 2u_i + u_{i-1}}{h^2}, \quad i = 2, \dots, N - 1.$$
(4.3.4)

Boundary conditions are essential to ensure the physical realism of the solution. We impose Neumann boundary conditions, which specify zero flux at the domain boundaries:

$$u_x(0,t) = A$$
, and  $u_x(1,t) = B$ .

### 4.3.1 Method of lines for path graph $P_2$

To start applying the method of lines on the network, we will start with the simple case  $P_2$  (see 4.3.1), which contains two vertices connected by a single edge. The boundary condition will be imposed on the vertices 1, 2. The concentration at spatial point is denoted by  $u_i^{(1)}$ , where 1 represents the edge index, and i represents the spatial node within the element. This section details how boundary conditions are incorporated into the numerical solution.

### **Boundary conditions**

At vertex 1, the zero-flux boundary condition is imposed, expressed as:

$$\frac{du_1^{(1)}}{dt} = f\left(u_1^{(1)}\right) + D\frac{1}{h^2}\left(u_2^{(1)} - 2u_1^{(1)} + u_0^{(1)}\right),\tag{4.3.5}$$

where  $u_0^{(1)}$  is a fictitious point outside the domain on edge  $e_{12}$ . To satisfy the zero-flux condition, we impose:

$$u_2^{(1)} - u_0^{(1)} = 0,$$
 (4.3.6)

which implies:

$$u_0^{(1)} = u_2^{(1)}. (4.3.7)$$

Substituting this relation into Equation (4.3.5), we obtain:

$$\frac{du_1^{(1)}}{dt} = f\left(u_1^{(1)}\right) + D\frac{1}{h^2}\left(2u_2^{(1)} - 2u_1^{(1)}\right). \tag{4.3.8}$$

At vertex 2, the zero-flux boundary condition is similarly expressed as:

$$\frac{du_N^{(1)}}{dt} = f\left(u_N^{(1)}\right) + D\frac{1}{h^2}\left(u_{N+1}^{(1)} - 2u_N^{(1)} + u_{N-1}^{(1)}\right),\tag{4.3.9}$$

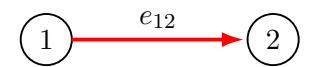


Figure 4.3.1: A path graph  $P_2$  with two vertices.

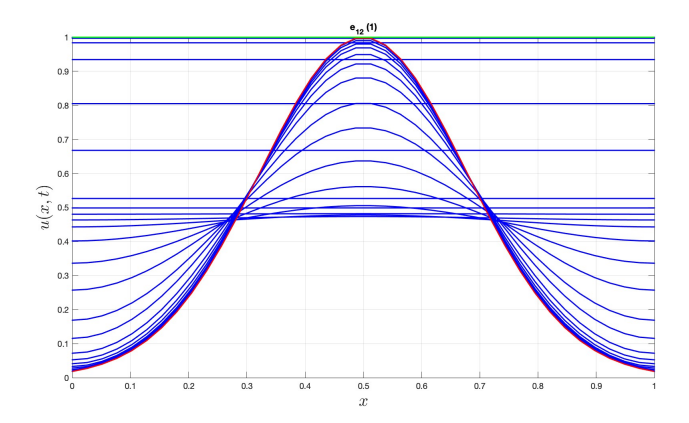


Figure 4.3.2: Evaluation of concentration u(x,t) over time for a Fisher equation.

where  $u_{N+1}^{(1)}$  is a fictitious point on the end of edge 1. To enforce the zero-flux condition, we impose:

$$u_{N+1}^{(1)} - u_{N-1}^{(1)} = 0, (4.3.10)$$

which implies:

$$u_{N+1}^{(1)} = u_{N-1}^{(1)}. (4.3.11)$$

Substituting this into Equation (4.3.9), we obtain:

$$\frac{du_N^{(1)}}{dt} = f\left(u_N^{(1)}\right) + D\frac{1}{h^2}\left(-2u_N^{(1)} + 2u_{N-1}^{(1)}\right). \tag{4.3.12}$$

For the interior mesh point on that network, we will apply the discretised equation (4.3.4).

### 4.3.2 Numerical results and analysis for path graph $P_2$

For the path graph  $P_2$ , (see Figure 4.3.1), numerical simulations were performed using the method of lines to solve the reaction-diffusion equation:

$$u_t = u(1 - u) + Du_{xx},$$

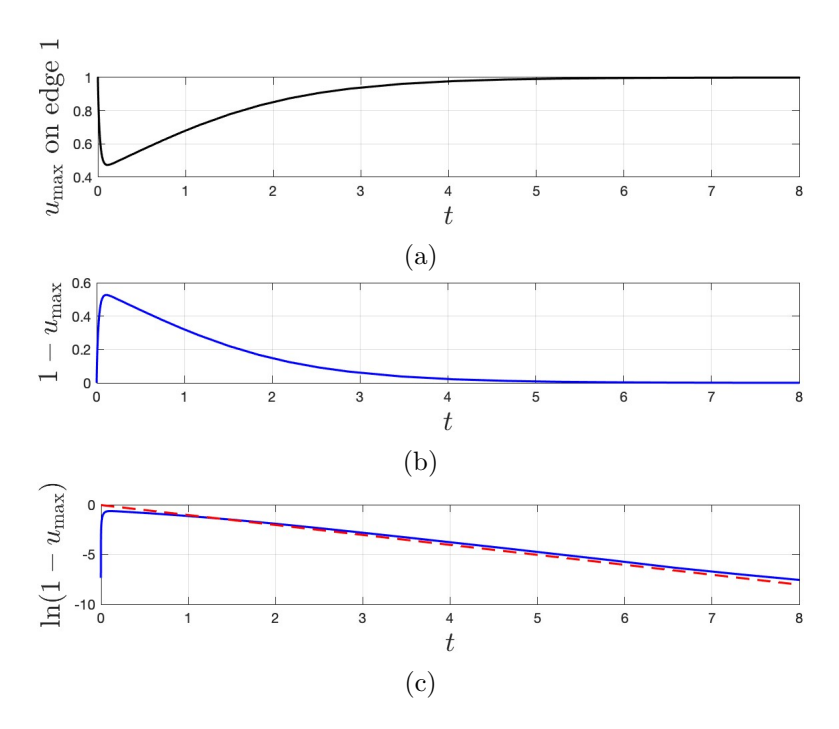


Figure 4.3.3: Solution on a  $P_2$  graph. (a) In the limit as time t tends to infinity, the maximum value of the concentration u, denoted as  $u_{\text{max}}$ , approaches 1. (b)In the limit as time t tends to infinity, the complement of the maximum value of u, denoted as  $1 - u_{\text{max}}$ , approaches 0. (c) Plot provides a visual representation of the decay behaviour of the logarithm of  $1 - u_{\text{max}}$  over time and compares it with the red dashed expected decay rate. The red dashed line has slope -1 which corresponds to the value of  $\mu$  given in (4.2.26) taking n = 0.

the topology of the graph was represented by its adjacency matrix. The following parameters were used for the calculation:

- Diffusivity (D): 1.0.
- Number of grid points at the edge (N): 80.
- Length of edge (L): 1.0.
- Time span:  $0 \le t \le 8.0$ .

The Neumann boundary conditions  $u_x(0,t) = u_x(1,t) = 0$  were applied. A Gaussian pulse was chosen as the initial condition.

Figure (4.3.2) shows the evolution of concentration u(x,t) over time. The initial Gaussian pulse (red curve) diffuses and reacts according to the Fisher equation.

At intermediate times, the profile is shown in blue and as  $t \to \infty$ , the solution approaches the final step (green line).

Figure (4.3.3) (a) shows the maximum concentration  $u_{\text{max}}$ ) that was tracked over time. Initially,  $u_{\text{max}}$  increases rapidly due to the dominating reaction term, before gradually approaching u = 1. Figure (4.3.3) (b)In the limit as time t tends to infinity, the complement of the maximum value of u, denoted as  $1 - u_{\text{max}}$ , approaches 0. Figure (4.3.3) (c) is a plot of  $\ln(1 - u_{\text{max}})$  versus t that exhibits a linear trend at large times, confirming the exponential convergence of the solution to the steady state. The observed decay rate matches the theoretical prediction (red dashed line) of -1, derived from the linearised reaction term at u = 1.

### 4.3.3 Method of Lines for path graph $P_3$

In this section, we consider a path graph  $P_3$  (see Figure 4.3.4) consisting of three vertices, which represent two edges to have a clear picture to start applying the method of lines on the network. The boundary conditions are imposed at the two boundary vertices (1 and 3), while vertex 2 serves as a common vertex between the two edges. The concentration at each spatial point is denoted by  $u_i^{(k)}$ , where k represents the edge index, and i represents the spatial discretization points within the edge. This section details how boundary conditions and continuity conditions are incorporated into the numerical solution.

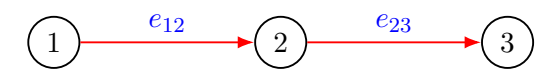


Figure 4.3.4: path graph  $P_3$  with three vertices connected by two edges.

#### Boundary vertices

At vertex 1, the zero-flux boundary condition is imposed, expressed as:

$$\frac{du_1^{(1)}}{dt} = f\left(u_1^{(1)}\right) + D\frac{1}{h^2}\left(u_2^{(1)} - 2u_1^{(1)} + u_0^{(1)}\right),\tag{4.3.13}$$

where  $u_0^{(1)}$  is a fictitious point outside the domain on edge  $e_{12}$ . To satisfy the zero-flux condition, we impose:

$$u_2^{(1)} - u_0^{(1)} = 0,$$
 (4.3.14)

which implies:

$$u_0^{(1)} = u_2^{(1)}. (4.3.15)$$

Substituting this relation into Equation (4.3.13), we obtain:

$$\frac{du_1^{(1)}}{dt} = f\left(u_1^{(1)}\right) + D\frac{1}{h^2}\left(2u_2^{(1)} - 2u_1^{(1)}\right). \tag{12.6}$$

At vertex 3, the zero-flux boundary condition is similarly expressed as:

$$\frac{du_N^{(2)}}{dt} = f\left(u_N^{(2)}\right) + D\frac{1}{h^2}\left(u_{N+1}^{(2)} - 2u_N^{(2)} + u_{N-1}^{(2)}\right),\tag{4.3.16}$$

where  $u_{N+1}^{(2)}$  is a fictitious point on edge 2. To enforce the zero-flux condition, we impose:

$$u_{N+1}^{(2)} - u_{N-1}^{(2)} = 0, (4.3.17)$$

which implies:

$$u_{N+1}^{(2)} = u_{N-1}^{(2)}. (4.3.18)$$

Substituting this into Equation (4.3.16), we obtain:

$$\frac{du_N^{(2)}}{dt} = f\left(u_N^{(2)}\right) + D\frac{1}{h^2}\left(-2u_N^{(2)} + 2u_{N-1}^{(2)}\right). \tag{12.8}$$

### Common vertex

At vertex 2, which is a common vertex between the two edges, the discretized equations for the mesh points N on the first edge and 1 on the second edge are given by:

$$\frac{du_N^{(1)}}{dt} = f\left(u_N^{(1)}\right) + D\frac{1}{h^2}\left(u_{N+1}^{(1)} - 2u_N^{(1)} + u_{N-1}^{(1)}\right),\tag{4.3.19}$$

$$\frac{du_1^{(2)}}{dt} = f\left(u_1^{(2)}\right) + D\frac{1}{h^2}\left(u_2^{(2)} - 2u_1^{(2)} + u_0^{(2)}\right). \tag{4.3.20}$$

Here,  $u_{N+1}^{(1)}$  on edge 1 and  $u_0^{(2)}$  on edge 2 are fictitious points used to enforce continuity of concentration and flux at the junction.

To ensure the continuity of concentration at vertex 2:

$$u_N^{(1)} = u_1^{(2)}. (4.3.21)$$

As well as to ensure the continuity of flux at vertex 2, the following condition is imposed:

$$u_{N+1}^{(1)} - u_{N-1}^{(1)} = u_2^{(2)} - u_0^{(2)}, (4.3.22)$$

which simplifies to:

$$u_0^{(2)} + u_{N+1}^{(1)} = u_{N-1}^{(1)} + u_2^{(2)}. (4.3.23)$$

Adding Equations (4.3.19) and (4.3.20), and using the continuity condition from Equation (4.3.23), we obtain:

$$\frac{d}{dt}\left(u_N^{(1)} + u_1^{(2)}\right) = \left(f\left(u_N^{(1)}\right) + f\left(u_1^{(2)}\right)\right) + \frac{2D}{h^2}\left(-u_N^{(1)} + u_{N-1}^{(1)} + u_2^{(2)} - u_1^{(2)}\right).$$
(4.3.24)

Let R denote the right-hand side of Equation (4.3.24), such that:

$$R = \left( f\left(u_N^{(1)}\right) + f\left(u_1^{(2)}\right) \right) + \frac{2D}{h^2} \left( -u_N^{(1)} + u_{N-1}^{(1)} + u_2^{(2)} - u_1^{(2)} \right). \tag{4.3.25}$$

Since  $u_N^{(1)} = u_1^{(2)}$ , the temporal evolution at the junction is given by:

$$\frac{du_N^{(1)}}{dt} = \frac{1}{2}R. (4.3.26)$$

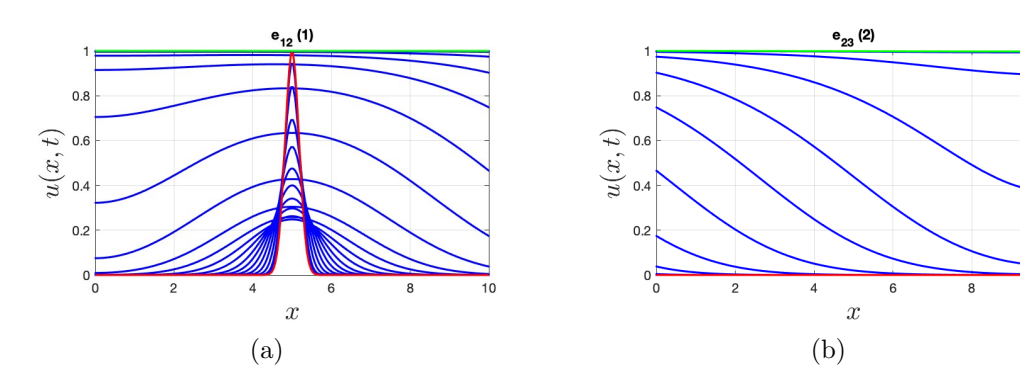


Figure 4.3.5: On the path graph  $P_3(a)$  the concentration profile u(x,t) over time for a Fisher equation for  $P_3$  on first edge. (b) the propagation of the concentration u(x,t) to the second edge due to the continuity condition apply.

#### 4.3.4 Numerical results and analysis for path graph $P_3$

For the path graph  $P_3$ , (see Figure 4.3.4), the numerical simulation obtained using the line method to solve the reaction-diffusion equation:

$$u_t = u(1 - u) + Du_{xx}$$

on  $P_3$  with the following parameters used:

- Diffusion coefficient D = 1.0.
- Spatial discretization: 200 grid points per edge.
- Edge length L = 10.0.
- Time interval:  $t \in [0, 15]$ .

The initial condition was a Gaussian pulse centred at x=5 on the first edge. The Neumann boundary conditions were applied on the boundary vertices, and the continuity of flux and concentration was applied on the common vertex. The results are as follows:

• Figure (4.3.5)(a,b) shows the evolution of the concentration u(x,t) over time on the graph  $P_3$ . The initial Gaussian pulse, applied on the first

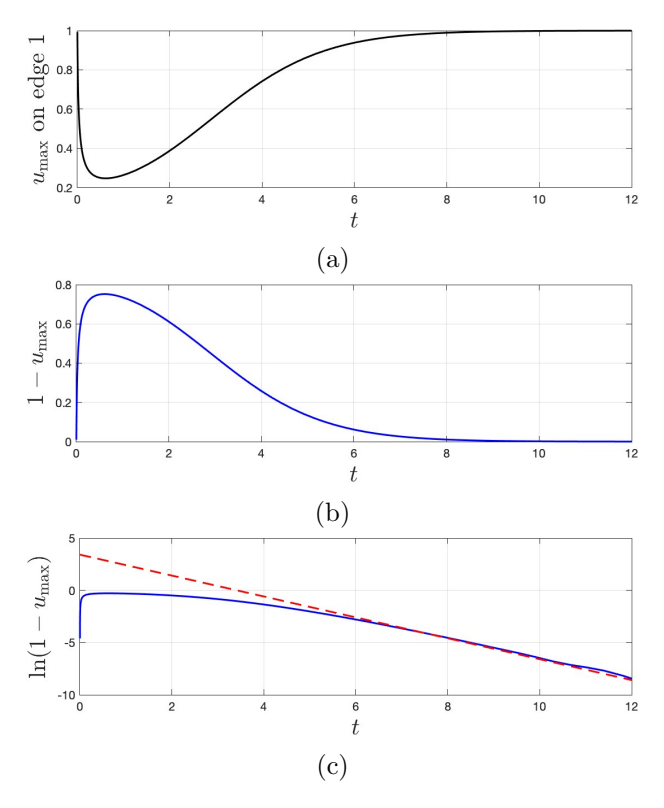


Figure 4.3.6: On the path graph  $P_3$ ,(a) In the limit as time t tends to infinity, the maximum value of the concentration u, denoted as  $u_{\text{max}}$ , approaches 1. (b)In the limit as time t tends to infinity, the complement of the maximum value of u, denoted as  $1-u_{\text{max}}$ , approaches 0. (c) Plot provides a visual representation of the decay behaviour of the logarithm of  $1-u_{\text{max}}$  over time and compares it with the red dashed expected decay rate.

edge (red curve), undergoes diffusion and reaction according to the non-linear diffusion equation. At intermediate times, the concentration profile (blue) shows the smoothing and spreading effects of diffusion. As  $t \to \infty$ , the solution stabilises and approaches the final steady-state profile (green line). Notably, the diffusion spreads to the second edge, as a result of the continuity conditions for both concentration and flux imposed at the common vertex. These conditions ensure a smooth transition and consistent flux across the network.

• Figure (4.3.6) (a) shows the flux at the boundaries of the first edge tracked over time. The flux initially oscillates as the concentration stabilises before settling into a steady-state value. (b) illustrates the maximum concentration  $u_{\text{max}}$  on the first edge, which increases rapidly at

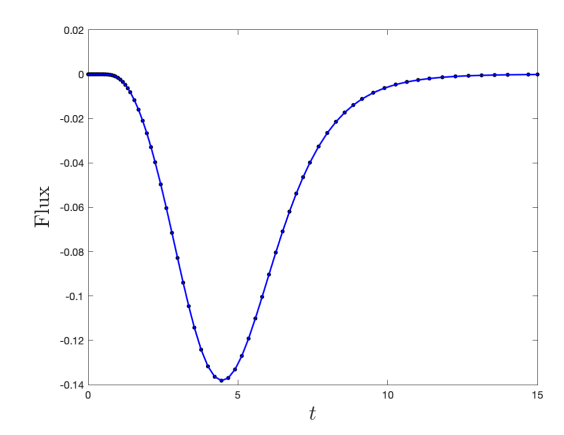


Figure 4.3.7: On the path graph  $P_3$ , the black dots represent the flux entering edge 2 through vertex 2 the tail of edge 1 and the blue curve shows the flux entering edge 2 through its head vertex 2.

first due to the non-linear growth term, then gradually converges to u = 1. (c) is a plot of  $\ln(1 - u_{\text{max}})$  versus t, showing a linear trend at large times. This confirms the exponential convergence of the solution to the steady state. The observed decay rate matches the theoretical prediction (red dashed line) derived from the linearised equation at u = 1.

• Figure (4.3.7) shows the flux dynamics at the edge boundary over time. The flux at the tail of the first edge is represented by the black dotted line, while the flux at the head of the second edge is shown in blue. Notably, the two flux profiles overlap perfectly, demonstrating the accurate enforcement of flux continuity across the common vertex. This result validates the implementation of both the continuity of flux and concentration conditions in the numerical simulation.

#### 4.3.5 Method of lines on general network

In this section, we analyse a network with N vertices. The boundary conditions outlined in Section (4.3.3) remain applicable to this general network. Here, we focus on interior mesh points along the edges, excluding the boundary grid points and the common vertices. Additionally, we address the behaviour at common vertices where more than two edges intersect. These will allow us to handle

different network topologies.

#### Network common vertices

To enforce the continuity of flux at the common vertices i, the flux balance equation is written as:

$$\sum_{k \in S_{\perp}^{(i)}} q_k^H - \sum_{k \in S_{-}^{(i)}} q_k^T = 0, \tag{4.3.27}$$

Here,  $q_k^H$  and  $q_k^T$  represent the head and tail fluxes for edges  $e_{ki}$  and  $e_{ik}$ , respectively, and where the sets:

- $S_{+}^{(i)} = \{j \in V : j > i \text{ and } a_{ij} = 1\}$  denotes the set of vertices connected to node i with indices greater than i.
- $S_{-}^{(i)} = \{j \in V : j < i \text{ and } a_{ij} = 1\}$  denotes the set of vertices connected to node i with indices less than i.

Here,  $a_{ij}$  is the  $ij^{th}$  element of the adjacency matrix A for the network, and V is the set of all vertices in the network. Using the finite difference approximation for the flux, we have:

For 
$$S_{+}^{(i)}: q_{k}^{H} = \frac{u_{2}^{(e)} - u_{0}^{(e)}}{2h}$$
, For  $S_{-}^{(i)}: q_{k}^{T} = \frac{u_{N+1}^{(e)} - u_{N-1}^{(e)}}{2h}$ ,

and e is the edge label. Substituting these into Equation (4.3.27), we obtain:

$$\sum_{e \in C_i^H} \frac{u_2^{(e)} - u_0^{(e)}}{2h} - \sum_{e \in C_i^T} \frac{u_{N+1}^{(e)} - u_{N-1}^{(e)}}{2h} = 0, \tag{4.3.28}$$

where  $C_i^H$  and  $C_i^T$  represent the edges group hosting vertex i as either head or tail at common vertex i, respectively.

At a common vertex i, the governing equation for the edges hosting node i as a

head is:

$$\frac{du_1^{(e)}}{dt} = f\left(u_1^{(e)}\right) + \frac{D}{h^2}\left(u_2^{(e)} - 2u_1^{(e)} + u_0^{(e)}\right), \quad \text{for } e \in C_i^H, \tag{4.3.29}$$

and as a tail is:

$$\frac{du_N^{(e)}}{dt} = f\left(u_N^{(e)}\right) + \frac{D}{h^2} \left(u_{N+1}^{(e)} - 2u_N^{(e)} + u_{N-1}^{(e)}\right), \quad \text{for } e \in C_i^T.$$
 (4.3.30)

Combining Equations (4.3.29) and (4.3.30), we can write the total contribution to the flux balance as:

$$\sum_{e \in C_i^H} \frac{du_1^{(e)}}{dt} + \sum_{e \in C_i^T} \frac{du_N^{(e)}}{dt} = Q,$$
(4.3.31)

where Q is given by:

$$Q = \sum_{e \in C_i^H} \left[ f\left(u_1^{(e)}\right) + \frac{D}{h^2} \left(u_2^{(e)} - 2u_1^{(e)}\right) \right]$$

$$+ \sum_{e \in C_i^T} \left[ f\left(u_N^{(e)}\right) + \frac{D}{h^2} \left(-2u_N^{(e)} + u_{N-1}^{(e)}\right) \right]$$

$$+ \frac{D}{h^2} \left[ \sum_{e \in C_i^H} u_0^{(e)} + \sum_{e \in C_i^T} u_{N+1}^{(e)} \right]. \tag{4.3.32}$$

From Equation (4.3.28), we can also express the flux continuity condition as:

$$\sum_{e \in C_i^H} u_0^{(e)} + \sum_{e \in C_i^T} u_{N+1}^{(e)} = S, \tag{4.3.33}$$

where:

$$S = \sum_{e \in C_i^H} u_2^{(e)} + \sum_{e \in C_i^T} u_{N-1}^{(e)}.$$
 (4.3.34)

Using the equality  $u_1^{(e)} = u_N^{(e)}$  for all  $e \in C_i^H \cup C_i^T$ , Equation (4.3.32) can be

rewritten as:

$$M\frac{du_1^{(e)}}{dt} = \sum_{e \in C_i^H} \left[ f\left(u_1^{(e)}\right) + D\frac{1}{h^2} \left(u_2^{(e)} - 2u_1^{(e)}\right) \right]$$

$$+ \sum_{e \in C_i^T} \left[ f\left(u_N^{(e)}\right) + D\frac{1}{h^2} \left(-2u_1^{(e)} + u_{N-1}^{(e)}\right) \right]$$

$$+ S, \qquad (4.3.35)$$

where M is the total number of edges hosting common vertex i.

#### 4.3.6 Numerical results and analysis for general network

In this section, we present numerical solutions to the reaction-diffusion equation

$$u_t = u(1 - u) + Du_{xx}, (4.3.36)$$

on different network structures using the method of lines. To ensure consistency, Neumann boundary conditions are applied at the boundary vertices (see Section 4.3.1) and continuity of concentration and flux is enforced at the common vertices, as discussed in detail in Section (4.3.5).

The connectivity of each network is described by its adjacency matrix  $\mathbf{A}$ , and the degree matrix  $\mathbf{D}$  is calculated as a diagonal matrix where each diagonal entry represents the degree of the corresponding vertex. The theoretical growth or decay rate of the solution is determined by the eigenvalues of the *modified Laplacian* matrix  $\mathbf{L}^*$ , defined as:

$$\mathbf{L}^* = \mathbf{A} - \cos(\nu)\mathbf{D}.\tag{4.3.37}$$

Here,  $\cos(\nu)$  corresponds to an eigenvalue  $\lambda$  such that  $\cos(\nu) = \lambda$ . Rewriting the equation, we have:

$$\mathbf{L}^* = \mathbf{A} - \lambda \mathbf{D}.\tag{4.3.38}$$

134

For any given network, the eigenvalues of the modified Laplacian matrix  $\mathbf{L}^*$  can be calculated numerically. Then, using the relation  $\cos^{-1}(\lambda) = \nu$ , we can compute the decay rate  $\nu$  for any network by choosing the smallest positive decay rate, which corresponds to the slowest mode of diffusion in the network. Then, compare it with the theoretical growth rate calculated using eigenvalue analysis. Now, we will discuss two specific examples to demonstrate this approach.

#### Triangle graph

In this section, we extend our analysis to a triangle graph (see Figure 4.3.8) which is a cycle graph with three vertices arranged as a triangle. The reaction diffusion equation

$$u_t = u(1 - u) + Du_{xx}$$

is solved numerically using the method of lines. As all vertices are common vertices, the continuity of flux and concentration is maintained at all the common vertices. The following parameters used:

- Diffusion coefficient D = 1.0.
- Spatial discretization: 200 grid points per edge.
- Edge length L = 15.0.
- Time interval:  $t \in [0, 16]$ .
- h = 0.0754

The numerical results of the calculation are as follows:

• Figure 4.3.9(a) The concentration profile of the Fisher equation on the triangle graph where the Gaussian is set as the initial condition at the first edge (red) and we can see the intermediate time (blue) until we approach the steady state u = 1. (b, c) Propagation of the concentration from the edge  $e_{12}$  to the other edges of the graph.

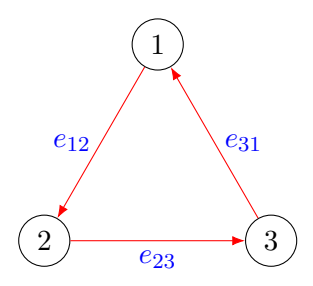


Figure 4.3.8: Cycle graph with 3 vertices arranged as a triangle

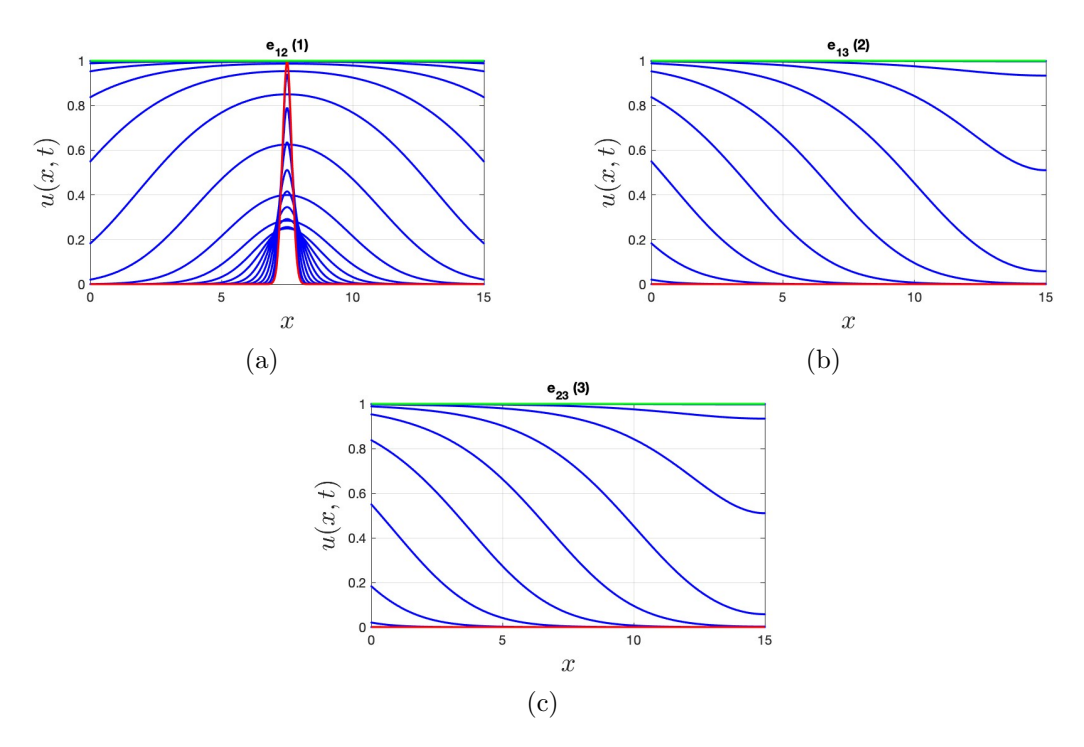


Figure 4.3.9: Solution on the triangle graph, (a) the concentration profile u(x,t) over time for a Fisher equation for triangle graph, the initial condition (red), the intermediate time steps (blue), and the final step (green). (b,c) the propagation of the concentration u(x,t) to rest of the edges due to the continuity condition apply.

- The numerical convergence of our results is established in Figure 4.3.10 (a) which shows that convergence is achieved on reducing the size of the mesh spacing h = 0.005 by reducing the edge length L = 1, and in figure 4.3.10 (b) which shows that convergence is achieved on increasing the size of the mesh spacing h = 0,15 by increasing the edge length L = 30.
- Figure 4.3.11(a) illustrates the plot of  $u_m$ , which represents the maximum value of the concentration u, as a function of time on the first element. This plot demonstrates the evolution of the maximum concentration value

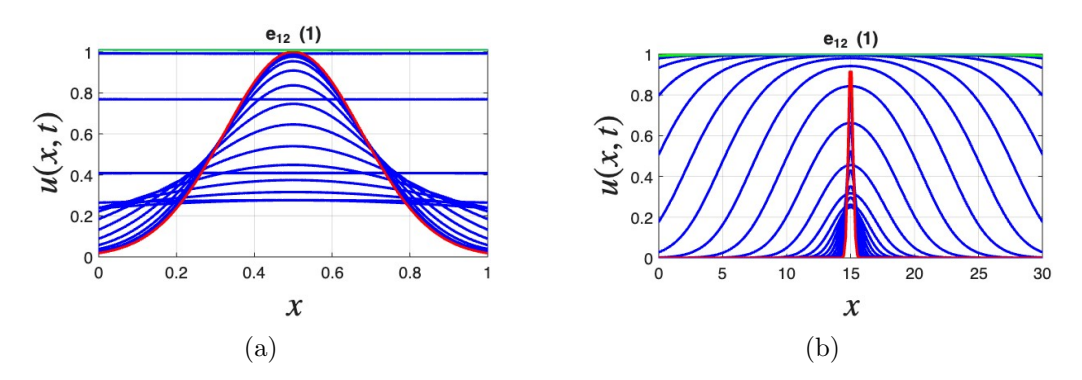


Figure 4.3.10: Numerical converge study in triangle graph. Showing the the concentration profile u(x,t) over time for a Fisher equation for triangle graph on edge  $e_{12}$ , condition (red), the intermediate time steps (blue), and the final step (green). Comparison shown for: (a) h = 0.005, L = 1, and (b) h = 0.15, L = 30.

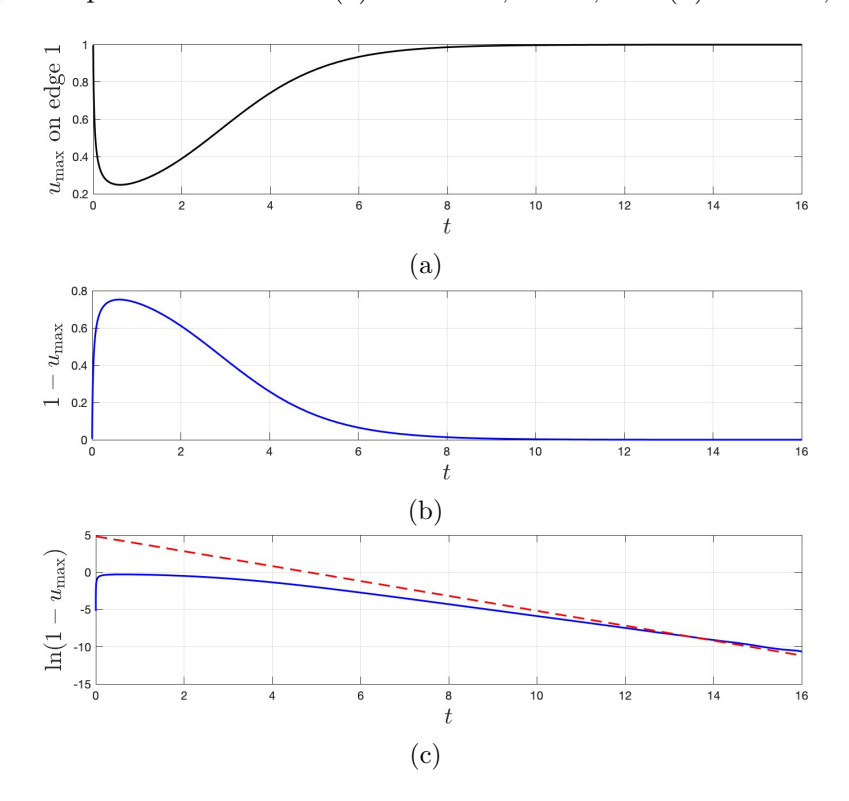


Figure 4.3.11: On the triangle graph,(a) In the limit as time t tends to infinity, the maximum value of the concentration u, denoted as  $u_{\text{max}}$ , approaches 1. (b)In the limit as time t tends to infinity, the complement of the maximum value of u, denoted as  $1-u_{\text{max}}$ , approaches 0. (c) Plot provides a visual representation of the decay behaviour of the logarithm of  $1-u_{\text{max}}$  over time and compares it with the red dashed expected decay rate.

on the first element over time. In particular, as time approaches infinity, it is evident that the concentration u tends to 1.

• Figure 4.3.11(b) shows the behaviour of the function 1-u, which represents

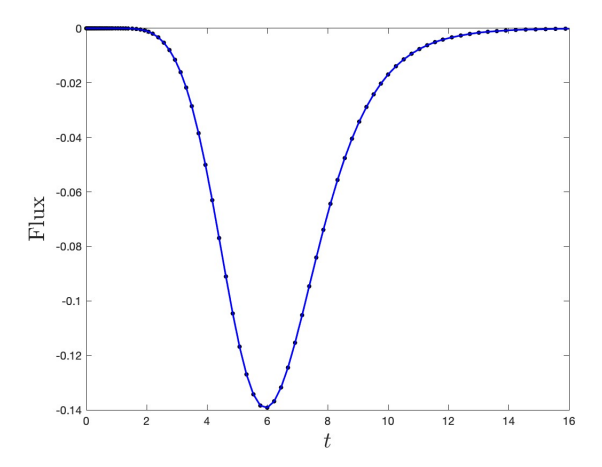


Figure 4.3.12: The flux entering edge  $e_{23}$  through vertex 2 as a tail of edge  $e_{12}$  (black dots) and as a head of edge  $e_{23}$  (blue)

the complement of the maximum concentration u, as a function of time. This plot shows the evolution of the complement of the maximum value of u over time. In particular, it is evident that the function tends to 0 as time approaches infinity.

- Figure 4.3.11(c) presents the plot of the natural logarithm of 1-u as a function of time. The dashed red line corresponds to the theoretical calculation based on equation (4.2.16), which represents a linear decay with time.
- Figure 4.3.12 shows the flux entering edge  $e_{23}$  through vertex 2 as a tail of edge  $e_{12}$  (black dots) and as a head of edge  $e_{23}$  (blue) which shows agreement of the flux as a result of continuity of concentration and flux conditions applied.

#### Tree graph with 6 vertices

In this section, we extend our analysis to a tree graph with six vertices (see Figure 4.3.13). The reaction diffusion equation

$$u_t = u(1 - u) + Du_{xx}$$

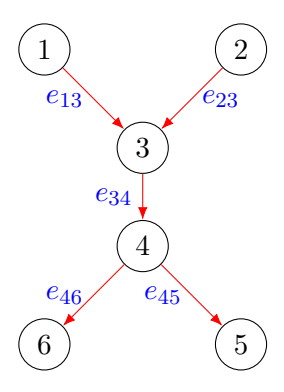


Figure 4.3.13: Tree graph with 6 vertices.

is solved numerically using the method of lines. The zero flux conditions are applied on the boundary vertex, and the continuity of concentration and flux are applied one the common vertices. The numerical result is obtained as follows:

- Figure (4.3.14)(a) The concentration profile of the Fisher equation on the tree graph with 6 vertices and 5 edges, where the Gaussian is set as the initial condition at the first edge (red) and we can see the intermediate time (blue) until we approach the steady state u = 1. (b, c, d, e) Propagation of the concentration from the edge  $e_{13}$  to the rest of edges of the graph.
- Figure (4.3.15(a)) illustrates the plot of  $u_m$ , which represents the maximum value of the concentration u, as a function of time on the first element. This plot demonstrates the evolution of the maximum concentration value on the first element over time. In particular, as time approaches infinity, it is evident that the concentration u tends to 1.
- (4.3.15(b)) shows the behaviour of the function 1 u, which represents the
  complement of the maximum concentration u, as a function of time. This
  plot shows the evolution of the complement of the maximum value of u
  over time. In particular, it is evident that the function tends to 0 as time
  approaches infinity.
- (4.3.15(c)) presents the plot of the natural logarithm of 1-u as a function of time. The dashed red line corresponds to the theoretical calculation based on equation (4.2.16), which represents a linear decay with time.

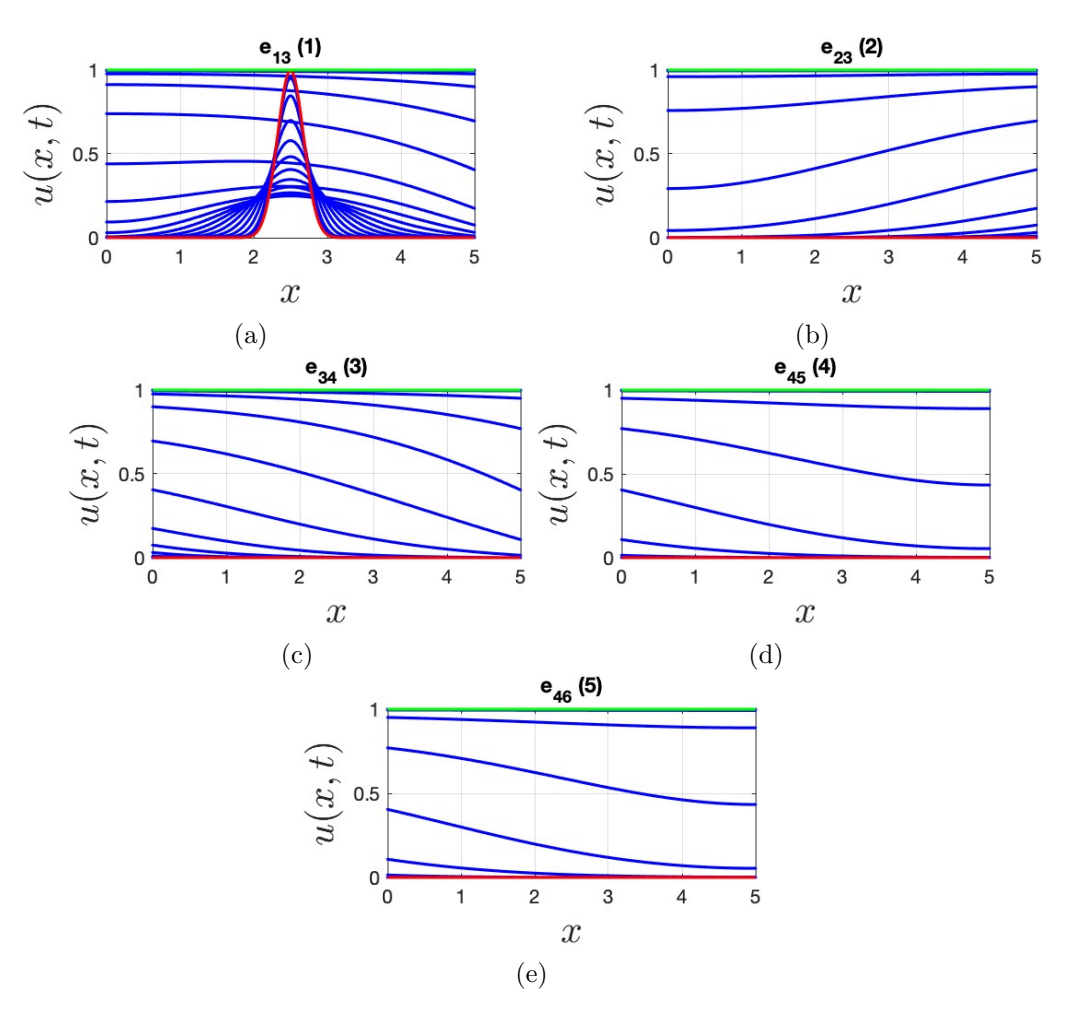


Figure 4.3.14: the concentration profile u(x,t) over time for a Fisher equation for tree graph with 6 edges. (a) on the first edge applied the initial condition (red), the intermediate time (blue), the final time (green).(b,c,c,d,e) the propagation of the concentration u(x,t) to the rest of edges on the graph as a result of the continuity conditions apply.

• Figure (4.3.16) shows the flux distribution at vertex 4, where it acts as the tail of edge  $e_{34}$  (black dots) and the head of edges  $e_{45}$  (blue dots) and  $e_{46}$  (red dashed line). The flux originating from edge  $e_{34}$  is evenly distributed between edges  $e_{45}$  and  $e_{46}$ , demonstrating the accurate enforcement of the continuity of both concentration and flux conditions at the common vertex.

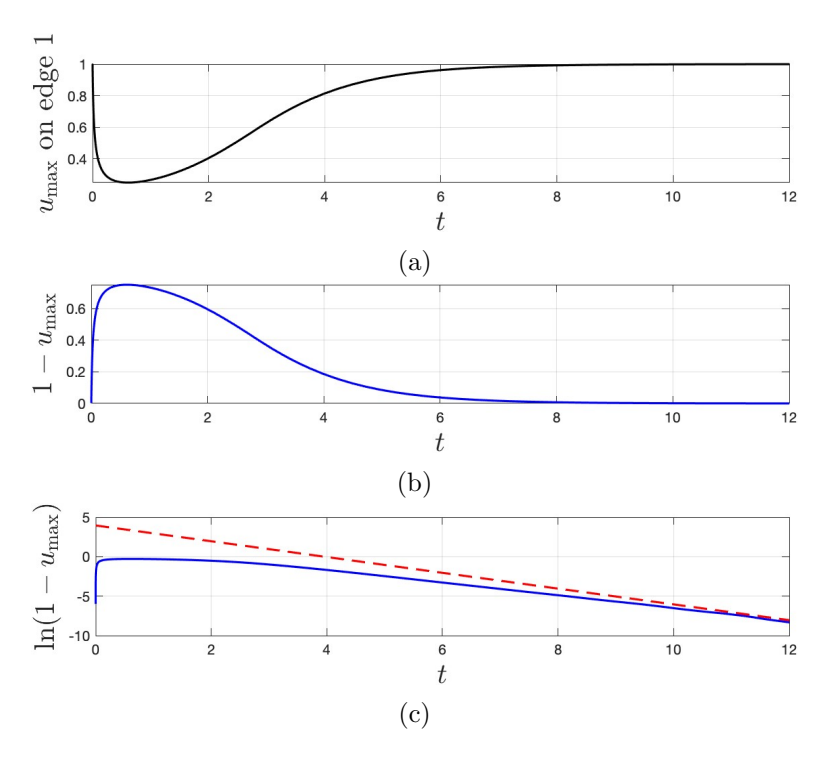


Figure 4.3.15: On the tree graph with 6 vertices,(a) In the limit as time t tends to infinity, the maximum value of the concentration u, denoted as  $u_{\text{max}}$ , approaches 1. (b)In the limit as time t tends to infinity, the complement of the maximum value of u, denoted as  $1-u_{\text{max}}$ , approaches 0. (c) Plot provides a visual representation of the decay behaviour of the logarithm of  $1-u_{\text{max}}$  over time and compares it with the red dashed expected decay rate.

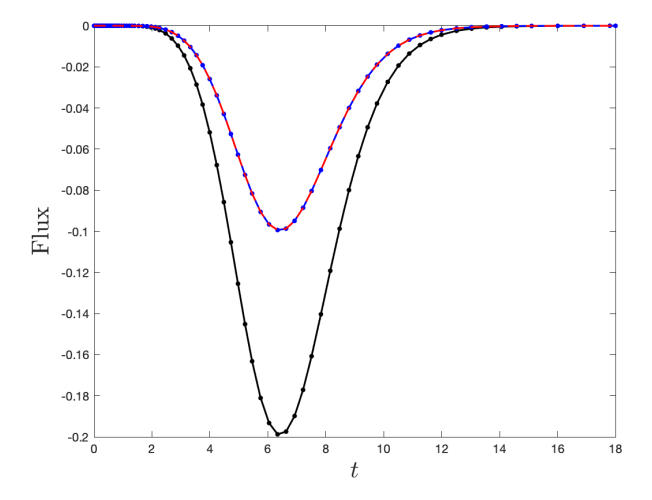


Figure 4.3.16: The flux entering edge  $e_{45}$  and  $e_{46}$  through vertex 4 as a tail of edge  $e_{34}$  (black dots) and as a head of edge  $e_{45}$  (blue dots) and  $e_{46}$  (red dashed).

# The FitzHugh–Nagumo model: simulation of pulse dynamics in network

In this chapter, we use the Fitzhugh-Nagumo (FHN) model to simulate pulse dynamics in network structures, inspired by Annalisa's observations of pulse-like phenomena in calcium wave dynamics. The model comprises two coupled reaction-diffusion equations for membrane potential and recovery variables, used to examine pulse propagation mechanisms in networks. Initial exploration focuses on simpler network topologies like path graphs, extending to complex configurations like Y-shaped networks. Pulses are initiated by external forces at head nodes, and their propagation is studied in one-dimensional and multi-edge networks. The chapter highlights how network topology affects pulse splitting and propagation at junctures. Additionally, it addresses boundary conditions, introduces numerical methods such as finite-difference and time-stepping techniques for solving FHN equations, and investigates bifurcation points and the stability of pulse solutions. The study concludes with findings on how pulse behaviour depends on network structure and parameters.

## 5.1 The FitzHugh-Nagumo model

In the 1960s, the FitzHugh-Nagumo (FHN) model was developed in neuroscience as a simplified model to represent the behaviour of excitable neuron cells. Despite its origins, this equation is also applicable in cardiac physiology, cell division, population dynamics, electronics, and other natural phenomena [16].

The present work builds upon the foundational study by Argentina (2000) [1], who investigated head-on collisions of pulses in the FitzHugh-Nagumo system on infinite one-dimensional domains. Argentina demonstrated that for negative values of parameter a, pulses can either annihilate or pass through each other depending on the parameter values. We adopt their parameters and model formulation as our starting point. However, our contribution extends this work in several novel directions:

- Network extension: While Argentina studied pulse dynamics in infinite 1D domains, we extend the FHN model to network structures, developing new boundary conditions and continuity constraints at network vertices.
- Pulse splitting discovery: We demonstrate a new phenomenon where
  pulses seamlessly split at network junctions, propagating along multiple
  edges while preserving their shape and amplitude a behaviour not
  present in the original 1D setting.
- Network specific analysis: We develop new mathematical tools including modified Laplacian matrices  $L^* \leftrightarrow (k)$  and network-adapted Chebyshev methods to analyse pulse dynamics across different network topologies.

In this chapter, we use the one-dimensional form of that model with non-zero diffusion coefficients for both species. The model is governed by two coupled reaction-diffusion equations [1]:

$$\frac{\partial u}{\partial t} = \frac{\partial^2 u}{\partial x^2} - u(u - 1)(u - a) - v, \tag{5.1.1}$$

$$\frac{\partial v}{\partial t} = \lambda(u - bv) + \delta \frac{\partial^2 v}{\partial x^2},\tag{5.1.2}$$

where u(x,t) represents the voltage in the axon and v(x,t) represents a recovery variable which allows the axon to return to its rest state. The parameter  $\lambda$  indicates the relative time scales of these variables and typically acts as a small parameter. The excitable dynamics are influenced by the parameter a, while the diffusivity ratio is represented by  $\delta > 0$  [1]. As is usual in the study of these equations, we assume that  $\lambda > 0$  and b > 0. Normally the assumption is that 0 < a < 1 (see, for example, [6]). Here, however, we will allow a to take either sign. This step is motivated by the work of Argentina [1], who found complex and interesting dynamics when a is negative. As is well known for the FHN system, there exist pulse solutions which propagate at constant speed, and it has been shown that the dynamics when two pulses are involved can pivot delicately on the choice of parameter values and that, in particular, two pulses that approach each other may either pass through each other or else annihilate, possibly leaving behind a non-uniform equilibrium state.

We shall investigate the dynamics of pulse solutions to the FHN equations on a network and determine non-uniform states and analyse their stability. The parameter values from Argentina provide the excitable system necessary for our network studies, but the phenomena we observe - particularly pulse splitting and network-topology-dependent bifurcations - are entirely new contributions to the field.

To study pulse dynamics on a network we employ the method of lines, as outlined in chapter 4, adapting it to solve the set of non-linear equations inclusive of the reaction term. This involves using discretization and explicit time-stepping techniques. Our investigation seeks to understand the impact of network topology

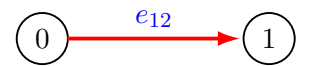


Figure 5.2.1: A path graph  $P_2$  with two vertices.

on spatio-temporal pulse behaviour.

### 5.2 Numerical simulation of pulse dynamics

#### 5.2.1 Forcing effects on a path graph $P_2$

In this section, we solve the FitzHugh-Nagumo model

$$\frac{\partial u}{\partial t} = \frac{\partial^2 u}{\partial x^2} - u(u - 1)(u - a) - v, \tag{5.2.1}$$

$$\frac{\partial v}{\partial t} = \lambda(u - bv) + \delta \frac{\partial^2 v}{\partial x^2},\tag{5.2.2}$$

on a path graph  $P_2$  connecting two vertices (see figure 5.2.1), by using the method of lines. Neumann boundary conditions are applied at both ends, and an external forcing function  $h(t) = -t^3 e^{-t}$  is applied exclusively to the head vertex which means setting the value of  $u_x$  at x = 0 to be h(t). This is done in order to stimulate the generation of a pulse solution.

The system is solved with the following specifications:

- Spatial domain: [0, L] with L = 65
- Spatial discretization: N = 100 points
- Temporal domain:  $t \in [0, 80]$
- h = 0.6566
- The parameters of the model a = 0.02, b = 0.01, c = 0.01,  $\lambda = 1$ , and  $\delta = 0$ .

The final profile of the calculation (see figures 5.2.4 and 5.2.5). When the forcing ceases, the system returns to a stable homogeneous state. This

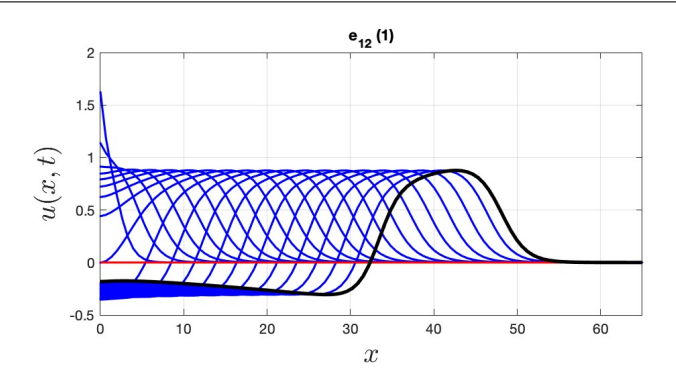


Figure 5.2.2: on  $P_2$  graph, pulse dynamics of u(x,t) under forcing at the head vertex. The blue curve represents the voltage in the axon, The red line represents the initial concentration, the black curve represents the final time profile of concentration, and the blue curves show intermediate profiles over time.

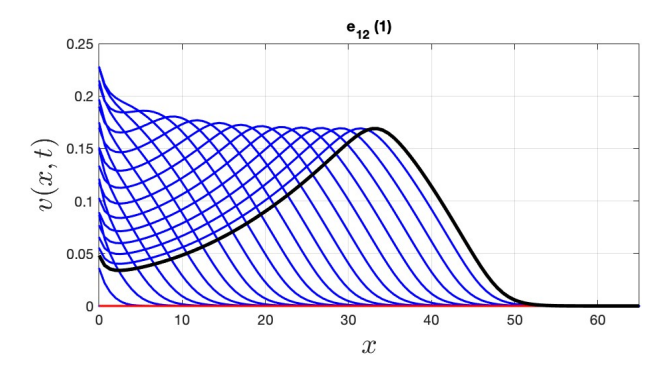


Figure 5.2.3: Recovery dynamics of v(x,t) on a  $P_2$  under forcing at the head node. The red line represents the initial concentration, the black curve represents the final time profile of concentration, and the blue curves show intermediate profiles over time.

behaviour highlights the localised impact of external stimuli on network dynamics.

This asymmetric stimulation induces localised oscillations in both u and v, which propagate along the edge and decay as they move away from the stimulus. Figures 5.2.2 and 5.2.3 illustrate the behaviour of u(x,t) and v(x,t) over time, respectively.

Figure (5.2.6) displays the temporal evolution of the maximum amplitudes for both the membrane potential (u) and recovery variable (v) as functions of time. The membrane potential u exhibits an initial rapid increase, reaching its global maximum shortly after t = 0. The recovery variable v shows a delayed response, consistent with its role as a slow variable in the system. The system approaches

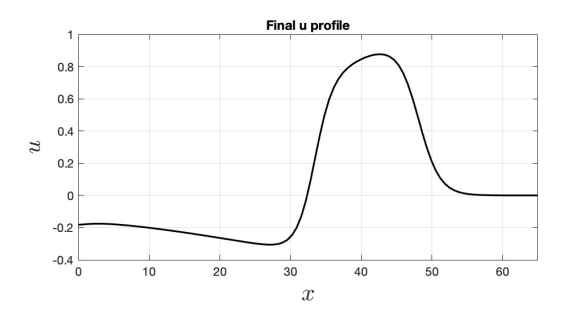


Figure 5.2.4: Final profile pulse of the voltage in the axon on  $P_2$ .

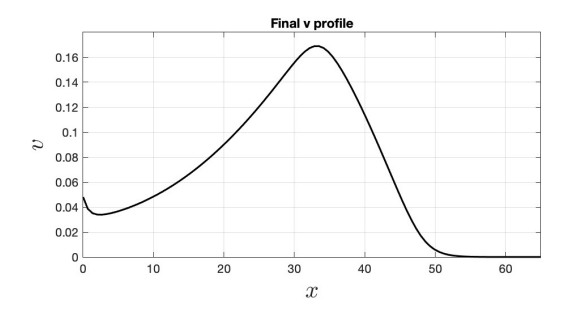


Figure 5.2.5: Final profile of recovery dynamics of v(x,t) on a  $P_2$ .

a steady state as  $t \to \infty$ .

#### 5.2.2 Forcing effects on a Y-shaped graph

In this section, we extend our analysis of pulse dynamics within a Y-shaped graph, as illustrated in Figure (5.2.7). In that graph, a force function denoted as  $h(t) = -t^3 e^{-t}$  is applied to vertex 1 located at the head of the edge  $e_{12}$ . This application of force to that edge initiates the propagation of a pulse over the network as a result of the continuity of concentration and flux conditions that are applied on the common vertex 2.

Upon reaching the common vertex (2) of that graph, the pulse seamlessly splits into two parts, each continuing its journey along the two downstream edges. This captivating phenomenon mirrors binary switching behaviours analogous to neuronal axon potentials at synapses. Significantly, the pulse retains its shape, speed, and amplitude after splitting, underlining the deterministic nature of the network topology, which consistently divides the pulse equally between the two branches see figure (5.2.8) and (5.2.9).

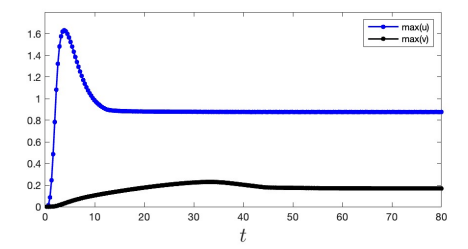


Figure 5.2.6: Temporal evolution of maximum amplitudes for membrane potential (u, blue) and recovery variable (v, black) over time.

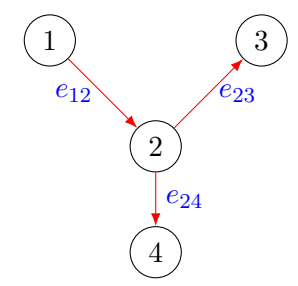


Figure 5.2.7: Y-shape graph with four vertices and three edges

The results presented in Figures (5.2.10) and (5.2.11) show the temporal evolution of the activator variable u and the inhibitor variable v across the network edges. The black lines represent the values at the head vertex of each edge, while the blue lines indicate the values at the tail vertex. For u, the initial Gaussian pulse propagates through the network, and its amplitude decreases over time due to dissipation. The inhibitor variable v follows behind u, as dictated by the FitzHugh-Nagumo model, and maintains a smaller amplitude compared to u. These dynamics highlight the interaction between the activation and recovery processes in the model. Additionally, the plots reveal how the network structure influences the timing and magnitude of the signals, emphasising the importance of continuity of concentration and flux conditions in ensuring smooth transitions between edges.

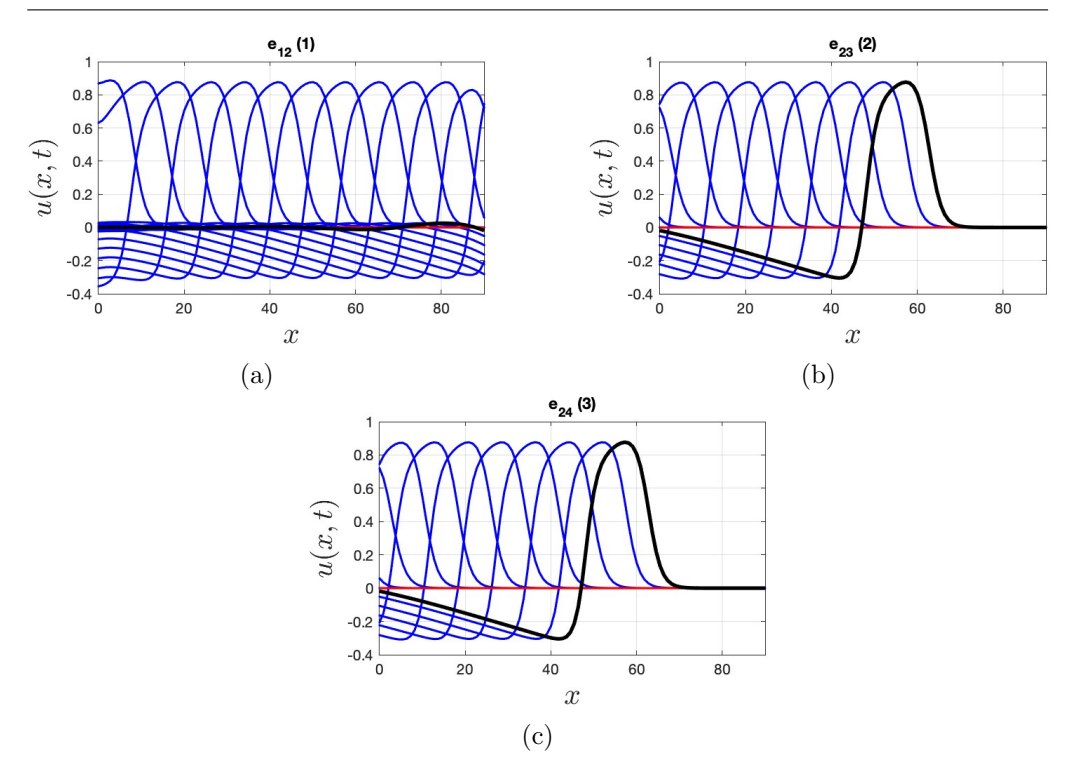


Figure 5.2.8: On the Y-shaped graph, the pulse which represent the voltage in the axon seamlessly splits into two parts, each continuing its journey along the two downstream edges. (a) shows the force function apply on vertex 1 at edge  $e_{12}$  then we see (b,c) the pulse splits between other edges at common vertex 2 as a result of the continuity of concentrations and flux conditions. The final time step (black), the intermediate time (blue) and the initial condition (red).

# 5.3 Spatial dynamics of FitzHugh-Nagumo system

#### 5.3.1 Analysis of stationary solutions

In this section we discuss stationary solutions to the FitzHugh-Nagumo equations, namely

$$u_t = -v - u(u-1)(u-a) + u_{xx}$$
(5.3.1)

and

$$v_t = \lambda(u - bv) + \delta v_{xx} \tag{5.3.2}$$

Note that the v equation includes a diffusion term. To analyse the spatial structure of stationary waves, we seek solutions where  $u_t = v_t = 0$  for Equations

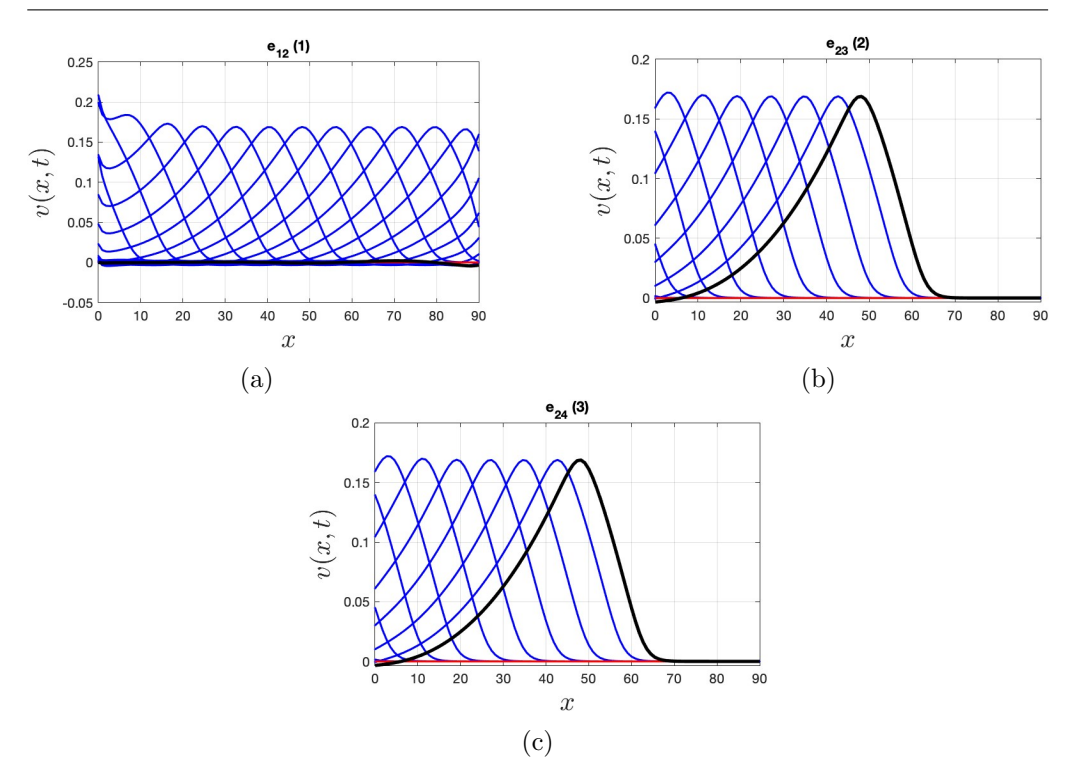


Figure 5.2.9: On the Y-shaped graph, the pulse which represent the recovery variable seamlessly splits into two parts, each continuing its journey along the two downstream edges. (a) shows the force function apply on vertex 1 at edge  $e_{12}$  then we see (b,c) the pulse splits between other edges at common vertex 2 as a result of the continuity of concentrations and flux conditions. The final time step (black), the intermediate time (blue) and the initial condition (red).

(5.3.1) and (5.3.2) and define  $\omega = \frac{\lambda}{\delta}$ . This yields the system:

$$u_{xx} = v + f(u) \tag{5.3.3}$$

and

$$v_{xx} = \omega(bv - u), \tag{5.3.4}$$

where f(u) = u(u - a)(u - 1) represents the non-linear reaction term.

In order to calculate stationary solutions numerically, the following manipulations are useful. We multiply equation (5.3.3) by  $\omega u_x$  and equation (5.3.4) by  $v_x$  yields the following expressions:

$$\omega u_x u_{xx} = \omega v u_x + \omega u_x f(u) \tag{5.3.5}$$

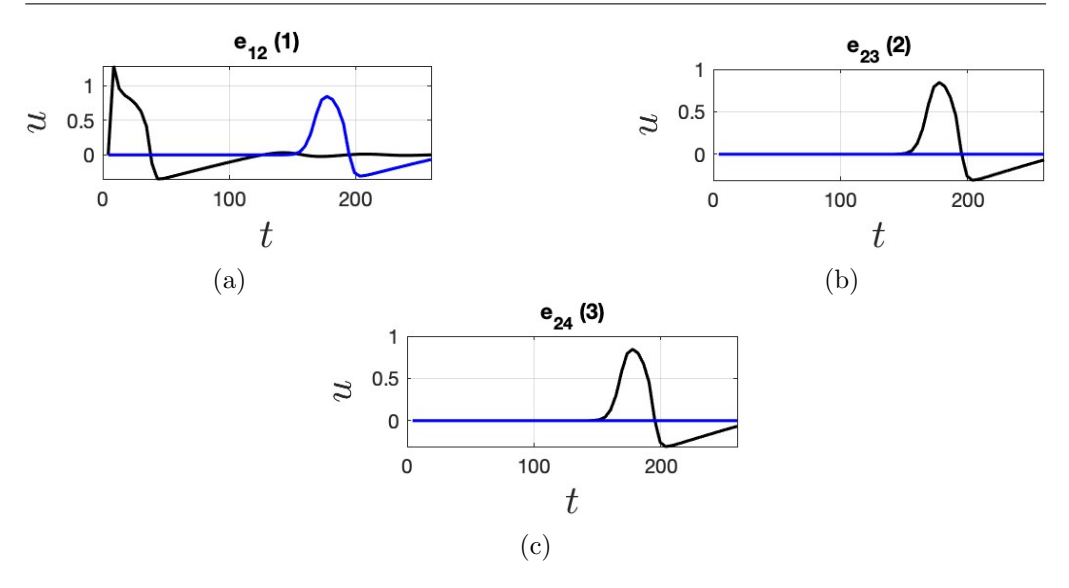


Figure 5.2.10: On the Y-shaped graph, Time evolution of the voltage in the axon variable u(x,t) for the edges in of the network. Each subplot represents the temporal behaviour within a edge. The blue curve highlights the early time evolution, while the black curve shows the progression toward steady-state. The figure illustrates how excitation propagates and stabilizes over time.

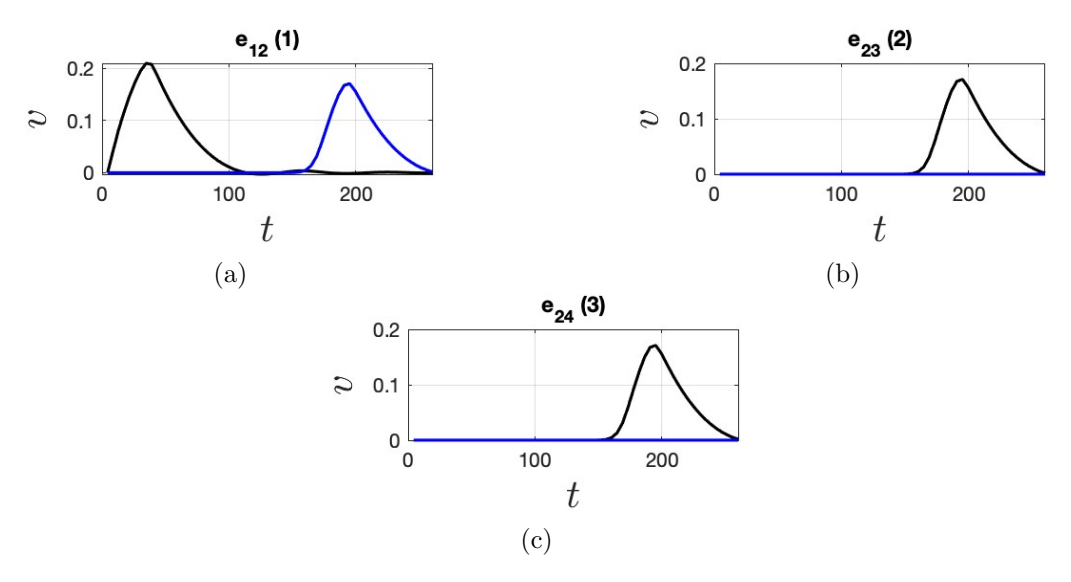


Figure 5.2.11: On the Y-shaped graph, Time evolution of the recovery variable v(t) for different edges in the network. Each subplot represents the temporal behaviour within an edge. The blue curve shows the early dynamics, while the black curve represents the progression toward steady-state. The recovery variable v(t) follows the excitation variable u(t), reflecting its inhibitory role in the system.

and

$$v_x v_{xx} = \omega(v_x b v - v_x u) \tag{5.3.6}$$

By subtracting equation (5.3.5) from equation (5.3.6), we obtain:

$$\omega u_x u_{xx} - v_x v_{xx} = \omega (v u_x + u v_x + u_x f(u) - b v v_x)$$

$$(5.3.7)$$

By integrating equation (5.3.7) with respect to x, we obtain:

$$\frac{1}{2}(\omega u_x^2 - v_x^2) = \omega(vu + g(u) - \frac{b}{2}v^2 + \kappa), \tag{5.3.8}$$

where  $\kappa$  is constant, and the function  $g(u) = \int f(u)$  which is define as:

$$g(u) = \frac{u^4}{4} - \frac{1}{3}(1+a)u^3 + \frac{au^2}{2}$$

To analyse the system numerically, we defined the following variables:

$$u_1 = u$$
,  $u_2 = u_x$ ,  $u_3 = v$ ,  $u_4 = v_x$ 

, Which is transforms the system into matrix form:

$$\begin{bmatrix} u_{1x} \\ u_{2x} \\ u_{3x} \\ u_{4x} \end{bmatrix} = \begin{bmatrix} u_2 \\ u_3 + u_1(u_1 - a)(u_1 - 1) \\ u_4 \\ \omega b u_3 - u_1 \end{bmatrix}.$$

Alternatively the system can be expressed as:

$$\begin{bmatrix} u_{1x} \\ u_{2x} \\ u_{3x} \end{bmatrix} = \begin{bmatrix} u_2 \\ u_3 + u_1(u_1 - a)(u_1 - 1) \\ \sqrt{\omega(u_2^2 + bu_3^2 - 2u_1u_3 - 2g - 2\kappa)} \end{bmatrix}$$

Evaluating this system at x = 0 yields:

$$\begin{bmatrix} u_1 \\ u_2 \\ u_3 \end{bmatrix} = \begin{bmatrix} \text{unknown} \\ 0 \\ \text{unknown} \end{bmatrix},$$

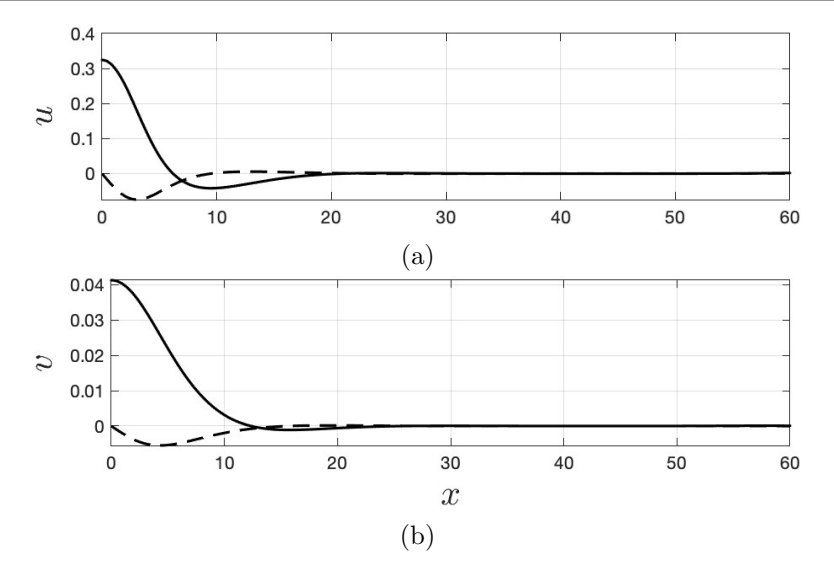


Figure 5.3.1: In the FitzHugh-Nagumo model on a path graph  $P_2$  with parameter values a = -0.04344,  $\lambda = 0.015$ ,  $\delta = 1.25$  and b = 3.5.(a) The spatial dynamics evolution of excitation u (solid line) and the derivative of u (dashed line). (b) The spatial dynamics evolution of recovery v (solid line) and the derivative of v (dashed line).

with the boundary conditions  $u_x = v_x = 0$  at x = 0, the constraint becomes:

$$uv + g(u) + \kappa - \frac{bv^2}{2} = 0$$

This results in a quadratic equation in v:

$$\frac{b}{2}v^2 - uv - (\kappa + g) = 0$$

Solving for v yields:

$$v = \frac{1}{b} \left[ u \pm \sqrt{u^2 + 4(\kappa + g)\frac{b}{2}} \right]$$
 (5.3.9)

The unknowns in this context are  $u_0 = u(0)$  and  $\kappa$ , with  $v_0 = v(0)$  given by equation (5.3.9). The boundary conditions at x = 0 and x = L are:

$$u_x = v_x = 0.$$

Using MATLAB and adjusting the parameters to a = -0.04344,  $\lambda = 0.015$ ,  $\delta = 1.25$  and b = 3.5, and setting the length of the element to 60, we obtain the following results for u as depicted in Figure 2 of Argentina's paper [1]. Setting

the initial value of  $u_0 = 0.32445$  the corresponding  $v_0$  calculated from equation (5.3.9), we obtained spatial profiles for both variables on a domain of length 60. Figure (5.3.1 (a)) shows the spatial profile of the excitation variable u (solid curve) and its derivative (dashed curve), while Figure (5.3.1 (b)) shows the corresponding profiles for the recovery variable v (solid curve) and its derivative (dashed curve).

#### 5.3.2 Small amplitude stationary solutions on $P_2$

In this subsection, we seek small amplitude stationary solutions to the timeindependent FitzHugh-Nagumo (FHN) system, namely,

$$u_{xx} = v + f(u),$$

$$\delta v_{xx} = \lambda(bv - u),$$
(5.3.10)

where f(u) = u(u - a)(u - 1) and f(0) = 0. We work on a path graph with two vertices,  $P_2$ . The Neumann boundary conditions  $u_x(0) = v_x(0) = 0$  and  $u_x(L) = v_x(L) = 0$  are imposed. We begin by noting that u = v = 0, for all x, is a trivial solution, and then we seek bifurcations from this state.

To proceed, we linearise about the zero solution. Accounting for the boundary condition at x = 0, we write

$$u = \varepsilon A \cos kx, \qquad v = \varepsilon B \cos kx,$$
 (5.3.11)

where  $\varepsilon \ll 1$ , and A and B are to be found. The boundary conditions at x = L then require that

$$\sin kL = 0$$

and hence

$$k = \frac{n\pi}{L} \equiv k_n, \tag{5.3.12}$$

for integer n.

Inserting into the main equations (5.3.10) we obtain the following linearised

equations:

$$-Ak^{2} = B + aA, \qquad -\delta Bk^{2} = \lambda(Bb - A).$$
 (5.3.13)

This leads to the matrix form:

$$\begin{bmatrix} a+k^2 & 1 \\ -\lambda & b\lambda + \delta k^2 \end{bmatrix} \begin{bmatrix} A \\ B \end{bmatrix} = \begin{bmatrix} 0 \\ 0 \end{bmatrix}$$

Solving, we obtain:

$$\delta k^4 + (b\lambda + a\delta)k^2 + \lambda(1 + ab) = 0. {(5.3.14)}$$

With  $k = k_n$ , where  $k_n$  is given by (5.3.12), we may rearrange the preceding expression to obtain the critical values of a, herein labelled  $a_c^n$ , at which stationary states emerge:

$$a_c^n = -\frac{(\delta k_n^4 + b k_n^2 \lambda + \lambda)}{\delta k_n^2 + b \lambda}.$$
 (5.3.15)

at which we expect a bifurcation to occur to a non-trivial state. Since, as was noted above,  $\lambda > 0$  and b > 0, it is clear that

$$a_c^n < 0.$$
 (5.3.16)

#### 5.3.3 Arbitrary amplitude stationary solutions on $P_2$

In the previous subsection we computed values of the parameter a at which we expect bifurcations to non-trivial stationary states to occur. Emerging from these bifurcation points we expect to find solution branches that lead to arbitrary amplitude stationary solutions. Such solutions cannot be found analytically and must be computed numerically. We address the latter in the current subsection. The computations will be done spectrally by expanding the unknown functions in series of Chebyshev polynomials.

Let us start by writing down the FitzHugh-Nagumo equations, viz,

$$u_t = -v - u(u - a)(u - 1) + u_{\xi\xi},$$
  

$$v_t = \lambda(bv - u) + \delta v_{\xi\xi},$$
(5.3.17)

where  $a, b, \lambda$ , and  $\delta$  are given constants. Here we use  $\xi$  as the independent variable defined over the single edge of the  $P_2$  graph, so that  $\xi \in [0, L]$ .

In the steady state  $(u_t = v_t = 0)$ , the equations reduce to:

$$0 = -v - u(u - a)(u - 1) + u_{\xi\xi},$$
  

$$0 = \lambda(bv - u) + \delta v_{\xi\xi}.$$
(5.3.18)

We seek static solutions with Neumann boundary conditions at the domain ends:

$$u_{\xi}(0) = u_{\xi}(L) = 0, \quad v_{\xi}(0) = v_{\xi}(L) = 0.$$
 (5.3.19)

Since we intend to use Chebyshev polynomials, which are defined canonically on the domain [-1,1], to prepare for the numerical method, we map the domain  $\xi \in [0,L]$  to  $x \in [-1,1]$  using the transformation:

$$x = \frac{2\xi}{L} - 1. (5.3.20)$$

Rewriting equation (5.3.18) in terms of x, we obtain:

$$0 = -v - u(u - a)(u - 1) + \left(\frac{2}{L}\right)^2 u_{xx},$$
  

$$0 = \lambda(bv - u) + \delta\left(\frac{2}{L}\right)^2 v_{xx}.$$
(5.3.21)

We compute a solution numerically using a Chebyshev collocation method (e.g. [14], [42]). The basic idea is to represent the solution as a Chebyshev series

$$u(x) = \sum_{n=0}^{N} a_n T_n(x), \qquad v(x) = \sum_{n=0}^{N} b_n T_n(x)$$
 (5.3.22)

for some truncation level N. We aim to compute the coefficients  $a_n$ . Note that (5.3.22) is a polynomial of degree N. We introduce a set of collocation points over [-1,1]. Since we are effectively performing an interpolation, instead of choosing equally-spaced points, which are known to lead to disastrous results, we instead select the Chebyshev points (also known as the Gauss-Lobatto points) (see [42])

$$x_j = \cos \theta_j, \quad \theta_j = \frac{j\pi}{N}, \quad 0 \le j \le N.$$
 (5.3.23)

The reason for doing this is twofold:

- Equally-spaced points have terrible interpolation properties. Chebyshev points cluster at the ends of the interval where interpolation problems are usually focussed.
- 2. We can then exploit the fact that

$$T_n(x) = \cos n\theta, \quad x = \cos \theta.$$
 (5.3.24)

Thus, evaluating (5.3.22) on the grid we have

$$u(x_j) = \sum_{n=0}^{N} a_n T_n(x_j) = \sum_{n=0}^{N} a_n \cos\left(\frac{n\pi j}{N}\right).$$
 (5.3.25)

Proceeding, we substitute (5.3.22) (and its v counterpart) into the governing equations and apply at each collocation point to obtain a system of 2(N+1) nonlinear algebraic equations in the unknown Chebyshev coefficients. In keeping with (5.3.19) we also demand that

$$u_x(-1) = u_x(1) = 0, \quad v_x(-1) = v_x(1) = 0.$$
 (5.3.26)

Differentiating  $T_n(x)$ :

$$T'_n(x) = -n\sin(n\theta)\frac{d\theta}{dx} = \frac{n\sin n\theta}{\sin \theta}.$$
 (5.3.27)

And we may differentiate again to get  $T''_n(x)$ . Expanding carefully about  $\theta = 0$ and  $\theta = \pi$ , we can deduce that

$$T'_n(-1) = -n^2 \cos n\pi,$$
  $T'_n(1) = n^2,$  (5.3.28)

$$T'_n(-1) = -n^2 \cos n\pi, \qquad T'_n(1) = n^2, \qquad (5.3.28)$$

$$T''_n(-1) = \frac{1}{3}n^2(n^2 - 1)\cos n\pi, \qquad T''_n(1) = \frac{1}{3}n^2(n^2 - 1). \qquad (5.3.29)$$

Using all of this, we solve the equations at the collocation points and the four boundary condition equations using Newton's method to get a solution.

The question arises immediately as to what initial guess to take for Newton's method to ensure that we latch onto a non-trivial state and don't simply converge to the known trivial solution u = v = 0. We choose to take the small amplitude linear solution discussed in the previous section. That solution took the form

$$u = \varepsilon A \cos k\xi, \qquad v = \varepsilon B \cos k\xi,$$

with  $k = k_n$  and  $k_n$  given by (5.3.12) (note the shift in notation for the independent variable from (5.3.11)). Unfortunately, this solution is written in terms of trigonometric functions, whereas our numerical method utilises Chebyshev polynomials. The one can be rationalised with the other, however. Before doing this, we must convert the independent variable. Recall that from (5.3.20)

$$x = \frac{2\xi}{L} - 1.$$

Hence

$$\xi = \frac{L}{2}(x+1).$$

Thus, since from (5.3.12),  $k = n\pi/L = k_n$ ,

$$\cos k\xi = \cos\left(\frac{kL}{2}(1+x)\right) = \cos\left(\frac{n\pi}{2}(1+x)\right) \tag{5.3.30}$$

Hence

$$\cos k\xi = \cos\left(\frac{n\pi}{2}\right)\cos\left(\frac{n\pi}{2}x\right) - \sin\left(\frac{n\pi}{2}\right)\sin\left(\frac{n\pi}{2}x\right). \tag{5.3.31}$$

Therefore:

$$n \text{ odd } : \cos k\xi = (-1)^{\frac{n+1}{2}} \sin\left(\frac{n\pi}{2}x\right);$$

$$n \text{ even } : \cos k\xi = (-1)^{\frac{n}{2}} \cos\left(\frac{n\pi}{2}x\right).$$

$$(5.3.32)$$

The next problem is to convert the trigonometric functions into Chebyshev polynomials. From Wünsche [47] eq. (3.20) we have

$$\cos r\xi = J_0(r) + 2\sum_{m=1}^{\infty} (-1)^m J_{2m}(r) T_{2m}(\xi), \qquad (5.3.33)$$

$$\sin r\xi = 2\sum_{m=0}^{\infty} (-1)^m J_{2m+1}(r) T_{2m+1}(\xi), \qquad (5.3.34)$$

where  $J_n(r)$  are the Bessel functions of the first kind.

#### 5.3.4 Small amplitude stationary solutions on a network

Up to now we have treated the stationary FitzHugh-Nagumo problem on a path graph  $P_2$ . More generally we would like to be able to determine solutions on any network. With that in mind we herein consider small amplitude solutions on a general network. The analysis essentially mimics that for a path graph  $P_2$ .

On any edge in the network we have the system of equations

$$u_{t} = -v - u(u - a)(u - 1) + u_{xx},$$

$$v_{t} = -\lambda(bv - u) + \delta v_{xx},$$
(5.3.35)

where  $a, b, \lambda, \delta$  are given constants, and x belongs to the interval [0, L]. We transform each edge from [0, L] into [0, 1] to be consistent with our discussion of networks earlier in the thesis (wherein each edge length was normalised to unity). Writing

$$\xi = x/L, \tag{5.3.36}$$

equations (5.3.35) become

$$u_t = -v - u(u - a)(u - 1) + \rho u_{\xi\xi},$$
 (5.3.37)

$$v_t = -\lambda(bv - u) + \delta\rho v_{\xi\xi},\tag{5.3.38}$$

where

$$\rho = 1/L^2, (5.3.39)$$

and  $\xi \in [0,1]$ . The steady form of these equations is

$$\rho u_{\xi\xi} = f(u, v), \tag{5.3.40}$$

$$\rho v_{\xi\xi} = g(u, v), \tag{5.3.41}$$

in which

$$f(u,v) = v + u(u-a)(u-1), (5.3.42)$$

$$g(u,v) = \hat{\lambda}(bv - u), \tag{5.3.43}$$

where we have defined

$$\hat{\lambda} = \lambda/\delta. \tag{5.3.44}$$

We seek a solution on a network. The boundary conditions are

$$u_{\xi} = v_{\xi} = 0 \tag{5.3.45}$$

at a boundary vertex; and  $u, v, u_{\xi}$ , and  $v_{\xi}$  are all continuous at a common vertex. We note that a solution is u = v = 0 everywhere.

If  $|u|, |v| \ll 1$ , we can Taylor expand the f, g terms as follows:

$$f(u,v) = f(0,0) + f_u(0,0)u + f_v(0,0)v + \cdots, \qquad (5.3.46)$$

$$g(u,v) = g(0,0) + g_u(0,0)u + g_v(0,0)v + \cdots$$
(5.3.47)

Here from (5.3.42) and (5.3.43) we compute

$$f_u(0,0) = a, \quad f_v(0,0) = 1,$$
 (5.3.48)

$$g_u(0,0) = -\hat{\lambda}, \quad g_v(0,0) = \hat{\lambda}b.$$
 (5.3.49)

Then (5.3.40) and (5.3.41) become (neglecting non-linear terms):

$$\rho u_{\xi\xi} = au + v, \tag{5.3.50}$$

$$\rho v_{\xi\xi} = \hat{\lambda}(bv - u) \tag{5.3.51}$$

Let us introduce the vector  $\boldsymbol{u} = (u, v)^T$ . Then the linearised system takes the form

$$\rho \boldsymbol{u}_{\xi\xi} = \boldsymbol{J}\boldsymbol{u},\tag{5.3.52}$$

where

$$J = \begin{pmatrix} a & 1 \\ -\hat{\lambda} & \hat{\lambda}b \end{pmatrix}. \tag{5.3.53}$$

To solve the system, we write the solution of the form

$$\boldsymbol{u} = e^{ik\xi}\boldsymbol{q},\tag{5.3.54}$$

for constant vector  $\boldsymbol{q}$  and real wavenumber k, then we have

$$(\boldsymbol{J} + \rho k^2 \boldsymbol{I})\boldsymbol{q} = 0. \tag{5.3.55}$$

We therefore require  $\det(\boldsymbol{J} + \rho k^2 \boldsymbol{I}) = 0$ , so that

$$(a + \rho k^2)(\hat{\lambda}b + \rho k^2) + \hat{\lambda} = 0$$
 (5.3.56)

and thus

$$\rho^2 k^4 + (a + \hat{\lambda}b)\rho k^2 + \hat{\lambda}(ab+1) = 0.$$
 (5.3.57)

This equation coincides with (5.3.14) on setting  $\rho = 1$  and recalling the definition

above that  $\hat{\lambda} = \lambda/\delta$ .

The result (5.3.57) represents a quartic equation for the wavenumber  $\sqrt{\rho} k = k/L$  on using (5.3.39). Given a value of  $\sqrt{\rho} k$  it imposes a condition on the parameters a, b and  $\hat{\lambda}$  for a bifurcation to a non-zero state to occur. Writing  $\kappa = \sqrt{\rho} k$ , (5.3.57) may be rewritten as  $F(\kappa) = 0$ , where

$$F(\kappa) = \kappa^4 + B\kappa^2 + C,\tag{5.3.58}$$

where  $B = a + \hat{\lambda}b$  and  $C = \hat{\lambda}(ab+1)$ . Now (5.3.58) has real roots for  $\kappa^2$  if  $B^2 - 4C \ge 0$ , i.e. if  $(a + \hat{\lambda}b)^2 - 4[\hat{\lambda}(ab+1)] \ge 0$ . The latter simplifies to

$$(a - \hat{\lambda}b)^2 \ge 4\hat{\lambda}.\tag{5.3.59}$$

If (5.3.59) holds then  $\kappa^2 \in \mathbb{R}$ , but it may be that  $\kappa^2 < 0$  for one or both of the two roots. Evidently

$$\kappa_{\pm}^2 = \frac{1}{2} \left( -B \pm (B^2 - 4C)^{1/2} \right),$$

and we can clearly arrange to get at least one positive root, for example by choosing parameters such that B>0 and C<0 and selecting  $\kappa_+^2>0$ . Then clearly  $\kappa_+>0$ .

For illustration let us set the parameter values (we shall return to these values later)

$$\lambda = 2.5, \qquad b = 3.5, \qquad \delta = 1.0.$$
 (5.3.60)

Then (5.3.59) requires

$$a < 5.588$$
 or  $a > 11.912$ 

Figure 5.3.2 shows F plotted against  $\kappa^2$  for the parameter values (5.3.60) and a = -5.0. Evidently the right-hand root is positive.

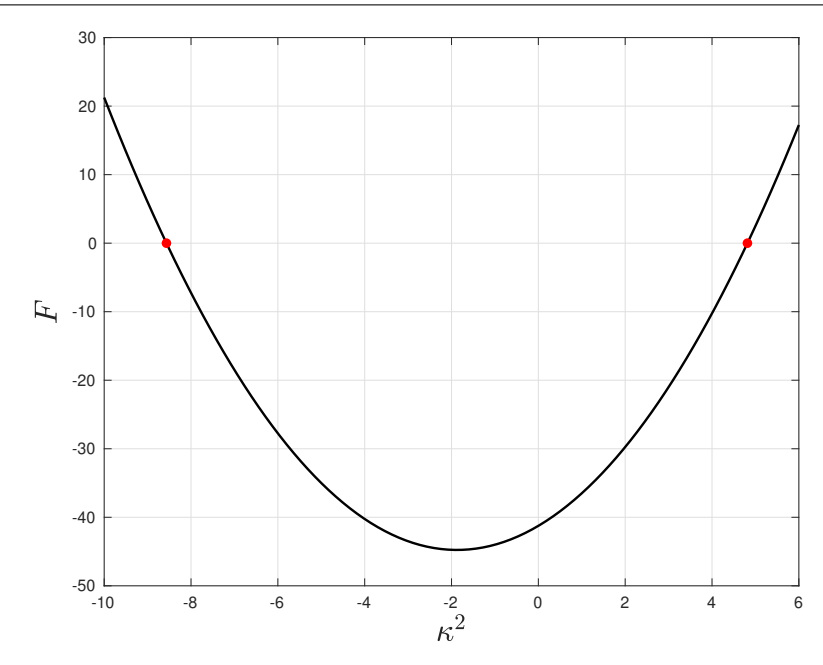


Figure 5.3.2: Plot of the function F, defined in (5.3.58), against  $\kappa^2$  for the parameter values  $a=-5,\ \lambda=2.5,\ b=3.5,\ and\ \delta=1.0.$  The red marker points indicate the zeros where F=0.

Having said this, it is not sufficient to establish that real  $\kappa$  and hence real k are possible for certain parameter choices. We must also ensure that the selected k value is such that the relevant boundary conditions across the network are satisfied. This is to say that we must ensure continuity of concentration at every vertex and continuity of flux at every vertex, as well as appropriate conditions at the boundary vertices. To move forward therefore, we should first establish the possible set of k values that are consistent with the network boundary conditions, and then select parameter values a, b,  $\hat{\lambda}$  that, together with a k value chosen from this set, satisfy (5.3.57). We discuss how to construct the set of acceptable k values in the next section.

# 5.3.5 Small amplitude stationary solution on a network: wave number compatibility

In the previous section we showed that it is possible to find parameter values corresponding to bifurcation points onto a branch of steady solutions to the FitzHugh-Nagumo equations on a network. However, we noted that the associated wavenumber must be consistent with the boundary conditions across the network. Herein we address the latter point and construct the set of allowable k.

Taking inspiration from the work in chapter 2 (specifically, see (2.2.16)), and referring to (5.3.54), now replacing  $\boldsymbol{u}$  with  $\boldsymbol{u}_{ij}$  to represent the solution on edge  $e_{ij}$ , we write, assuming  $\sin k \neq 0$ ,

$$\mathbf{u}_{ij}(\xi) = (\sin k)^{-1} (\mathbf{U}_i \sin k\xi + \mathbf{U}_i \sin k(1-\xi)),$$
 (5.3.61)

where  $U_i$  are the vertex values, i.e.  $u_{ij}(0) = U_i$  and  $u_{ij}(1) = U_j$ . Here  $U_i = (u_i, v_i)^T$ , where  $u_i$ ,  $v_i$  are the values of u and v, respectively, at vertex i. The form (5.3.61) satisfies the linearised governing equation (5.3.52) provided that (5.3.57) holds and that  $U_i$ ,  $U_j$  both satisfy (5.3.55). Thus we need all vertex vectors  $U_i$  to satisfy the constraint

$$(\mathbf{J} + \rho k^2 \mathbf{I}) \mathbf{U}_i = 0 \tag{5.3.62}$$

for i = 1, 2, ..., N, where N is the total number of vertices. It is via this constraint that the independent variables (for Fitzhugh-Nagumo these are u and v) interact with one another. From the definition for J in (5.3.53), the constraint (5.3.62) becomes

$$\begin{pmatrix} a + \rho k^2 & 1 \\ -\hat{\lambda} & \hat{\lambda}b + \rho k^2 \end{pmatrix} U_i = 0.$$
 (5.3.63)

To consider the case  $\sin k = 0$  it's helpful to first rewrite (5.3.61) as

$$\mathbf{u}_{ij}(\xi) = (\sin k)^{-1} [\mathbf{U}_j - \mathbf{U}_i \cos k] \sin k\xi + \mathbf{U}_i \cos k\xi.$$
 (5.3.64)

This forces

$$U_j - U_i \cos k = 0 \qquad \Longrightarrow \qquad U_i = (-1)^k U_j, \qquad (5.3.65)$$

leaving the eigenfunction

$$\mathbf{u}_{ij}(\xi) = \mathbf{U}_i \cos k\xi, \qquad \mathbf{U}_i = (-1)^k \mathbf{U}_j. \tag{5.3.66}$$

and again we have the requirement that  $U_i$  satisfies (5.3.62).

Let us now define the vertex concentration vectors

$$\mathbf{x}_u = (u_1, u_2, \dots, u_N)^T, \qquad \mathbf{x}_v = (v_1, v_2, \dots, v_N)^T,$$
 (5.3.67)

where N is the total number of vertices in the network. To correctly determine these vectors two points need to be considered

- (i) The concentrations must be compatible with all flux and continuity conditions across the network.
- (ii) The concentrations must be compatible with the dynamics imposed by the FitzHugh-Nagumo system.

To address point (i) first we now apply the flux-continuity conditions to the vertex concentrations  $u_i$ , i = 1, 2, ..., N across the network. To do this, we know from chapter 2 that the following condition must hold:

$$\boldsymbol{L}^*(k)\boldsymbol{x}_u = 0, \tag{5.3.68}$$

where

$$\boldsymbol{L}^*(k) = \boldsymbol{A} - (\cos k)\boldsymbol{D} \tag{5.3.69}$$

is the modified Laplacian for the network (see chapter 2 equation (2.3.7)). Therefore the possible k values must satisfy the equation

$$\det \mathbf{L}^*(k) = 0, \tag{5.3.70}$$

whose precise form is dictated by the network structure.

Now that  $x_u$  is determined (to within a multiplicative constant as is normal for an eigenvector), to address point (ii) we fix the  $v_i$  concentrations by choosing, at

each vertex,  $v_i$  such that (5.3.63) holds, namely

$$\begin{pmatrix} a + \rho k^2 & 1 \\ -\hat{\lambda} & \hat{\lambda}b + \rho k^2 \end{pmatrix} \begin{pmatrix} u_i \\ v_i \end{pmatrix} = 0.$$
 (5.3.71)

As noted above, this equation can hold only if (5.3.57) holds. Assuming it does,  $v_i$  is then determined in terms of  $u_i$  via (5.3.71). Necessarily, each  $v_i$  is proportional to  $u_i$ , for all i = 1, 2, ..., N. Since the latter is true it follows that

$$\boldsymbol{L}^*(k)\boldsymbol{x}_v = 0,$$

and continuity of concentration and flux of v across the network is assured.

#### Summary

To recap and summarise:

- 1. We determine the set of acceptable wavenumbers, k, for the network by solving (5.3.70), viz. det  $L^*(k) = 0$ . We then determine the set of acceptable concentration vectors  $x_u$  for the network by solving  $L^*(k)x_u = 0$ . This problem has already been discussed for various networks in chapter 2.
- **2.** Once the set of possible k values is computed, we select one particular k value. We then fix the parameter set  $\{a, b, \hat{\lambda}, \rho\}$  so that  $det(J + \rho k^2 I) = 0$  holds, i.e. (5.3.57) holds, viz

$$\rho^2 k^4 + (a + \hat{\lambda}b)\rho k^2 + \hat{\lambda}(ab+1) = 0.$$
 (5.3.72)

3. Finally, the vertex concentration vector  $\boldsymbol{x}_v$  is found by solving (5.3.63) at each vertex, namely

$$\begin{pmatrix} a + \rho k^2 & 1 \\ -\hat{\lambda} & \hat{\lambda}b + \rho k^2 \end{pmatrix} U_i = \begin{pmatrix} a + \rho k^2 & 1 \\ -\hat{\lambda} & \hat{\lambda}b + \rho k^2 \end{pmatrix} \begin{pmatrix} u_i \\ v_i \end{pmatrix} = 0, \quad (5.3.73)$$

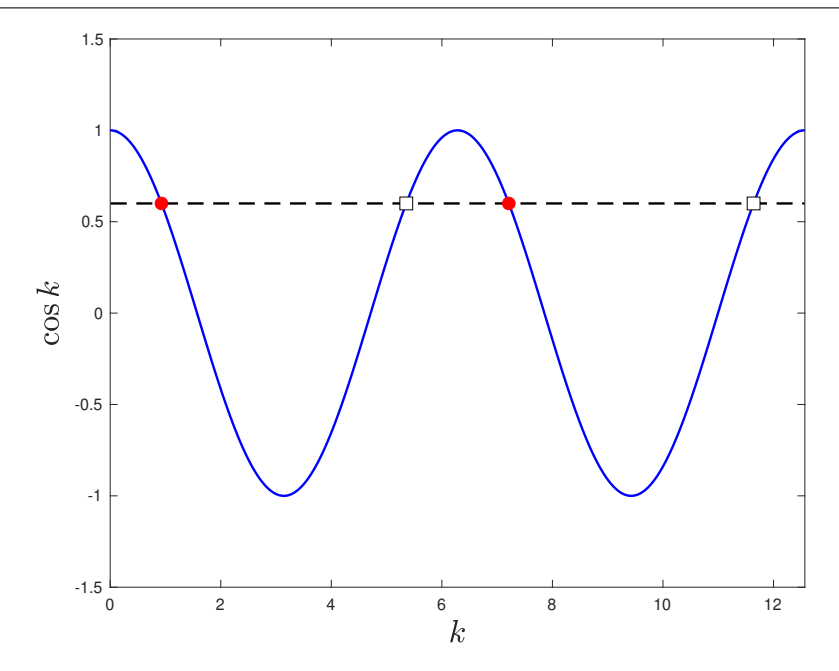


Figure 5.3.3: Demonstrating the set of possible k values for a given value of  $\cos k$ . The black dashed line indicates the value  $\cos k = 0.6$  for illustration. The red dots indicate the values  $\cos^{-1}(0.6) = 0.9273 + 2n\pi$ , for integer n. The white-filled squares indicate the values  $\cos^{-1}(0.6) = 5.356 + 2n\pi$ , for integer n.

for i = 1, 2, ..., N.

In practice, we shall start by selecting a network structure (e.g. a Y-shaped graph, for example), and then follow steps 1-3 as described above. Typically, we will select values for b,  $\hat{\lambda}$  (=  $\lambda/\delta$ ) and  $\rho$  (=  $1/L^2$ ), and use the relation (5.3.72) to fix a, i.e. we set  $a = a_c^n$ , where

$$a_c^n = -\frac{\rho^2 k^4 + \hat{\lambda} b \rho k^2 + \hat{\lambda}}{\hat{\lambda} b + \rho k^2} < 0.$$
 (5.3.74)

For a network with N vertices the condition (5.3.70) fixes N possible (and possibly repeated) values of  $\cos k$ . Each value of  $\cos k$  then corresponds to an infinite set of possible k values, as is illustrated in Figure 5.3.3.

# 5.3.6 Small amplitude stationary solution on a network: examples

In this section we give a couple of examples of networks and compute the relevant small amplitude solution according to the prescription laid out in the previous section.

#### • Path graph $P_2$

In this case

$$\mathbf{A} = \begin{pmatrix} 0 & 1 \\ 1 & 0 \end{pmatrix}, \qquad \mathbf{D} = \begin{pmatrix} 1 & 0 \\ 0 & 1 \end{pmatrix}. \tag{5.3.75}$$

In this case condition (5.3.70), namely det  $L^*(k)x_u = 0$  requires

$$\begin{vmatrix} -\cos k & 1 \\ 1 & -\cos k \end{vmatrix} = 0 \implies \cos k = \pm 1 \tag{5.3.76}$$

and so  $k = n\pi$  for integer n.

For  $k = 2n\pi$  (cos k = 1), the corresponding eigenvector satisfies

$$\begin{pmatrix} -1 & 1 \\ 1 & -1 \end{pmatrix} \begin{pmatrix} u_1 \\ u_2 \end{pmatrix} = \begin{pmatrix} 0 \\ 0 \end{pmatrix} \tag{5.3.77}$$

We find

$$m{x}_u = egin{pmatrix} u_1 \ u_2 \end{pmatrix} = egin{pmatrix} 1 \ 1 \end{pmatrix}.$$

For  $k = (2n+1)\pi$  (cos k = -1) the corresponding eigenvector satisfies

$$\begin{pmatrix} 1 & 1 \\ 1 & 1 \end{pmatrix} \begin{pmatrix} u_1 \\ u_2 \end{pmatrix} = \begin{pmatrix} 0 \\ 0 \end{pmatrix} \tag{5.3.78}$$

This yields

$$x_u = \begin{pmatrix} u_1 \\ u_2 \end{pmatrix} = \begin{pmatrix} 1 \\ -1 \end{pmatrix}.$$

In either case we find  $x_v$  by solving (5.3.63). Since if either  $k = 2n\pi$  or  $k = (2n+1)\pi$  we have  $\sin k = 0$ , the form of the eigenfunctions on the edge is given by (5.3.66). So we have

$$u_{12}(\xi) = U_1 \cos k\xi, \qquad U_1 = (-1)^k U_2,$$

## $\bullet$ Path graph $P_3$

In this case

$$\mathbf{A} = \begin{pmatrix} 0 & 1 & 0 \\ 1 & 0 & 1 \\ 0 & 1 & 0 \end{pmatrix}, \quad \mathbf{D} = \begin{pmatrix} 1 & 0 & 0 \\ 0 & 2 & 0 \\ 0 & 0 & 1 \end{pmatrix}. \tag{5.3.79}$$

Thus we need

$$\begin{vmatrix} -\nu & 1 & 0 \\ 1 & -2\nu & 1 \\ 0 & 1 & -\nu \end{vmatrix} = 0, \tag{5.3.80}$$

where  $\nu = \cos k$ . Expanding, we find  $\nu(1 - \nu^2) = 0$ . So

$$\cos k = 0, \pm 1 \tag{5.3.81}$$

and thus  $k = n\pi/2$  for integer n.

For  $k = n\pi$  with n even  $(\nu = \cos k = 1)$ , the eigenvector satisfies

$$\begin{pmatrix} -1 & 1 & 0 \\ 1 & -2 & 1 \\ 0 & 1 & -1 \end{pmatrix} \begin{pmatrix} u_1 \\ u_2 \\ u_3 \end{pmatrix} = \begin{pmatrix} 0 \\ 0 \\ 0 \end{pmatrix}$$
 (5.3.82)

We find

$$m{x}_u = egin{pmatrix} u_1 \ u_2 \ u_3 \end{pmatrix} = egin{pmatrix} 1 \ 1 \ 1 \end{pmatrix}.$$

For  $k = n\pi$  with n odd ( $\nu = \cos k = -1$ ), the eigenvector satisfies

$$\begin{pmatrix} 1 & 1 & 0 \\ 1 & 2 & 1 \\ 0 & 1 & 1 \end{pmatrix} \begin{pmatrix} u_1 \\ u_2 \\ u_3 \end{pmatrix} = \begin{pmatrix} 0 \\ 0 \\ 0 \end{pmatrix}$$
 (5.3.83)

We find

$$m{x}_u = egin{pmatrix} u_1 \ u_2 \ u_3 \end{pmatrix} = egin{pmatrix} 1 \ -1 \ 1 \end{pmatrix}.$$

For  $k = n\pi/2$  with n odd ( $\nu = \cos k = 0$ ), the eigenvector satisfies

$$\begin{pmatrix} 0 & 1 & 0 \\ 1 & 0 & 1 \\ 0 & 1 & 0 \end{pmatrix} \begin{pmatrix} u_1 \\ u_2 \\ u_3 \end{pmatrix} = \begin{pmatrix} 0 \\ 0 \\ 0 \end{pmatrix}$$
 (5.3.84)

We find

$$\boldsymbol{x}_u = \begin{pmatrix} u_1 \\ u_2 \\ u_3 \end{pmatrix} = \begin{pmatrix} 1 \\ 0 \\ -1 \end{pmatrix}.$$

# 5.3.7 Small amplitude stationary solution on a network: initial guess for the numerical method

We will obtain the solution over a network numerically using a Chebyshev expansion approach, similar to what we did earlier. To this end we need to map  $\xi \in [0,1]$  on each edge to the canonical interval  $x \in [-1,1]$ . We do this by

setting

$$x = 2\xi - 1$$
  $\Longrightarrow$   $\xi = \frac{1}{2}(1+x).$  (5.3.85)

Then (5.3.40) and (5.3.41) become

$$\tilde{\rho}u_{xx} = f(u, v), \tag{5.3.86}$$

$$\tilde{\rho}v_{xx} = g(u, v), \tag{5.3.87}$$

where  $\tilde{\rho} = (2/L)^2$ .

To compute the static solution, we expand U(x) and V(x) as finite Chebyshev series:

$$U(x) = \sum_{n=0}^{N} U_n T_n(x), \qquad V(x) = \sum_{n=0}^{N} V_n T_n(x),$$

where  $T_n(x)$  are the Chebyshev polynomials of the first kind. By inserting these expansions into the equation (5.5.7) and evaluating at M collocation points  $x_i$ , we obtain a system of 2N non-linear algebraic equations,

$$f(U) + DU_{xx} = F(x) = 0,$$
 (5.3.88)

where  $\boldsymbol{x} = (U_1, U_2, \dots, U_N, V_1, \dots, V_N)^T$  and  $\boldsymbol{F} \in \mathbb{R}^{2N}$ . The static solution can be found via Newton's method, where each iteration proceeds as follows:

$$x^{n+1} = x^n - \mathbf{H}^{-1} \mathbf{F}(x^n), \tag{5.3.89}$$

with the Jacobian matrix

$$\boldsymbol{H} = \boldsymbol{J}, \text{ where } \boldsymbol{J_{ij}} = \frac{\partial f_i}{\partial x_j}.$$
 (5.3.90)

The initial guess for Newton's method is constructed using the small amplitude solution over a network discussed earlier. The complication in doing this is that we must cross-refer between trigonometric functions and Chebyshev polynomials. Our eigenfunctions (5.3.61) or (5.3.66) contain terms  $\sin k\xi$  and  $\cos k\xi$ . We note that

$$\cos k\xi = \cos\left(\frac{k}{2}(1+x)\right) = \cos\frac{k}{2}\cos\frac{kx}{2} - \sin\frac{k}{2}\sin\frac{kx}{2},\tag{5.3.91}$$

and

$$\sin k\xi = \sin\left(\frac{k}{2}(1+x)\right) = \sin\frac{k}{2}\cos\frac{kx}{2} + \cos\frac{k}{2}\sin\frac{kx}{2}.$$
 (5.3.92)

Thus the eigenfunction (5.3.64) is:

$$\mathbf{u}_{ij} = (\sin k)^{-1} [\mathbf{U}_j - \mathbf{U}_i \cos k] \sin k\xi + \mathbf{U}_i \cos k\xi$$
 (5.3.93)

$$= \mathbf{A_c} \cos \frac{kx}{2} + \mathbf{A_s} \sin \frac{kx}{2}, \tag{5.3.94}$$

where

$$\mathbf{A}_{c} = \frac{\sin(k/2)}{\sin k} (\mathbf{U}_{j} - \mathbf{U}_{i} \cos k) + \cos(k/2) \mathbf{U}_{i}$$

$$(5.3.95)$$

$$\mathbf{A}_{s} = \frac{\cos(k/2)}{\sin k} (\mathbf{U}_{j} - \mathbf{U}_{i} \cos k) - \sin(k/2) \mathbf{U}_{i}. \tag{5.3.96}$$

The eigenfunction (5.3.66) is

$$u_{ij} = U_i \cos k\xi = A_c \cos \frac{kx}{2} + A_s \sin \frac{kx}{2},$$

with

$$\mathbf{A_c} = \mathbf{U}_i \cos(k/2), \qquad \mathbf{A_s} = -\mathbf{U}_i \sin(k/2).$$

The next problem is to convert the trigonometric functions into Chebyshev polynomials. From Wünsche [47] (eq. 3.20) we have, for constant  $\kappa$ ,

$$\cos \kappa x = J_0(\kappa) + 2\sum_{m=1}^{\infty} (-1)^m J_{2m}(\kappa) T_{2m}(x),$$

$$\sin \kappa x = 2 \sum_{m=0}^{\infty} (-1)^m J_{2m+1}(\kappa) T_{2m+1}(x).$$

# 5.4 Uniform solution on a network

In the previous sections, we have concentrated on computing non-uniform stationary solutions of the FitzHugh-Nagumo equations on a general network. In this section, we address the simpler problem of determining uniform solutions, that is, solutions for which the concentrations u and v are everywhere constant over the network. The problem is, of course, equivalent to determining constant solutions to the FitzHugh-Nagumo equations on a single edge, the geometry of the network being irrelevant since all of the network boundary conditions (continuity of flux, etc.) are automatically satisfied.

To determine constant solutions, we require the functions f and g to vanish. Recall that

$$f(u,v) = v + u(u-a)(u-1)$$

$$g(u, v) = \hat{\lambda}(bv - u).$$

Thus we require

$$v + u(u - a)(u - 1) = 0 (5.4.1)$$

$$\hat{\lambda}(bv - u) = 0 \tag{5.4.2}$$

Hence

$$u = bv. (5.4.3)$$

Using this result and simplifying the first equation, we obtain:

$$u\left(u^2 - (1+a)u + a + \frac{1}{b}\right) = 0, (5.4.4)$$

a cubic for u with, in general, three solutions. The trivial solution u=0 gives v=0. Non-trivial solutions occur if the quadratic

$$u^{2} - (1+a)u + a + \frac{1}{b} = 0 {(5.4.5)}$$

has real solutions. This requires that

$$(1-a)^2 > \frac{4}{b}$$
.

This condition evidently holds if a is sufficiently large. In general the solutions to the quadratic equation (5.4.5) are given by:

$$u = \frac{1}{2}(1+a) \pm \frac{1}{2}\left((1-a)^2 - \frac{4}{b}\right)^{\frac{1}{2}}.$$
 (5.4.6)

In the next two subsections we consider the cases of a large and positive/negative separately.

Case I:  $a \gg 1$ .

We consider the case where  $a \gg 1$  with a > 0. We can use the binomial expansion to obtain the approximations

$$u_{+} \sim a - \frac{1}{ba}, \qquad u_{-} \sim 1 + \frac{1}{ba}.$$
 (5.4.7)

Case II:  $a = -\kappa$  with  $\kappa \gg 1$ .

Now, let us examine the case where  $a = -\kappa$  with  $\kappa \gg 1$ . Equation (5.4.6) takes the form

$$u = \frac{1}{2}(1 - \kappa) \pm \frac{1}{2}\left((1 + \kappa)^2 - \frac{4}{b}\right)^{\frac{1}{2}}.$$
 (5.4.8)

Following a similar approach as before, we expand using the binomial theorem to obtain

$$u_{+} \sim 1 + \frac{1}{ba}, \qquad u_{-} \sim a - \frac{1}{ba},$$
 (5.4.9)

valid when  $-a \gg 1$ .

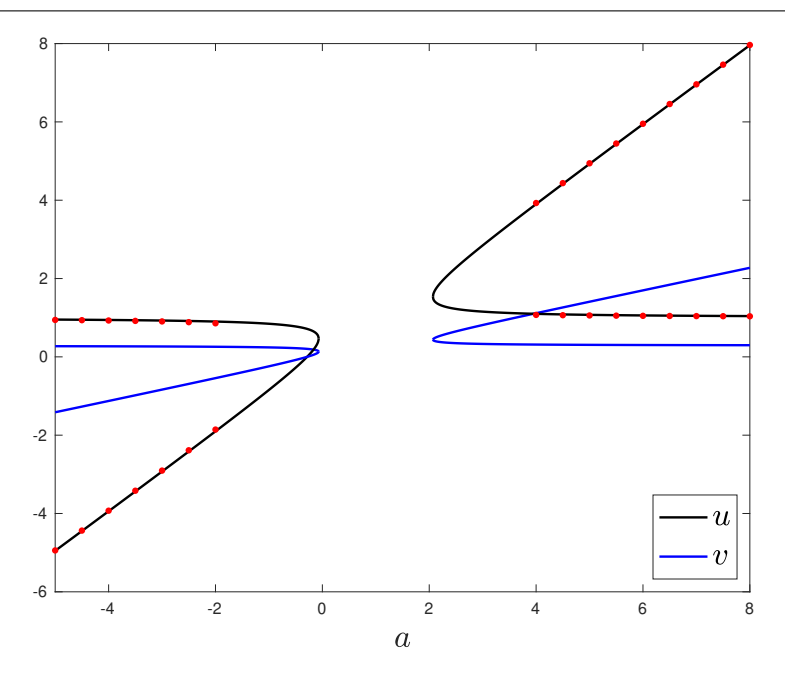


Figure 5.4.1: The space of uniform solutions for the case b = 3.5. Note that there is no uniform solution over the range -0.0690 < a < 2.069. The red dots indicate the asymptotic approximations (5.4.7) and (5.4.9).

In Figure 5.4.1 we show the possible uniform solutions, given by (5.4.6) and (5.4.3), for the case when b = 3.5. The values of u and v are shown plotted against the remaining parameter, a. Note that there is no solution over the range where  $(1-a)^2 < 4/b$ , i.e.

$$1 - \frac{2}{\sqrt{b}} < a < 1 + \frac{2}{\sqrt{b}}.$$

This is because if a lies within this range then (5.4.6) yields a complex u. In the present case this range is -0.0690 < a < 2.069. This appears as a gap between the solution curves in the figure. The asymptotic approximations (5.4.7) and (5.4.9) are also shown and can be seen to agree very well with the exact solutions.

# 5.5 Stationary solutions on a network: stability

Having discussed stationary solutions to the FitzHugh-Nagumo system on a network at some length, we now turn our attention to the stability of such solutions.

We recall that the governing equations are

$$u_t = f(u, v) + u_{XX}, \qquad v_t = g(u, v) + \delta v_{XX},$$
 (5.5.1)

where the functions f(u, v) and g(u, v) have been stated several times, and are repeated below for convenience. On any edge of the network we have  $X \in [0, L]$ . To map the problem on each edge onto the canonical interval  $x \in [-1, 1]$ , we apply the transformation

$$x = \frac{2}{L}X - 1. (5.5.2)$$

Under this transformation, the equations become

$$u_t = f(u, v) + \hat{\rho}u_{xx}, \qquad v_t = g(u, v) + \hat{\rho}\delta v_{xx},$$
 (5.5.3)

where

$$\hat{\rho} = \left(\frac{2}{L}\right)^2. \tag{5.5.4}$$

The non-linear functions f(u, v) and g(u, v) are given by

$$f(u,v) = u(u-a)(1-u) - v,$$
  $g(u,v) = \lambda(u-bv).$  (5.5.5)

In vector form, the system (5.5.3) can be expressed as

$$\boldsymbol{u}_t = \boldsymbol{f}(\boldsymbol{u}) + \boldsymbol{D}\boldsymbol{u}_{xx}, \tag{5.5.6}$$

where

$$m{u} = \begin{pmatrix} u \\ v \end{pmatrix}, \quad m{f}(m{u}) = \begin{pmatrix} f(u,v) \\ g(u,v) \end{pmatrix}, \quad m{D} = \begin{pmatrix} \hat{
ho} & 0 \\ 0 & \hat{
ho}\delta \end{pmatrix}.$$

Assume that we have computed a static solution

$$oldsymbol{u} = oldsymbol{U} = egin{pmatrix} U \ V \end{pmatrix},$$

where U = U(x) and V = V(x), which satisfies the static form of the system:

$$\mathbf{0} = \mathbf{f}(\mathbf{U}) + \mathbf{D}\mathbf{U}_{xx}.\tag{5.5.7}$$

To analyse the stability of the static solution, we perturb it by writing

$$\boldsymbol{u} = \boldsymbol{U} + \epsilon \boldsymbol{\eta}(x, t), \tag{5.5.8}$$

where  $\epsilon \ll 1$  and  $\eta$  is to be found. Stability is determined by the large time behaviour of  $\eta$ , i.e. if  $|\eta| \to 0$  as  $t \to \infty$  then the static solution is stable, and if  $|\eta| \to \infty$  as  $t \to \infty$  then the static solution is unstable.

Linearising around the static solution, we obtain

$$\eta_t = J\eta + D\eta_{xx},\tag{5.5.9}$$

where

$$J = \begin{pmatrix} \alpha_1 & \alpha_2 \\ \beta_1 & \beta_2 \end{pmatrix} \tag{5.5.10}$$

with

$$\alpha_1(x) = f_u(U, V) = -3U^2 + 2(1+a)U - a,$$
 (5.5.11)

$$\alpha_2(x) = f_v(U, V) = -1,$$
(5.5.12)

$$\beta_1(x) = g_u(U, V) = \lambda, \tag{5.5.13}$$

$$\beta_2(x) = g_v(U, V) = -\lambda b.$$
 (5.5.14)

Note that the elements of J in general depend on x. Assuming that we can separate the variables, we write

$$oldsymbol{\eta}(x,t) = e^{st}oldsymbol{p}(x), \qquad oldsymbol{p}(x) = egin{pmatrix} p(x) \ q(x) \end{pmatrix}.$$

This leads to the following eigenvalue problem

$$s\mathbf{p} = J\mathbf{p} + D\mathbf{p}'', \tag{5.5.15}$$

Written out in components this is

$$\hat{\rho}p'' + \alpha_1 p + \alpha_2 q = sp, \qquad \hat{\rho}\delta q'' + \beta_1 p + \beta_2 q = sq.$$
 (5.5.16)

Stability hinges on the sign of s, which we must determine. To this end we express p(x) and q(x) as Chebyshev series truncated at a finite level N, where N is to be chosen:

$$p(x) = \sum_{n=0}^{N} p_n T_n(x), \qquad q(x) = \sum_{n=0}^{N} q_n T_n(x), \qquad (5.5.17)$$

Inserting these into the stability equations (5.5.15), we obtain the generalized eigenvalue problem:

$$Jw = s\hat{T}w, \tag{5.5.18}$$

where  $\mathbf{w} = (p_1, \dots, p_N, q_1, \dots, q_N)^T$ , and  $\mathbf{J}$  was defined in (5.3.90). Note that the Jacobian matrix  $\mathbf{J}$  was already computed as part of Newton's method for the

static problem. We have also defined (for path graph  $P_2$ )

$$T = \begin{pmatrix} T_0(x_1) & T_1(x_1) & \cdots & T_N(x_1) & 0 & 0 & \cdots & 0 \\ \vdots & \vdots & \ddots & \vdots & 0 & 0 & \cdots & 0 \\ T_0(x_M) & T_1(x_M) & \cdots & T_N(x_M) & 0 & 0 & \cdots & 0 \\ 0 & 0 & \cdots & 0 & T_0(x_1) & T_1(x_1) & \cdots & T_N(x_1) \\ 0 & 0 & \cdots & 0 & \vdots & \vdots & \ddots & \vdots \\ 0 & 0 & \cdots & 0 & T_0(x_M) & T_1(x_M) & \cdots & T_N(x_M) \end{pmatrix}$$
(5.5.19)

The matrix  $\hat{T}$  is obtained by replacing the rows in T corresponding to the boundary conditions with zeros.

In summary, to determine the stability we must solve the generalized eigenvalue problem (5.5.18) for s.

### 5.5.1 Stability of the uniform state

Simplifications occur in the stability analysis when we consider the stability of the uniform state discussed in section 5.4. In this case U and V are constants and so the coefficients given in (5.5.11), and hence the elements of the Jacobian matrix J, are constants. In this case the eigenvalue problem (5.5.15), namely,

$$s\mathbf{p} = J\mathbf{p} + D\mathbf{p}'', \tag{5.5.20}$$

can be solved exactly. We write

$$p = (p, q)^T = e^{ikx}a, \qquad a = (A, B)^T.$$
 (5.5.21)

Then we have the matrix eigenvalue problem

$$\tilde{\boldsymbol{J}}(k) \begin{pmatrix} A \\ B \end{pmatrix} = s \begin{pmatrix} A \\ B \end{pmatrix}. \tag{5.5.22}$$

Here we have defined

$$\tilde{\boldsymbol{J}}(k) = \boldsymbol{J} - k^2 \boldsymbol{D} = \begin{pmatrix} m_1 & m_2 \\ m_3 & m_4 \end{pmatrix}$$
 (5.5.23)

with matrix elements

$$m_1 = \alpha_1 - \hat{\rho}k^2$$
,  $m_2 = -1$ ,  $m_3 = \lambda$ ,  $m_4 = -\lambda b - \hat{\rho}\delta k^2$ . (5.5.24)

Note that  $\alpha_1$  was given in (5.5.11). The eigenvalues s hence satisfy

$$s^2 - (\operatorname{tr}\tilde{\boldsymbol{J}})s + \det \tilde{\boldsymbol{J}} = 0, \tag{5.5.25}$$

where

$$\operatorname{tr}\tilde{\boldsymbol{J}} = m_1 + m_4 = (\alpha_1 - \lambda b) - \hat{\rho}(1+\delta)k^2,$$
 (5.5.26)

$$\det \tilde{J} = m_1 m_4 - m_2 m_3 = \lambda - (\alpha_1 - \hat{\rho}k^2)(\lambda b + \hat{\rho}\delta k^2). \tag{5.5.27}$$

Formula (5.5.25) simplifies further if we specialise to the zero state U = V = 0. In this case

$$\alpha_1 = f_u(0,0) = -a, \qquad \alpha_2 = f_v(0,0) = -1,$$

and

$$\beta_1 = g_u(0,0) = \lambda, \qquad \beta_2 = g_v(0,0) = -\lambda b.$$

The quadratic (5.5.25) becomes

$$s^{2} + (a + \lambda b + \hat{\rho}(1+\delta)k^{2})s + (a + \hat{\rho}k^{2})(\hat{\rho}\delta k^{2} + \lambda b) + \lambda = 0.$$
 (5.5.28)

(As an aside we note that if s = 0 this becomes, writing  $k^* = \sqrt{\hat{\rho}} k$ ,

$$\delta k^{*4} + (\lambda b + a\delta)k^{*2} + \lambda(1 + ab) = 0.$$
 (5.5.29)

This quadratic for  $k^{*2}$  coincides with that for  $k^2$  given in (5.3.14). The latter was the condition we derived for a small amplitude solution to exist and such a solution occurs at the bifurcation to stationary branch. It is therefore coincident with what is found via the present stability analysis when s = 0.)

Writing (5.5.28) in the form  $s^2 + \alpha s + \beta = 0$ , the solution is

$$s = \frac{1}{2} \left( -\alpha \pm \sqrt{\alpha^2 - 4\beta} \right), \tag{5.5.30}$$

where

$$\alpha = a + \lambda b + \hat{\rho}(1+\delta)k^2, \qquad \beta = (a+\hat{\rho}k^2)(\hat{\rho}\delta k^2 + \lambda b) + \lambda$$

Stability is determined by the sign of the real part of s, which in general may be complex depending on the sign of  $\alpha^2 - 4\beta$ .

It is worth at this point to summarise where we are. We have obtained the formula (5.5.30) for the stability about a uniform state and about the zero state. This formula involves the parameters a, b,  $\lambda$ ,  $\delta$  and  $\hat{\rho}$  and the wave number k. The situation is now similar to that discussed at the end of section 5.3.5. We proceed therefore via the following steps.

Step 1. We fix values of the parameters  $a, b, \lambda, \delta$  and  $\hat{\rho}$ .

Step 2. We ensure wave number compatibility of the ansatz (5.5.21) with the network by solving det  $L^*(k) = 0$ , where the modified Laplacian  $L^*$  was defined in (5.3.69). This determines the set K of k values that are compatible with the concentration and flux continuity conditions across the network.

Step 3. We choose a  $k \in K$  and solve for s either by solving (5.5.25) for a general uniform state, or by utilising formula (5.5.30) for the zero state.

Step 4. For the given pair (k, s), and the parameters  $a, b, \lambda, \delta$  and  $\hat{\rho}$  fixed, the vertex values of the perturbation eigenfunction for u are found by solving  $L^*x_u$ , where  $x_u$  is analogous to the vector defined in (5.3.67). The vertex values of the

perturbation eigenfunction for v are then found by solving for a the equation

$$s\boldsymbol{a} = (\boldsymbol{J} - k^2 \boldsymbol{D}) \boldsymbol{a}.$$

Step 5. Finally, the perturbation eigenfunctions are constructed across the network using either (5.3.64) or (5.3.66), depending on the value of k.

To determine stability of the uniform state at a particular set of parameter values  $\{a, b, \lambda, \delta, L\}$ , we must determine the sign of

$$s_M = \max_{k \in K} s.$$

If  $s_M > 0$  then the state is unstable; if  $s_M < 0$  then the state is stable.

For example, in the simplest case of the graph with one edge,  $P_2$ , and choosing the parameters

$$\delta = 1.0, \qquad L = 1.0,$$

we have for the zero state U = V = 0 from (5.5.30),

$$s = \frac{1}{2} \left( -\alpha \pm \sqrt{\alpha^2 - 4\beta} \right),$$

where

$$\alpha = a + \lambda b + 2k^2, \qquad \beta = (a + k^2)(k^2 + \lambda b) + \lambda$$

Then the discriminant is found be independent of k with  $\alpha^2 - 4\beta = (b\lambda + a)^2 - 4\lambda$ . Then

$$s_{\pm} = -k^2 + \phi_{\pm}(a, b, \lambda), \qquad \phi_{\pm} \equiv -\frac{1}{2}(a + \lambda b) \pm \frac{1}{2}\sqrt{(a + \lambda b)^2 - 4\lambda(1 + ab)}.$$

Evidently for a fixed parameter set  $\{a, b, \lambda, \delta, L\}$ , the maximum value of s occurs when k = 0. Thus

$$s_M = \phi_+(a, b, \lambda).$$

We recall that  $\lambda > 0$ . It follows that if 1 + ab > 0 then  $\operatorname{Re} \phi_{\pm} < 0$  so that

Re  $s_M < 0$  and the zero state is stable. If 1 + ab < 0 then  $\phi_+ > 0$  and  $s_M > 0$  and the zero state is unstable. We note that the point where 1 + ab = 0 coincides with the bifurcation to the non-zero uniform branch according to (5.5.29) (setting  $k^* = 0$  in that equation). We conclude that the zero state U = V = 0 is stable to the right of the bifurcation to the non-zero uniform state, and unstable to the left of it.

The non-zero uniform state is rather similar. We again fix  $\delta = L = 1$ . Solving the quadratic (5.5.25), the discriminant is again found to be independent of k, and we obtain

$$s_{\pm} = -k^2 + \tilde{\phi}_{\pm}(a, b, \lambda)$$

with

$$\tilde{\phi}_{\pm} \equiv -\frac{1}{2}(\alpha_1 - \lambda b) \pm \frac{1}{2}\sqrt{(\alpha_1 - \lambda b)^2 - 4\lambda(1 - \alpha_1 b)}.$$

Again the maximum growth rate occurs when k = 0 so that

$$s_M = \tilde{\phi}_+(a, b, \lambda). \tag{5.5.31}$$

Notice that  $s_{+} = 0$  when  $1 - \alpha_{1}b = 0$ , which corresponds to det  $\mathbf{J} = 0$ , where the Jacobian matrix for the spatially-independent stability problem, namely  $\mathbf{J} = \tilde{\mathbf{J}}(0)$ , where  $\tilde{\mathbf{J}}(k)$  was defined in (5.5.23).

Following the preceding remarks, in figures 5.5.1 and 5.5.2 we show the stability of the uniform state, using a solid line to indicate a stable part of a branch, and a dashed line to indicate an unstable part of a branch. As can be seen the uniform state is everywhere unstable.

Finally, we remark that it is possible to have a bifurcation at which s=0 is double. The eigenvalues s for a general uniform state satisfy the quadratic equation (5.5.25). This has the form  $s^2 - (\operatorname{tr} \tilde{\boldsymbol{J}}) s + \det \tilde{\boldsymbol{J}} = 0$ . So we have a single eigenvalue s=0 if  $\det \tilde{\boldsymbol{J}} = 0$ , and a double eigenvalue s=0 if both  $\det \tilde{\boldsymbol{J}} = 0$  and  $\operatorname{tr} \tilde{\boldsymbol{J}} = 0$  simultaneously. From (5.5.26) and (5.5.27) the latter two

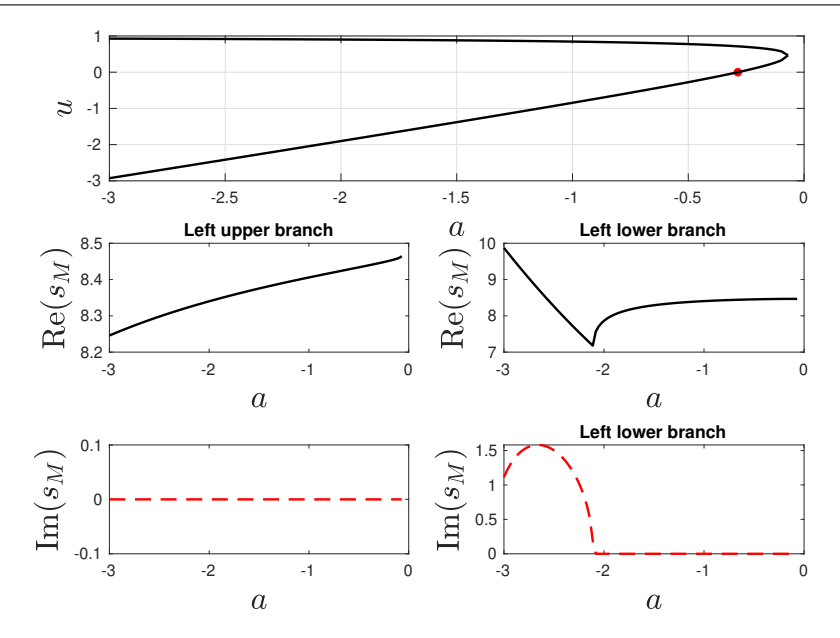


Figure 5.5.1: Stability properties of the left branch of the non-zero uniform state, with  $\lambda = 2.5$  and b = 3.5. The real and imaginary parts of the growth rate  $s_M$ , defined in (5.5.31) are shown.

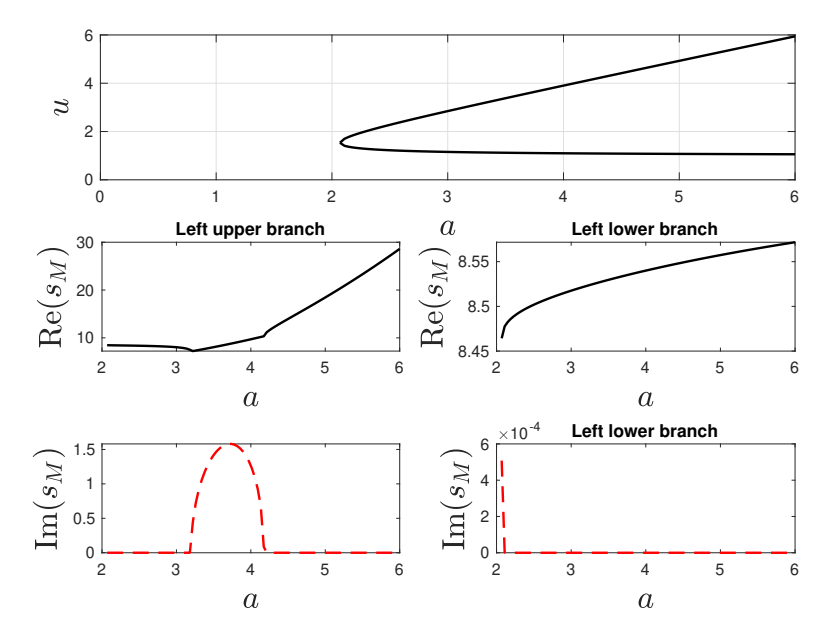


Figure 5.5.2: Stability properties of the right branch of the non-zero uniform state, with  $\lambda = 2.5$  and b = 3.5. The real and imaginary parts of the growth rate  $s_M$ , defined in (5.5.31) are shown.

equations demand

$$a + \hat{\lambda}b + 2\rho k^2 = 0, (5.5.32)$$

$$\rho^2 k^4 + (a + \hat{\lambda}b)\rho k^2 + \hat{\lambda}(ab + 1) = 0, \tag{5.5.33}$$

respectively. Viewing  $\hat{\lambda}$  and k as being fixed we may solve this pair of equations for a and b. Doing this we find

(i) 
$$a = -\rho k^2 + \sqrt{\hat{\lambda}}, \qquad b = -\frac{\rho k^2 + \sqrt{\hat{\lambda}}}{\hat{\lambda}}$$
 (5.5.34)

or

(ii) 
$$a = -\rho k^2 - \sqrt{\hat{\lambda}}, \qquad b = \frac{\sqrt{\hat{\lambda} - \rho k^2}}{\hat{\lambda}}.$$
 (5.5.35)

In choosing parameters later we will typically take b > 0, in which case option (ii) is of greater interest.

## 5.6 Numerical results

In the previous sections we have shown how we may compute both uniform and spatially-varying stationary solutions across an arbitrary network and how we can determine their stability. For uniform stationary solutions the stability properties are determined via relatively simple formula. For spatially-dependent stationary solutions, the stability spectrum must be determined numerically. In this section we present some numerical results to illustrate the application of the theory to various networks.

We choose to use a as a bifurcation parameter. To this end we fix the other parameters in the system, namely b,  $\lambda$ ,  $\hat{\rho}$  and  $\delta$  and we vary a. Our strategy is as follows. We know that the zero state u=v=0 everywhere across the network) is a solution to the Fitzhugh-Nagumo system. Varying a we expect to determine a sequence of bifurcation points at which side branches to non-zero states occur. These may be branches on which the solution is everywhere uniform across the network, or side branches on which the solution is spatially varying.

Having selected a network structure, we determine the possible set K of wave numbers k that are compatible with the network by solving det  $L^*(k) = 0$ . From

this finite set we may construct an extended, infinite set of K values by taking

$$k = \arccos(\cos(k)) + 2\pi n, \quad n \in \mathbb{Z}^+. \tag{5.6.1}$$

Bifurcations to non-zero states occur at values of a that satisfy in (5.5.29), namely

$$\delta k^{*4} + (\lambda b + a\delta)k^{*2} + \lambda(1 + ab) = 0.$$
 (5.6.2)

where  $k^* = \sqrt{\hat{\rho}} k$ . Since this is linear in a there is only one possible a value for given parameters. Call it  $a_c = a(k^*, b, \lambda, \delta)$ . Rearranging (5.6.2) we find

$$a_c = -\frac{\delta k^{*4} + \lambda b k^{*2} + \lambda}{\delta k^{*2} + \lambda b} < 0.$$
 (5.6.3)

Starting at or near to  $a_c$ , we use the small amplitude solution constructed in section 5.3.4 as an initial guess for Newton's method in our numerical code developed to handle solutions of arbitrary amplitude discussed earlier. In this way we aim to latch onto the relevant side branch. Once this is achieved, the remainder of the branch is computer via parameter continuation.

We start with a discussion of the simplest network choice, namely the path graph  $P_2$ .

## 5.6.1 The path graph $P_2$

We herein investigate the behaviour of solutions to the Fitzhugh-Nagumo equations on a path graph  $P_2$ , illustrated in Figure 5.6.1. Recall that in this case we have

$$\mathbf{A} = \begin{pmatrix} 0 & 1 \\ 1 & 0 \end{pmatrix}, \qquad \mathbf{D} = \begin{pmatrix} 1 & 0 \\ 0 & 1 \end{pmatrix} \tag{5.6.4}$$

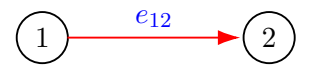


Figure 5.6.1: A path graph  $P_2$  with two vertices.

and det  $L^*(k)x_u = 0$  requires that  $\cos k = \pm 1$  and so  $k = n\pi = k_n$ , say, for integer n. The critical values of the parameter a are given by (5.6.3), viz

$$a_c^n = -\frac{\delta \hat{\rho}^2 k_n^4 + \lambda b \hat{\rho} k_n^2 + \lambda}{\delta \hat{\rho} k^2 + \lambda b} < 0.$$

We fix the following parameters

$$b = 3.5, \qquad \lambda = 2.5, \qquad \delta = 1.0, \qquad L = 1.0.$$

(Recall from that  $\hat{\rho} = 1/L^2$ .) Then we have

$$(k_0, a_c^0) = (0, -0.286), (k_1, a_c^1) = (\pi, -10.004)$$
 (5.6.5)

$$(k_2, a_c^2) = (2\pi, -39.530), \qquad (k_3, a_c^3) = (3\pi, -88.852).$$
 (5.6.6)

The bifurcation diagram for  $P_2$  is shown in Figure 5.6.2. In this diagram we plot ||u|| against the bifurcation parameter a. The diagram incorporates branches corresponding to uniform solutions (corresponding to k = 0) (solid black lines) and asymptotic behaviour for large |a| (dashed black lines).

the stability of the uniform solution branch discussed in subsection 5.5.1.

For the non-uniform branches, the dashed lines in the figure (5.6.2) indicate instability for non-uniform branches, which is discussed in section 5.5. Further details of the diagram are as follows:

- 1. The leftmost black curve corresponds to the branch  $k=k_0=0$  (uniform solution). This curve bifurcates from the point  $a=a_c^0=-0.286$ .
- 2. The blue curve corresponds to the branch  $k=k_1=\pi$ . This curve bifurcates from the point  $a=a_c^1=-10.004$ .

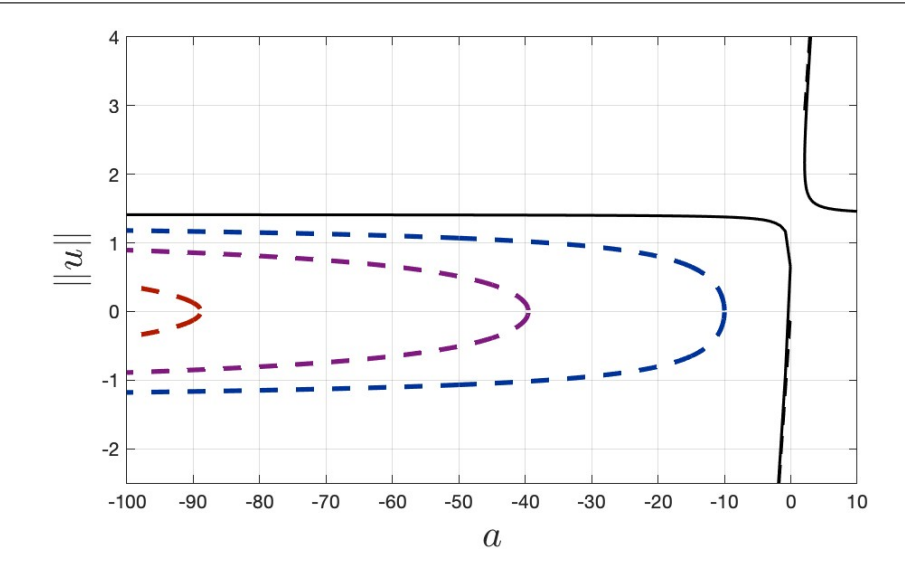


Figure 5.6.2: Bifurcation diagram for the Fitzhugh-Nagumo equations on the path graph  $P_2$ . The plot shows ||u|| versus the parameter a when b=3.5,  $\lambda=2.5$ ,  $\delta=1.0$ , L=1.0. Solid black lines show exact uniform (k=0) solutions; the dashed black lines indicate the large |a| asymptotic behaviours for the uniform solutions given by (5.4.7) and (5.4.9). The blue, purple, and red curves represent first  $(k=k_1=\pi)$ , second  $(k=k_2=2\pi)$ , and third  $(k=k_3=3\pi)$  non-uniform solutions, respectively. The dashed mean that bifurcation point is not stable

- 3. The purple curve corresponds to the branch  $k=k_2=2\pi$ . This curve bifurcates from the point  $a=a_c^2=-39.530$ .
- 4. The red curve corresponds to the branch  $k = k_3 = 3\pi$ . This curve bifurcates from the point  $a = a_c^3 = -88.852$ .

These non-uniform solution branches demonstrate the system's capacity to support spatially non-uniform states, each characterised by distinct spatial profiles and bifurcation points. The observed bifurcation structure elucidates the rich dynamics of the Fitzhugh-Nagumo system on a  $P_2$  graph, showcasing the interplay between uniform and non-uniform solutions as the parameter a varies.

#### 5.6.2 The path graph $P_3$

We extend our analysis to show the behaviour of solutions to the Fitzhugh-Nagumo equations on path graph  $P_3$  (see figure 5.6.3). Recall that in this case

we have

$$\mathbf{A} = \begin{pmatrix} 0 & 1 & 0 \\ 1 & 0 & 1 \\ 0 & 1 & 0 \end{pmatrix}, \quad \mathbf{D} = \begin{pmatrix} 1 & 0 & 0 \\ 0 & 2 & 0 \\ 0 & 0 & 1 \end{pmatrix}. \tag{5.6.7}$$

Then  $\det \mathbf{L}^*(k) = 0$  requires

$$\begin{vmatrix} -\cos k & 1 & 0 \\ 1 & -2\cos k & 1 \\ 0 & 1 & -\cos k \end{vmatrix} = 0.$$
 (5.6.8)

This leads to  $\cos k = \pm 1$ , 0. Hence  $k_n = n\pi/2$  for integer n. The bifurcation points are given by (5.6.3), namely

$$a_c^n = -\frac{\delta \hat{\rho}^2 k_n^4 + \lambda b \hat{\rho} k_n^2 + \lambda}{\delta \hat{\rho} k^2 + \lambda b}.$$

We use the same parameter values as before, namely

$$b = 3.5, \qquad \lambda = 2.5, \qquad \delta = 1.0, \qquad L = 1.0,$$

and so  $\hat{\rho} = 1$ . Then we have

$$(k_0, a_c^0) = (0, -0.286), (k_1, a_c^1) = (\pi/2, -2.6902),$$

$$(k_2, a_c^2) = (\pi, -10.004), (k_3, a_c^3) = (3\pi/2, -22.287),$$

$$(k_4, a_c^4) = (2\pi, -39.530), (k_5, a_c^5) = (5\pi/2, -61.72052),$$

$$(k_6, a_c^6) = (3\pi, -88.852).$$

$$(5.6.9)$$

Comparing these with the  $k_n$  values for  $P_2$  given in (5.6.5) we see that, as expected, the set of  $\{k_n\}$  for  $P_3$  includes that for  $P_2$ . The bifurcation diagram for  $P_3$  is shown in Figure 5.6.4. In this diagram we plot ||u|| against the bifurcation parameter a. The diagram incorporates branches corresponding to uniform solutions (corresponding to k=0) (solid black lines) and asymptotic behaviour for large |a| (dashed black lines), remains unchanged for any network as it is from the previous section path graph  $P_2$ , as detailed the reason in



Figure 5.6.3: path graph  $P_3$  with three vertices connected by two edges.

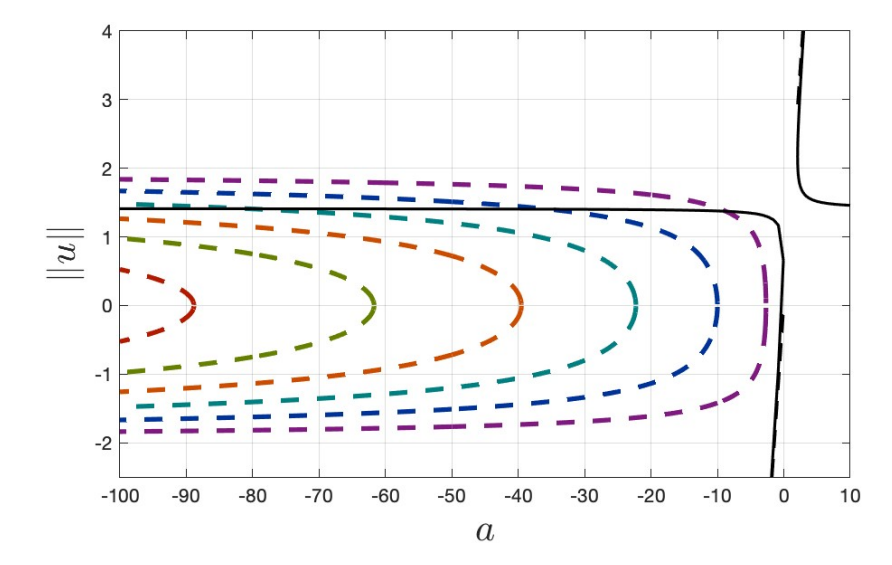


Figure 5.6.4: On a path graph  $P_3$ , bifurcation diagram for the Fitzhugh-Nagumo equations. The plot shows the norm of u versus the parameter a. Solid black lines show exact solutions for k=0, and dashed black lines indicate asymptotic behaviour for large |a| given by (5.4.7) and (5.4.9). The purple, blue, teal green, orange, olive green, and dark red curves represent a non-uniform solutions. Parameters:  $b=3.5, \lambda=2.5, \delta=1.0, L=1.0$  (domain length). The dashed curve indicates that the bifurcation points unstable.

Section (5.4). Note that the uniform solution bifurcates from  $a = a_c^0 = -0.286$  to create the left-hand solid black line in the figure. As is clear from the discussion in section 5.4 and in particular from Figure 5.4.1 the right-hand uniform branch does not bifurcate from the zero state.

The bifurcation diagram in Figure 5.6.4 highlights several key features:

- 1. The leftmost black curve corresponds to the branch  $k=k_0=0$  (uniform solution). This curve bifurcates from the point  $a=a_c^0=-0.286$ .
- 2. The purple curve corresponds to the branch  $k=k_1=\pi/2$ . This curve bifurcates from the point  $a=a_c^1=-2.6902$ .
- 3. The blue curve corresponds to the branch  $k=k_2=\pi$ . This curve bifurcates from the point  $a=a_c^2=-10.004$ .

- 4. The teal green curve corresponds to the branch  $k = k_3 = 3\pi/2$ . This curve bifurcates from the point  $a = a_c^3 = -22.287$ .
- 5. The orange curve corresponds to the branch  $k=k_4=2\pi$ . This curve bifurcates from the point  $a=a_c^4=-39.530$ .
- 6. The olive green curve corresponds to the branch  $k = k_5 = 5\pi/2$ . This curve bifurcates from the point  $a = a_c^5 = -61.721$ .
- 7. The dark red curve corresponds to the branch  $k=k_6=3\pi$ . This curve bifurcates from the point  $a=a_c^6=-88.852$ .

The non-uniform solution branches demonstrate that all branches are unstable, as indicated by the dashed curves in the bifurcation diagram. This observation highlights the rich dynamical behaviour of the Fitzhugh-Nagumo system on the  $P_3$  graph. Specifically, it reveals the interplay between uniform and non-uniform solutions as the parameter a varies, emphasising the system's tendency to favour instability in spatially heterogeneous states.

#### 5.6.3 The Y-shaped graph

We extend our analysis to show the behaviour of solutions to the Fitzhugh-Nagumo equations on path graph Y-shaped graph (see figure 5.6.5). Recall that in this case we have

$$\mathbf{A} = \begin{pmatrix} 0 & 0 & 1 & 0 \\ 0 & 0 & 1 & 0 \\ 1 & 1 & 0 & 1 \\ 0 & 0 & 1 & 0 \end{pmatrix}, \quad \mathbf{D} = \begin{pmatrix} 1 & 0 & 0 & 0 \\ 0 & 1 & 0 & 0 \\ 0 & 0 & 3 & 0 \\ 0 & 0 & 0 & 1 \end{pmatrix}. \tag{5.6.10}$$

Thus  $\det \mathbf{L}^*(k) = 0$  requires

$$\begin{vmatrix} -\cos k & 0 & 1 & 0 \\ 0 & -\cos k & 1 & 0 \\ 1 & 1 & -3\cos k & 1 \\ 0 & 0 & 1 & -\cos k \end{vmatrix} = 0.$$
 (5.6.11)

This is leads to

$$-\cos k \begin{vmatrix} -\cos k & 1 & 0 \\ 1 & -3\cos k & 1 \\ 0 & 1 & -\cos k \end{vmatrix} + \begin{vmatrix} 0 & -\cos k & 0 \\ 1 & 1 & 1 \\ 0 & 0 & -\cos k \end{vmatrix} = 0.$$
 (5.6.12)

Then, we have

$$\det \mathbf{L}^*(k) = 3\cos^2 k(\cos^2 k - 1) = -3\sin^2 k \cos^2 k = -\frac{3}{4}\sin^2 2k = 0.$$

Hence  $\cos k = 0$ , 0,  $\pm 1$ ; and  $k = n\pi/2 = k_n$ , for integer n.

Despite the difference in the graph structure compared to the previous section, we observe that the critical wave numbers  $k_n$  remain the same. This implies that the bifurcation values for the parameter a are also identical. These values,  $a_c^n$ , are given by

$$a_c^n = -\frac{\delta \hat{\rho}^2 k_n^4 + \lambda b \hat{\rho} k_n^2 + \lambda}{\delta \hat{\rho} k_n^2 + \lambda b}.$$

As before we choose the parameter values

$$b = 3.5, \quad \lambda = 2.5, \quad \delta = 1.0, \quad L = 1.0,$$

(and recall that  $\hat{\rho} = 1/L^2$ . Substituting these values, we compute the critical

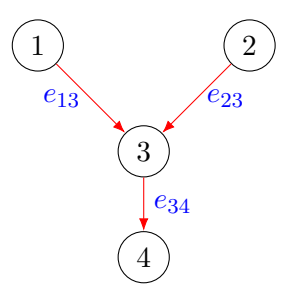


Figure 5.6.5: Y-shape graph with four vertices and three edges

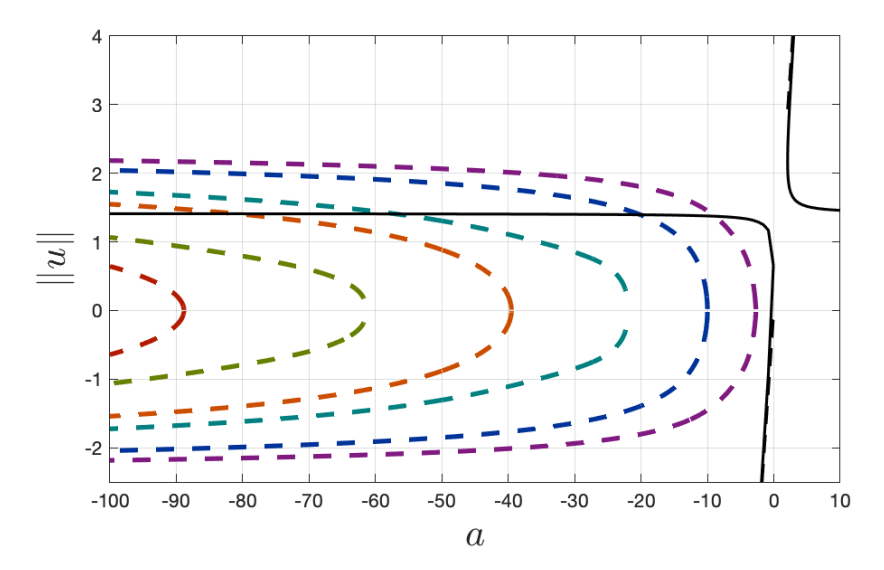


Figure 5.6.6: On a Y-shaped graph, bifurcation diagram for the Fitzhugh-Nagumo equations. The plot shows the norm of u versus the parameter a. Solid black lines show exact solutions for k=0, and dashed black lines indicate asymptotic behaviour for large |a| given by (5.4.7) and (5.4.9). The purple, blue, teal green, dark orange, olive green, and dark red curves represent a non-uniform solutions. Parameters: b=3.5,  $\lambda=2.5$ ,  $\delta=1.0$ , L=1.0 (domain length). The dashed curve indicates that the bifurcation points unstable.

pairs  $(k_n, a_c^n)$  as follows:

$$(k_0, a_c^0) = (0, -0.286), (k_1, a_c^1) = \left(\frac{\pi}{2}, -2.6902\right),$$

$$(k_2, a_c^2) = (\pi, -10.004), (k_3, a_c^3) = \left(\frac{3\pi}{2}, -22.287\right),$$

$$(k_4, a_c^4) = (2\pi, -39.530), (k_5, a_c^5) = \left(\frac{5\pi}{2}, -61.721\right),$$

$$(k_6, a_c^6) = (3\pi, -88.852).$$

The consistency in the values of  $k_n$  and  $a_c^n$  across different graph structures

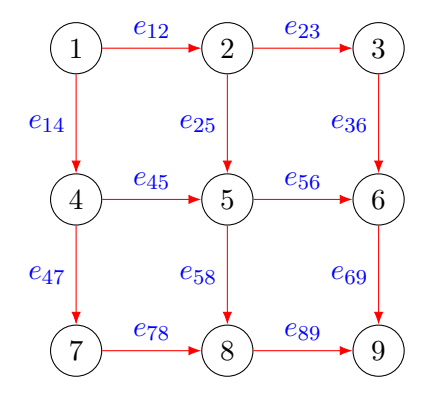


Figure 5.6.7: Square grid graph  $3 \times 3$ .

highlights the robustness of the bifurcation analysis. Specifically:

- The uniform solution branch (k = 0) remains unchanged, as it is independent of the graph topology.
- The non-uniform branches  $(k_n \neq 0)$  exhibit the same critical values  $a_c^n$ , suggesting that the bifurcation structure is primarily governed by the wave number  $k_n$  rather than the graph's shape.

#### 5.6.4 Square grid graph $3 \times 3$

We extend our analysis to show the behaviour of solutions to the Fitzhugh-Nagumo equations on a square grid graph  $3 \times 3$  (see figure 5.6.7). Recall that in this case we need to find the determinant of  $\det \mathbf{L}^* = \det(\mathbf{A} - \nu \mathbf{D}) = 0$ , as

follows

$$\begin{vmatrix} -2\nu & 1 & 0 & 1 & 0 & 0 & 0 & 0 & 0 \\ 1 & -3\nu & 1 & 0 & 1 & 0 & 0 & 0 & 0 \\ 0 & 1 & -2\nu & 0 & 0 & 1 & 0 & 0 & 0 \\ 1 & 0 & 0 & -3\nu & 1 & 0 & 1 & 0 & 0 \\ 0 & 1 & 0 & 1 & -4\nu & 1 & 0 & 1 & 0 \\ 0 & 0 & 1 & 0 & 1 & -3\nu & 0 & 0 & 1 \\ 0 & 0 & 0 & 1 & 0 & 0 & -2\nu & 1 & 0 \\ 0 & 0 & 0 & 0 & 1 & 0 & 1 & -3\nu & 1 \\ 0 & 0 & 0 & 0 & 0 & 1 & 0 & 1 & -2\nu \end{vmatrix} = 0,$$

where  $\nu = \cos k$ . We use Matlab to obtain the determinant:

$$\nu^{3}(9\nu^{6} - 15\nu^{4} + 7\nu^{2} - 1) = \nu^{3}(\nu - 1)(\nu + 1)(3\nu^{2} - 1)^{2} = 0.$$

This leads to

$$\nu = \cos k = 0, 0, 0, \pm 1, \frac{1}{\sqrt{3}}, \frac{1}{\sqrt{3}}, -\frac{1}{\sqrt{3}}, -\frac{1}{\sqrt{3}}$$

So the general expression for  $k = k_n$  is given by:

$$k_n = \begin{cases} n\pi/2 & \text{for } \cos k = \pm 1, 0, \\ \pm \arccos\left(\frac{1}{\sqrt{3}}\right) + n\pi & \text{for } \cos k = \pm \frac{1}{\sqrt{3}}, \end{cases}$$

where  $n \in \mathbb{Z}^+$ .

The important value for parameter a are specified by (5.6.3), namely

$$a_c^n = -\frac{\delta \hat{\rho}^2 k_n^4 + \lambda b \hat{\rho} k_n^2 + \lambda}{\delta \hat{\rho} k^2 + \lambda b}.$$

As in the previous cases we set the following parameter values

$$b = 3.5, \qquad \lambda = 2.5, \qquad \delta = 1.0, \qquad L = 1.0.$$

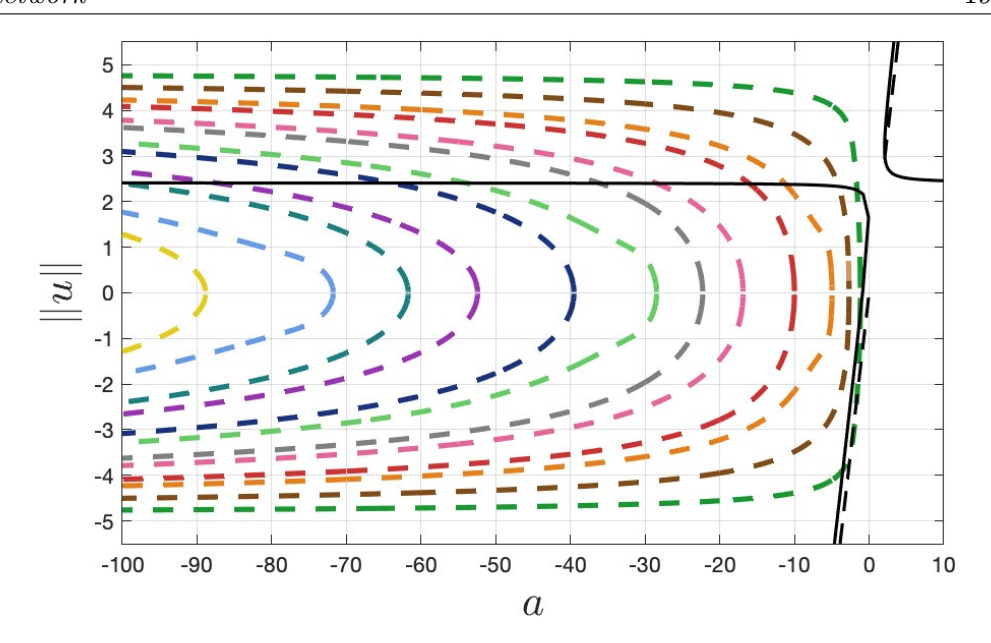


Figure 5.6.8: On a  $3\times 3$  square grid graph, bifurcation diagram for the Fitzhugh-Nagumo equations. The plot shows the norm of u versus the parameter a. Solid black lines show exact solutions for k=0, and dashed black lines indicate asymptotic behaviour for large |a| given by (5.4.7) and (5.4.9).The non-uniform bifurcation points represent by 12 different colour. Parameters:  $b=3.5, \ \lambda=2.5, \ \delta=1.0, \ L=1.0$  (domain length).The dashed curve indicates that the bifurcation points unstable.

(Recall from that  $\hat{\rho} = 1/L^2$ .) Then we have

$$(k_0, a_c^0) = (0, -0.286), \qquad (k_1, a_c^1) = \left(\arccos\left(\frac{1}{\sqrt{3}}\right), -1.1714\right),$$

$$(k_2, a_c^2) = (\pi/2, -2.6902), \qquad (k_3, a_c^3) = \left(-\arccos\left(\frac{1}{\sqrt{3}}\right) + \pi, -4.9646\right),$$

$$(k_4, a_c^4) = (\pi, -10.0039), \qquad (k_5, a_c^5) = \left(\left(\arccos\left(\frac{1}{\sqrt{3}}\right) + \pi, -16.8826\right),$$

$$(k_6, a_c^6) = (3\pi/2, -22.2874), \qquad (k_7, a_c^7) = \left(-\arccos\left(\frac{1}{\sqrt{3}}\right) + 2\pi, -28.4535\right),$$

$$(k_8, a_c^8) = (2\pi, -39.53025), \qquad (k_9, a_c^9) = \left(\arccos\left(\frac{1}{\sqrt{3}}\right) + 2\pi, -52.4368\right),$$

$$(k_{10}, a_c^{10}) = (5\pi/2, -61.72052), \qquad (k_{11}, a_c^{11}) = \left(-\arccos\left(\frac{1}{\sqrt{3}}\right) + 3\pi, -71.7629\right),$$

$$(k_{12}, a_c^{12}) = (3\pi, -88.85206),$$

$$(5.6.13)$$

The bifurcation diagram in Figure 5.6.8 highlights several key features:

1. The leftmost black curve corresponds to the branch  $k = k_0 = 0$  (uniform

solution). This curve bifurcates from the point  $a = a_c^0 = -0.286$ .

- 2. The green curve corresponds to the branch  $k=k_1=\arccos\left(\frac{1}{\sqrt{3}}\right)$ . This curve bifurcates from the point  $a=a_c^1=-1.1714$ .
- 3. The brown curve corresponds to the branch  $k=k_2=\pi/2$ . This curve bifurcates from the point  $a=a_c^2=-2.6902$ .
- 4. The Orange curve corresponds to the branch  $k = k_3 = -\arccos\left(\frac{1}{\sqrt{3}}\right) + \pi$ . This curve bifurcates from the point  $a = a_c^3 = -4.9646$ .
- 5. The red curve corresponds to the branch  $k=k_4=3\pi$ . This curve bifurcates from the point  $a=a_c^4=-10.0039$ .
- 6. The pink curve corresponds to the branch  $k = k_5 = \arccos\left(\frac{1}{\sqrt{3}}\right) + \pi$ . This curve bifurcates from the point  $a = a_c^5 = -16.8826$ .
- 7. The gray curve corresponds to the branch  $k=k_6=3\pi/2$ . This curve bifurcates from the point  $a=a_c^6=-22.287$ .
- 8. The light green curve corresponds to the branch  $k = k_7 = -\arccos\left(\frac{1}{\sqrt{3}}\right) + 2\pi$ . This curve bifurcates from the point  $a = a_c^7 = -28.4535$ .
- 9. The dark blue curve corresponds to the branch  $k=k_8=2\pi$ . This curve bifurcates from the point  $a=a_c^8=-39.530$ .
- 10. The purple curve corresponds to the branch  $k = k_9 = \arccos\left(\frac{1}{\sqrt{3}}\right) + 2\pi$ . This curve bifurcates from the point  $a = a_c^9 = -52.4368$ .
- 11. The dark green curve corresponds to the branch  $k=k_{10}=5\pi/2$ . This curve bifurcates from the point  $a=a_c^{10}=-61.721$ .
- 12. The light blue curve corresponds to the branch  $k = k_{11} = -\arccos\left(\frac{1}{\sqrt{3}}\right) + 3\pi$ . This curve bifurcates from the point  $a = a_c^{11} = -71.7629$ .
- 13. yellow curve corresponds to the branch  $k=k_{12}=3\pi$ . This curve bifurcates from the point  $a=a_c^{12}=-88.852$ .

The non-uniform solution branches demonstrate that all branches are unstable, as indicated by the dashed curves in the bifurcation diagram. This observation highlights the rich dynamical behaviour of the Fitzhugh-Nagumo system on the  $3 \times 3$  square grid graph. Specifically, it reveals the interplay between uniform and non-uniform solutions as the parameter a varies, emphasising the system's tendency to favour instability in spatially heterogeneous states.

# Conclusion

# 6.1 Summary and conclusions

This thesis investigates the propagation of signals through networks modelled by diffusion and by reaction-diffusion, the latter modelled using Fisher equation and the FitzHugh-Nagumo system of equations. The primary objective of this work was to explore the effects of network topology on signal dynamics, focusing on diffusion processes and the excitable nature of reactions within networked systems. By employing both analytical approaches and numerical simulations, this study derived solutions for the diffusion equation, the Fisher equation, and the FitzHugh-Nagumo model on various network structures, providing insights into the dynamics of signals as they propagate and interact with their topological structures.

The thesis begins with a detailed analysis of diffusion processes on networks as discussed in chapter 2. The fundamental principles of diffusion, including concentration, flux, and the diffusion coefficient, were presented through Fick's Law. The chapter derived the one-dimensional diffusion equation based on mass conservation and adapted these continuous diffusion principles to a discrete network structure. Special attention was given to solving the diffusion equation on networks, where boundary and continuity conditions specific to network structure were considered. A key method employed was eigenvalue analysis using adjacency and degree matrices, with Gershgorin's theorem providing

bounds on eigenvalues. The results revealed the influence of network structure on the diffusion process, especially in regular graphs and square grid graphs, where eigenvalues were shown to play a key role in diffusion behaviour. Computational techniques confirmed the theoretical findings, particularly in the study of eigenvalue asymptotic as network size increases for square grid graphs.

Chapter 3 concentrates on the finite-difference method (FDM) for solving the diffusion equation on networks. The chapter demonstrated how discretising the spatial domain and enforcing continuity conditions for flux and concentration could numerically solve the diffusion problem. The Crank-Nicholson method was introduced as a second-order method for diffusion equations and applied to path graphs  $P_2$  and  $P_3$ . The method was extended to more complex network structures, including square grid and Y-shaped graphs. Numerical simulations validated the approach, with results showing excellent agreement with theoretical predictions for concentration profiles and decay rates. The method proved effective for handling networks with multiple edges and vertices, providing accurate solutions for concentration evolution and flux continuity.

The reaction-diffusion equation was applied to network structures, focusing on the stability and dynamics of concentration profiles in chapter 4. The Method of Lines (MOL) was used to numerically solve the Fisher equation on networks, allowing for the study of concentration dynamics in reaction-diffusion systems. Steady-state solutions were analysed, and the stability of these states was assessed. It was found that the steady-state solutions for the Fisher equation were constrained to be constant, either u=0 or u=1, with u=1 being stable. Numerical simulations of concentration dynamics on path and Y-shaped networks demonstrated how external forcing at vertices could initiate pulse propagation, which would subsequently propagate, split, and decay as it moved through the network. The results showed that network topology significantly influences the way pulses propagate and split, revealing the importance of continuity conditions at network vertices.

We extended the analysis in chapter 5 to the FitzHugh-Nagumo (FHN) model, a system of coupled reaction-diffusion equations that model excitable systems, such as neurons. The FitzHugh-Nagumo equations were solved on various network structures, including path graphs and Y-shaped graphs, to investigate pulse dynamics and the interaction between excitation and recovery variables. Stationary solutions were derived, and their stability was analysed. The chapter also explored small-amplitude and arbitrary-amplitude stationary solutions, computed numerically using Chebyshev polynomials and Newton's method. The analysis of the FitzHugh-Nagumo model on networks demonstrated that network topology significantly affects the dynamics of excitability and pulse formation, with bifurcation diagrams revealing the transition from uniform to non-uniform solutions as parameters varied.

In summary, this thesis provides a comprehensive exploration of how diffusion and reaction-diffusion processes behave on networks. It integrates mathematical techniques, such as eigenvalue analysis, finite-difference methods, and the Method of Lines, to model and simulate the diffusion and reaction-diffusion equations on various network topologies. The results highlight the profound effect that network structure has on the propagation of signals, especially in reaction-diffusion systems like the FitzHugh-Nagumo model, where network topology can lead to complex phenomena such as pulse splitting and stable or unstable states of bifurcation points. This work contributes to the understanding of networked systems in biological, physical, and chemical contexts, offering a foundation for further research on signal dynamics in complex networks.

#### 6.2 Future work

The thesis establishes a foundational understanding of diffusion and reactiondiffusion processes on network structures, which can be interpreted through graph theory. For future research, we need to identify numerous pathways to improve our understanding of network dynamics. While this thesis focused on relatively simple network topologies such as tree graphs, Y-shaped graphs, and square grid graphs, future research could extend to more complex network structures. This could include networks with more intricate interactions between nodes, such as feedback loops, adaptive connections, or hierarchical structures.

The models developed in this thesis can be applied to real-world networks, for instance, neural or social networks, and adjusted with experimental data to explore how network topology influences signal transmission in natural systems. Also, exploring higher-dimensional networks, such as 2D or 3D grids, would enhance the understanding of signal propagation in complex, spatially organized systems. Future work could explore how dynamic changes in network structure (e.g., adding/removing vertices or edges) affect the propagation of signals, which is especially relevant for communication and biological networks.

In summary, future research could focus on extending the models to more complex and dynamic networks, applying them to real-world systems, and incorporating experimental data to refine predictions. These advancements would provide a deeper understanding of signal dynamics in natural and artificial networks.

## $\mathbf{A}$

# Find the eigenvalue of square grid graph by applying Klopotek's equation

## A.1 Case of $3 \times 3$ square grid graph

The following table is obtained by MATLAB calculation of the eigenvalue problem. It shows the modified Laplacian eigenvalue  $\lambda$ , the Normalized Laplacian eigenvalue  $\tau$ , and their multiplicity.

λ	multiplicity	au
-1.0000000000000000	1	2.00000000000000000
-0.577350269189626	2	1.577350269189626
0.0000000000000000	3	1.00000000000000000
0.577350269189626	2	0.422649730810374
1.00000000000000000	1	0.0000000000000000

The following table is obtained by plotting the phases of  $(\delta_1, \delta_2) \in [0, (n-1)\pi)$  to determine the initial values of these parameters. Subsequently, the eigenvalues of the normalized Laplacian  $\tau$  are computed for a grid graph  $3 \times 3$  for all cases where  $(z_1, z_2) = (1, 0), (1, 1), \text{ or } (0, 0)$ .

	$(\delta_1,\delta_2)$	au
(0,0)	(0,0)	2
(0,0)	(0.7854, 3.92699)	1
(0,0)	(0.7854, 2.3562)	1
(0,0)	(2.3562, 5.4978)	1
(0,0)	(2.3562, 0.7854)	1
(0,0)	(3.92699, 5.4978)	1
(0,0)	(3.92699, 0.7854)	1
(0,0)	(5.4978, 3.92699)	1
(0,0)	(5.4978, 2.3562)	1
(0,0)	$(\pi \;, \pi)$	0
(1,1)	$(0\;,\pi)$	1
(1,1)	$(\pi \;, \pi)$	1
(1,0)	$(0.2928 \;, 0.5236)$	1.57735
(1,0)	(0.2928 , 5.7596)	1.57735
(1,0)	(2.8487, 5.7596)	1.57735
(1,0)	(2.8487 , 0.5236)	1.57735
(1,0)	(3.4344, 3.6652)	0.42265
(1,0)	(3.4344, 2.61799)	0.42265
(1,0)	(5.9903, 3.6652)	0.42265
(1,0)	(5.9903, 2.61799)	0.42265

# A.1.1 Observation on the table for odd number of vertices along one side n=3

For the square grid graph  $4\times 4$  we got the eigenvalue of the Normalized Laplacian  $\tau$  as follows:

• Right multiplicity when  $\tau=2,0$  where  $(z_1,z_2)=(0,0)$  and (1,1), respectively.

• For case  $(z_1, z_2) = (0, 0)$  we got  $\tau = 1$  with the following choices of

$$0.7854 \rightarrow \{2.3562, 3.92699\},$$

$$\delta_1 \rightarrow \delta_2:$$

$$2.3562 \rightarrow \{0.7854, 5.4978\},$$

$$3.92699 \rightarrow \{0.7854, 5.4978\},$$

$$5.4978 \rightarrow \{2.3562, 3.92699\},$$

There is 8 multiplicity of this eigenvalue, but if we look to table we can see  $\tau = 1$  is appear when  $(z_1, z_2) = (1, 1)$  twice as well with the following choices of

$$\delta_1 \to \delta_2:$$
 $0 \to \pi,$ 
 $\pi \to \pi,$ 

which lead to have 10 multiplicity while we just need 3 which means we can reduce our search on the interval as

- Right multiplicity when  $\tau = 2,0$  where  $(z_1,z_2) = (0,0)$  and (1,0), respectively.
- For case  $(z_1, z_2) = (1, 0)$  we got  $\tau = 1.57735$  with the following choices of

$$\delta_1 \rightarrow \delta_2: \begin{tabular}{l} 0.2928 \rightarrow \{0.5236, 5.7596\}, \\ 2.8487 \rightarrow \{0.5236, 5.7596\}, \end{tabular}$$

There is 4 multiplicity of this eigenvalue ,and we need only 2 multiplicity to reduce our search on interval  $\delta_1, \delta_2 \in [0, (n-2)\pi]$ .

• For case  $(z_1, z_2) = (1, 0)$  we got  $\tau = 0.42265$  with the following choices of

$$\delta_1 \rightarrow \delta_2: \begin{tabular}{ll} 3.4344 \rightarrow \{2.61799, 3.6652\}, \\ 5.9903 \rightarrow \{2.61799, 3.6652\}, \end{tabular}$$

There is 4 multiplicity of this eigenvalue ,and we need only 2 multiplicity to reduce our search on interval  $\delta_1, \delta_2 \in (\pi, (n-1)\pi)$ .

## A.2 Case of $4 \times 4$ square grid graph

The following table is obtained by MATLAB calculation of the eigenvalue problem. It shows the modified Laplacian eigenvalue  $\lambda$ , the Normalized Laplacian eigenvalue  $\tau$ , and their multiplicity.

λ	multiplicity	au
-1.0000000000000000	1	2.0000000000000000
-0.781735959970572	2	1.781735959970572
-0.50000000000000000	1	1.5000000000000000
-0.3333333333333333	2	1.333333333333333
-0.0000000000000000	4	1.0000000000000000
0.3333333333333333	2	0.66666666666666666667
0.5000000000000000	1	0.5000000000000000
0.781735959970572	2	0.218264040029428
1.00000000000000000	1	-0.0000000000000000

The following table is obtained by plotting the phases of  $(\delta_1, \delta_2) \in [0, (n-1)\pi)$  to determine the initial values of these parameters. Subsequently, the eigenvalues of the normalized Laplacian  $\tau$  are computed for a grid graph  $4 \times 4$  for all cases where  $(z_1, z_2) = (1, 0), (1, 1), \text{ or } (0, 0).$ 

$  \{z_1,z_2\} $	$(\delta_1,\delta_2)$	au
(0,0)	(0,0)	2
(0,0)	(0.80217 , 6.7762)	1.3333
(0,0)	(0.8021734, 2.648612)	1.3333
(0,0)	(2.6486, 8.6226)	1.3333
(0,0)	(2.6486, 0.8022)	1.3333
(0,0)	(6.7762, 8.62260)	1.3333
(0,0)	(6.7762 , 0.8022)	1.3333
(0,0)	(8.6226 , 6.7762)	1.3333

	$(\delta_1,\delta_2)$	au
(0,0)	(8.6226, 2.6486)	1.3333
(0,0)	(3.1416, 6.2832)	0.5
(0,0)	(3.1416, 3.1416)	0.5
(0,0)	$(6.2832 \; ,  6.2832)$	0.5
(0,0)	(6.2832, 3.1416)	0.5
(1,1)	$(2\pi , 2\pi)$	0
(1,1)	(3.6346 , 7.0854)	0.6667
(1,1)	(3.6346, 5.4810)	0.6667
(1,1)	(5.4810, 8.9318)	0.6667
(1,1)	(5.4810, 3.6346)	0.6667
(1,1)	(7.0854, 8.9318)	0.6667
(1,1)	(7.0854, 3.6346)	0.6667
(1,1)	(8.9318, 7.0854)	0.6667
(1,1)	(8.9318, 5.4810)	0.6667
(1,1)	( 3.1416 , 3.1416)	1.5
(1,1)	$(0,\pi)$	1.5
(1,0)	(0.2083, 8.9408)	1.781736
(1,0)	(0.2083, 0.48396)	1.781736
(1,0)	(2.9333, 8.9408)	1.781736
(1,0)	(2.9333, 0.48394)	1.781736
(1,0)	(5.79923, 6.07487)	0.21826
(1,0)	(5.7992, 3.3499)	0.21826
(1,0)	(6.7671, 3.3499)	0.21826
(1,0)	(6.76714, 6.0749)	0.21826
(1,0)	(3.45575, 6.59734)	1
(1,0)	(3.4557, 2.8274)	1
(1,0)	(5.3407, 8.4823)	1
(1,0)	(5.3407, 0.9425)	1

$\boxed{\{z_1, z_2\}}$	$(\delta_1,\delta_2)$	au
(1,0)	(7.2257, 8.4823)	1
(1,0)	(7.2257, 0.9425)	1
(1,0)	(9.1106, 6.5973)	1
(1,0)	(9.1106, 2.8274)	1

## A.2.1 Observation on the table for even number of vertices along one side n=4

For the square grid graph  $4 \times 4$  we got the eigenvalue of the Normalized Laplacian  $\tau$  as follows:

- Right multiplicity when  $\tau = 2,0$  where  $(z_1,z_2) = (0,0)$  and (1,1), respectively.
- For case  $(z_1, z_2) = (0, 0)$  we got  $\tau = 1.3333$  whith the following choices of

$$0.80217 \rightarrow \{2.6486, 6.7762\},$$
 
$$2.6486 \rightarrow \{0.80217, 8.6226\},$$
 
$$6.7762 \rightarrow \{0.80217, 8.6226\},$$
 
$$8.6226 \rightarrow \{2.6486, 6.7762\},$$

There is 8 multiplicity of this eigenvalue while we just need 2 multiplicity which means we can reduce our search on the interval as  $\delta_1, \delta_2 \in (0, (n-3)\pi)$ .

• For case  $(z_1, z_2) = (0, 0)$  we got  $\tau = 0.5$  with the following choices of

$$\delta_1 \to \delta_2:$$

$$\pi \to \{\pi, 2\pi\},$$

$$2\pi \to \{\pi, 2\pi\},$$

There is 4 multiplicity of this eigenvalue while we just need 1 multiplicity

which means we can reduce our search on the interval as  $\delta_1, \delta_2 \in (0, (n-3)\pi]$ .

• For case  $(z_1, z_2) = (1, 1)$  we got  $\tau = 0.6667$  with the following choices of

$$3.6346 \rightarrow \{5.4810, 7.0854\},$$
 
$$\delta_1 \rightarrow \delta_2:$$
 
$$5.4810 \rightarrow \{3.6346, 8.9318\},$$
 
$$7.0854 \rightarrow \{3.6346, 8.9318\},$$
 
$$8.9318 \rightarrow \{5.4810, 7.0854\},$$

There is 8 multiplicity of this eigenvalue while we just need 2 multiplicity which means we can reduce our search on the interval as  $\delta_1, \delta_2 \in (\pi, (n-2)\pi]$ .

• For case  $(z_1, z_2) = (1, 1)$  we got  $\tau = 1.5$  with the following choices of

$$\delta_1 \to \delta_2 : 0 \to \pi$$

$$\pi \to \pi,$$

There is 2 multiplicity of this eigenvalue while we just need 1 multiplicity which means we can reduce our search on the interval as  $\delta_1 \in [0, \pi)$  and  $\delta_2 \in (0, \pi]$ .

• For case  $(z_1,z_2)=(1,0)$  we got  $\tau=1.781736$  with the following choices of

$$\delta_1 \rightarrow \delta_2:$$

$$0.2083 \rightarrow \{0.48396, 8.9408\},$$

$$2.9333 \rightarrow \{0.48394, 8.9408\}$$

There is 4 multiplicity of this eigenvalue while we just need 2 multiplicity which means we can reduce our search on the interval as  $\delta_1, \delta_2 \in (\frac{n}{n-1}\pi, (n-1)\pi)$ .

• For case  $(z_1, z_2) = (1, 0)$  we got  $\tau = 0.21826$  with the following choices of

$$\delta_1 \rightarrow \delta_2:$$
 5.79923  $\rightarrow$  {3.3499, 6.07487}, 6.7671  $\rightarrow$  {3.3499, 6.07487}

There is 4 multiplicity of this eigenvalue while we just need 2 multiplicity which means we can reduce our search on the interval as  $\delta_1, \delta_2 \in (\frac{n}{n-1}\pi, (n-1)\pi)$ .

• For case  $(z_1, z_2) = (1, 0)$  we got  $\tau = 1$  with the following choices of

$$3.45575 \rightarrow \{2.8274, 6.59734\},$$
 
$$\delta_1 \rightarrow \delta_2:$$
 
$$5.3407 \rightarrow \{0.9425, 8.4823\},$$
 
$$7.2257 \rightarrow \{0.9425, 8.4823\},$$
 
$$9.1106 \rightarrow \{2.8274, 6.5973\},$$

There is 8 multiplicity of this eigenvalue while we just need 4 multiplicity which means we can reduce our search on the interval as  $\delta_1 \in (\pi, (n-2)\pi)$ ,  $\delta_2 \in (0, (n-2)\pi)$ .

### A.3 Case of $5 \times 5$ square grid graph

The following table is obtained by MATLAB calculation of the eigenvalue problem. It shows the modified Laplacian eigenvalue  $\lambda$ , the Normalized Laplacian eigenvalue  $\tau$ , and their multiplicity.

The following table is obtained by plotting the phases of  $(\delta_1, \delta_2) \in [0, (n-1)\pi)$  to determine the initial values of these parameters. Subsequently, the eigenvalues of the normalized Laplacian  $\tau$  are computed for a grid graph  $5 \times 5$  for all cases where  $(z_1, z_2) = (1, 0), (1, 1), \text{ or } (0, 0).$ 

	$(\delta_1,\delta_2)$	au
(0,0)	(0,0)	2
(0,0)	(0.777156, 2.7794)	1.55277
(0,0)	(0.777156, 9.7869)	1.55277
(0,0)	(2.7794, 0.777156)	1.55277
(0,0)	(2.7794, 11.7892)	1.55277
(0,0)	(9.7869, 0.777156)	1.55277
(0,0)	(9.7869, 11.7892)	1.55277
(0,0)	(11.7892 , 2.7794)	1.55277
(0,0)	(11.7892, 9.7869)	1.55277

$\  \{z_1, z_2\}$		
	$(\delta_1,\delta_2)$	τ
(0,0)	(1.04719755, 5.23599)	1
(0,0)	(1.0472 , 7.3304)	1
(0,0)	$(\pi\;,\pi)$	1
(0,0)	$(\pi , 3\pi)$	1
(0,0)	(5.23599, 1.0472)	1
(0,0)	(5.23599, 11.5192)	1
(0,0)	(7.3304, 1.0472)	1
(0,0)	(7.3304, 11.5192)	1
(0,0)	$(3\pi ,\pi )$	1
(0,0)	$(3\pi , 3\pi)$	1
(0,0)	(11.5192, 5.23599)	1
(0,0)	(11.5192 , 7.3304)	1
(0,0)	(3.50375, 5.50603)	0.4472
(0,0)	(3.50375, 7.0603)	0.4472
(0,0)	(5.50603, 3.50375)	0.4472
(0,0)	(5.50603, 9.0626)	0.4472
(0,0)	(7.0603, 3.5038)	0.4472
(0,0)	(7.0603, 9.0626)	0.4472
(0,0)	(9.0626 , 5.5060)	0.4472
(0,0)	$(9.0626 \; ,  7.0603)$	0.4472
(0,0)	$(2\pi \ , \ 2 \ \pi)$	0
(1,1)	$(0,\pi)$	1.7071
(1,1)	$(\pi \ ,  \pi)$	1.7071
(1,1)	( 3.6652 , 5.7596)	1
(1,1)	(3.6652, 9.9484)	1
(1,1)	(5.7596, 3.6652)	1
(1,1)	(5.7596, 12.0428)	1
(1,1)	(9.9484, 3.6652)	1

$\boxed{\{z_1, z_2\}}$	$(\delta_1,\delta_2)$	au
(1,1)	(9.9484, 12.0428)	1
(1,1)	(12.0428 , 5.7596)	1
(1,1)	(12.0428 , 9.9484)	1
(1,1)	$(2\pi \ , \ 2\pi \ )$	0.29289
(1,1)	$(2\pi \ ,  3\pi)$	0.29289
(1,1)	$(3\pi \ ,  2\pi)$	0.29289
(1,1)	$(3\pi , 3\pi)$	0.29289
(1,0)	(0.1629 , 0.4473)	1.8687
(1,0)	(0.1629, 12.1191)	1.8687
(1,0)	(2.9787, 0.4473)	1.8687
(1,0)	(2.9787, 12.1191)	1.8687
(1,0)	(3.4319, 2.9048)	1.3577
(1,0)	(3.4319, 9.6616)	1.3577
(1,0)	(12.2760, 2.9048)	1.3577
(1,0)	(12.2760, 9.6616)	1.3577
(1,0)	(3.7828 , 5.3194)	0.78106
(1,0)	(3.7828, 7.2469)	0.78106
(1,0)	(11.9252 , 5.3195)	0.78106
(1,0)	(11.9252, 7.2469)	0.78106
(1,0)	(5.6420, 0.9637)	1.2189
(1,0)	( 5.6420 , 11.6027)	1.2189
(1,0)	( 10.0659 , 0.96371)	1.2189
(1,0)	( 10.0659 , 11.6027)	1.2189
(1,0)	( 5.9928 , 3.3784)	0.6423
(1,0)	( 5.9928 , 9.18799)	0.6423
(1,0)	( 9.71513 , 3.37838)	0.6423
(1,0)	( 9.71513 , 9.18799)	0.6423
(1,0)	(6.4461, 5.8359)	0.1313

$\boxed{\{z_1, z_2\}}$	$(\delta_1,\delta_2)$	au
(1,0)	(6.4461, 6.7305)	0.1313
(1,0)	$(9.2618 \; ,  5.8359 \; )$	0.1313
(1,0)	$(9.2618 \; ,  6.73048 \; )$	0.1313

## A.3.1 Case of $6 \times 6$ square grid graph

λ	multiplicity	au
-1.0000000000000000	1	2.0000000000000000
-0.912769316065670	2	1.912769316065670
-0.809016994374948	1	1.809016994374948
-0.686259466680336	2	1.686259466680336
-0.562065445787390	2	1.562065445787390
-0.404270466768019	2	1.404270466768019
-0.309016994374948	1	1.309016994374947
-0.259129927208275	2	1.259129927208275
-0.156203793861273	2	1.156203793861273
-0.000000000000000	6	1.0000000000000000
0.156203793861273	2	0.843796206138727
0.259129927208275	2	0.740870072791725
0.309016994374947	1	0.690983005625053
0.404270466768018	2	0.595729533231982
0.562065445787390	2	0.437934554212610
0.686259466680336	2	0.313740533319664
0.809016994374948	1	0.190983005625052
0.912769316065670	2	0.087230683934330
1.00000000000000000	1	-0.0000000000000000

П		
$\boxed{\{z_1, z_2\}}$	$(\delta_1,\delta_2)$	au
(0,0)	$(0\;,0)$	2
(0,0)	(1.0682 , 5.529)	1.1562
(0,0)	(1.0682, 10.1794)	1.1562
(0,0)	(5.5285, 1.0682)	1.1562
(0,0)	(5.5285, 14.63976)	1.1562
(0,0)	(10.1794, 1.068201)	1.1562
(0,0)	(10.1794, 14.6398)	1.1562
(0,0)	(14.6398, 5.5285)	1.1562
(0,0)	(14.6398, 10.1794)	1.1562
(0,0)	(0.7439, 2.85319)	1.6862
(0,0)	(0.7439, 12.8548)	1.6862
(0,0)	(2.85319, 0.743889)	1.6862
(0,0)	(2.85319, 14.9641)	1.6862
(0,0)	(12.8548, 0.7439)	1.6862
(0,0)	(12.8548, 14.9641)	1.6862
(0,0)	( 14.9641 , 2.85319)	1.6862
(0,0)	(14.9641, 12.8548)	1.6862
(0,0)	$(\pi\;,\pi)$	1.30909
(0,0)	$(\pi , 4\pi)$	1.30909
(0,0)	$(4\pi , \pi)$	1.30909
(0,0)	$(4\pi , 4\pi)$	1.30909
(0,0)	(3.5384, 5.7729)	0.7409
(0,0)	( 3.53837 ,9.93505)	0.7409
(0,0)	(5.7729, 3.5384)	0.7409
(0,0)	(9.93505, 3.53837)	0.7409
(0,0)	(5.7729, 12.1696)	0.7409
(0,0)	(9.9350, 12.1696)	0.7409
(0,0)	(12.1696, (5.7729)	0.7409
Ш		

$\boxed{\{z_1, z_2\}}$	$(\delta_1,\delta_2)$	au
(0,0)	(12.1696, (9.9350)	0.7409
(0,0)	$(2\pi , 2\pi)$	0.19098
(0,0)	$(2\pi , 3\pi)$	0.19098
(0,0)	$(3\pi, 2\pi)$	0.19098
(0,0)	$(3\pi,3\pi)$	0.19098
(1,1)	$(3\pi , 3\pi)$	0
(1,1)	(6.5717, 8.6809)	0.3137
(1,1)	(6.5717, 10.1687)	0.3137
(1,1)	( 8.6809 , 6.5717 )	0.3137
(1,1)	( 8.6809 , 12.27789)	0.3137
(1,1)	$(10.1687 \; , \; 6.5717)$	0.3137
(1,1)	(12.27789, 8.6809)	0.3137
(1,1)	(10.1687, 12.277897)	0.3137
(1,1)	(12.27789, 10.1687)	0.3137
(1,1)	$(2\pi \ ,  2\pi)$	0.69098
(1,1)	$(2\pi \ ,  4\pi)$	0.69098
(1,1)	$(4\pi \ ,  2\pi)$	0.69098
(1,1)	$(4\pi \ ,  4\pi)$	0.69098
(1,1)	(3.8962 , 8.3566)	0.8438
(1,1)	(3.8962, 10.49298)	0.8438
(1,1)	$(8.3566\ ,3.8962\ )$	0.8438
(1,1)	(8.3566, 14.9533)	0.8438
(1,1)	(10.49298 , 3.8962)	0.8438
(1,1)	(10.49298 , 14.9533)	0.8438
(1,1)	(14.9533, 8.3566)	0.8438
(1,1)	(14.9533, 10.49298)	0.8438
(1,1)	(3.6519, 5.8864)	1.2591
(1,1)	(3.6519, 12.9631)	1.2591

	$(\delta_1,\delta_2)$	au
(1,1)	(5.8864, 3.6519)	1.2591
(1,1)	(5.8864, 15.1977)	1.2591
(1,1)	(12.9631, 3.6519)	1.2591
(1,1)	(12.9631, 15.1976877)	1.2591
(1,1)	(15.19769, 5.8864)	1.2591
(1,1)	$(15.19769 \;,\; 12.9631)$	1.2591
(1,1)	$(0\;,\pi)$	1.8090
(1,1)	$(\pi \;, \pi)$	1.8090
(1,0)	(5.7976, 0.9532)	1.4043
(1,0)	(5.7976, 14.7547)	1.4043
(1,0)	(13.0519 , 0.9532)	1.4043
(1,0)	(13.0519, 14.7547)	1.4043
(1,0)	(3.81479, 5.60999)	1
(1,0)	(3.81479, 10.09798)	1
(1,0)	(6.0588, 3.36599)	1
(1,0)	(6.0588, 12.34197)	1
(1,0)	(8.3028, 1.121997)	1
(1,0)	(8.3028, 14.5857)	1
(1,0)	(10.5468, 1.121997)	1
(1,0)	(10.5468, 14.5857)	1
(1,0)	(12.7908, 3.36599)	1
(1,0)	(12.7908, 12.34197)	1
(1,0)	(15.0348, 5.60999)	1
(1,0)	(15.0348, 10.09798)	1
(1,0)	(3.4051 , 2.9486)	1.5621
(1,0)	(3.4051, 12.7593)	1.5621
(1,0)	(15.4444, 2.9486)	1.5621
(1,0)	(15.4444, 12.759 3)	1.5621

$\boxed{\{z_1, z_2\}}$	$(\delta_1,\delta_2)$	au
(1,0)	(8.4716, 3.6272)	0.5957
(1,0)	(8.4716, 12.0808)	0.5957
(1,0)	(10.37799, 3.62716)	0.5957
(1,0)	(10.37799, 12.0808)	0.5957
(1,0)	(6.47616 , 6.0197)	0.4379
(1,0)	(6.47616 , 9.6883)	0.4379
(1,0)	(12.373 , 6.0197)	0.4379
(1,0)	(12.373 , 9.6883)	0.4379
(1,0)	(6.4174, 9.00822)	0.0872
(1,0)	(9.00822, 6.4174)	0.0872
(1,0)	(9.00822, 9.29058)	0.0872
(1,0)	(9.8413, 6.4174)	0.0872
(0,1)	(0.1342, 0.4166)	1.9128
(0,1)	(0.1342, 15.2914)	1.9128
(0,1)	(3.007396, 0.4166)	1.9128
(0,1)	(3.007396, 15.2914)	1.9128
(0,1)	$(\pi,0)$	1.9128

#### A.3.2 Observation

• For  $(z_1, z_2) = (0, 0)$  on interval  $(\delta_1, \delta_2) \in [0, (n-1)\pi)$  for all cases of n that I tried I noticed that, If the correct multiplicity of eigenvalue is 2 I got 8 of multiplicity of eigenvalue with in that range. as well as if the correct multiplicity of eigenvalue is 1. I got 4 of multiplicity of eigenvalue with in that range. the exceptional of this observation that odd n produced  $\tau = 1$  when  $(z_1, z_2) = (0, 0)$  with multiplicity  $(n \times 2) + 2$  the correct multiplicity when produced  $\tau = 1$  for both n even or odd and only If n odd,  $\tau = 0$  with interval  $(\delta_1 = \delta_2 = (n - 3)\pi)$  and the only exceptional in this interval is case n = 3 where is  $(\delta_1 = \delta_2 = \pi)$ .

• For  $(z_1, z_2) = (1, 0)$ , if n is even we will have double multiplicity of  $\tau = 1$ .

## **Bibliography**

- [1] M. Argentina, P. Coullet, and V. Krinsky. Head-on collisions of waves in an excitable fitzhugh–nagumo system: a transition from wave annihilation to classical wave behavior. *Journal of theoretical biology*, 205(1):47–52, 2000.
- [2] A. Barrat, M. Barthélemy, and A. Vespignani. Dynamical Processes on Complex Networks. Cambridge University Press, Cambridge, 2008.
- [3] M. Barthélemy. Spatial networks. Physics reports, 499(1-3):1–101, 2011.
- [4] A. Bellandi, D. Papp, A. Breakspear, J. Joyce, M. Johnston, J. Keijzer, E. Raven, M. Ohtsu, T. Vincent, A. Miller, Sanders. D., S. Hogenhout, R. J. Morris, and C. Faulkner. Diffusion & bulk flow of amino acids mediate calcium waves in plants. *Science Advances*, 8(42):eabo6693, 2022.
- [5] E. Bender and S. Williamson. Lists, decisions and graphs. with an introduction to probability (2010).
- [6] J. Billingham and A. C. King. Wave motion. Number 24. Cambridge university press, 2000.
- [7] J. Bondy and U. Murty. Graph theory with applications, volume 290.Macmillan London, 1976.
- [8] L. Böttcher and M. Porter. Dynamical processes on metric networks. arXiv preprint arXiv:2401.00735, 2024.
- [9] R. Boukrab and A. Pagès-Zamora. Random-walk laplacian for frequency analysis in periodic graphs. *Sensors*, 21(4):1275, 2021.

- [10] M. Breakspear. Dynamic models of large-scale brain activity. *Nature* neuroscience, 20(3):340–352, 2017.
- [11] M. Brio, J.-G. Caputo, and H. Kravitz. Spectral solutions of pdes on networks. Applied Numerical Mathematics, 172:99–117, 2022.
- [12] A. Brouwer and W. Haemers. Spectra of graphs. Springer Science & Business Media, 2011.
- [13] I. Bárány and J. Solymosi. Gershgorin disks for multiple eigenvalues of nonnegative matrices. A Journey Through Discrete Mathematics, pages 123–133, 2017.
- [14] C. Canuto, M. Hussaini, A. Quarteroni, and T. Zang. Spectral Methods: Evolution to Complex Geometries and Applications to Fluid Dynamics. Springer.
- [15] T. Cebeci. Convective Heat Transfer. Springer Berlin Heidelberg, 2002.
- [16] D. Cebrían-Lacasa, P. Parra-Rivas, D. Ruiz-Reynés, and L. Gelens. Six decades of the fitzhugh-nagumo model: A guide through its spatio-temporal dynamics and influence across disciplines. arXiv preprint arXiv:2404.11403, 2024.
- [17] D. Centola. The spread of behavior in an online social network experiment. science, 329(5996):1194–1197, 2010.
- [18] V. Chandraker, Awasthi A., and S. Jayaraj. Implicit numerical techniques for fisher equation. *Journal of Information and Optimization Sciences*, 39(1):1– 13, 2018.
- [19] H. Chen and F. Zhang. Resistance distance and the normalized laplacian spectrum. *Discrete applied mathematics*, 155(5):654–661, 2007.
- [20] W. Chen. Graph theory and its engineering applications, volume 5. World Scientific, 1997.

- [21] K. Chong, A. Boresi, S. Saigal, and J. Lee. Numerical methods in mechanics of materials: with applications from nano to macro scales. CRC Press, 2017.
- [22] F. Chung. Spectral graph theory, volume 92. American Mathematical Soc., 1997.
- [23] A. Coco and G. Russo. High order finite-difference ghost-point methods for elliptic problems in domains with curved boundaries. arXiv preprint arXiv:2405.13986, 2024.
- [24] J. Crank. The Mathematics of Diffusion. Oxford University Press, Oxford, 1975.
- [25] J. Enderle and J. Bronzino. Introduction to biomedical engineering.

  Academic press, 2012.
- [26] W. Gao, H. Wu, M. Siddiqui, and A. Baig. Study of biological networks using graph theory. Saudi journal of biological sciences, 25(6):1212–1219, 2018.
- [27] G. Grimmett and D. Stirzaker. Probability and Random Processes. Oxford University Press, Oxford, 2001.
- [28] J. Gross and J. Yellen. Graph Theory and Its Applications, Second Edition (Discrete Mathematics and Its Applications). Chapman & Hall/CRC, 2005.
- [29] M. Keeling and K. Eames. Networks and epidemic models. Journal of the royal society interface, 2(4):295–307, 2005.
- [30] M. Kłopotek. Spectral analysis of laplacians of an unweighted and weighted multidimensional grid graph-combinatorial versus normalized and random walk laplacians. arXiv preprint arXiv:1707.05210, 2017.
- [31] P. Kuchment. Quantum graphs: an introduction and a brief survey. arXiv preprint arXiv:0802.3442, 2008.
- [32] L. Lovász. Random walks on graphs: A survey. pages 1–46, 1993.

- [33] F. Malliaros and M. Vazirgiannis. Clustering and community detection in directed networks: A survey. *Physics reports*, 533(4):95–142, 2013.
- [34] R. Marappan, S. Raja, Sh. Raja, and Sa. Raja. Check if a graph is bipartite or not & bipartite graph coloring using java. *International Journal of Mathematical, Engineering, Biological & Applied Computing*, pages 61–67.
- [35] M. Newman. Networks: An Introduction. Oxford University Press, 2010.
- [36] M. Newman. Networks: An Introduction. Oxford University Press, Oxford, 2018.
- [37] S. Priyadarshini and S. Rodda. Geometric multi-way frequent subgraph mining approach to a single large database. In Smart Intelligent Computing and Applications, pages 233–244. Springer, 2020.
- [38] W. Schiesser and G. Griffiths. A compendium of partial differential equation models: method of lines analysis with Matlab. Cambridge University Press, 2009.
- [39] B. Sennaiyan and T. Suresh. Graph coloring on bipartite graphs. International Journal of Mathematical, Engineering, Biological & Applied Computing, pages 56–60, 2022.
- [40] Z. Shi, S. Watanabe, K. Ogawa, and H. Kubo. Structural Resilience in Sewer Reconstruction - From Theory to Practice. 08 2017.
- [41] M. Stone and P. Goldbart. Mathematics for Physics. Cambridge University Press, Cambridge, 2004.
- [42] N. Trefethen. Approximation Theory and Approximation Practice. SIAM.
- [43] A. Turing. The chemical basis of morphogenesis. *Philosophical Transactions* of the Royal Society B, 237(641):37–72, 1952.
- [44] V. Volpert and S. Petrovskii. Reaction–diffusion waves in biology. *Physics of life reviews*, 6(4):267–310, 2009.

- [45] D. West. Introduction to Graph Theory. Prentice Hall, Upper Saddle River, NJ, 2001.
- [46] R. Wilson. Introduction to Graph Theory. Pearson Education India, 1996.
- [47] A. Wünsche. Duality between bessel functions and chebyshev polynomials in expansions of functions. Advances in Pure Mathematics, 13(8):504–536, 2023.